

1991

Partial Melting Experiments On Phlogopite-bearing Model Mantle Sources And The Role Of Carbon Dioxide- And Alkali-rich Melts In Metasomatic Processes

Yves Thibault

Follow this and additional works at: <https://ir.lib.uwo.ca/digitizedtheses>

Recommended Citation

Thibault, Yves, "Partial Melting Experiments On Phlogopite-bearing Model Mantle Sources And The Role Of Carbon Dioxide- And Alkali-rich Melts In Metasomatic Processes" (1991). *Digitized Theses*. 1961.
<https://ir.lib.uwo.ca/digitizedtheses/1961>

This Dissertation is brought to you for free and open access by the Digitized Special Collections at Scholarship@Western. It has been accepted for inclusion in Digitized Theses by an authorized administrator of Scholarship@Western. For more information, please contact tadam@uwo.ca, wlsadmin@uwo.ca.

**PARTIAL MELTING EXPERIMENTS
ON PHLOGOPITE-BEARING MODEL MANTLE SOURCES
AND THE ROLE OF CO₂- AND ALKALI-RICH MELTS
IN METASOMATIC PROCESSES**

by

Yves Thibault

Department of Geology

**Submitted in partial fulfilment
of the requirements for the degree of
Doctor of Philosophy**

**Faculty of Graduate Studies
The University of Western Ontario**

London, Ontario

November, 1990

© Yves Thibault 1990



National Library
of Canada

Bibliothèque nationale
du Canada

Canadian Theses Service Service des thèses canadiennes

Ottawa, Canada
K1A 0N4

The author has granted an irrevocable non-exclusive licence allowing the National Library of Canada to reproduce, loan, distribute or sell copies of his/her thesis by any means and in any form or format, making this thesis available to interested persons.

The author retains ownership of the copyright in his/her thesis. Neither the thesis nor substantial extracts from it may be printed or otherwise reproduced without his/her permission.

L'auteur a accordé une licence irrévocable et non exclusive permettant à la Bibliothèque nationale du Canada de reproduire, prêter, distribuer ou vendre des copies de sa thèse de quelque manière et sous quelque forme que ce soit pour mettre des exemplaires de cette thèse à la disposition des personnes intéressées.

L'auteur conserve la propriété du droit d'auteur qui protège sa thèse. Ni la thèse ni des extraits substantiels de celle-ci ne doivent être imprimés ou autrement reproduits sans son autorisation.

ISBN 0-315-64280-7

Canada

ABSTRACT

Experiments at 3.0 GPa were done to define the nature of near-solidus melts formed from phlogopite lherzolite (PLZ) and carbonated phlogopite lherzolite (CPL) model mantle sources. The reactivity of these melts towards harzburgite and wehrlite were then investigated at 2.0 GPa and 1000°C.

At 3.0 GPa and 1225°C, PLZ yields 7 wt% of melt. The partial breakdown of phlogopite to olivine and liquid results in a silicate melt enriched in K, OH, Al and Fe and a residual phlogopite enriched in Ti. This alkaline silicate melt is only slightly reactive towards harzburgite and wehrlite at 2.0 GPa and 1000°C.

In CPL, at 3.0 GPa and 1100°C, 4 wt% of alkali-bearing dolomitic melt coexists with residual garnet phlogopite lherzolite. The alkalinity is related to the partial breakdown of phlogopite to olivine and pyrope yielding K and OH to the melt. At 2.0 GPa and 1000°C, this dolomitic melt metasomatizes a harzburgite to a phlogopite wehrlite, whereas infiltration into wehrlite could result in the formation of calcite- and phlogopite-bearing dunite.

A process active below continental rifts is proposed in which a carbonated phlogopite lherzolite horizon, formed at the base of the lithosphere by the release of dense alkaline

fluids, migrates via *melting-migrating-solidifying/reacting* cycles. The results of the CPL and PLZ experiments suggest that fractional melting of the carbonated phlogopite lherzolite horizon at 100 km depth could yield a dolomitic melt followed by an alkali-rich silicate melt. The consecutive infiltration of these distinct agents into lithospheric mantle at 65km depth could result in a decoupled metasomatic/enrichment event. The dissociation of the carbonate components of the dolomitic melt will create an harzburgite -> wehrlite metasomatic trend. The infiltration of the silicate melt will enrich the metasomatized rocks in clinopyroxene and phlogopite. The variety of rocks that result bear similarities with a suite of mantle xenoliths from the West Eifel, Germany.

ACKNOWLEDGEMENTS

In the first place, I would like to express my sincere gratitude to Dr. Alan D. Edgar for allowing me to undertake this project. His critical supervision and continuous encouragement during the various stages of this study are greatly appreciated.

I strongly benefitted from the assistance of Dr. Felicity E. Lloyd. I especially thank her for sharing her vast knowledge on metasomatic processes, for guiding me through the many quarries of the Eifel volcanic region, and for providing suitable materials needed for this study. Thanks, also, to all her family for their warm hospitality during my one-week stay in Reading.

The assistance and guidance of Robert Barnett and Dave Kingston with the microprobe work were indispensable. Many thanks to John Forth for quickly preparing thin sections of great quality and to Ron Shirran for keeping the high-pressure laboratory in perfect order.

Sincere gratitude to Dr. Danilo Vukadinovic for his encouragement and his objective review of earlier versions of this thesis and to Dr. Sandro Conticelli for sharing his knowledge of potassic magmatism and more importantly for his friendship. Thanks to Diane Forsyth for showing me, with great patience, the high-pressure experimental procedures.

Financial support was provided by the "Fonds pour la formation de chercheurs et l'aide à la recherche" (FCAR) through a doctoral sholarship. The analytical expenses were covered by an operating grant from the Natural Sciences and Engineering Research Council of Canada (NSERC) to Dr. Alan D. Edgar. A field trip to the West Eifel vocanic region, Germany, was funded by a collaborative research grant from NATO.

TABLE OF CONTENTS

	<u>Page</u>
CERTIFICATE OF EXAMINATION.....	ii
ABSTRACT.....	iii
ACKNOWLEDGEMENTS.....	v
TABLE OF CONTENTS.....	vii
LIST OF TABLES.....	xi
LIST OF FIGURES.....	xiv
LIST OF APPENDICES.....	xvii
CHAPTER 1: INTRODUCTION.....	1
1.1 Definition of metasomatism.....	1
1.2 Types of mantle metasomatism and enrichment..	3
1.3 Potential metasomatic agents.....	4
1.4 Objectives of the thesis.....	5
1.5 Comments on the use of the terms metasomatism and enrichment.....	6
1.6 Comments on the use of the terms fluids, melts and low-density fluids.....	7
CHAPTER 2 : REVIEW OF PREVIOUS EXPERIMENTAL STUDIES RELEVANT TO MANTLE METASOMATIC PROCESSES.....	8
2.1 Review of theoretical and experimental data characterizing properties of low-density fluids as potential metasomatic agents.....	8
2.1.1 Volatile species of C-O-H low-density fluids and existence of carbonates in the upper mantle.....	8
2.1.2 Buffering capacity of peridotite with respect to H ₂ O-CO ₂ low-density fluids.....	10
2.1.3 Solubility and reactivity of H ₂ O-CO ₂ low-density fluids in the upper mantle.....	11
2.2 Review of recent theoretical and experimental data characterizing the properties of melts as potential metasomatic agents.....	16
2.2.1 Theoretical aspects of the mobility of melts in the upper mantle.....	16

2.2.2 Experimental data on the nature and reactivity of melts.....	18
2.3 Implications for the present study.....	21
CHAPTER 3: EXPERIMENTAL AND ANALYTICAL TECHNIQUES...	22
3.1 Starting material.....	22
3.1.1 Synthesis of mantle source and mantle protolith compositions.....	22
3.1.2 Synthesis of stimated melt composition for "sandwich-type" experiments and interaction experiments.....	28
3.2 Experimental apparatus.....	32
3.3 Experimental charge preparation.....	33
3.3.1 Encapsulation.....	33
3.3.2 Sandwich-type experiments.....	34
3.4 Comments on experimental conditions.....	35
3.4.1 Experimental times and attainment of equilibrium.....	35
3.4.2 Oxygen fugacity.....	36
3.5 Phase indentification and analytical techniques.....	38
CHAPTER 4: PARTIAL MELTING OF A PHLOGOPITE LHERZOLITE (PLZ) AT P = 3.0 GPA: EXPERIMENTAL RESULTS.....	42
4.1 General statement on phase relationships.....	42
4.2 Chemical composition of minerals.....	44
4.2.1 $X_{MgFe_{tot}}$ of silicate minerals and related comments on iron loss.....	44
4.2.2 Olivine.....	50
4.2.3 Orthopyroxene.....	50
4.2.4 Clinopyroxene.....	51
4.2.5 Phlogopite.....	67
4.2.6 Garnet.....	75
4.3 Determination of melt composition in equilibrium with PLZ at 1225°C: sandwich experiments.....	78
4.3.1 Details of the experimental approach.....	78
4.3.2 Sandwich experiment on PLZ using SDW2 as a middle layer.....	79
4.3.3 Sandwich experiment on PLZ using SDW3 as a middle layer.....	85
4.4 Interaction experiments with HAR and WHR protoliths.....	91
4.5 Summary.....	97

CHAPTER 5: PARTIAL MELTING OF A CARBONATED PHLOGOPITE LHERZOLITE (CPL) AT P = 3.0 GPA: EXPERIMENTAL RESULTS.....	98
5.1 General statement on phase relationships.....	98
5.2 Chemical composition of minerals.....	100
5.2.1 Carbonates.....	100
5.2.2 Olivine.....	104
5.2.3 Orthopyroxene.....	104
5.2.4 Clinopyroxene.....	104
5.2.5 Phlogopite.....	105
5.2.6 Garnet.....	111
5.3 Determination of melt composition in equilibrium with CPL at 1100°C: sandwich experiments.....	114
5.3.1 Details of the experimental approach.....	114
5.3.2 Sandwich experiment on CPL using S-DOL as a middle layer.....	114
5.3.3 Sandwich experiment on CPL using S/P-DOL as a middle layer.....	120
5.4 Interaction experiments with HAR and WHR protoliths.....	124
5.5 Summary.....	128
CHAPTER 6: NATURE OF THE MELTING AND METASOMATIC REACTIONS.....	130
6.1 Melting reactions in PLZ and CPL.....	130
6.1.1 Generalized melting reaction and degree of partial melting at 1225°C in the PLZ source.....	130
6.1.2 Generalized melting reaction and degree of partial melting at 1100°C in the CPL source.....	143
6.1.3 Additional comments on the degree of partial melting.....	149
6.2 Metasomatic reactions in HAR and WHR.....	150
6.2.1 Metasomatic reactions involving CARMET.....	151
6.2.1.1 Metasomatic reactions between CARMET and HAR.....	151
6.2.1.2 Metasomatic reactions between CARMET and WHR.....	155
6.2.1.3 Progressive metasomatism involving CARMET.....	157
6.2.2 Metasomatic reactions involving SILMET	163
6.2.3 Chemical modification of the protolith.....	166
6.3 Summary.....	169
CHAPTER 7: PETROLOGICAL IMPLICATIONS.....	172
7.1 Multi-cycle metasomatic/enrichment process active in a continental rifting environment....	172

7.1.1	A basic assumption: the movement and infiltration of small melt fractions.....	172
7.1.2	A thermal framework for an active continental rifting environment.....	174
7.1.3	Proposed early metasomatic/enrichment cycles.....	182
7.1.4	Late decoupled metasomatic/enrichment cycle from 100 to 65 km depth.....	185
7.1.5	Limitations of the proposed model.....	190
7.2	Two well-documented occurrences of modal mantle metasomatism in continental rifting environments.....	193
7.2.1	Heterogeneous nature of the upper mantle below the West Eifel volcanic province, Germany: the possible result of a decoupled metasomatic/enrichment event?...	193
7.2.2	Mantle xenoliths sampled by ultrapotassic magmas in southwest Uganda: widespread metasomatism in the western branch of the East African Rift?.....	201
7.3	Summary.....	205
CHAPTER 8: CONCLUSIONS.....		208
APPENDIX A: DETAILS OF FUGACITY CALCULATION.....		211
APPENDIX B: MINERAL AND MELT CHEMICAL COMPOSITIONS..		215
B1	Experiment for oxygen fugacity estimation.....	216
B2	Experiments on PLZ.....	220
B3	Experiments on CPL.....	257
B4	Interaction experiments.....	293
APPENDIX C: LEAST-SQUARES MASS BALANCE CALCULATIONS.		307
REFERENCES.....		319
VITA.....		338

LIST OF TABLES

<u>Table</u>	<u>Description</u>	<u>Page</u>
3.1	List of all the starting materials used in this study.....	23
3.2	Mantle sources and mantle protoliths compositions.....	26
3.3	Average microprobe analyses of mineral separates from mantle xenolith F48Y.....	30
3.4	Average microprobe analyses of other minerals used in starting materials.....	31
3.5	Comparison of accepted analyses of natural standards with their analyses during the different probe sessions.....	40
3.6	List of all melt compositions cited in this study.....	41
4.1	Results of partial melting experiments on PLZ at P = 3.0 GPa.....	43
4.2	Microprobe analyses of melt pools observed in the products of the partial melting experiments on PLZ.....	80
4.3	Synthesized melt compositions used in sandwich experiments with the PLZ model mantle source.....	82
4.4	Average of microprobe analyses of "quench" liquid in the middle layer of the sandwich experiments performed on PLZ.....	86
4.5	Comparison of the composition of primary and quench clinopyroxene grains in sandwich experiment PLZ40.....	88

4.6	Comparison of the composition of the minerals in the standard experiment PLZ30 and in the sandwich experiment PLZ40.....	90
4.7	Bulk composition of SILMET, HAR+SILMET and WHR+SILMET.....	93
4.8	Results of standard experiments on HAR and WHR and interaction experiments with SILMET...	94
4.9	Comparison of average composition of SILMET and of the cryptocrystalline assemblage in HAR-SILMET and WHR-SILMET.....	96
5.1	Results of partial melting experiments on CPL at P = 3.0 GPa.....	99
5.2	Synthesized melt compositions used in sandwich experiments with the CPL model mantle source..	116
5.3	Composition of quench carbonate analyzed in sandwich experiment CPL14 performed at 1100°C and 3.0 GPa.....	118
5.4	Microprobe analyses of melt in large melt pools of sandwich experiment CPL14 performed at 1100°C and 3.0 GPa.....	119
5.5	Comparison of the composition of the minerals in the standard experiment CPL10 and in the sandwich experiment CPL16.....	122
5.6	Microprobe analyses of melt in large melt pools of sandwich experiment CPL16 performed at 1100°C and 3.0 GPa.....	123
5.7	Bulk composition of CARMET, HAR+CARMET and WHR+CARMET.....	126
5.8	Results of standard experiments on HAR and WHR and interaction experiments with CARMET...	127
6.1	Results of the least-squares mass balance calculations on PLZ at subsolidus and suprasolidus conditions.....	132
6.2	Normative composition of the melt in equilibrium with PLZ at 3.0 GPa and 1225°C....	137
6.3	Results of the least-squares mass balance calculations on CPL in the magnesite field, the dolomite field and at suprasolidus conditions.....	145

6.4	Results of the least-squares mass balance calculations for the interaction experiment with HAR and CARMET.....	153
6.5	Results of the least-squares mass balance calculations for the interaction experiment with WHR and CARMET.....	156
6.6	Density of the silicates magnesian end members.....	162
6.7	Results of the least-squares mass balance calculations for the interaction experiment with HAR and SILMET.....	164

LIST OF FIGURES

<u>Figure</u>	<u>Description</u>	<u>Page</u>
4.1	Variation of $100X_{MgFe}$ of the silicate minerals against temperature (PLZ standard experiments).....	46
4.2	Variation of the $K_D^{ol/opx}(Fe/Mg)$ against temperature (PLZ standard experiments).....	49
4.3	Variations of the wollastonite proportion and of the $(Al_2O_3 + Cr_2O_3)$ content of orthopyroxene against temperature (PLZ standard experiments).....	53
4.4	Compositions of clinopyroxene plotted in the Wo-En-Fs ternary diagram (PLZ standard experiments).....	55
4.5	Variations of the Ti/Q , Na/Q and (Al_{tot}/Q) in clinopyroxene against temperature (PLZ standard experiments).....	58
4.6	Variation between Al^{IV} and Ti in clinopyroxene (PLZ standard experiments).....	60
4.7	Variation between Al^{IV} and $(Al^{VI}+Cr+2Ti)$ in clinopyroxene (PLZ standard experiments).....	62
4.8	Variation between Na and Cation Excess in clinopyroxene (PLZ and CPL standard experiments).....	66
4.9	Variation of the $Ti:K$ atomic ratio of phlogopite against temperature (PLZ standard experiments).....	70
4.10	Variation of Ti against $[(6-Si-Al^{VI}-Cr-Ca)/2]$, $[6-OSO]$, and $[(6-Si-Al^{VI}-Cr-Ca)/2] + [6-OSO]$ in phlogopite(PLZ standard experiments).....	73
4.11	Garnet compositions on a $Mg-Fe^{2+}-Ca$ ternary diagram (PLZ experiments).....	77

4.12	Backscattered electron micrographs of: a) products of sandwich experiment PLZ33 b) melt pools filled by quench carbonates in sandwich experiment CPL14.....	84
5.1	Carbonate compositions plotted on a Mg-Ca-(Fe+Mn) ternary diagram (CPL standard experiments).....	103
5.2	Variation of the Ti:K atomic ratio of phlogopite against temperature (CPL standard experiments).....	108
5.3	Variation of Ti against [(6-Si-Al ^{VI} -Cr-Ca)/2], [6-OSO], and [(6-Si-Al ^{VI} -Cr-Ca)/2] + [6-OSO] in phlogopite (CPL standard experiments).....	110
5.4	Variation between TiO ₂ and Cr ₂ O ₃ in garnets (PLZ and CPL standard experiments).....	113
6.1	Calculated phase proportions in the PLZ source at subsolidus conditions and at 7.1 wt% of partial melting.....	134
6.2	Normative composition of the PLZ equilibrium partial melt at 3.0 GPa and 1225°C plotted in the quaternary system DI-OL-KZ-QZ; a) on the OL-KS-QZ plane projected from diopside b) on the DI-OL-LC plane projected from quartz.....	140 142
6.3	Calculated phase proportions in the CPL source in the subsolidus magnesite field, the subsolidus dolomite field and at 4.3 wt% partial melting.....	147
6.4	Effects of the progressive metasomatism of a harzburgite protolith by the infiltration of CARMET plotted on an olivine- orthopyroxene-clinopyroxene ternary diagram..	159
6.5	Effects of the progressive metasomatism of a harzburgite protolith by the infiltration of CARMET plotted on an (olivine+orthopyroxene)-clinopyroxene- phlogopite ternary diagram.....	161
6.6	Chemical modification of HAR by infiltration of 10 wt% of CARMET and SILMET.....	168

7.1	Geotherms expressing a hypothetical thermal evolution in the mantle beneath a continental rift.....	176
7.2	Hypothetical sections representing the thermal conditions in the lithospheric mantle beneath a continental rift a) and b)..... c) and d).....	179 181
7.3	Sketch and olivine-orthopyroxene-clinopyroxene ternary diagram illustrating the diversity of ultramafic rocks resulting from a decoupled metasomatic/enrichment event at 65 km depth..	189
7.4	Modal compositions of representative samples of ultramafic xenoliths from Gees, West Eifel, Germany plotted on a olivine-orthopyroxene-clinopyroxene ternary diagram.....	196
7.5	Modal compositions of representative samples of ultramafic xenoliths from Gees, West Eifel, Germany plotted on a (olivine+orthopyroxene)-clinopyroxene-phlogopite ternary diagram.....	196

LIST OF APPENDICES

<u>Appendix</u>	<u>Page</u>
APPENDIX A	
Details of oxygen fugacity calculation method.....	211
APPENDIX B	
Mineral and melt chemical compositions.....	215
B1	
Experiment for oxygen fugacity estimation.....	216
B2	
Experiment on PLZ.....	220
B3	
Experiment on CPL.....	257
B4	
Interaction experiments.....	293
APPENDIX C	
Least-squares mass balance calculations.....	307

The author of this thesis has granted The University of Western Ontario a non-exclusive license to reproduce and distribute copies of this thesis to users of Western Libraries. Copyright remains with the author.

Electronic theses and dissertations available in The University of Western Ontario's institutional repository (Scholarship@Western) are solely for the purpose of private study and research. They may not be copied or reproduced, except as permitted by copyright laws, without written authority of the copyright owner. Any commercial use or publication is strictly prohibited.

The original copyright license attesting to these terms and signed by the author of this thesis may be found in the original print version of the thesis, held by Western Libraries.

The thesis approval page signed by the examining committee may also be found in the original print version of the thesis held in Western Libraries.

Please contact Western Libraries for further information:

E-mail: libadmin@uwo.ca

Telephone: (519) 661-2111 Ext. 84796

Web site: <http://www.lib.uwo.ca/>

CHAPTER 1

INTRODUCTION

1.1 Definition of metasomatism

Goldschmidt (1922, p.106) has defined metasomatism as:

"... a process of alteration which involves enrichment of the rock by new substances brought in from the outside. Such enrichment takes place by definite chemical reaction between the original minerals and the enriching substances.

...The newly introduced substances may take the form of either gases, aqueous solutions or melts, and their reactions with the original constituents of the rock result in the formation of metasomatic and possible accessory minerals."

The idea that metasomatic processes should be active in the upper mantle gained significant credibility at the First International Kimberlite Conference held in Cape Town in 1973. Lloyd and Bailey (1975), who studied mantle nodules sampled by primitive ultrapotassic and sodi-potassic volcanics from southwest Uganda and west Eifel (Germany) volcanic provinces, suggested that hydrous alkali clinopyroxenite showing deformation textures and replacement fabrics were the end product of extensive metasomatism of anhydrous peridotite related to the degassing of a large portion of the underlying asthenospheric mantle through a narrow rift zone. Harte et al. (1975) and Gurney et al.

(1975) suggested that metasomatism under mantle conditions was responsible for the formation of phlogopite, ilmenite, rutile and sulphides in some peridotite xenoliths from the Matsoku kimberlite pipe, Lesotho. Erlank (1973) and Boyd and Nixon (1975) concluded that primary phlogopite (Carswell, 1975) observed in nodules sampled by kimberlites from Kimberley (Erlank), Northern Lesotho and the Monastery Mine (Boyd and Nixon) were probably formed by mantle metasomatic processes. Since then so much work has been done on the subject that, in 1987, three books were published in which mantle metasomatism processes were discussed in detail (Menzies and Hawkesworth, 1987; Morris and Pasteris, 1987; Nixon, 1987). However, a controversy still existed on restricting or not the use of "metasomatism" to processes where the enriching "agents" consist primarily of low-density fluids (e.g. H₂O, CO₂), leading Boettcher (1987) to comment:

"In response to this semantic dispute, I see no advantage in defining too narrowly the processes of metasomatism until we are capable of distinguishing petrographically, chemically or isotopically the differences between alteration produced by silicate-rich liquids (magmas) and that resulting from hydrothermal fluids - both are the results of percolating solutions."

In this context, the suggestion of Harte (1987) to emphasize that a metasomatic process has to involve "...definite chemical reaction between the original minerals and the enriching substance" (Goldschmidt, 1922, p.106) is

preferred here. Therefore, it is not the nature of the introduced "enriching substance" that defines a process as metasomatic but rather evidence that this substance (agent), be it a low-density fluid or a melt, clearly reacts with the original minerals of the solid material (protolith) it infiltrates.

1.2 Types of mantle metasomatism and enrichment

Dawson (1982, 1984) recognized two contrasting types of mantle metasomatism: (i) "patent" metasomatism where evidence is found of textural replacement of the rock's original minerals by later "generally" hydrous phases, and (ii) "cryptic" metasomatism where peridotites, generally strongly depleted in "basaltic" components, exhibit anomalously high trace-element (e.g. LILE, LREE) abundances.

Based essentially on textural and chemical data from peridotite xenoliths sampled by kimberlites, Harte (1983, 1987) identified three types of "enrichment" processes: (i) modal metasomatism, (ii) major-minor-trace element enrichment and (iii) isolated trace element enrichment. Modal metasomatism, comparable to patent metasomatism, involves changes in major-minor-trace element composition associated with recognizable modification in modal mineralogy (changes in mineral proportions or introduction of new mineral species: Harte, 1983; Harte and Hawkesworth, 1989). Major-minor-trace element enrichment involves

chemical modification without changes in modal composition. Isolated trace element enrichment is essentially synonymous with cryptic metasomatism. This term is preferred by Harte (1987) due to the difficulty in finding evidence concerning the nature of the exact processes responsible for this type of enrichment. In any of these types, depending on the timing of the metasomatic event, the enrichment in trace elements may or may not be coupled by a change in radiogenic isotopic ratios (e.g. $^{143}\text{Nd}/^{144}\text{Nd}$, $^{87}\text{Sr}/^{86}\text{Sr}$; e.g. Harte, 1983; Menzies and Murthy, 1980; Roden and Murthy, 1985).

Bailey (1987) indicated that the major lithophile-element-bearing minerals in mantle xenoliths showing replacement of pre-existing peridotite minerals or being associated with metasomatism are biotite, amphibole, clinopyroxene and carbonates, whereas the usual minor ones are phosphates, titanates, oxides and sulphides. He added that, chemically, most documented mantle metasomatism occurrences involve enrichment in some or all of the following elements: H, C, F, Na, Al, P, S, Cl, K, Ca, Ti, Fe, Rb, Y, Nb, Ba and rare earths (REE).

1.3 Potential metasomatic agents

The most important agents that have been called upon as responsible for metasomatic processes in the upper mantle are essentially silicate melts (e.g. Wilshire and Shervais, 1975; Harte et al., 1975, 1987; Dawson and Smith, 1977; Frey

and Prinz, 1978; Ehrenberg, 1979; Jones et al., 1982; Kramers et al., 1983; Wilshire, 1987; Edgar et al., 1989; Waters et al., 1989; Lloyd et al., 1990a), CO₂-rich melts (e.g. Menzies et al., 1987; Meen, 1987; Green and Wallace, 1988; Meen et al., 1989) and low-density fluids composed mainly of volatile species of the C-O-H system (e.g. Bailey, 1972, 1982, 1985; Lloyd and Bailey, 1975; Schneider and Eggler, 1986; Stosch and Lugmair, 1986; Lloyd, 1987; Kempton et al., 1988). Depending of their specific nature, low-density fluids and melts will have distinct properties that will constrain their abilities to be responsible for any particular occurrence of mantle metasomatism. In this context, experimental studies investigating the nature of potential metasomatic agents at mantle conditions can yield valuable information.

1.4 Objectives of the thesis

The present study is an experimental investigation of the properties of small melt fractions, formed in equilibrium with phlogopite-bearing model mantle sources, as potential metasomatic agents. In more detail, the main objectives are:

- 1) To determine the composition of melts formed at small degrees of partial melting of a phlogopite lherzolite and carbonated phlogopite lherzolite at a pressure of 3.0 GPa

and to characterize the nature of the melting reactions involved. The pressure chosen (3.0 GPa) is believed to be representative of mantle depth conditions in excess of the amphibole stability (cf. Green, 1973; Mysen and Boettcher, 1975) and where phlogopite should therefore be the characteristic hydrous phase present in peridotitic rocks.

2) To estimate the reactivity of these melts towards harzburgitic and wehrlitic protoliths at 2.0 GPa and 1000°C and to propose reactions that define their effectiveness as potential metasomatic agents. The pressure-temperature conditions for these experiments are considered to be representative of conditions that these melts may encounter during their ascent in the lithospheric mantle.

3) To integrate the experimental results in a petrological framework characterizing metasomatic and enrichment processes that could be active in the lithospheric mantle of a continental rifting environment.

4) To test the applicability of the proposed model to two well-documented occurrences of mantle metasomatism: the West Eifel volcanic province, Germany, and the southwest Uganda volcanic fields in the western branch of the East African Rift.

1.5 Comments on the use of the terms metasomatism and enrichment

In the present study, discussion of metasomatic

processes will usually deal with modal metasomatism caused by melts. A melt will be considered as a good metasomatic agent if the newly formed minerals are clearly the product of significant replacement of the original minerals of the protolith. If the new minerals are essentially the product of crystallization of the infiltrating melt without significant replacement of the original minerals of the protolith, the process will be rather considered as an enrichment.

1.6 Comments on the use of the terms fluids, melts and low-density fluids

Wyllie (1987) described fluid as a (p. 611): "... term applicable in geological contexts to liquid (melt, magma, silicate melt with dissolved volatile components), vapour (dense gas, pneumatolytic gas, hydrothermal solution), supercritical solution, or to undefined fluid phase." In the present study, this definition will be used implying that melts, vapours and supercritical solutions are all fluids. Vapour and supercritical fluids dominated by volatile species such as H_2O , CO_2 , CH_4 , F, Cl, etc... will usually be referred to as low-density fluids in order to retain a distinction with melts.

CHAPTER 2

REVIEW OF PREVIOUS EXPERIMENTAL STUDIES RELEVANT TO MANTLE METASOMATIC PROCESSES

The present study was undertaken, in part, to complement previous experimental studies that have characterized the properties of low-density fluids and melts as potential metasomatic agents. A brief review of theoretical and experimental data relevant to mantle metasomatism is presented below.

2.1 Review of theoretical and experimental data characterizing properties of low-density fluids as potential metasomatic agents

2.1.1 Volatile species of C-O-H low-density fluids and existence of carbonates in the upper mantle

If present in the upper mantle, the volatile species in C-O-H low-density fluids are controlled by the oxidation state of the mantle and change, at graphite or diamond saturation, from essentially $\text{CO}_2 + \text{H}_2\text{O}$ at oxygen fugacities between the fayalite-magnetite-quartz (FMQ) and the wüstite-magnetite (WM) buffers to mixtures of CH_4 and H_2 under

strongly reducing conditions with fO_2 's near and below the iron-wüstite (IW) buffer (e.g. Ryabchikov et al., 1981; Egglar and Baker, 1982; Woermann and Rosenhauer, 1985; Holloway, 1987). Egglar and Baker (1982) have also shown that if carbonates are stable in the mantle, the fO_2 will be defined, in the presence of graphite or diamond, by the existence of: enstatite-magnesite-olivine-diamond (EMOD), enstatite-magnesite-olivine-graphite (EMOG) or graphite-enstatite-diopside-olivine-dolomite (GEDOD). All these carbonated assemblages define fO_2 s near MW at mantle pressure-temperature conditions (Egglar, 1987 and references therein).

Most recent studies attempting to estimate upper mantle oxygen fugacity were based on thermodynamic data for heterogeneous equilibria involving coexisting phases in mantle xenolith mineral assemblages: olivine-orthopyroxene-ilmenite (Egglar, 1983), olivine-orthopyroxene-spinel (O'Neill and Wall, 1987; Mattioli and Wood, 1988; Mattioli et al., 1989; Wood and Virgo, 1989), and olivine-pyroxenes-garnet (Luth et al., 1990). The results of these studies are all consistent with fO_2 values above the WM buffer and usually closer to the FMQ buffer in the mantle regions represented by most mantle xenoliths. Therefore, C-O-H low-density fluids should be generally dominated by CO_2 and H_2O and carbonates should be stable in the upper mantle.

2.1.2 Buffering capacity of peridotite with respect to H₂O-CO₂ low-density fluids

In the upper mantle, the composition of H₂O-CO₂ low-density fluids will be buffered by reaction involving amphibole, phlogopite and carbonates as long as the peridotitic material is not completely hydrated (e.g. Wyllie, 1978; Eggler, 1978). The buffering capacity of fertile mantle peridotite (e.g. pyrolite) is approximately 0.4 wt% H₂O (Green, 1973; Wyllie, 1978) as long as amphibole is stable. At pressures exceeding amphibole stability, phlogopite becomes the only stable hydrous phase and the buffering capacity of peridotite relative to H₂O, which is then essentially related to the amount of K₂O, will drop to approximately 0.02 wt% (Wyllie, 1978). With respect to CO₂, the buffering capacity of peridotite is enormous (e.g. Schneider and Eggler, 1986). For example, at pressures greater than approximately 2.0 GPa, no free CO₂ vapor phase can coexist with peridotitic mineralogy because it will be consumed through two major carbonation reactions: "Forsterite + Diopside + CO₂ => Enstatite + Dolomite" and "Forsterite + CO₂ => Enstatite + Magnesite" (Falloon and Green, 1989).

In conclusion, because the buffering capacity of peridotite is small relative to H₂O but very large with respect to CO₂, low-density fluids should be dominated by

H₂O. Nevertheless, the significantly higher buffering capacity of amphibole peridotite compared to phlogopite peridotite with respect to H₂O, should drive H₂O-rich low-density fluid entering the mantle region of amphibole stability towards slightly more CO₂-rich composition. However, this will only be true as long as the buffering capacity is not exhausted (Schneider and Eggler, 1986).

2.1.3 Solubility and reactivity of H₂O-CO₂ low-density fluids in the upper mantle

Ryabchikov and Boettcher (1980) determined experimentally the amount of K₂O in aqueous vapour in equilibrium with synthetic phlogopite-bearing mantle assemblage at pressures from 1.0 to 3.0 GPa and temperatures between 1050° and 1100°C. They observed an important increase in the proportion of solute in the vapour phase with increasing pressure, ranging from about 14 wt% at 1.1 GPa to about 55 wt% at 3.0 GPa. At 3.0 GPa, the K₂O solubility was estimated at 25 wt% and the other major components quantitatively partitioned in the vapour phase were considered to be SiO₂ and Al₂O₃ with a K₂O/Al₂O₃ molecular ratio close to unity. Ryabchikov and Boettcher (1980) concluded that aqueous low-density fluids are very efficient agents for transporting K₂O.

Ryabchikov et al. (1982) performed a series of experiments bearing on the solubilities of Na in pure H₂O

low-density fluid in equilibrium with omphacitic pyroxene (70 mol% $\text{CaMgSi}_2\text{O}_6$; 30 mol% $\text{NaAlSi}_2\text{O}_6$) at pressures of 2.0 and 3.0 GPa and a temperature of 900°C. With increasing fluid to solid ratio, they observed a decrease in Na and an increase of the Tschermak's components ($\text{CaAl}_2\text{SiO}_6$ - $\text{MgAl}_2\text{SiO}_6$) in the clinopyroxene phase. Ryabchikov et al. (1982), therefore, concluded that the content of Na in the aqueous phase was substantial and that it was present, at least partly in the form of sodium silicate components. For a constant fluid to solid ratio, the distribution of Na between the aqueous and pyroxene phases did not appear to be pressure dependent in contrast to the behaviour of K in phlogopite-bearing assemblage (see above; Ryabchikov and Boettcher, 1980). Based on this contrasting behavior of these two major alkali elements, Ryabchikov et al. (1982) proposed that, during upward transport of alkali-bearing low-density fluids in the mantle, the major part of potassium may be fixed in phlogopite at deeper levels, while sodium would be preferentially retained in the low-density fluid until the amphibole stability is reached.

Schneider and Eggler (1986) performed comparable experiments on the solubilities of oxides in H_2O and $\text{H}_2\text{O}-\text{CO}_2$ low-density fluids equilibrated with phlogopite peridotite, amphibole peridotite and jadeite peridotite, at pressures ranging from 1.3 to 2.0 GPa and temperatures between 600° and 1100°C. They observed that the composition of the solute in H_2O low-density fluid was dominated by normative

quartzofeldspathic components (K_2O or Na_2O , Al_2O_3 , SiO_2), peraluminous ($Al > K+Na$), and not enriched in Mg, Fe and Ti. The maximum amount of solute recorded in pure H_2O fluid in equilibrium with phlogopite peridotite at 2.0 Gpa, was approximately 12 wt% (K_2O solubility of ≈ 1 wt%). In this context, Schneider and Eggler (1986) doubted that the far greater K_2O solubility of 25 wt% determined by Ryabchikov and Boettcher (1980) at 3.0 GPa is reasonable and suggested that it could be the result of the use of gels rather than crystalline phlogopite in the Ryabchikov-Boettcher study.

Solute contents in H_2O-CO_2 low-density fluid were found by Schneider and Eggler (1986) to be far less than in pure H_2O even at very low value of X_{CO_2} (0.1-0.2). Moreover solute compositions in H_2O-CO_2 fluids, although also dominated by normative feldspathic components, were significantly more alkaline. Schneider and Eggler (1986) suggested that the increased alkalinity of the solute in H_2O-CO_2 low-density fluids is probably related to carbonate complexing (K_2CO_3 and Na_2CO_3 complexes). However, Eggler (1987) noted that the carbonate complexing is certainly not extensive as shown by the dramatic lowering of the total solubility in CO_2 -bearing low-density fluids compared to pure H_2O (Schneider and Eggler, 1986; Eggler, 1987).

In the context of mantle metasomatism, Schneider and Eggler (1986) envisioned the subsolidus lithosphere in terms of two major regions: 1) a region of carbonate phlogopite peridotite at depths greater than 70 km in which

34

undersaturated H₂O-rich low-density fluids could leach a significant amount of K, Na, Al and Si and 2) a shallower region of amphibole peridotite, where, as pointed out in section 2.1.2, the solute-bearing low-density fluid should become more CO₂-rich. Because of the drastic lowering of the total solubility of elements in CO₂-bearing fluids, Schneider and Egger (1986) suggested that this shallower region should be characterized by widespread precipitation from the low-density fluids resulting in metasomatism of the surrounding mantle rocks.

Nevertheless, Schneider and Egger (1986) considered that low-density fluids are probably inefficient metasomatic agents resulting in part from rather low solubilities especially in CO₂-bearing fluids. They finally suggested that melts are probably more attractive metasomatic agents because the solubilities of major elements are far greater than in low-density fluids.

In an experimental study designed to model K-metasomatism at P-T conditions near that of the continental geotherm, Edgar and Arima (1984) investigated the effects of the interaction of model mantle pyrolite with H₂O low-density fluid containing minor CO₂ and varying concentrations of K₂O in solution. At a pressure of 3.0 GPa and temperatures of 850° and 950°C, a progressive increase in the relative proportion of phlogopite with increasing concentration of K₂O in the aqueous solution, up to 3.6g K₂O/10g solution, was observed. At higher K₂O

concentrations, the amount of phlogopite decreased and the presence of glass suggested that the lower relative amount of phlogopite was related to the preferential partitioning of K into a melt phase. At 2.0 GPa and 950°C, phlogopite showed an increase relative to the other minerals and no glass was observed even at very high K₂O concentrations. An amphibole was detected at very low concentrations of K₂O, but it rapidly disappeared with increasing K₂O in solution, suggesting that it was not a K-bearing amphibole. Their results indicated reactions for phlogopite formation involving garnet, olivine and orthopyroxene at 3.0 GPa and spinel, amphibole, olivine, orthopyroxene and clinopyroxene at 2.0 GPa. Edgar and Arima (1984) also argued that the antipathetic relation between amphibole and phlogopite at 2.0 GPa suggests that in the absence of appreciable sodium, the diagnostic K-rich metasomatic mineral at depths equivalent to 2.0 GPa is phlogopite rather than K-rich amphibole.

In order to model experimentally Na-dominated metasomatism, McNeil (1987) and McNeil and Edgar (1987) investigated experimentally the effects of the interaction of pyrolite with H₂O low-density fluid containing minor CO₂ and varying proportions of Na₂O and both Na₂O and K₂O in solution at a pressure of 2.0 GPa and a temperature of 950°C. With increasing alkali concentration up to 3.0g alkalies/10g solution, the amount of amphibole (pargasitic to edenitic in composition) and olivine was found to

increase, whereas orthopyroxene and clinopyroxene decreased. The amount of Na in the amphibole also increased with increasing alkali concentration and McNeil and Edgar (1987) considered that the dominant substitution mechanism was $(\text{Na},\text{K}) + \text{Si} \rightleftharpoons \text{Al} + \text{Ca}$. They showed that the experimentally-produced amphiboles are closely related to natural pargasite-edenite but not to natural Ti-pargasite found in metasomatized mantle xenoliths. Based on these observations, they suggested that variations in natural amphiboles from Ti-pargasite to pargasite-edenite may represent a transition between precipitation from a silicate melt and metasomatism caused by a residual hydrous fluid. They observed that the solidus boundary appeared to be reached at less than 950°C with solution with more than 3.0g alkalis/10g solution, and concluded that this may be an important mechanism for generating alkali enriched magma which might subsequently caused alkali metasomatism of wallrock through which it passes.

2.2 Review of recent theoretical and experimental data characterizing the properties of melts as potential metasomatic agents

2.2.1 Theoretical aspects of the mobility of melts in the upper mantle

Assuming that the rocks above the source of melt are

27

non-porous, the liquid can migrate upwards by two mechanisms (Watson and Brenan, 1987): magma ascent can be done by propagation of melt-filled cracks through the lithosphere (e.g. Spera, 1984, 1987) or the melt can penetrate grain edges by dissolution/re-precipitation or, more simply, infiltration (e.g. Watson, 1982; Watson and Brenan, 1987).

The ability of a melt to propagate through non-porous rocks by infiltration is directly related to the melt/rock surface energy configuration. If the dihedral (wetting) angle formed between the melt and the crystalline residuum is less than 60° , the melt will form a framework of interconnected channels along solid grain edges at all melt fractions (e.g. Hunter and McKenzie, 1989 and references therein) and the local interfacial energy will be lower at wet grain edges than at dry ones (Watson, 1982). This implies that the wet configuration is energetically favoured and, consequently, the melt, driven by its low density, can ascend by infiltrating the dry grain edges of the mantle material above. For basic silicate (Beeré, 1975; Waff and Bulau, 1979; McKenzie, 1985) and carbonatite (Hunter and McKenzie, 1989) melts, the dihedral angle is less than 60° . These melts should, therefore, form an interconnected network at all melt fractions and, consequently, should have a tendency to infiltrate adjacent dry rocks.

Given a low density and a dihedral angle less than 60° , the other most important property of the melt that will control the efficiency of infiltration is the viscosity.

McKenzie (1985) estimated that alkali-rich basic silicate melts can segregate from their mantle sources and migrate by infiltration at melt fractions of approximately 1%. For carbonatite melts, the minimum fraction for segregation would be as low as 0.02%, due to their extremely low viscosities (Hunter and McKenzie, 1989).

McKenzie (1989) argued that because such small melt fractions transport little heat, they will rarely reach the surface. Moreover, because they are probably rich in alkalis, water and carbonates, the reaction of such melts with the lithosphere as they percolate upwards could result in mantle metasomatism.

2.2.2 Experimental data on the nature and reactivity of melts

The high-pressure phase relationships of complex peridotite systems with small amount of H₂O and CO₂ have been investigated by Olafsson and Eggler (1983) and Wallace and Green (1988). With increasing pressure, Olafsson and Eggler (1983) characterized three distinct subsolidus assemblages: a amphibole-peridotite ($P < 1.7$ GPa), a carbonate-amphibole-peridotite ($1.7 \text{ GPa} < P < 2.2 \text{ GPa}$), a carbonate-phlogopite-peridotite ($> 2.2 \text{ GPa}$). They considered that amphibole, phlogopite and carbonate should melt completely at temperatures very close to the solidus and found the near-solidus melt of carbonate-amphibole-

peridotite to be nephelinitic (carbonated alkali-rich silicate melt). They could not obtain compositions of melts produced in the carbonate-phlogopite-peridotite field but presumed that they should also be carbonate-rich and probably potassic.

Considering the results of Olafsson and Eggler (1983), Meen (1987) and Meen et al. (1989) suggested that the rise of such nephelinitic melts could be a powerful method of creating distinct enriched mantle regions. Consequently, they studied experimentally the interaction of a carbonated alkaline magma composition (Ijolite + 5 wt% CO₂) with harzburgitic material. Based on their experimental results, they characterized different mineral assemblages that could be produced by metasomatism involving the interaction of a hydrous and carbonated alkaline magma with a peridotite as a function of pressure, temperature and "melt:harzburgite" ratio. At high temperatures (> 1100°C), and with a high "melt:harzburgite" ratio (> 1), olivine and orthopyroxene of the protolith are partially dissolved in the melt and an olivine clinopyroxenite assemblage is produced. At lower temperature and lower "melt:harzburgite" ratio, the product is related to pressure. At pressures less than 1.7 GPa, an amphibole-lherzolite is formed with release of CO₂ low-density fluid, whereas, at pressures exceeding 1.7 GPa, an amphibole-carbonate-lherzolite would be produced. Some of the non-silicate minerals that could occur would be ilmenite and, at high temperatures, whitlockite (Ca₃[PO₄]₂) (Meen et

al., 1989)

More recently, Wallace and Green (1988) have characterized the phase relationships of a vapour-undersaturated carbonate- and amphibole-bearing peridotite. Up to a pressure of 3.0 GPa, the different solidus assemblages that they determined were: an amphibole-lherzolite ($P < 2.1$ GPa), a dolomite-amphibole-lherzolite ($2.1 < P < 2.8$ GPa) and a magnesite-amphibole-lherzolite ($P > 2.8$ GPa). In contrast to the experimental study of Olafsson and Eggler (1983), the results of Wallace and Green (1988) revealed a suprasolidus field in which the carbonate has completely broken down and a melt coexists with amphibole-bearing lherzolite indicating the persistence of amphibole to temperatures clearly in excess of the solidus temperature. Wallace and Green (1988) characterized the composition of the near-solidus melt at 2.2 GPa by a series of sandwich experiments and found it to be dolomitic ($\text{CO}_2 > 40$ wt%), rich in Na ($\text{Na}_2\text{O} \approx 5$ wt%) and very poor in Si ($\text{SiO}_2 \approx 3$ wt%). P_2O_5 was also found to be strongly partitioned in the dolomitic melt.

Green and Wallace (1988) have investigated experimentally the efficiency of such a carbonatite melt as a potential metasomatic agent. They concluded that at pressures less than 2.1 GPa and temperatures of 950° to 1050°C, infiltration of the sodic dolomitic melt could modally alter spinel lherzolite to apatite-bearing wehrlite. In this transformation, the dolomitic component of the melt

81

reacts with enstatite to yield olivine, diopside and CO_2 , whereas the sodic component of the melt reacts with alumina contained in orthopyroxene and spinel to form clinopyroxene and pargasite components (Green and Wallace, 1988). Finally apatite formation is related to the significant amount of P_2O_5 brought by the melt.

2.3 Implications for the present study

In the context of McKenzie's (1984, 1985, 1989) proposition regarding the segregation and migration of small volumes of melts by pervasive infiltration, the results of the recent experimental studies investigating the nature of small melt fractions formed in equilibrium with hydrated and carbonated peridotite (e.g. Olafsson and Eggler, 1983; Wallace and Green, 1988) and estimating the effectiveness of such melts as potential metasomatic agents (Meen, 1987; Green and Wallace, 1988; Meen et al, 1989) are quite valuable. These experimental investigations have dealt, however, essentially with amphibole-bearing sources. The present study, which deals essentially with phlogopite-bearing peridotitic sources, is believed to represent a reasonable complement to these previous studies.

CHAPTER 3

EXPERIMENTAL AND ANALYTICAL TECHNIQUES

3.1 Starting material

Because of the large number of starting materials needed for this study, the abbreviations used to identify each of them and the Tables where their compositions can be found are all listed in Table 3.1.

3.1.1 Synthesis of mantle source and mantle protolith compositions

-Comments on the compositions of the "model" mantle sources.

The mantle source materials used for the melting experiments at a pressure of 3.0 GPa are considered representative of carbonated phlogopite lherzolite (CPL mixture, Table 3.2) and phlogopite lherzolite (PLZ mixture, Table 3.2) - two types of mantle rocks often referred to as potential sources of many primary alkaline magmas. However, compared to most "normal" mantle materials, the proportion of olivine incorporated in the mixtures was kept at the minimum limit for a peridotite (40% olivine relative to the total of olivine and pyroxenes; based on the classification

Table 3.1 : List of all the starting materials used in this study with their corresponding abbreviations.

<u>Abbreviation</u>	<u>Description of the material</u>	<u>Table</u>
<i>Mantle sources and protoliths</i>		
PLZ	Phlogopite lherzolite	3.2
CPL	Carbonated phlogopite lherzolite	3.2
HAR	Harzburgite	3.2
WHR	Wehrlite	3.2
<i>Synthesized compositions used as middle layer in sandwich experiments</i>		
SDW2	Silicate glass used in sandwich experiment on PLZ	4.3
SDW3	Silicate glass used in sandwich experiment on PLZ	4.3
S-DOI	Sodic-dolomitic composition used in sandwich experiment on CPL	5.2
S/P-DOL	Sodic-potassic-dolomitic composition used in sandwich experiment on CPL	5.2
<i>Synthesized composition used for interaction experiments</i>		
SILMET	Silicate glass used in interaction experiments with HAR and WHR	4.7
CARMET	Dolomitic mixture used in interaction experiments with HAR and WHR	5.7

Notes: The compositions can be found in the specified Tables.

of Streckeisen, 1973). This technique is relatively similar to the one used by Green and Ringwood (1970) in which a significant amount of olivine is subtracted from the starting composition in order to "...facilitate the identification and microprobe analysis of minor phases" (Mengel and Green, 1989, p.572). This method is especially useful in experiments investigating phase relationships at low degrees of partial melting.

As one of the objectives of the partial melting experiments on CPL is a comparison with the recent experiments performed on a carbonated amphibole lherzolite (Wallace and Green, 1988), the amount of carbonate added to the CPL mixture is such that the compositional characteristics, especially the CO₂ content and the CO₂:H₂O ratio, are comparable to the ones for the starting material used by Wallace and Green (1988, p.344, Table 1, Analysis 1). However, relative to Wallace and Green's (1988) composition, the CPL mixture (Table 3.2) is poorer in TiO₂, Al₂O₃ and FeO, richer in MgO. Moreover, although the total abundance of alkalis is quite similar, the K₂O/Na₂O value is significantly higher in CPL (K₂O:Na₂O weight ratio of 3.05 in CPL compared to 0.18 for Wallace and Green's composition), a characteristic of many phlogopite-bearing garnet lherzolites (e.g. Erlank et al., 1987, p.277, Table IVb; Menzies et al., 1987, p.328, Table III).

The PLZ composition (Table 3.2) is comparable with the starting material used by Mengel and Green (1989, p.572,

Table 7.1, Analysis C) in their investigation of the stability of amphibole and phlogopite in a metasomatized peridotite at water-undersaturated conditions. A very significant difference, however, is the H₂O/alkalies value which in Mengel and Green's study is such that when amphibole breaks down at high pressure, there is an excess of water relative to the amount needed to form phlogopite, creating a significant "backbending" (lowering) of the solidus between 2.5 and 2.8 GPa (Mengel and Green, 1989, Fig. 7.5B, p. 577). In the PLZ composition, because water is added in the form of phlogopite, no such excess of H₂O can occur. Consequently the solidus of PLZ at 3.0 GPa occurs at considerably higher temperature than for Mengel and Green's composition (see details in Chapter 4).

-Comments on the compositions of the "model" mantle protoliths.

Mg-rich peridotite consisting essentially of olivine and orthopyroxene with only a little clinopyroxene, garnet and/or spinel (harzburgite and clinopyroxene-poor lherzolite) are abundant and widespread in the mantle xenolith population representative of the lithospheric mantle (e.g. Harte and Hawkesworth, 1989). Therefore, a harzburgite is considered a good candidate as the protolith of many metasomatized mantle rocks. Consequently, one of the mantle protolith compositions chosen for the interaction experiments at 2.0 GPa is of harzburgitic composition (HAR

Table 3.2: Mantle sources and mantle protoliths compositions (minerals in italics are separates from xenolith E48Y)

<u>CPL</u>				<u>PLZ</u>			
	(wt%)		(wt%)		(wt%)		(wt%)
<i>OL</i>	34.87	SiO ₂	45.07	<i>OL</i>	36.40	SiO ₂	47.04
<i>OPX</i>	34.87	TiO ₂	0.29	<i>OPX</i>	36.40	TiO ₂	0.30
<i>CPX</i>	17.44	Al ₂ O ₃	4.05	<i>CPX</i>	18.20	Al ₂ O ₃	4.23
<i>SP</i>	2.87	Cr ₂ O ₃	0.69	<i>SP</i>	3.00	Cr ₂ O ₃	0.72
<i>PHL-8</i>	5.75	FeO*	6.44	<i>PHL-8</i>	6.00	FeO*	6.72
CaCO ₃	3.50	MnO	0.11			MnO	0.12
Na ₂ CO ₃	0.70	MgO	33.92			MgO	35.40
		NiO	0.11			NiO	0.11
		CaO	6.09			CaO	4.32
		Na ₂ O	0.60			Na ₂ O	0.20
		K ₂ O	0.58			K ₂ O	0.61
		H ₂ O	0.22			H ₂ O	0.23
		CO ₂	1.83			CO ₂	0.00
Total	100.00	Total	100.00	Total	100.00	Total	100.00
		X _{MgFe_{tot}}	0.90			X _{MgFe_{tot}}	0.90

<u>HAR</u>				<u>WHR</u>			
	(wt%)		(wt%)		(wt%)		(wt%)
<i>OL</i>	50.00	SiO ₂	48.31	<i>OL</i>	72.75	SiO ₂	42.33
<i>OPX</i>	50.00	TiO ₂	0.01	<i>CPX</i>	24.25	TiO ₂	0.03
		Al ₂ O ₃	1.52	<i>SP</i>	3.00	Al ₂ O ₃	2.36
		Cr ₂ O ₃	0.15			Cr ₂ O ₃	0.65
		FeO*	7.43			FeO*	7.62
		MnO	0.13			MnO	0.12
		MgO	42.00			MgO	40.96
		NiO	0.15			NiO	0.22
		CaO	0.28			CaO	5.50
		Na ₂ O	0.02			Na ₂ O	0.21
		K ₂ O	0.00			K ₂ O	0.00
		H ₂ O	0.00			H ₂ O	0.00
		CO ₂	0.00			CO ₂	0.00
Total	100.00	Total	100.00	Total	100.00	Total	100.00
		X _{MgFe_{tot}}	0.91			X _{MgFe_{tot}}	0.91

mixture; Table 3.2).

The other synthesized mantle protolith for this study is a spinel wehrlite (WHR mixture; Table 3.2). Two main reasons justify this choice of composition. First, it allows a study of the interaction of agents with clinopyroxene and spinel which, besides olivine and orthopyroxene, are the most common minerals found in mantle xenoliths sampled by alkali basalts (e.g. Nixon, 1987). Secondly, Cr-diopside wehrlite xenoliths are sometimes reported as part of the mantle xenolith population in areas like the West Eifel, Germany (e.g. Lloyd and Bailey, 1975; Stosch and Lugmair, 1986; Lloyd, 1987; Kempton et al., 1988; Edgar et al., 1989; Lloyd et al., 1990a), Victoria, Australia (e.g. Green and Wallace, 1988) and San Carlos, Arizona (Frey and Prinz, 1978). These wehrlites are sometimes interpreted as being the end product of metasomatism of spinel lherzolite by carbonatite melts (Green and Wallace, 1988) or by silicate liquids (Frey and Prinz, 1978; Stosch and Lugmair, 1986; Lloyd et al., 1990a).

-Preparation.

CPL, PLZ, HAR and WHR compositions were prepared using natural olivine, orthopyroxene, clinopyroxene, spinel and phlogopite. "Spec-Pure" CaCO_3 and "Fisher certified" Na_2CO_3 were used as a source of CO_2 in the CPL composition.

Olivine, orthopyroxene, clinopyroxene and spinel were separated from a spinel lherzolite xenolith (E48Y) from

Meerfeld Maar, West Eifel, Germany, kindly donated by Dr. Felicity Lloyd. The source of phlogopite was a single xenocryst (E-8) also sampled from the West Eifel. The compositions of these minerals are shown in Tables 3.3 and 3.4.

The separation of minerals from E48Y was done by hand, choosing only crystals free of visible inclusions and alteration as seen under a binocular microscope. Subsequently, each of the mineral separates from E48Y and the phlogopite xenocryst (E-8) were ground individually under acetone in an agate mortar. All materials were then dried at 110°C for at least 24 hours and cooled in a dessicator. Finally, each of the starting compositions was prepared using the desired amounts of dried materials that were mixed and ground together manually and mechanically in an agate mortar for periods of at least 2 hours. Based on observations of the products after experiments, it is believed that the average grain size of the mixtures is approximately 10µm or less. Table 3.2 shows the proportions of mineral separates and carbonates used for each mixture and the resulting bulk compositions for the two model mantle sources (CPL and PLZ) and the two protoliths (HAR and WHR).

3.1.2 Synthesis of estimated melt composition for "sandwich-type" experiments and interaction experiments

Synthesized water-bearing silicate melt and dolomitic

melt compositions were needed for sandwich-type melting experiments (see section 3.3.2) of mantle sources (CPL and PLZ) and interaction experiments with mantle protoliths (HAR and WHR). Some of the materials used in the synthesis of these melt compositions were "Fisher certified" TiO_2 , MgO , Na_2CO_3 , K_2CO_3 , "Analar grade" Al_2O_3 , "Spec-Pure" CaCO_3 and pre-ground 99.9% pure quartz. Natural fayalite (FAY-1), brucite (BRU-1) and dolomite (DOL-1) were used respectively as the main sources of FeO , H_2O and CO_2 . The compositions of FAY-1, BRU-1 and DOL-1 are shown in Table 3.4.

-Preparation of water-bearing silicate glasses

The water-bearing silicate melt compositions were synthesized as glasses in a two-stage process.

In the first step, the desired amounts of pre-dried SiO_2 , TiO_2 , Al_2O_3 , MgO , CaCO_3 , Na_2CO_3 , and K_2CO_3 were mixed, under acetone, by mechanical and hand grinding in an agate mortar for a period of at least 1 hour. The mixture was then transferred to a platinum crucible, melted in air at 1350°C for 25 minutes in order to remove all CO_2 , and quenched to a homogeneous transparent glass. Microprobe analyses of these prepared glasses show that the sodium loss is insignificant ($<0.5\text{wt}\%$).

In the second step, appropriate amounts of pre-dried and pre-ground synthesized glass (see above), FAY-1 and BRU-1 were mixed in an agate mortar under acetone for a period of 1 hour and dried at 110°C for 24 hours. About 40 mg of this

Table 3.3: Average microprobe analyses of mineral separates from mantle xenolith E48Y.

	<u>CPX</u> (n=7)	<u>OPX</u> (n=6)	<u>OL</u> (n=5)	<u>SP</u> (n=5)
SiO ₂	53.22(0.37)	56.08(0.44)	40.69(0.26)	-----
TiO ₂	0.07(0.03)	0.02(0.02)	0.01(0.01)	0.03(0.02)
Al ₂ O ₃	3.55(0.18)	3.03(0.14)	0.01(0.01)	50.01(0.50)
Cr ₂ O ₃	0.59(0.07)	0.29(0.05)	0.01(0.02)	16.68(0.40)
FeO*	2.71(0.10)	5.82(0.21)	9.07(0.27)	13.38(0.26)
MnO	0.09(0.05)	0.13(0.03)	0.13(0.08)	0.11(0.07)
MgO	16.59(0.28)	33.97(0.35)	50.19(0.24)	20.03(0.53)
NiO	-----	-----	0.31(0.02)	-----
CaO	22.65(0.32)	0.52(0.10)	0.04(0.01)	-----
Na ₂ O	0.86(0.03)	0.05(0.01)	0.00(0.01)	-----
K ₂ O	0.00(0.00)	0.00(0.00)	0.00(0.00)	-----
Total	100.33	99.91	100.46	100.24
X _{MgFe_{tot}}		0.92	0.91	0.91

Notes : The number in brackets is one standard deviation for the "n" microprobe analyses. "-----" means that the element was not analysed. FeO* refers to the total Fe expressed as FeO. X_{MgFe_{tot}} is Mg/(Mg+Fe_{total}).

Table 3.4: Average microprobe analyses of other minerals used in starting materials

	<u>PHL-8</u>	<u>FAY-1</u>	<u>DOL-1</u>	<u>BRU-1</u>
	(n=9)	(n=9)	(n=5)	(n=2)
SiO ₂	36.96(0.28)	30.59(0.16)	-----	0.00[0.00]
TiO ₂	4.56(0.08)	0.00(0.00)	-----	0.00[0.00]
Al ₂ O ₃	16.36(0.36)	0.02(0.01)	-----	0.00[0.00]
Cr ₂ O ₃	0.00(0.00)	0.00(0.01)	-----	0.00[0.00]
FeO*	6.96(0.18)	66.20(0.28)	6.56(0.29)	0.32[0.33]
MnO	0.09(0.02)	0.67(0.07)	0.15(0.02)	0.99[1.01]
MgO	20.23(0.12)	2.37(0.05)	18.02(0.15)	66.50[67.96]
CaO	0.02(0.02)	0.04(0.01)	29.18(0.20)	0.00[0.00]
BaO	0.45(0.02)	-----	-----	-----
Na ₂ O	0.35(0.02)	0.01(0.02)	-----	0.00[0.00]
K ₂ O	10.11(0.13)	0.00(0.00)	-----	0.00[0.00]
H ₂ O#	3.79	-----	-----	30.05[0.00]
CO ₂ #	-----	-----	46.68	-----
F	0.19(0.05)	-----	-----	-----
O=>F	0.08	-----	-----	-----
Total	99.99	99.90	100.59	97.86[100.00]

Notes :

"n" is the number of microprobe analyses
 number in curved brackets is one standard deviation
 number in square brackets is the value recalculated for 100wt% total
 -----: not analysed
 PHL-8: phlogopite xenocryst from west Eifel
 FAY-1: fayalite
 DOL-1: single crystal of dolomite
 BRU-1: single crystal of brucite
 H₂O# and CO₂# are not analysed but calculated

38

mixture was sealed in a 12 mm long, 2.5 mm diameter platinum capsule and melted in a piston-cylinder apparatus at 1.2 GPa and 1350°C for a period of 5 minutes. The final products were dark brown water-bearing silicate glasses whose compositions were checked by microprobe analysis. The glass was then ground, dried at 110°C and cooled in a dessicator.

-Preparation of dolomitic melt compositions

The dolomitic melt compositions were synthesized as simple mixtures using the appropriate amounts of pre-dried and pre-ground DOL-1, CaCO₃, Na₂CO₃, K₂CO₃, and BRU-1. After mixing under acetone in an agate mortar for at least 2 hours, the mixture was dried at 110°C for 24 hours and cooled in a dessicator.

3.2 Experimental apparatus

The pressure (2.0 and 3.0 GPa) and temperature (900° to 1300°C) conditions needed for this study were achieved using a 1.27 cm-diameter piston-cylinder apparatus (Boyd and England, 1960) The solid pressure-transmitting medium consisted of a talc-pyrex sleeve in which a graphite furnace was introduced. The temperature, generated by passing a current through the graphite furnace, was monitored using a Pt-Pt₉₀Rh₁₀ thermocouple.

Pressures and temperatures were calibrated at the kyanite-sillimanite transition at 2.2 GPa and 1300°C

(Richardson et al., 1968) and at the jadeite + quartz → albite reaction at 1.63 GPa and 600°C (Johannes et al., 1971; Holland, 1980). No frictional correction was applied to pressure nor a pressure correction to the emf of the Pt-Pt₉₀Rh₁₀ thermocouple. In principle, pressure and temperature could be controlled to within ± 0.05 GPa and ± 5°C of the stated value. However, the effect of possible contamination of the Pt-Pt₉₀Rh₁₀ thermocouple at high temperature and long run times (Presnall et al., 1973) was not taken into account. Windom and Unger (1988, see fig. 3, p. 392) performed some tests in which they monitored temperatures controlled by a Pt-Pt₉₀Rh₁₀ thermocouple with a W₉₅Re₅-W₇₄Re₂₆ thermocouple. Based on these tests, the maximum change in temperature in the present study would be an increase of approximately 8°C, occurring in the experiments performed at temperatures over 1200°C for a duration of 20 hours.

A hot piston-out technique was used in which an initial pressure 10% higher than required was maintained for 15 to 45 minutes (at run temperature) and then reduced to the desired value.

3.3 Experimental charge preparation

3.3.1 Encapsulation

Approximately 8 mg of starting material was loaded into 7 mm long, 1 mm diameter capsule welded at one end. In order

to minimize iron loss, Ag₅₀Pd₅₀ capsules were used at temperatures up to 1250°C. For the two experiments performed at temperatures of 1275° and 1300°C, Fe-soaked platinum capsules (Ford, 1978) were employed. After the capsule was filled, it was sealed by electrical welding.

3.3.2 Sandwich-type experiments

In order to define the equilibrium liquid composition at low degrees of partial melting of the two mantle sources (CPL and PLZ), a "sandwich" technique, in which 10 to 18 wt% of a melt composition was added between two layers of the peridotitic source, was used. This technique, extensively used in melting experiments (e.g. Stolper, 1980; Takahashi and Kushiro, 1983; Fujii and Scarfe, 1984, 1985; Falloon and Green, 1988; Falloon et al., 1988; Wallace and Green, 1988; Mengel and Green, 1989), ensures that large areas of equilibrated melt, whose composition is not affected by quench overgrowths on primary crystal phases, are available for defocused beam microprobe analysis (Fujii and Scarfe, 1984). The use of a defocused electron beam for melt analysis also prevents important volatilization of Na and K.

3.4 Comments on experimental conditions

3.4.1 Experimental times and attainment of equilibrium

Experimental times were chosen in order to offer the best compromise between attainment of equilibrium and prevention of unacceptable iron loss. Normally, durations of the experiments varied from 28 hours at subsolidus conditions down to 4 hours at 1300°C. Shorter times were sometimes used in sandwich experiments.

In the experimental products, most crystal phases are compositionally uniform and are therefore considered to be fully equilibrated. However, especially at suprasolidus conditions, some crystals occasionally show small compositional zonation. For example, clinopyroxene crystal rims, nearer to the melting regions, are generally poorer in Na₂O, richer in Al₂O₃ and Cr₂O₃, and have higher $X_{Mg/Fe_{tot}}$ ($Mg/[Mg+Fe_{total}]$) values compared to the cores. The preservation of relict compositions in the clinopyroxene cores is probably due to the slow rate of intracrystalline diffusion preventing achievement of complete equilibrium, a problem well documented by Raheim and Green (1974) and Green (1976). The possible option of using longer experimental times to eliminate this problem was rejected on two grounds: first, as noted above, to prevent unacceptable iron loss; secondly, in previous studies in which mineral separates were used in sandwich experiments,

unequilibrated relict compositions were still preserved in the cores of pyroxenes even with durations up to 72 hours (Fujii and Scarfe, 1984, 1985).

Nevertheless, in the experimental products of this study, the unreacted central portions of crystals are relatively small relative to the equilibrated rims, and although it does not appear that perfect equilibrium throughout the charge has been reached, the melt is believed to be in equilibrium with all the crystal phases (cf. Fujii and Scarfe, 1984; Falloon and Green, 1987). Considering the objectives of the melting experiments in this study these equilibrium conditions are acceptable.

3.4.2 Oxygen fugacity

Although the oxygen fugacity (f_{O_2}) was not controlled in the experiments, a rough calculation was attempted in one experimental run by taking advantage of the coexistence of olivine, orthopyroxene and spinel in the mantle source compositions (CPL and PLZ). As pointed out by Mattioli and Wood (1988), knowledge of activity-composition relationships and thermodynamic data for the equilibrium



[3.1]

enables calculation of fO_2 by the relation

$$\log fO_2^{T,P} = [-24222/T + 8.64 - 6\log a_{Fe_2SiO_4}(ol) + 3\log a_{Fe_2Si_2O_6}(opx) + 2\log a_{Fe_3O_4}(sp)] - [(1/2.303RT) x\Delta\bar{V} (P-1)] \quad [3.2]$$

where T is temperature in $^{\circ}K$, $\Delta\bar{V}$ is partial molar volume in $J \text{ bar}^{-1}\text{mol}^{-1}$, P is pressure in bar, R is the gas constant in $J \text{ mol}^{-1}\text{K}^{-1}$ and $a_x(y)$ is the activity of component x in phase y .

Because the partial melting experiments on lherzolitic material (CPL and PLZ) presented in this study are done at 3.0 GPa and consequently outside the spinel stability field, one experiment (run PLZ36) using the PLZ starting material was performed at 2.0 GPa and 1000 $^{\circ}C$ (in the spinel stability field) for a time of 30 hours (longest run time of this study). A temperature of 1000 $^{\circ}C$ was chosen because the activity-composition relationship for the magnetite component in spinel is based on the experimental calibration of Mattioli and Wood (1988) across the $MgAl_2O_4$ - Fe_3O_4 join done at 900 $^{\circ}$ and 1000 $^{\circ}C$. The details of the calculation can be found in Appendix A.

The calculated $\log fO_2$ for experiment PLZ36 ranges from -8.03 to -7.49, which is 1.14 to 1.68 log units over the pressure-corrected fayalite-magnetite-quartz ($\log fO_2[\text{FMQ}] = -9.17$) oxygen buffer. It is believed that this result represents a rough estimate of the fO_2 conditions in the

experimental runs performed in this study, at least for the experiments using the PLZ composition.

3.5 Phase identification and analytical techniques

Longitudinal sections of the experimental charges were mounted and polished for microprobe analysis purposes. For "sandwich" experiments using the CPL composition, the suggestion of Wallace and Green (1988), to avoid all use of water in the thin section preparation, was followed in order to prevent dissolution of possible alkali-bearing carbonate phases.

Wavelength dispersive analyses of all mineral and melt phases were done on a JEOL JXA-8600 electron microprobe equipped with TRACOR NORTHERN 5500 automation. All elements were analysed at 15 kv accelerating voltage with a 1×10^{-8} A beam current. Matrix corrections were made using the TRACOR NORTHERN "ZAF" program. The excellent backscattered electron imaging facility of the JEOL 8600 microprobe was very useful in the determination of textural relationships.

In order to assess the precision and accuracy of the electron microprobe analyses the average compositions and variations (expressed as 1 standard deviation) of repeated analyses of natural standards done during the different probe sessions are compared to the accepted compositions of these standards in Table 3.5.

-Calculation of chemical formulae

Chemical formulae of crystal phases were calculated on the basis of a fixed number of oxygens. An estimate of the ferric iron was done for spinel and garnet analyses assuming a perfect stoichiometry.

-Distinction between quench and primary phases

In the few sandwich experiments where distinction between quench and primary clinopyroxene crystals was necessary, textural and chemical criteria were used. Quench clinopyroxene grains were found to be smaller, acicular and chemically richer in TiO_2 , and Al_2O_3 with a lower $X_{\text{MgFe}_{\text{tot}}}$ value.

-Notes on melt compositions obtained

A large number of melt compositions were obtained throughout this study. A description of what they represent, and the Tables where these compositions can be found are listed in Table 3.6.

Table 3.5: Comparison of accepted analyses of natural standards with their analyses during the different probe sessions

	<u>Olivine P-140</u>			<u>Orthopyroxene R2537</u>		
	Acc.	Ave. (n=25)	1Std.	Acc.	Ave. (n=23)	1Std.
SiO ₂	40.85	40.80	0.27	52.20	52.51	0.43
TiO ₂	0.00	0.00	0.01	0.20	0.14	0.04
Al ₂ O ₃	0.13	0.00	0.01	2.00	1.77	0.10
Cr ₂ O ₃	0.00	0.00	0.01	0.00	0.02	0.03
FeO*	7.23	7.37	0.27	21.20	21.53	0.44
MnO	0.07	0.07	0.05	0.60	0.55	0.12
MgO	51.63	51.39	0.37	22.50	22.68	0.35
NiO	0.30	0.31	0.05	-----	-----	
CaO	0.00	0.00	0.01	0.75	0.71	0.25
Na ₂ O	0.00	0.00	0.01	-----	0.01	0.02
K ₂ O	0.00	0.00	0.00	-----	0.00	0.00
Total	100.21	99.94		99.45	99.92	

	<u>Wakefield diopside</u>			<u>Kaersutite</u>		
	Acc.	Ave. (n=25)	1Std.	Acc.	Ave. (n=23)	1Std.
SiO ₂	55.41	55.11	0.46	39.49	39.81	0.34
TiO ₂	-----	0.06	0.03	5.65	5.69	0.16
Al ₂ O ₃	0.00	0.07	0.04	14.09	14.52	0.24
Cr ₂ O ₃	0.00	0.01	0.02	-----	0.01	0.02
FeO*	0.00	0.05	0.04	12.01	12.19	0.28
MnO	0.00	0.03	0.04	0.12	0.10	0.04
MgO	18.62	18.54	0.23	11.25	11.41	0.15
NiO	-----	-----		-----	-----	
CaO	26.44	26.26	0.21	9.88	9.70	0.14
Na ₂ O	0.03	0.00	0.01	2.85	2.89	0.07
K ₂ O	-----	0.00	0.01	1.71	1.63	0.07
Total	100.50	100.13		97.05	97.95	

Notes: "Acc." is the accepted analysis of the standard; "Ave." is the average of the "n" analyses performed on the standard during different probe sessions; "1Std." is one "standard deviation" for these "n" analyses; ----- means not analysed.

Table 3.6: List of all melt compositions cited in this study

<u>Description</u>	<u>Tables</u>
--------------------	---------------

Melts related to PLZ

Melt compositions obtained at 1225°C and 1235°C by direct electron microprobe analyses of melt pools 4.2

Equilibrated liquid composition obtained by sandwich experiments on PLZ 4.4

SILMET: glass synthesized to a composition as close as possible to the partial melt formed from PLZ at 1225°C 4.7

Equilibrated liquid composition obtained by sandwich experiment on PLZ with corrected and calculated amount of FeO and Fe₂O₃ 6.2

Melts related to CPL

Equilibrated liquid compositions obtained in sandwich experiment using the S/DOL middle layer and CPL at 1100°C 5.4

Equilibrated liquid compositions obtained in sandwich experiment using the S/P-DOL middle layer and CPL at 1100°C 5.6

CARMET: mixture synthesized to a composition as close as possible to the partial melt formed from CPL at 1100°C 5.7

Notes: The compositions can be found in the specified Tables.

CHAPTER 4

PARTIAL MELTING OF A PHLOGOPITE LEHRZOLITE (PLZ) AT P = 3.0

GPA: EXPERIMENTAL RESULTS

4.1 General statement on phase relationships

Temperatures for the partial melting experiments on the PLZ model mantle source at 3.0 GPa ranged from 1125° to 1300°C, and the phases observed in each experimental product are summarized in Table 4.1.

Based on the appearance of interstitial glass and on a significant decrease in the abundance of phlogopite, the solidus of PLZ at 3.0 GPa is estimated at 1175°C, which is in accord with solidus temperatures determined in experiments performed on a comparable phlogopite lherzolite by Wendlandt and Egger (1980, Figure 1, p.429). However, as pointed out by Modreski and Boettcher (1972) and Wendlandt and Egger (1980), the solidus temperature in such vapor-absent experiments can be underestimated due to the presence of pore spaces in the charge. These pores are regions of reduced pressure where phlogopite may decompose to produce traces of melt below the ideal solidus temperature. Therefore, the estimated solidus temperature should probably be considered as a minimum.

Table 4.1: Results of partial melting experiments on PLZ at P=3.0GPa

Run#	T (°C)	Time (hours)	Sdw comp.	Phases observed
PLZ31	1125	28	----	ol, opx, cpx, phl, gar, (sp)
PLZ37	1150	28	----	ol, opx, cpx, phl, gar, (sp)
PLZ21	1175	20	----	ol, opx, cpx, phl, gar, (sp, liq?)
PLZ22	1200	20	----	ol, opx, cpx, phl, gar, liq, (sp)
PLZ30	1225	19	----	ol, opx, cpx, phl, gar, liq, (sp)
PLZ23	1235	20	----	ol, opx, cpx, phl, gar, liq, (sp)
PLZ32	1250	10	----	ol, opx, cpx, phl, gar, liq, (sp)
PLZ29	1275	6	----	ol, opx, cpx, phl, liq
PLZ35	1300	5	----	ol, opx, cpx, liq
<i>(sandwich experiments)</i>				
PLZ33	1225	8	SDW2	ol, opx, cpx, phl, gar, liq, (sp)
PLZ40	1225	1	SDW3	ol, opx, cpx, phl, gar, liq, (sp)

Notes: Sdw comp. is the identification of the composition used as a middle layer in sandwich experiments; phases in curved brackets are phases in trace amounts; all runs done in Ag₅₀Pd₅₀ capsules except PLZ29 and PLZ35 done in Fe-soaked Pt capsules. ol: olivine; opx: orthopyroxene; cpx: clinopyroxene; phl: phlogopite; gar: garnet; liq: liquid; sp: spinel.

Olivine, orthopyroxene, and clinopyroxene are present at all investigated temperatures. Phlogopite, whose partial breakdown defines the solidus (1175°C), disappears completely between 1275° and 1300°C, and therefore melts over a temperature interval of about 100°C. Garnet is observed up to 1250°C. Relicts of unreacted spinel are preserved in most experimental products but in trace amounts only.

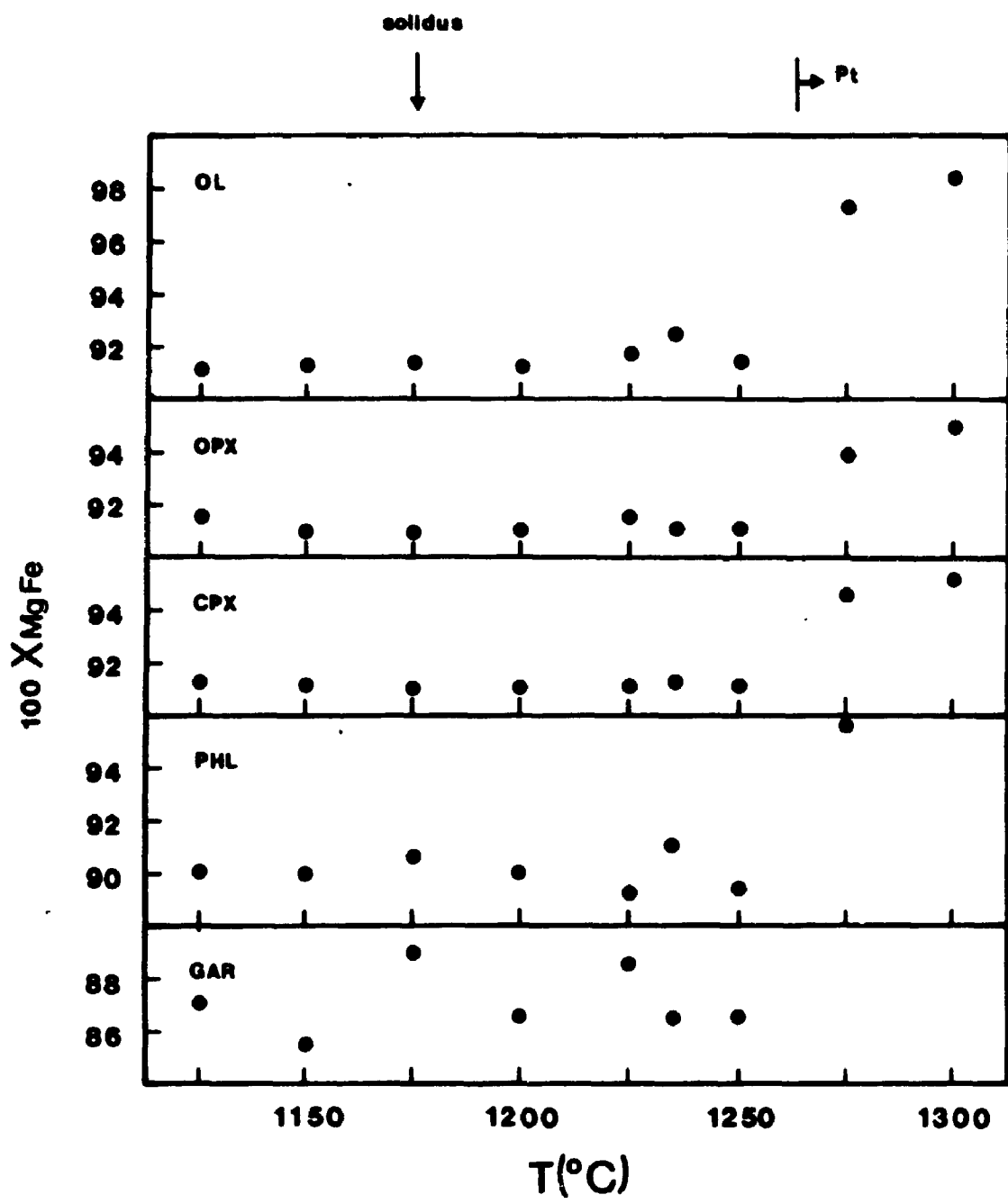
4.2 Chemical composition of minerals

The chemical composition of the mineral grains analysed in the products of the PLZ series of experiments and the calculated structural formulae are presented in Appendix B2. Generally, about four grains of each mineral present in the experimental products were analyzed and the average composition of these analyses was calculated. In the following, the content of a component in a mineral refers to this calculated average composition.

4.2.1 $X_{MgFe_{tot}}$ of silicate minerals and related comments on iron loss

The variations in $X_{MgFe_{tot}}$ for all silicate minerals in the PLZ experiments are plotted against temperature in Figure 4.1. From 1125° to 1250°C, the $X_{MgFe_{tot}}$ values are relatively constant for olivine, orthopyroxene,

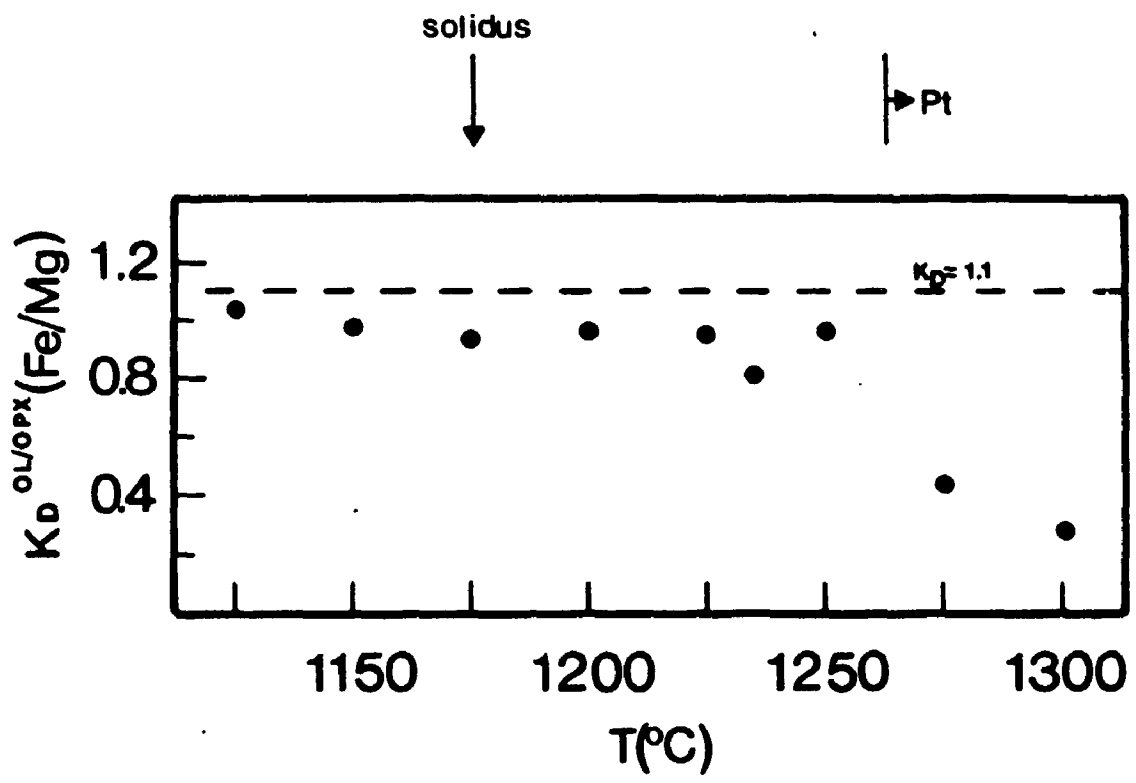
Figure 4.1 : (PLZ standard experiments) Variation of $100X_{MgFe}$ (calculated as $100 \times Mg/[Mg+Fe_{total}]$) of the silicate minerals against temperature (T). OL: olivine; OPX: orthopyroxene; CPX: clinopyroxene; PHL: phlogopite; GAR: garnet. Pt indicates the temperatures at which iron-soaked platinum capsules were used instead of $Ag_{50}Pd_{50}$ capsules.



clinopyroxene and phlogopite, with no apparent increase from subsolidus to suprasolidus conditions. This constancy in $X_{MgFe_{tot}}$ suggests that at suprasolidus conditions ($\geq 1175^{\circ}C$), and at least up to $1250^{\circ}C$, the melt fraction present is small (e.g. Green, 1976; Mengel and Green, 1989). Although garnet does not show any systematic trend with temperature, it nevertheless displays significant $X_{MgFe_{tot}}$ variation. This may suggest that the Fe/Mg equilibrium between garnet and the other silicate phases is not completely achieved.

The sharp increase in $X_{MgFe_{tot}}$ observed in the silicate minerals at $1275^{\circ}C$ coincides with the change from $Ag_{50}Pd_{50}$ to Fe-soaked Pt capsules, and is probably explained by more severe alloying of iron with platinum. The $K_p^{ol/opx}(Fe/Mg)$ (i.e. $[Fe/Mg]^{olivine} : [Fe/Mg]^{orthopyroxene}$ ratio) is usually considered to be insensitive to temperature and pressure in peridotitic systems with a value of 1.1 ± 0.1 (e.g. Mori and Green, 1978; Jaques and Green, 1979) and is therefore a good indicator of Fe/Mg equilibrium between these two silicate phases. As shown in Figure 4.2, the $K_p^{ol/opx}(Fe/Mg)$ values up to $1250^{\circ}C$ are very close to the equilibrium value suggesting small iron loss and good equilibration between olivine and orthopyroxene. On the other hand, the significantly lower $K_p^{ol/opx}(Fe/Mg)$ values of 0.43 and 0.28 at temperatures of 1275° and $1300^{\circ}C$ respectively suggest a difference in the rate of adjustment to iron loss of olivine and orthopyroxene producing a non-equilibrium assemblage (cf. Jaques and Green, 1979, p. 1318). Based on the relative changes in

Figure 4.2 : (PLZ standard experiments) Variation of the $K_D^{ol/opx}(Fe/Mg)$ (i.e. $[Fe/Mg]^{olivine}/[Fe/Mg]^{orthopyroxene}$) against temperature (T). The dashed line represents a constant K_D value of 1.1 considered to be representative of peridotitic systems (Mori and Green, 1978; Jaques and Green, 1979). Pt indicates the temperatures at which iron-soaked platinum capsules were used instead of $Ag_{50}Pd_{50}$ capsules.



$X_{MgFe_{tot}}$ for the different silicate minerals (Figure 4.1), the iron appears to be lost preferentially in the order olivine > phlogopite > pyroxenes. These observations indicate that more confidence should be given to the results of the experiments using Ag₅₀Pd₅₀ capsules and care should be taken in the interpretation of the compositional characteristics of minerals at 1275° and 1300°C.

4.2.2 Olivine

From 1125° up to 1250°C, the NiO (0.20 to 0.31 wt%) and CaO (0.13 to 0.25 wt%) contents (Appendix B2), and the $X_{MgFe_{tot}}$ (0.91 to 0.93, Figure 4.1) of olivine remain relatively constant. This compositional constancy is probably related to the weak participation of this mineral (at least relative to its abundance) in the melting reactions occurring from the solidus temperature to 1250°C.

The chemical characteristics of olivine at higher temperatures (1275° and 1300°C) are more difficult to interpret because, as noted above, the extremely high $X_{MgFe_{tot}}$ and also the low NiO content (0.10 wt% at 1300°C) are mainly due to the loss of Fe and Ni to the Pt capsules.

4.2.3 Orthopyroxene

Orthopyroxene in the PLZ series of experiments is an aluminian enstatite (Morimoto, 1988) of relatively constant

81

composition suggesting that, as for olivine, its participation in the reactions producing the small melt fraction occurring between 1175° and 1250°C is not important. Nevertheless, the Wo proportion (wollastonite proportion calculated as $100 \times \text{Ca}/[\text{Ca}+\text{Mg}+\text{Fe}+\text{Mn}]$) and the $(\text{Al}_2\text{O}_3 + \text{Cr}_2\text{O}_3)$ content appear to be correlated with temperature (Figure 4.3). Such increases in the solubilities of the Wo component and of $(\text{Al}_2\text{O}_3 + \text{Cr}_2\text{O}_3)$ with temperature are consistent with previous experimental studies of phase equilibria in simple pyroxene systems (e.g. Lindsley, 1982; Gasparik and Lindsley, 1982) and in garnet lherzolites (e.g. Mori and Green, 1978). However, the drastic increase in $X_{\text{MgFe}_{\text{tot}}}$ at 1275° and 1300°C due to the iron loss to the Pt capsules could also have a significant effect on these variations in the Wo proportion and the $(\text{Al}_2\text{O}_3 + \text{Cr}_2\text{O}_3)$ content.

4.2.4 Clinopyroxene

All clinopyroxene grains analyzed in the partial melting experiments of PLZ are Ca-Mg-Fe pyroxenes. According to the classification of Morimoto (1988), they range from aluminian-chromian diopside at lower temperatures (1125°-1200°C) to aluminian-chromian augite at higher temperatures (1225°-1300°C) (Figure 4.4). This systematic decrease in the Wo component is consistent with the narrowing of the miscibility gap between Ca-rich and Ca-poor pyroxenes with

Figure 4.3 : (PLZ standard experiments) Variations of the wollastonite proportion ($Wo = Ca/[Ca+Mg+Fe+Mn]$) and of the ($Al_2O_3 + Cr_2O_3$) content (in wt%) of orthopyroxene against temperature (T). Pt indicates the temperatures at which iron-soaked platinum capsules were used instead of $Ag_{50}Pd_{50}$ capsules.

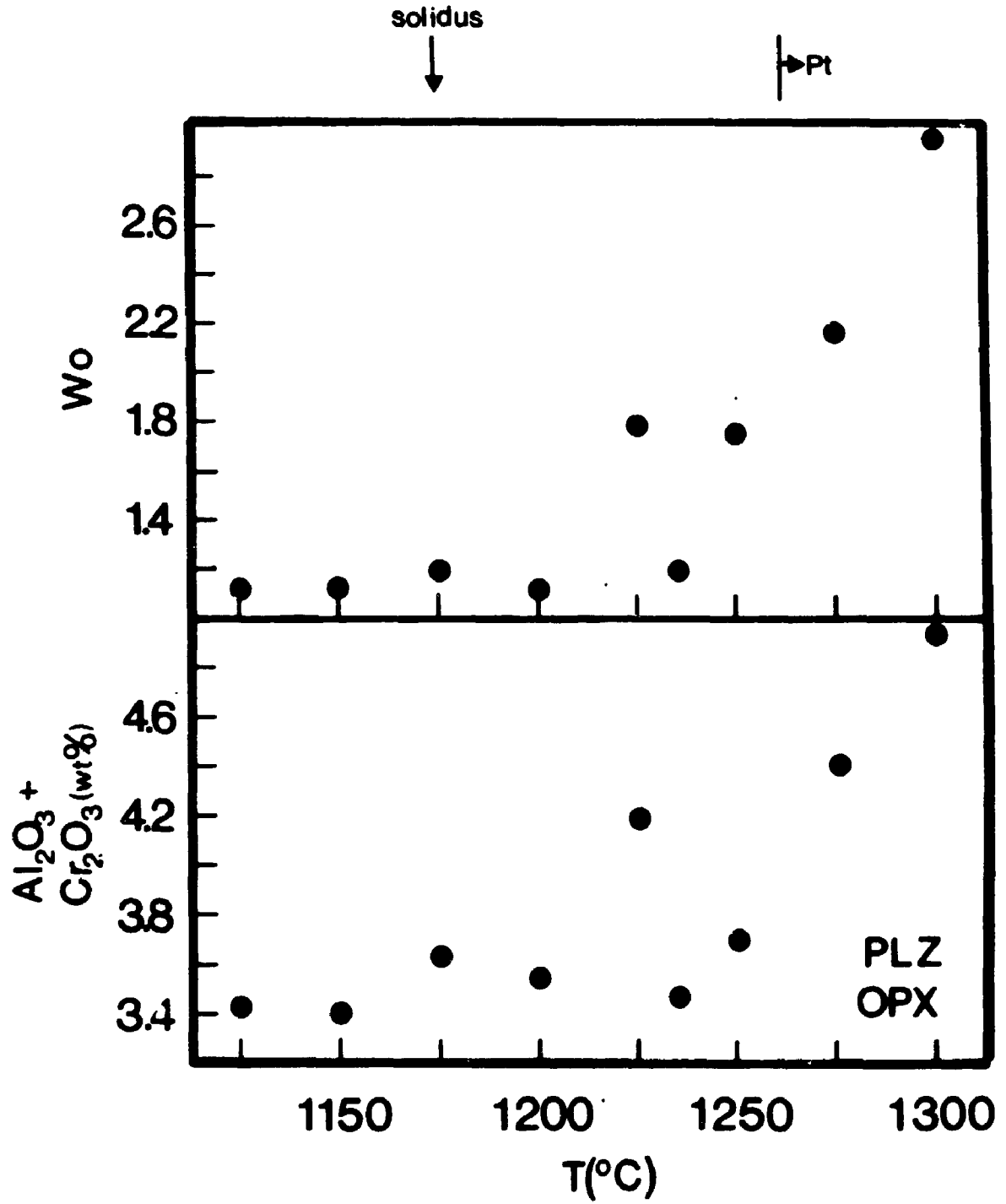
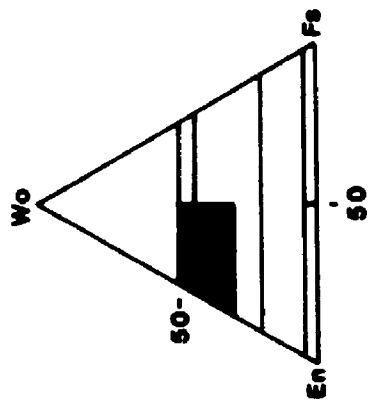
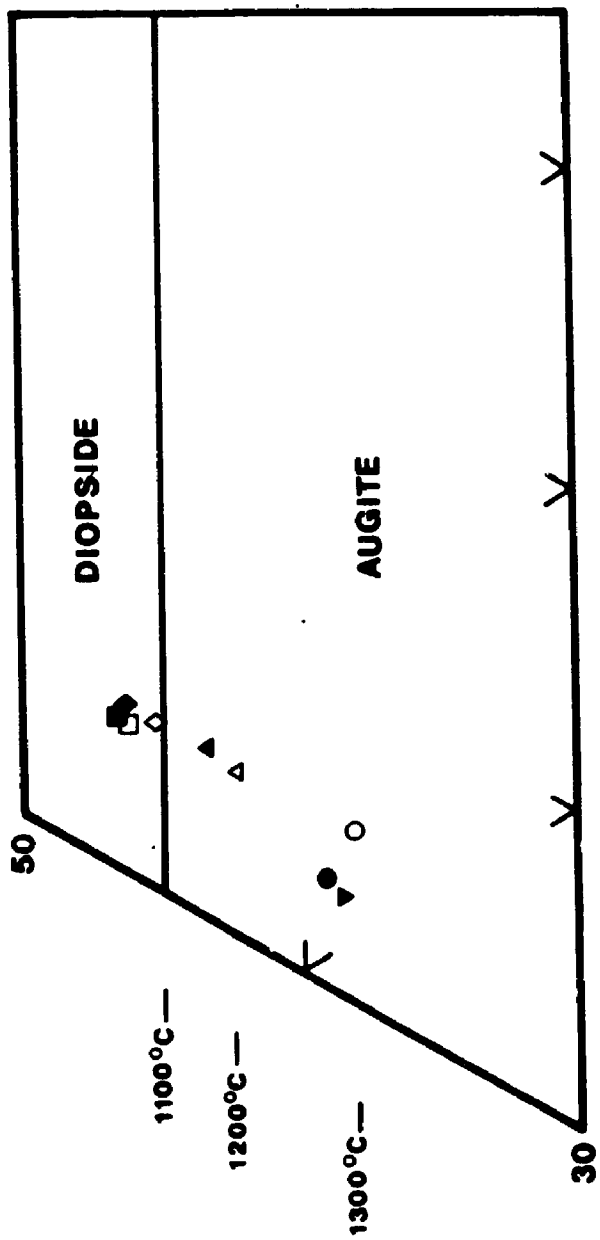


Figure 4.4 : (PLZ standard experiments) Compositions of clinopyroxene plotted in the Wollastonite-Enstatite-Ferrosilite (Wo-En-Fs) ternary diagram. The composition fields are those of Morimoto (1988). The temperatures indicated on the Wo-En join are for the simple system CaO-MgO-SiO₂ with excess Mg₂SiO₄ at 2.0 GPa and are taken from Lindsley and Dixon (1976, Figure 1). ■: 1125°C; □: 1150°C; ◆: 1175°C; ◇: 1200°C; ▲: 1225°C; △: 1235°C; ○: 1250°C; ●: 1275°C; ▼: 1300°C.



increasing temperature (e.g. Lindsley and Dixon, 1976; Mori and Green, 1978; Lindsley, 1982).

In addition to the main "Quad" cations (Ca+Mg+Fe+Mn; Papike et al., 1974), the clinopyroxenes contain a significant proportion of Na, Al, Cr, Ti, and, although not analyzed directly, possibly Fe³⁺. Of these minor cations, Ti is the least abundant with contents of 0.0027 to 0.0083 atoms per formula unit calculated on a basis of 6 oxygens (pfu/6), whereas Na abundance varies from 0.0263 to 0.0644 pfu/6. Cr and Al_{tot} (total Al) contents range from 0.0148 to 0.0407 pfu/6 and from 0.1670 to 0.2114 pfu/6 respectively.

In order to evaluate the effects of PLZ partial melting on these minor cations in clinopyroxene, the variations in Ti/Quad, Na/Quad and [Al_{tot} + Cr]/Quad (atomic ratios) are plotted against temperature in Figure 4.5. From the estimated solidus to higher temperatures, there is a clear decrease in Na, and an increase in Ti and (Al_{tot} + Cr) relative to the "Quad" cations. These chemical characteristics of the clinopyroxene complex solid solution suggest a significant contribution of this mineral in the melting reactions occurring in PLZ between 1175° and 1300°C.

The different valencies of the minor cations (Na, Al, Cr and Ti) relative to Ca, Mg, Fe, and Mn (divalent) require special coupled cation substitutions in order to preserve charge balance (Papike et al., 1974; Papike, 1982). To characterize the specific substitutions responsible for the observed variation in Ti, Na and (Al_{tot} + Cr) with

Figure 4.5 : (PLZ standard experiments) Variations of 100 Ti/Q (refers to 100 x Ti/[Quadrilateral components] with quadrilateral components = Ca+Mg+Fe+Mn), Na/Q, and (Al_{tot}+Cr)/Q in clinopyroxene against temperature (T). Pt indicates the temperatures at which iron-soaked platinum capsules were used instead of Ag₅₀Pd₅₀ capsules.

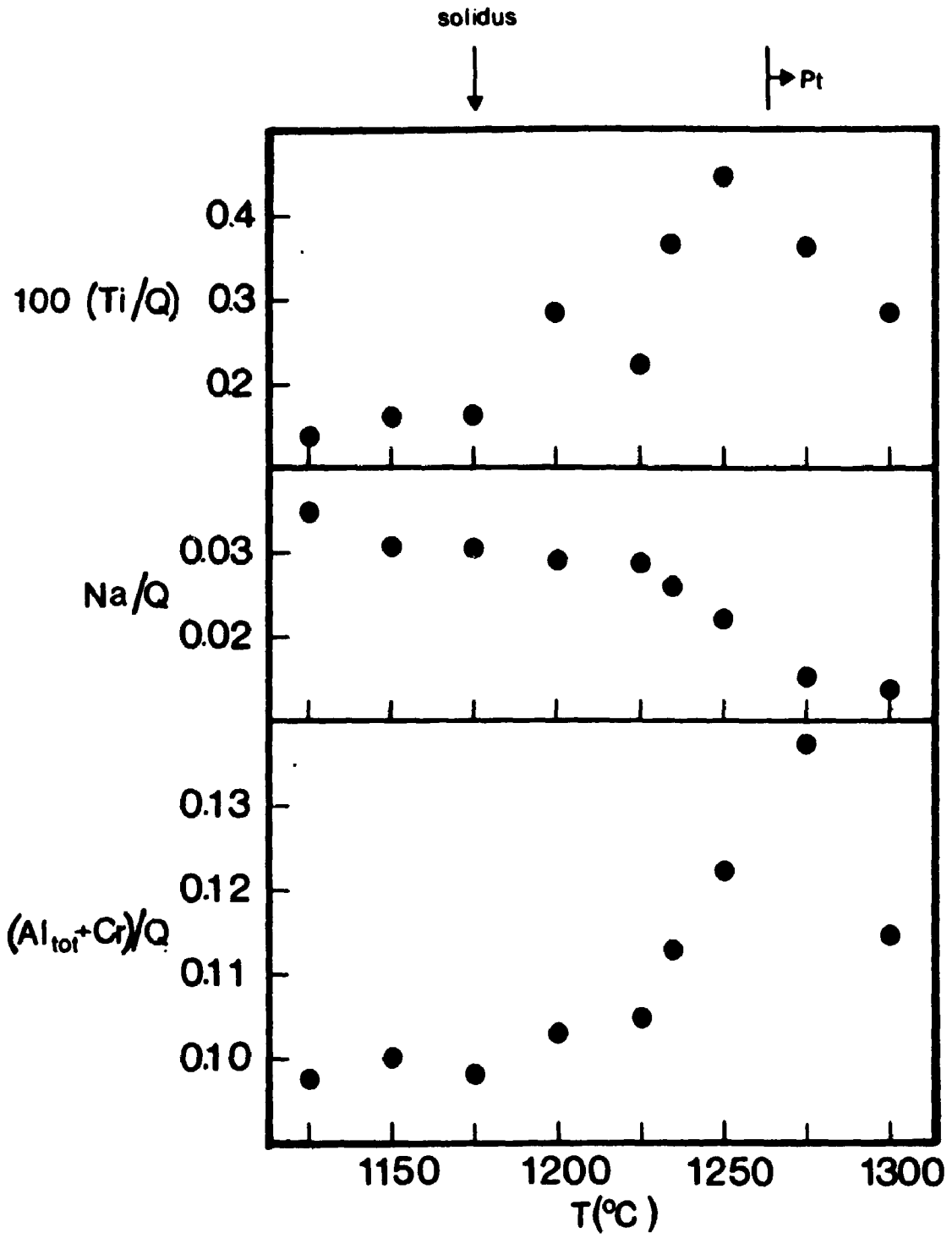


Figure 4.6 : (PLZ standard experiments) Variation between Al^{IV} and Ti in clinopyroxene. Al^{IV} and Ti are expressed in cations per formula unit calculated on a basis of 6 oxygens. The drawn line represents a $Al^{IV}:Ti$ ratio of 2:1.

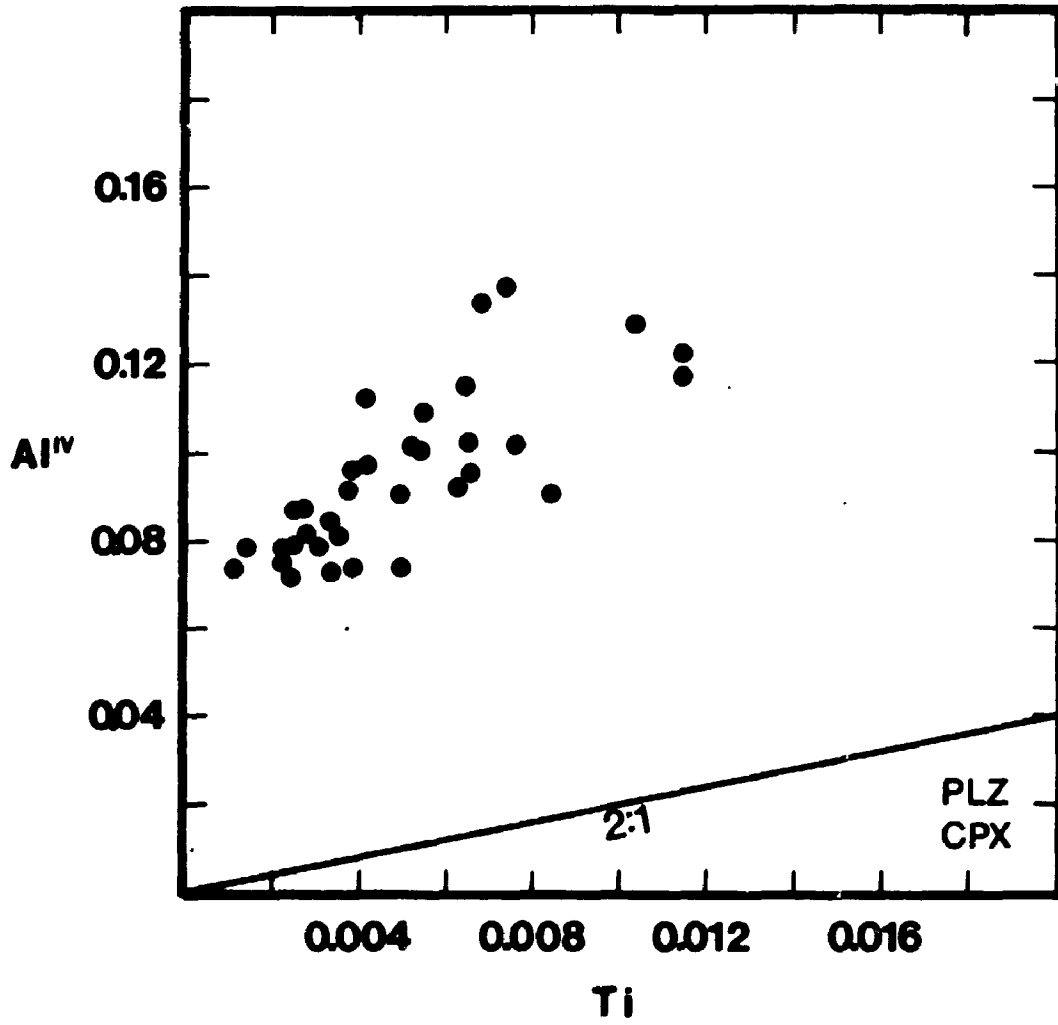
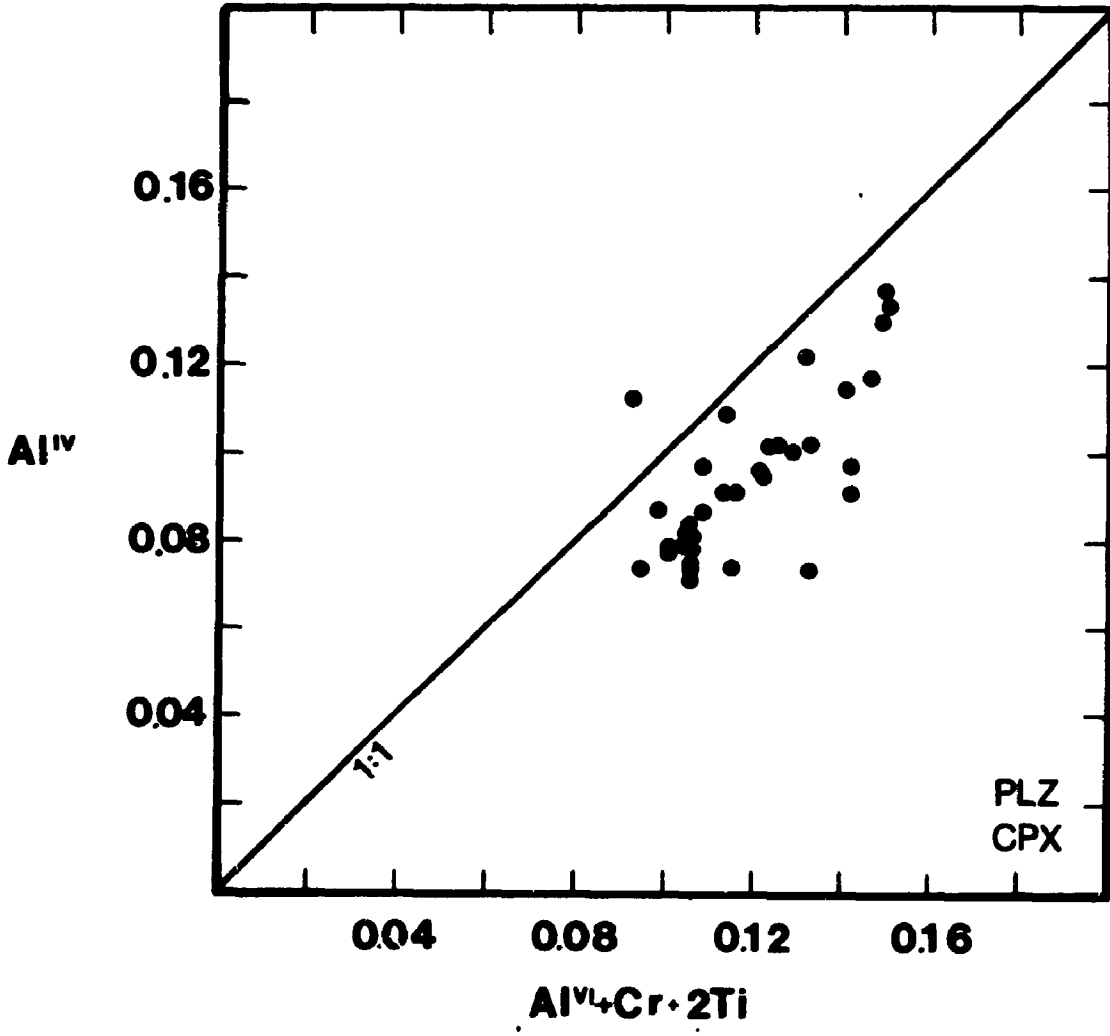


Figure 4.7 : (PLZ standard experiments) Variation between Al^{IV} and $(Al^{VI}+Cr+2Ti)$ in clinopyroxene. Al^{IV} and $(Al^{VI}+Cr+2Ti)$ are expressed in cations per formula unit calculated on a basis of 6 oxygens. The drawn line represents a $Al^{IV}:(Al^{VI}+Cr+2Ti)$ ratio of 1:1.



temperature (and degree of melting), different plots correlating Na and Al^{IV} (creating charge deficiency) to some of the different cations causing an excess of charge are shown in Figures 4.6, 4.7 and 4.8.

Figure 4.6 illustrates the relation of Al^{IV} with Ti and is therefore a measure of the importance of the substitutional couple 2Al^{IV}-Ti^{VI} (Papike, 1982; meaning that the excess of charge created by one Ti cation replacing one of the divalent cations in the octahedral site is counterbalanced by two Al cations substituting for two Si cations in the tetrahedral site). The positive correlation of Al^{IV} with Ti suggests that Ti is coupled with Al^{IV}. However, because the data plot far from the "Al^{IV}:Ti = 1:2" line (Figure 4.6), this substitutional couple can account only for a small amount of the variation in Al^{IV}.

In Figure 4.7, Al^{IV} is plotted against (Al + Cr + 2Ti)^{VI} expressing the combination of the 2Al^{IV}-Ti^{VI} and the Al^{IV}-(Al + Cr)^{VI} substitutional couples. The fact that the data fall near the 1:1 line in Figure 4.7 suggests that the variation in Al, Cr, and Ti are all coupled, with Al^{IV}-(Al + Cr)^{VI} being clearly dominant.

Because Na decreases when Al, Cr and Ti increase (Figure 4.5), the variation in Na cannot be coupled with any of these three cations. The remaining cation that can plausibly be coupled with Na is Fe³⁺. Although no direct measurement or calculation of the oxidation state of iron was done, an approximation of the importance of Fe³⁺ in the pyroxene

66

formula is the discrepancy between the total number of cations in the pyroxene structural formula calculated on the basis of 6 oxygens and the ideal total of 4. If the electron microprobe analyses are of good quality and the possible vacancies or excesses in the different sites are ignored, an increase in Fe^{3+} should be proportional to the "Cation Excess" (Cation excess = total of cations - 4). Accordingly, in order to reveal the possible presence of the substitutional couple Na- Fe^{3+} , a plot of Na in function of "cation excess" is presented in Figure 4.8. Except for a few individual analyses, Na correlates relatively well with the excess of cations and the data plot very near the Na:Cation Excess = 3:1 line defining the substitutional couple Na- Fe^{3+} . It is therefore concluded that almost all the variation in Na is coupled with ferric iron (Na- Fe^{3+}) as the acmite component.

In summary, throughout the melting interval of PLZ investigated in this study, the compositional characteristics of the clinopyroxene solid solution change significantly. With increasing temperature and degree of melting, the Wo component decreases and the abundance of the minor cations relative to the major "Quad" divalent cations changes through the following major coupled substitutions:

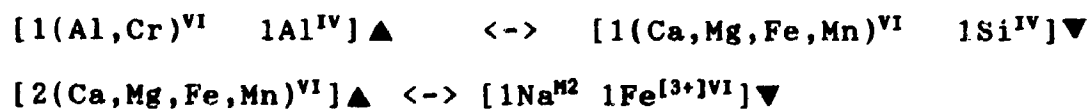
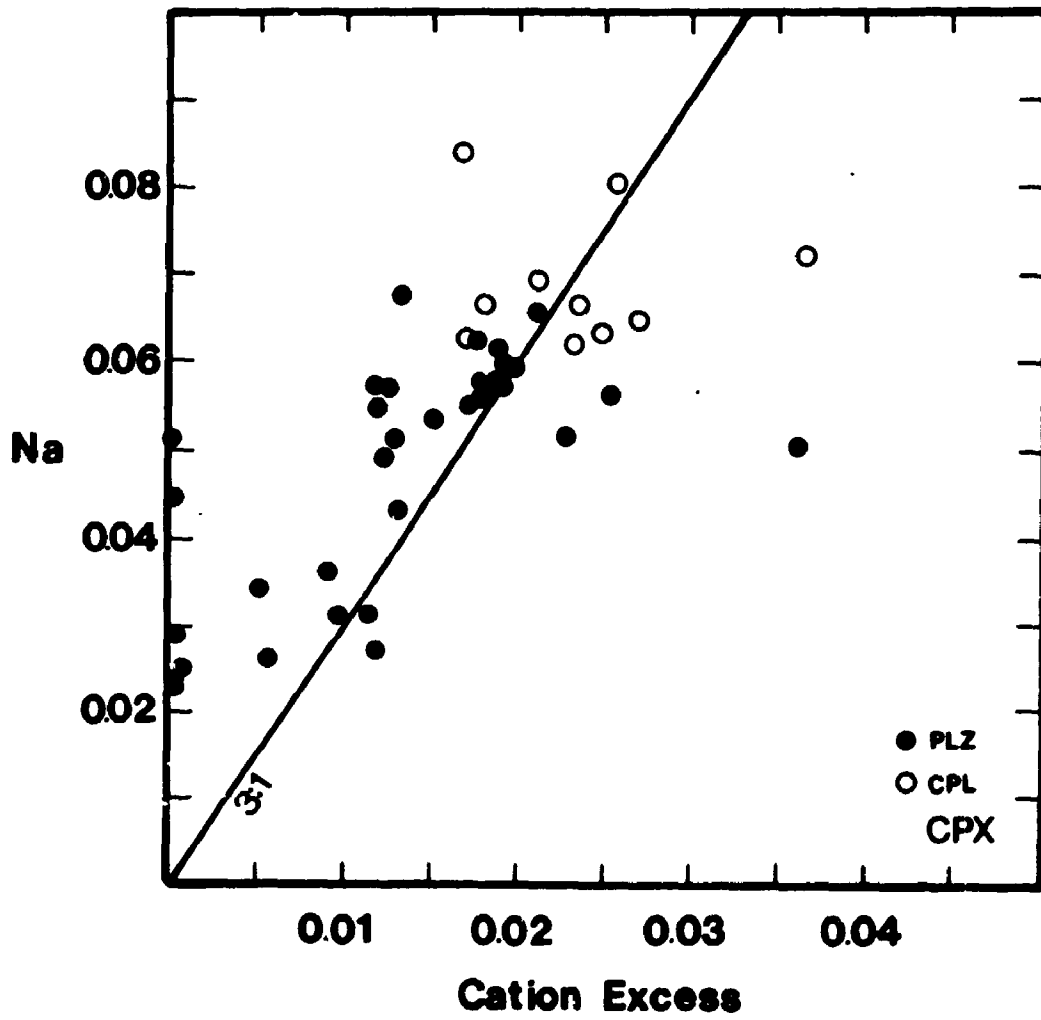


Figure 4.8 : (PLZ and CPL standard experiments) Variation between Na and Cation Excess in clinopyroxene. Na is expressed in cation per formula unit on a basis of 4 oxygens. Cation Excess represents the total of all the analyzed cations in the clinopyroxene minus the ideal total of 4. The drawn line represents a Na:Cation Excess ratio of 3:1 which defines the substitutional couple Na-Fe³⁺. For PLZ (●), individual analyses are plotted. For CPL (○) only average for each experimental product are plotted.



where \blacktriangle and \blacktriangledown means increasing and decreasing respectively. These substitutions can probably be seen as simplified melting reactions where Na, Fe^{3+} , Ca and Si are preferentially incorporated in the melt. This results in a decrease in the total proportion of clinopyroxene which becomes enriched especially in the Tschermak's ($[\text{Ca}, \text{Mg}, \text{Fe}] \text{Al}_2 \text{SiO}_6$) and in the Enstatite-Ferrosilite ($[\text{Mg}, \text{Fe}] \text{Si}_2 \text{O}_6$) components.

4.2.5 Phlogopite

Because the abundance of phlogopite decreases significantly from the solidus temperature to final disappearance at a temperature between 1275° and 1300°C, its compositional evolution should have an important effect on the nature of the silicate liquid present in the investigated melting interval of PLZ.

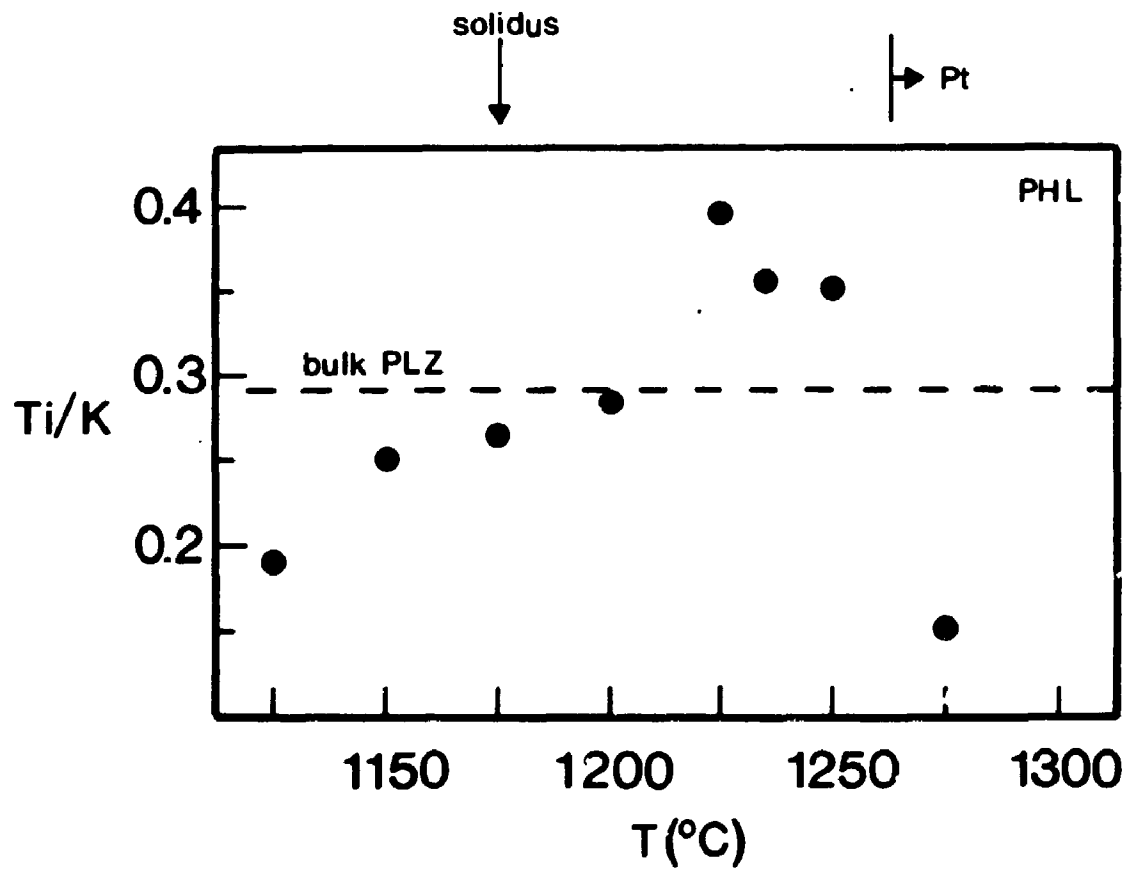
SiO_2 (37.78 to 40.75 wt%) and Al_2O_3 (15.75 to 17.53 wt%) contents in phlogopite are such that, in the structural formula, Si is always smaller than 6 pfu/22 (atoms per formula unit calculated on a basis of 22 oxygens) and the tetrahedral site can be filled completely by Si and Al ($\text{Si} + \text{Al}_{\text{tot}} > 8$ pfu/22). From 1125° to 1250°C, Cr_2O_3 contents range between 1.17 to 2.49 wt% with no systematic variation with temperature. At 1275°C, however, the Cr_2O_3 content is very low (0.13 wt%). In the interlayer site, the K is quite constant ($\text{K}_2\text{O} = 9.18\text{-}10.58$ wt%) and the amount of Na is

extremely low ($\text{Na}_2\text{O} = 0.00\text{-}0.11$ wt%). The phlogopites are all rich in TiO_2 with contents ranging from 2.34 to 7.04 wt%.

The variation in Ti/K (atomic ratio) is plotted against temperature in Figure 4.9. Except for its anomalously low value at 1275°C, Ti/K increases steadily with temperature. Because the amount of K is relatively constant, this increase in Ti/K reflects essentially a variation in the abundance of Ti. This systematic enrichment in TiO_2 is in accordance with previous experimental studies that have demonstrated a significant increase in the solubility of Ti in phlogopite with increasing temperature (e.g. Forbes and Flower, 1974; Robert, 1976; Trønnnes, 1985; Trønnnes et al., 1985). As long as phlogopite represents the only K-bearing phase, however, the Ti/K value of 0.29, calculated for the PLZ phlogopite lherzolite bulk composition (Table 3.2), should define the maximum TiO_2 content that phlogopite can contain. Therefore, the Ti/K values higher than 0.29 observed in phlogopite from 1200° to 1250°C (Figure 4.9) implies that an additional K-bearing phase with a Ti/K lower than 0.29 should exist in the experimental product at these temperatures. Because no other K-bearing mineral is observed, this additional phase, at these suprasolidus conditions, is likely the silicate liquid.

Previous studies have shown that the main mechanisms responsible for the variation in TiO_2 in biotite and phlogopite are the Ti-Tschermak's ($\text{Ti-Tsch: Ti}^{\text{VI}}2\text{Al}^{\text{IV}} \rightleftharpoons$

Figure 4.9 : (PLZ standard experiments) Variation of the Ti:K atomic ratio (Ti/K) of phlogopite against temperature (T). The dashed line represents the Ti/K value calculated for the PLZ phlogopite lherzolite bulk composition. Pt indicates the temperatures at which iron-soaked platinum capsules were used instead of Ag₅₀Pd₅₀ capsules.

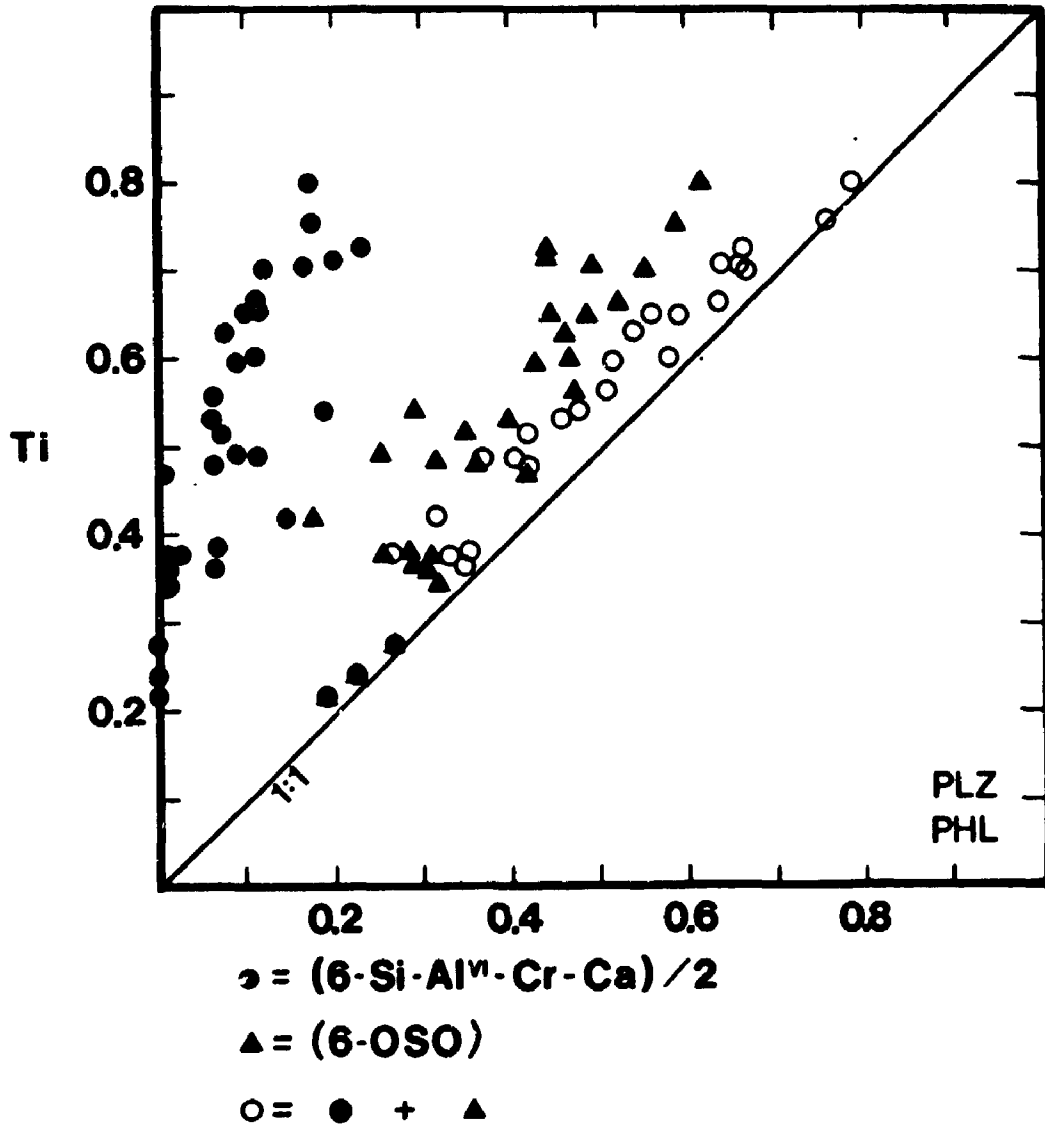


[Mg,Fe,Mn]^{VI}2Si^{IV}) and the Ti-Vacancy (Ti-Vac: Ti^{VI} □^{VI} ⇌ 2[Mg,Fe,Mn]^{VI} where □^{VI} refers to vacant octahedral site) substitutions (e.g. Forbes and Flower, 1974; Robert, 1976; Arima and Edgar, 1981; Trønnnes et al., 1985; Abrecht and Hewitt, 1988; Foley, 1989). In order to evaluate the importance of these substitutions, the Ti content of phlogopite in the PLZ series of experiments is plotted against the following parameters in Figure 4.10 : [(6-Si^{IV}-Al^{VI}-Cr-Ca)/2] and [6-OSO] (where OSO refers to the octahedral site occupancy). The [6-OSO] parameter evaluates the deficiency in the octahedral site resulting from the Ti-Vac substitution, whereas the [(6-Si^{IV}-Al^{VI}-Cr-Ca)/2] parameter is a measure of the decrease in Si^{IV} caused by the Ti-Tsch substitution corrected for the additional effects of the substitutional couples [Al^{VI}-Al^{IV}], [Cr^{VI}-Al^{IV}] and [Ca^{interlayer}-Al^{IV}] (Trønnnes, 1985).

In Figure 4.10, Ti is correlated to [6-OSO], [(6-Si-Al^{VI}-Cr-Ca)/2] and to the combination of these two parameters. The fact that all the data plot almost on the Ti: ([6-OSO] + [(6-Si-Al^{VI}-Cr-Ca)/2]) = 1:1 line suggests that the Ti-Tsch and Ti-Vac substitutions can account for almost all the titanium variation in the PLZ phlogopites. However, as shown by the relation of Ti relative to the [6-OSO] and [(6-Si-Al^{VI}-Cr-Ca)/2] parameters taken individually (Figure 4.10), although both substitutions are operative, the Ti-Vac is clearly dominant.

In conclusion, through the investigated temperature

Figure 4.10 : (PLZ standard experiments) Variation of Ti against $[(6\text{-Si-Al}^{\text{VI}}\text{-Cr-Ca)}/2]$ (\bullet), $[6\text{-OSO}]$ (\blacktriangle), and $[(6\text{-OSO}) + ((6\text{-Si-Al}^{\text{VI}}\text{-Cr-Ca)}/2)]$ (\circ) in phlogopite. OSO refers to the cations in the octahedral site ($\text{Al}^{\text{VI}} + \text{Cr} + \text{Ti} + \text{Mg} + \text{Fe} + \text{Mn}$). All cations are expressed in cations per formula unit calculated on a basis of 22 oxygens.



interval, the largest compositional variation observed in phlogopite is in its Ti content. At subsolidus conditions, the proportion of phlogopite is fixed by the total amount of K in PLZ, and the small increase in Ti is probably caused by exchange with the other existing solid phases (garnet and pyroxenes). However, the abundance of Ti in the mica between 1200° and 1250°C implies that phlogopite has partially melted with the formation of a silicate liquid which incorporates K preferentially relative to Ti. The Ti/K in the melt should therefore be less than in the coexisting phlogopite. An increase in the Ti/K value of the residual mica with progressive melting is consistent with the fact that titanium-rich phlogopite is stable at higher temperatures than titanium-absent phlogopite (Forbes and Flower, 1974).

Finally, the sharp decrease in the titanium content of phlogopite at 1275°C (Figure 4.9), just before its disappearance, suggests an important change in the distribution coefficient of Ti between the mica and the silicate liquid. Although $K_D^{phl/liquid}TiO_2$ has been shown to decrease as a function of temperature in experiments on some potassic magmas (Esperança and Holloway, 1986, 1987), the main factor influencing the low amount of titanium at 1275°C could well be the drastic change in the $X_{MgFe_{tot}}$ of phlogopite (from 0.90 to 0.96, Figure 4.1) caused by the change from a Ag₅₀Pd₅₀ to a Pt capsule. Indeed, a good negative correlation between Ti and $X_{MgFe_{tot}}$ is often observed in

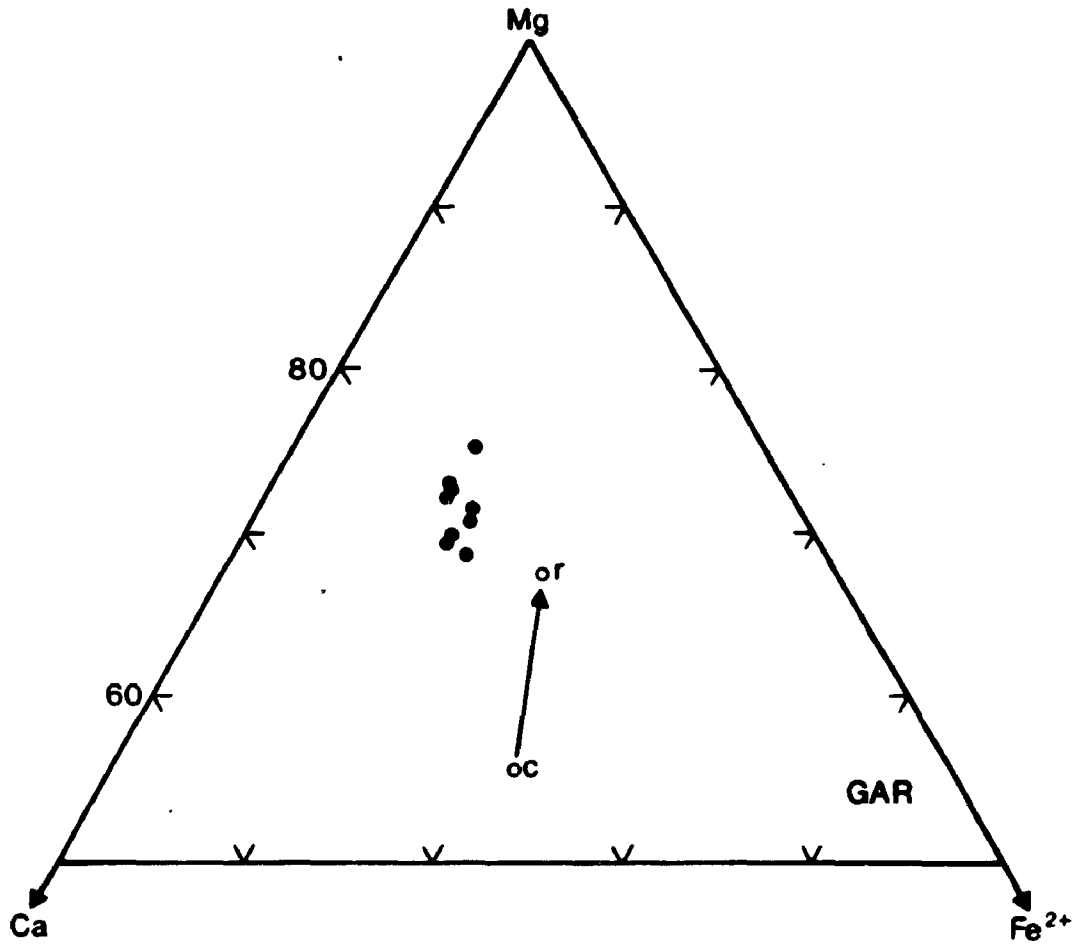
biotite and phlogopite found in nature (e.g. Delaney et al., 1980; Abrecht and Hewitt, 1988; Arai and Takahashi, 1989) as well as in experimental studies (Esperança and Holloway, 1986, 1987; Abrecht and Hewitt, 1988).

4.2.6 Garnet

Garnets in the PLZ experiments show proportions of the pyrope component between 68.9 and 72.5 mol% (Figure 4.11). These values are comparable with pyrope proportions in garnets observed in different peridotite xenoliths (e.g. Cox et al. 1987; Ehrenberg, 1982). CaO contents are relatively constant, varying between 6.67 and 7.71 wt%. Cr₂O₃ and TiO₂ contents range from 1.24 to 3.11 wt% and 0.49 to 1.10 wt% respectively with no systematic variation with temperature.

Garnet is not observed in the experiments at 1275° and 1300°C. The breakdown of garnet at those higher temperatures is probably due to the significant increase in the solubility of aluminum (and chromium) observed in the pyroxenes (sections 4.2.3, 4.2.4).

Figure 4.11 : (PLZ experiments) Garnet compositions plotted on a Mg-Fe²⁺-Ca ternary diagram (cationic proportions). Filled circles refer to the garnets in the products of the standard experiments. Empty circles refers to the core (c) and rim (r) of zoned garnet in sandwich experiment PLZ33 (see details in section 4.3.2).



4.3 Determination of melt composition in equilibrium with PLZ at 1225°C: sandwich experiments

4.3.1 Details of the experimental approach

In order to define the compositional nature of the silicate liquid in the melting interval where phlogopite is stable (1175° to 1275°C), experiments using a sandwich technique (see section 3.3.2) were performed at 1225°C. The success of such an approach depends significantly on the nature of the added glass layer which evidently changes the bulk composition of the system (e.g Falloon and Green, 1987). Therefore the following iterative method was adopted: the composition of the equilibrated melt layer, determined after a first sandwich experiment, is then used as a guide for the synthesis of the glass layer in the subsequent sandwich experiment (cf. Wallace and Green, 1988). Because the proportion of the peridotitic material (PLZ) is high relative to the glass layer (PLZ:Glass \approx 82:18), the equilibrated melt after each iterative step is believed to converge compositionally towards the ideal liquid in equilibrium with PLZ at 1225°C.

Two different synthesized glass compositions were needed (SDW2 and SDW3; Table 3.1). The sandwich experiments were performed at 1225°C and a summary of the experimental conditions and results is presented in Table 4.1. Chemical compositions of the analyzed minerals and melts are

presented in Appendix B2.

4.3.2 Sandwich experiment on PLZ using SDW2 as a middle layer

The choice of a composition for the synthesized glass used in the first sandwich experiment was based partially on the only three direct microprobe analyses of small melt "pools" that could be done in the standard experiments on PLZ performed at 1225° and 1235°C (Table 4.2). The composition of such interstitial melt is, however, probably modified significantly by quench overgrowth on surrounding primary crystals and by partial iron loss (Green, 1976). Moreover, significant volatilization (especially of Na and K) can occur during the microprobe analyses of the melt "pools" due to the necessary use of a focused electron beam. Therefore, some subjective corrections were done in order to arrive at a composition for the synthesized glass that was used in the first sandwich experiments. The main ones are summarized in the following paragraph.

In order to estimate the amount of water in the melt, the H_2O/K_2O value of the phlogopite was considered to be constant through the investigated melting interval of PLZ. This assumption is believed to be valid because the mica used in the starting material has a low F content (0.19 wt%; Table 3.4) suggesting that the "OH anionic site" is filled almost completely by water, and K is the only major cation

Table 4.2: Microprobe analyses of melt pools observed in the products of the partial melting experiments on PLZ

	<u>PLZ30 (1225°C)</u>		<u>PLZ23 (1235°C)</u>	
SiO ₂	37.62	39.40	35.35	
TiO ₂	3.02	2.33	1.73	
Al ₂ O ₃	15.57	14.23	13.22	
Cr ₂ O ₃	0.00	0.00	0.11	
FeO*	5.01	4.95	4.51	
MnO	0.06	0.10	0.09	
MgO	8.73	14.05	10.82	
CaO	6.86	6.94	6.61	
Na ₂ O	0.80	0.62	0.80	
K ₂ O	7.41	5.68	5.81	
Total	85.08	88.30	79.05	
X_{MgFe_{tot}}	0.76	0.83	0.81	

Notes : FeO* refers to the total Fe expressed as FeO. X_{MgFe_{tot}} is [Mg/(Mg+Fe_{tot})]

occupying the interlayer site (see section 4.2.5). Consequently, because phlogopite is the only phase that supplies potassium and water to the melt, the value of H_2O/K_2O should be almost identical (and constant) in the silicate liquid and in the coexisting phlogopite during progressive melting. A H_2O/K_2O (weight ratio) of 0.38, typical of ideal stoichiometry in mica, is believed to be a good approximation. Secondly, to compensate for iron loss, the FeO content was corrected assuming a $K_D^{olivine/liquid}(Fe/Mg)$ of 0.3 (Roeder and Emslie, 1970; Jaques and Green, 1979). Finally the composition was recalculated to 100 wt%. The glass was then synthesized using the method described in section 3.1.2. The composition of this synthesized glass (SDW2, Table 3.1), used as a middle layer in the first sandwich experiment, is presented in Table 4.3.

Backscattered electron images of the product of the sandwich experiment using PLZ and SDW2 in the proportion 82:18 (Table 4.1; Experiment PLZ33) show that large grains ($> 50 \mu m$) of zoned garnets are distributed homogeneously throughout the SDW2 middle layer (Figure 4.12a). Besides garnet, the SDW2 layer also contains primary phlogopite, quench clinopyroxene and glass. This particular assemblage is interpreted to be the product of reequilibration between PLZ and SDW2 during the experiment. The SDW2 glass was probably too rich in Al_2O_3 and K_2O to be in equilibrium with PLZ. Consequently, it reacted with the minerals of PLZ causing crystallization of garnet and phlogopite. The

Table 4.3: Synthesized melt compositions used in sandwich experiments with the PLZ model mantle source (based on microprobe analyses of the glasses using a defocused beam of 10 to 30 μm).

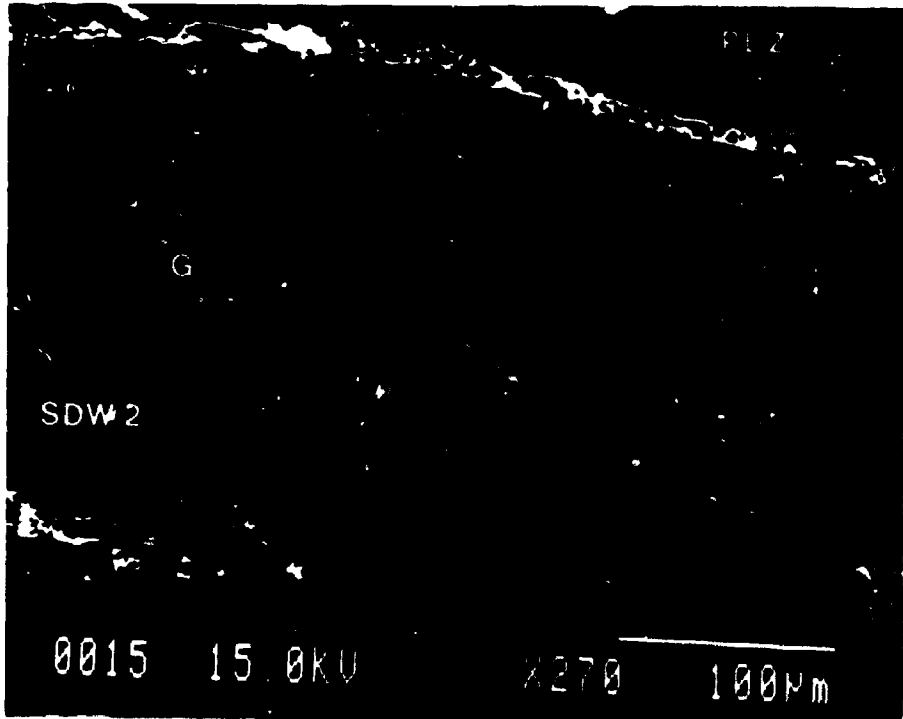
	<u>SDW2 (3wt% H₂O)</u> (n=5)			<u>SDW3 (2.5wt% H₂O)</u> (n=5)		
	Anal. (wt%)	1Std.	Rec. (wt%)	Anal. (wt%)	1Std.	Rec. (wt%)
SiO ₂	44.14	0.55	44.83	46.64	0.26	47.16
TiO ₂	2.08	0.06	2.12	2.59	0.06	2.62
Al ₂ O ₃	15.23	0.77	15.48	11.55	0.42	11.68
FeO*	7.24	0.30	7.36	6.45	0.60	6.52
MnO	0.10	0.03	0.10	0.18	0.04	0.19
MgO	11.28	0.18	11.46	10.84	1.09	10.95
CaO	5.97	0.05	6.06	9.77	0.39	9.87
Na ₂ O	1.11	0.06	1.13	1.74	0.16	1.76
K ₂ O	8.17	0.23	8.30	6.63	0.34	6.70
H ₂ O#			3.16			2.55
Total	95.32		100.00	96.39		100.00
X_{MgFe_{tot}}	0.74		0.74	0.75		0.75

Notes : "Anal." is the average of the "n" analyses performed on the glass. "1Std." is the standard deviation for the "n" analyses. "Rec." is "Anal." recalculated to 100wt% so that the H₂O:K₂O weight ratio is equal to 0.38. H₂O# is the calculated water content found by the ratio. This calculated water content can be compared with the water content that was intended in the preparation (see in curved brackets besides the glass identification). FeO* refers to the total Fe expressed as FeO. X_{MgFe_{tot}} is Mg/(Mg+Fe_{total}).

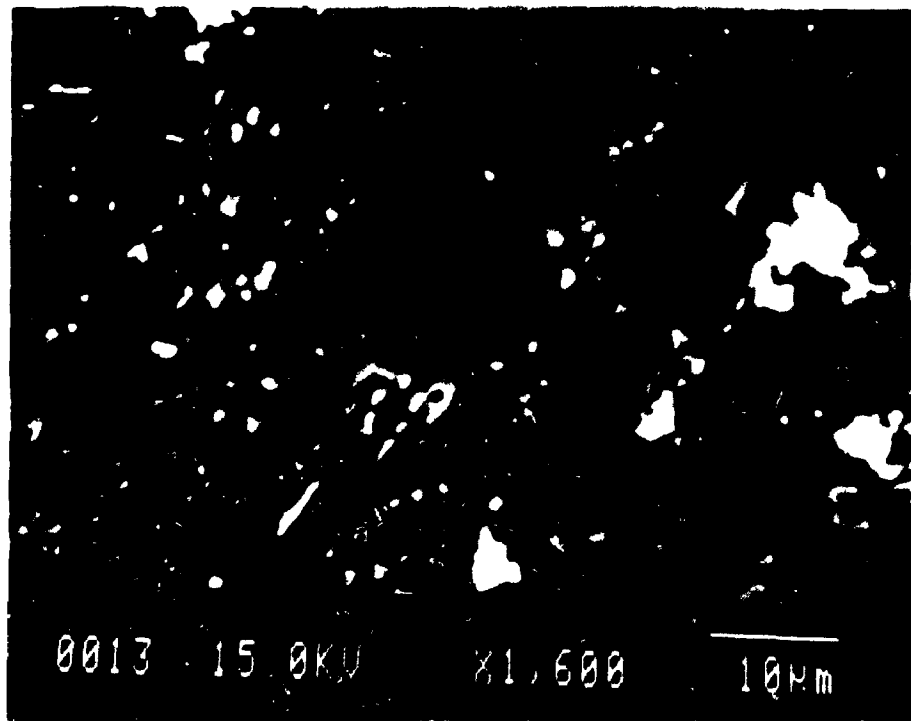
Figure 4.12

a) Backscattered electron micrograph of the products of experiment PLZ33 (P= 3.0 GPa, T= 1225°C, time= 8 hours) in which the SDW2 composition was used as a middle layer in phlogopite lherzolite (PLZ) material. Large grains of zoned garnets (G) are distributed homogeneously throughout the SDW2 middle layer. In addition to garnet, the SDW2 layer is composed of primary phlogopite, quench clinopyroxene and glass. See details in section 4.3.2.

b) Backscattered electron micrograph of a large melt "pool" in the product of experiment CPL14 (P= 3.0 GPa, T= 1100°C, time= 9 hours 30 minutes) in which S-DOL composition was used as a middle layer in carbonated phlogopite lherzolite (CPL) material. The melt has not quenched to a glass but to an assemblage of large elongated dolomite grains (D) and small acicular alkali- and calcium-rich carbonate crystals (aC). This texture bear strong similarities with the one observed by Wallace and Green (1988) in carbonatite melt "pools" in their experiments on the phase relationships of carbonated amphibole-bearing peridotite (see Wallace and Green, 1988, Figure 2, p. 345). S refers to primary silicates (clinopyroxene) at the border of the melt "pool". See details in section 5.3.2)



a



b

chemical zonation of the garnets suggests, however, that the residual liquid (now glass + quench clinopyroxene) converged compositionally towards the ideal partial melt in equilibrium with PLZ at 1225°C: from core to rim, the composition of these garnets changes significantly with the proportion of the pyrope component passing from 55% to a significantly higher value of 68%, comparable to that of the garnets found in the standard experiments on PLZ (Figure 4.11).

The residual liquid (glass + quench clinopyroxene) was analyzed with the microprobe using a defocused electron beam of 5 to 10 μm diameter. The eight analyses performed are presented in Appendix B2 and the average, recalculated to 100 wt% with a fixed $\text{H}_2\text{O}/\text{K}_2\text{O}$ of 0.38, is presented in Table 4.4 (analysis I). Relative to SDW2 (Table 4.3), the residual liquid (Table 4.4; analysis I) is indeed poorer in Al_2O_3 and K_2O and also richer in CaO . The $X_{\text{MgFe}_{\text{tot}}}$ is quite high (≈ 0.83), probably due to a relatively important iron loss of the liquid to the capsule.

4.3.3 Sandwich experiment on PLZ using SDW3 as a middle layer

The composition of the residual liquid obtained in the first sandwich experiment (section 4.3.2) was used as a basis for the synthesis of the glass layer in the second sandwich experiment (Table 4.1; Experiment PLZ40). The

Table 4.4: Average of microprobe analyses of "quench" liquid (glass + quench clinopyroxene) in the middle layer of the sandwich experiments performed on PLZ.

	<u>I</u> PLZ33 (1225°C) with SDW2 layer (n=8)			<u>II</u> PLZ40 (1225°C) with SDW3 layer (n=8)		
	Anal. (wt%)	1Std.	Rec. (wt%)	Anal. (wt%)	1Std	Rec. (wt%)
SiO ₂	47.26	1.35	47.64	46.32	1.16	47.63
TiO ₂	1.48	0.66	1.49	1.62	0.03	1.67
Al ₂ O ₃	11.87	1.00	11.97	10.59	0.44	10.89
Cr ₂ O ₃	0.04	0.05	0.04	0.28	0.59	0.29
FeO*	4.48	0.19	4.52	5.46	0.12	5.62
MnO	0.09	0.03	0.09	0.14	0.03	0.14
MgO	12.72	1.49	12.82	12.75	0.68	13.11
CaO	10.35	1.95	10.44	11.19	0.46	11.51
Na ₂ O	1.30	0.27	1.31	1.69	0.18	1.74
K ₂ O	6.96	1.52	7.02	5.21	0.53	5.36
H ₂ O [#]			2.66			2.04
Total	96.55		100.00	95.25		100.00
X _{MgFe_{tot}}	0.83		0.83	0.81		0.81

Notes : "Anal." is the average of the "n" analyses performed. "1Std." is the standard deviation for the "n" analyses. "Rec." is "Anal." recalculated to 100 weight % so that the H₂O:K₂O weight ratio is equal to 0.38. H₂O[#] is the calculated water content found by the ratio. FeO* refers to the total Fe expressed as FeO. X_{MgFe_{tot}} is Mg/(Mg+Fe_{total})

87

essential corrections done were, again, to fix the H_2O/K_2O value at 0.38 and to add FeO so that the $K_D^{olivine/liquid}(Fe/Mg) \approx 0.3$. The composition of the synthesized glass (SDW3) is presented in Table 4.3. In this second step, the duration of the experiment was reduced to one hour to minimize iron loss from the liquid (cf. Mengel and Green, 1989).

Backscattered electron images of the experimental product show a very homogeneous texture throughout the SDW3 middle layer, which consists essentially of glass and small acicular grains of clinopyroxene. Microprobe analyses of these small clinopyroxene grains indicate that they are anomalously rich in Al_2O_3 , K_2O and TiO_2 , poor in CaO and have a low $X_{MgFe_{tot}}$ when compared to the larger grains of clinopyroxene found in the PLZ layers (Table 4.5). These acicular crystals are therefore considered to be quenched, and this suggests that the middle layer was in a fully liquid state. At the boundaries between the SDW3 and PLZ layers, the liquid appears to have infiltrated the PLZ mineral assemblage. All these observations suggest that the middle layer represents a quench liquid equilibrated with the residual minerals found in the PLZ layer. The composition of this quench liquid should be close to the ideal partial melt in equilibrium with PLZ at 1225°C if the residual mineral assemblage is the same as in the standard experiment (non-sandwich) done at the same temperature (Table 4.1; Experiment PLZ30), and also if the composition of the residual minerals are comparable.

Table 4.5: Comparison of the composition of primary and quench clinopyroxene grains in sandwich experiment PLZ40.

	<u>Primary</u> (n=4)	<u>Quench</u>	<u>Quench</u>
SiO ₂	52.47	49.03	51.25
TiO ₂	0.13	1.28	0.95
Al ₂ O ₃	3.84	7.27	6.63
Cr ₂ O ₃	0.64	0.00	0.04
FeO*	3.09	5.61	5.02
MnO	0.07	0.14	0.19
MgO	17.74	14.45	17.42
CaO	20.87	15.97	15.16
Na ₂ O	0.81	0.84	1.05
K ₂ O	0.04	1.14	1.01
Total	99.70	95.73	98.72
X _{MgFe_{tot}}	0.91	0.82	0.86

Notes : "Primary" is an average of 4 analyses (n=4) of primary clinopyroxene grains. Each "Quench" represents an individual analysis of quench clinopyroxene. FeO* refers to the total Fe expressed as FeO. X_{MgFe_{tot}} is Mg/(Mg+Fe_{total}).

As indicated in Table 4.1, the residual mineral assemblage in the sandwich experiment using SDW3 as a middle layer (Experiment PLZ40) is indeed the same as that in the standard experiment on PLZ at 1225°C (Experiment PLZ30). In Table 4.6, the average compositions of the different residual minerals found in PLZ40 and PLZ30 are compared. No major differences in the compositions of the phases are observed with the exception of TiO_2 which is significantly lower in phlogopite of the sandwich experiment. Based on all these observations, it is considered that the composition of the equilibrated quench liquid in sandwich experiment PLZ40 is reasonably close to the ideal partial melt in equilibrium with PLZ at 1225°C.

Eight analyses of the quench liquid (glass + quench clinopyroxene) were performed with the microprobe using a defocused electron beam of 10 to 30 μm diameter. These analyses all yield comparable results (Appendix B2). The calculated average composition and corresponding standard deviation are presented in Table 4.4 (analysis II). This analyzed silicate liquid shows the main compositional characteristics that were deduced from the study of the chemical variations in the minerals (section 4.2). For example, of the components that can be supplied by clinopyroxene, the liquid is preferentially enriched in Na_2O and CaO . Moreover, the high K_2O content (5.35 wt%) supports the important role of phlogopite in the melting reactions. The Ti/K of the liquid (0.18) is significantly lower than

Table 4.6: Comparison of the composition of the minerals in the standard experiment PLZ30 and in the sandwich experiment PLZ40.

	<u>Olivine</u>		<u>Orthopyroxene</u>	
	<u>PLZ30</u>	<u>PLZ40</u>	<u>PLZ30</u>	<u>PLZ40</u>
SiO ₂	40.91	41.00	55.46	55.66
TiO ₂	0.01	0.01	0.05	0.01
Al ₂ O ₃	0.17	0.00	3.77	3.12
Cr ₂ O ₃	0.06	0.07	0.43	0.29
FeO _{total}	8.02	9.18	5.61	6.01
MnO	0.07	0.13	0.04	0.11
MgO	49.91	49.77	33.60	33.64
CaO	0.25	0.13	0.93	0.57
Na ₂ O	0.02	0.00	0.08	0.01
K ₂ O	0.01	0.00	0.00	0.00
Total	99.43	100.29	99.97	99.42

	<u>Clinopyroxene</u>		<u>Phlogopite</u>	
	<u>PLZ30</u>	<u>PLZ40</u>	<u>PLZ30</u>	<u>PLZ40</u>
SiO ₂	52.69	52.47	37.81	39.41
TiO ₂	0.15	0.13	7.04	4.35
Al ₂ O ₃	4.15	3.84	16.12	16.49
Cr ₂ O ₃	0.61	0.64	1.54	0.51
FeO _{total}	3.08	3.09	4.04	4.45
MnO	0.06	0.07	0.06	0.03
MgO	17.51	17.74	19.03	19.97
CaO	20.84	20.87	0.21	0.24
Na ₂ O	0.76	0.81	0.03	0.14
K ₂ O	0.00	0.04	10.43	9.80
Total	99.85	99.70	96.31	95.39

	<u>Garnet</u>	
	<u>PLZ30</u>	<u>PLZ40</u>
SiO ₂	42.40	41.66
TiO ₂	0.62	1.11
Al ₂ O ₃	20.27	21.25
Cr ₂ O ₃	3.11	1.13
FeO _{total}	4.93	6.21
MnO	0.21	0.28
MgO	20.85	20.98
CaO	7.14	6.95
Na ₂ O	0.00	0.00
K ₂ O	0.00	0.00
Total	99.53	99.57

the value of 0.29 for the PLZ bulk composition. Finally, the high K_2O/Na_2O (weight ratio) of 3.1 of the melt is, in part, a reflection of the high K_2O/Na_2O in the PLZ starting material. It should be noted that the $X_{MgFe_{tot}}$ value of 0.81 is probably too high and is explained by preferential iron loss of the liquid.

4.4 Interaction experiments with HAR and WHR protoliths

This part of the study was not intended to be detailed and in this respect can be considered as preliminary work. The main objective was to get an idea of how reactive the partial melt in equilibrium with PLZ at 1225°C and 3.0 GPa, whose composition was estimated in the previous section (4.3), would be towards harzburgitic and wehrlitic materials (HAR and WHR; Table 3.2) at 1000°C and 2.0 GPa.

The experimental approach taken was straightforward. First a glass of composition as close as possible to the estimated PLZ equilibrium partial melt (Table 4.4, analysis II) was synthesized using the method described in section 3.1.2. This synthesized glass (SILMET; Table 3.1) was then ground and mixed thoroughly with each of the peridotitic protoliths (HAR or WHR) Two mixtures were prepared with the harzburgite protolith: HAR-SILMET(A) and HAR-SILMET(B) in the weight proportions 10:90 and 25:75 respectively. One mixture (WHR-SILMET) with the weight proportion 10:90 was prepared with the wehrlite protolith. The compositions of

92

SILMET, as estimated by five defocused beam microprobe analyses, and of the three prepared mixtures (HAR-SILMET(A), HAR-SILMET(B), WHR-SILMET) are presented in Table 4.7.

The pure HAR and WHR compositions and the three mixtures were all equilibrated to a pressure of 2.0 GPa and temperature of 1000°C. HAR-SILMET(B) was held at 1225°C for one hour to induce melting and then cooled slowly (2 hours) to the temperature of the experiment (1000°C; cf. Meen, 1987). The experimental results are summarized in Table 4.8 and the chemical composition of the mineral grains analyzed for each experiment is presented in Appendix B4.

The resulting mineral assemblage of the standard experiment on HAR consists evidently of olivine and orthopyroxene. The HAR-SILMET(A) interaction experiment shows essentially the same assemblage, and the olivine and orthopyroxene compositions are the same as those in the HAR experiment (Appendix B4). The SILMET material can be distinguished and is distributed homogeneously throughout the charge, forming small veins and pockets where the glass seems to have devitrified to cryptocrystalline material. It was not possible to analyze the individual cryptocrystals, but, in a few pockets, the bulk composition of the cryptocrystalline assemblage could be determined by microprobe analysis using a 5 μm diameter electron beam. As can be seen in Table 4.9, the composition of the cryptocrystalline material is almost the same as the original composition of the SILMET glass. The only

Table 4.7: Bulk composition of SILMET, HAR+SILMET and WHR+SILMET.

	<u>SILMET</u> (n=5)	<u>HAR:90wt%</u> <u>SILMET:10wt%</u>	<u>HAR:75wt%</u> <u>SILMET:25wt%</u>	<u>WHR:90wt%</u> <u>SILMET:10wt%</u>
	(wt%)	(wt%)	(wt%)	(wt%)
SiO ₂	45.81	48.04	47.68	42.67
TiO ₂	1.67	0.18	0.43	0.19
Al ₂ O ₃	12.14	2.58	4.18	3.34
Cr ₂ O ₃	0.00	0.14	0.11	0.59
FeO*	6.51	7.34	7.20	7.51
MnO	0.00	0.12	0.10	0.11
MgO	11.75	38.97	34.44	38.03
NiO	0.00	0.14	0.11	0.20
CaO	11.29	1.38	3.03	6.08
Na ₂ O	2.27	0.25	0.58	0.42
K ₂ O	6.20	0.62	1.55	0.62
H ₂ O	2.36	0.24	0.59	0.24
CO ₂	0.00	0.00	0.00	0.00
Total	100.00	100.00	100.00	100.00
X _{MgFe_{tot}}	0.76	0.90	0.90	0.90

Notes : The composition of SILMET is an average of 5 microprobe analyses performed on the synthesized glass, using a defocused electron beam. FeO* refers to the total Fe expressed as FeO. X_{MgFe_{tot}} is Mg/(Mg+Fe_{total}).

Table 4.8: Results of standard experiments on HAR and WHR and interaction experiments with SILMET.

Run#	T (°C)	Time (hours)	Weight Prop.	Phases observed
HAR	1000	28	-----	ol,opx
HAR-SILMET(A)	1000	20	90:10	ol,opx,cryptocrystals
HAR-SILMET(B)	1200-> 1000	1-> 22	75:25	ol,opx,cpx,phl
WHR	1000	28	-----	ol,cpx,sp
WHR-SILMET	1000	20	90:10	ol,cpx,sp,cryptocrystals

Notes : Weight Prop. is the respective weight proportion of the different materials used in the interaction experiments. All runs done in Ag₅₀Pd₅₀ capsules. ol: olivine; opx: orthopyroxene; cpx: clinopyroxene; sp: spinel; phl: phlogopite. Cryptocrystals refers to a crystalline assemblage whose specific crystals, due to their small size, could not be identified.

significant differences are lower contents in K_2O and Al_2O_3 , and a higher $X_{MgFe_{tot}}$ value. The resulting mineral assemblage in the HAR-SILMET(B) interaction experiment consists of olivine, orthopyroxene, clinopyroxene and phlogopite.

The mineral assemblages of the standard experiment on WHR and interaction experiment WHR-SILMET consist essentially of olivine, clinopyroxene and spinel, and the compositions of these minerals are almost the same in the two experiments (Appendix B4). The SILMET glass in WHR-SILMET has devitrified to a cryptocrystalline assemblage whose bulk composition, presented in Table 4.9, shows the same characteristics as that of the cryptocrystalline material in HAR-SILMET(A).

These results suggest that, at the experimental conditions described above (2.0 GPa, 1000°C for 20 hours), SILMET, representative of a partial melt in equilibrium with a phlogopite lherzolite at 3.0 GPa, is not particularly reactive towards harzburgitic and wehrlitic compositions. This conclusion is based on the fact that, except for some evident partial reequilibration with the surrounding harzburgite or wehrlite, SILMET crystallized to a mineral assemblage whose bulk composition is close to that of the original glass. A more detailed investigation of these experimental results is presented in Chapter 6.

Table 4.9: Comparison of average composition of SILMET and of the cryptocrystalline assemblage in HAR-SILMET and WHR-SILMET.

	<u>Synthesized glass</u>	<u>Cryptocrystalline assemblage bulk composition (CRYPT)</u>	
	<u>SILMET</u>	<u>HAR-SILMET</u>	<u>WHR-SILMET</u>
	(wt%)	(n=2) (wt%)	(n=2) (wt%)
SiO ₂	45.81	47.29	47.51
TiO ₂	1.67	1.95	2.04
Al ₂ O ₃	12.14	10.33	10.93
Cr ₂ O ₃	0.00	0.06	0.10
FeO*	6.51	5.24	4.63
MnO	0.00	0.00	0.00
MgO	11.75	14.18	13.48
CaO	11.29	12.78	13.47
Na ₂ O	2.27	1.38	1.01
K ₂ O	6.20	3.81	4.74
Total	97.64	97.02	97.91
X_{MgFe_{tot}}	0.76	0.83	0.84

Notes : See Table 4.8 for details on composition of SILMET glass. For the cryptocrystalline assemblage the composition is an average of two microprobe analyses using a 5 μm diameter electron beam. FeO* refers to the total Fe expressed as FeO. X_{MgFe_{tot}} is Mg/(Mg+Fe_{total}).

4.5 Summary

At 3.0 GPa, the solidus of the phlogopite lherzolite model mantle source (PLZ) is estimated at 1175°C. The phlogopite-present melting interval ranges from 1175° to 1275°C with phlogopite and clinopyroxene as the main participants in the melting reactions. At 1225°C, the equilibrium partial melt coexists with olivine, orthopyroxene, clinopyroxene, garnet and phlogopite. The compositional characteristics of this melt are consistent with the chemical variations observed in the minerals through the investigated temperature interval. Notably, the equilibrium silicate melt is rich in alkalis with a strongly potassic affinity. The value of Ti/K in the melt is lower than in the coexisting phlogopite. The amount of water in the silicate liquid is probably limited by the K₂O content to a relatively constant H₂O/K₂O (weight ratio) of approximately 0.38, typical of a hydrous phlogopite. Finally, this water-bearing silicate melt, if put in contact with harzburgitic or wehrlitic material at 2.0 GPa and 1000°C for 20 hours, is only slightly reactive towards these peridotitic compositions and, therefore, crystallizes to a mineral assemblage with only minor compositional change.

CHAPTER 5

PARTIAL MELTING OF A CARBONATED PHLOGOPITE LHERZOLITE (CPL)

AT P = 3.0 GPA: EXPERIMENTAL RESULTS

5.1 General statement on phase relationships

Temperatures for the experiments on the carbonated phlogopite lherzolite (CPL) at a pressure of 3.0 GPa ranged from 900° to 1150°C and the phases present in each experimental product are summarized in Table 5.1.

Olivine, orthopyroxene, clinopyroxene and phlogopite are stable at all temperatures. Garnet is quite abundant from 1075° to 1150°C and its absence at lower temperature is probably due to the lack of time for subsolidus reaction between spinel and pyroxenes at such low temperatures. This relatively high abundance of garnet suggests that this mineral plays a significant role in the melting relation of the CPL mantle source (see section 5.2.6)

A crystalline carbonate phase is stable up to 1050°C. The subsequent breakdown of the carbonate is interpreted as being related to the formation of a CO₂-rich melt phase, a melting reaction observed in many high-pressure experiments on CO₂-bearing simple systems (e.g. Eggler, 1975, 1976, 1978; Wyllie and Huang, 1975, 1976; Wyllie et al., 1983) and

Table 5.1: Results of partial melting experiments on CPL at P=3.0GPa

Run#	T (°C)	Time (hours)	Sdw comp.	Phases observed
CPL2	900	28	-----	ol, opx, cpx, phl, mag, (sp, dol)
CPL4	925	28	-----	ol, opx, cpx, phl, mag, (sp, dol)
CPL5	975	20	-----	ol, opx, cpx, phl, mag, (sp, dol)
CPL11	1000	28	-----	ol, opx, cpx, phl, mag, (sp, dol)
CPL8	950->1025	21->5	-----	ol, opx, cpx, phl, dol, mag, (sp)
CPL9	950->1050	20->5	-----	ol, opx, cpx, phl, dol, (sp)
CPL7	950->1075	21->4.5	-----	ol, opx, cpx, phl, gar, liq, (sp)
CPL10	950->1100	20->5	-----	ol, opx, cpx, phl, gar, liq, (sp)
CPL13	950->1125	20->4	-----	ol, opx, cpx, phl, gar, liq, (sp)
CPL12	950->1150	20->4	-----	ol, opx, cpx, phl, gar, liq, (sp)
<i>(sandwich experiments)</i>				
CPL14	1100	9.5	S-DOL	ol, opx, cpx, gar, liq, (sp)
CPL16	1100	9.5	S/P-DOL	ol, opx, cpx, phl, gar, liq, (sp)

Notes : Sdw comp. is the identification of the composition used as a middle layer in sandwich experiments; phases in curved brackets are phases in trace amounts; all runs done in Ag₅₀Pd₅₀ capsules. The notations m->n and x->y for temperature and time respectively mean that the experiment was run x hours at m°C then brought to n°C for y hours. ol: olivine; opx: orthopyroxene; cpx: clinopyroxene; phl: phlogopite; gar: garnet; mag: magnesite; dol: dolomite; liq: liquid; sp: spinel.

CO₂-bearing peridotitic systems (e.g. Wendlandt and Mysen, 1980; Olafsson and Eggler, 1983; Wyllie and Rutter, 1986; Wallace and Green, 1988; Falloon and Green, 1989, 1990). Therefore, the solidus for the CPL composition at 3.0 GPa occurs at a maximum temperature between 1050° and 1075°C. However, the possibility that the carbonate phase melts over a temperature interval and that the solidus occurs at a temperature slightly lower than 1050°C cannot be discarded.

The persistence of phlogopite up to, at least, 1150°C implies that the assumed CO₂-rich melt is in equilibrium with a phlogopite-bearing lherzolite in a temperature interval of more than 75°C. Hence, one of the main objectives of the experiments on CPL is to define the nature of the melt in this phlogopite-present melting interval.

5.2 Chemical composition of minerals

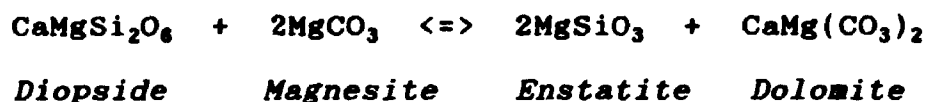
The detailed results of the microprobe analyses performed on the different minerals formed in the partial melting experiments on CPL are presented in Appendix B3. In the following, as in Chapter 4, the content of a component refers to the average mineral compositions calculated for each of the experimental products.

5.2.1 Carbonates

From 900° to 1000°C, the stable carbonate phase is

magnesite (MgCO_3 content: 85.03 to 87.01 mol%; Figure 5.1). At 1025°C, magnesite and dolomite coexist. At 1050°C, the only observed carbonate phase is dolomite (MgCO_3 content: 47.47 mol%; CaCO_3 content: 48.82 mol%; Figure 5.1).

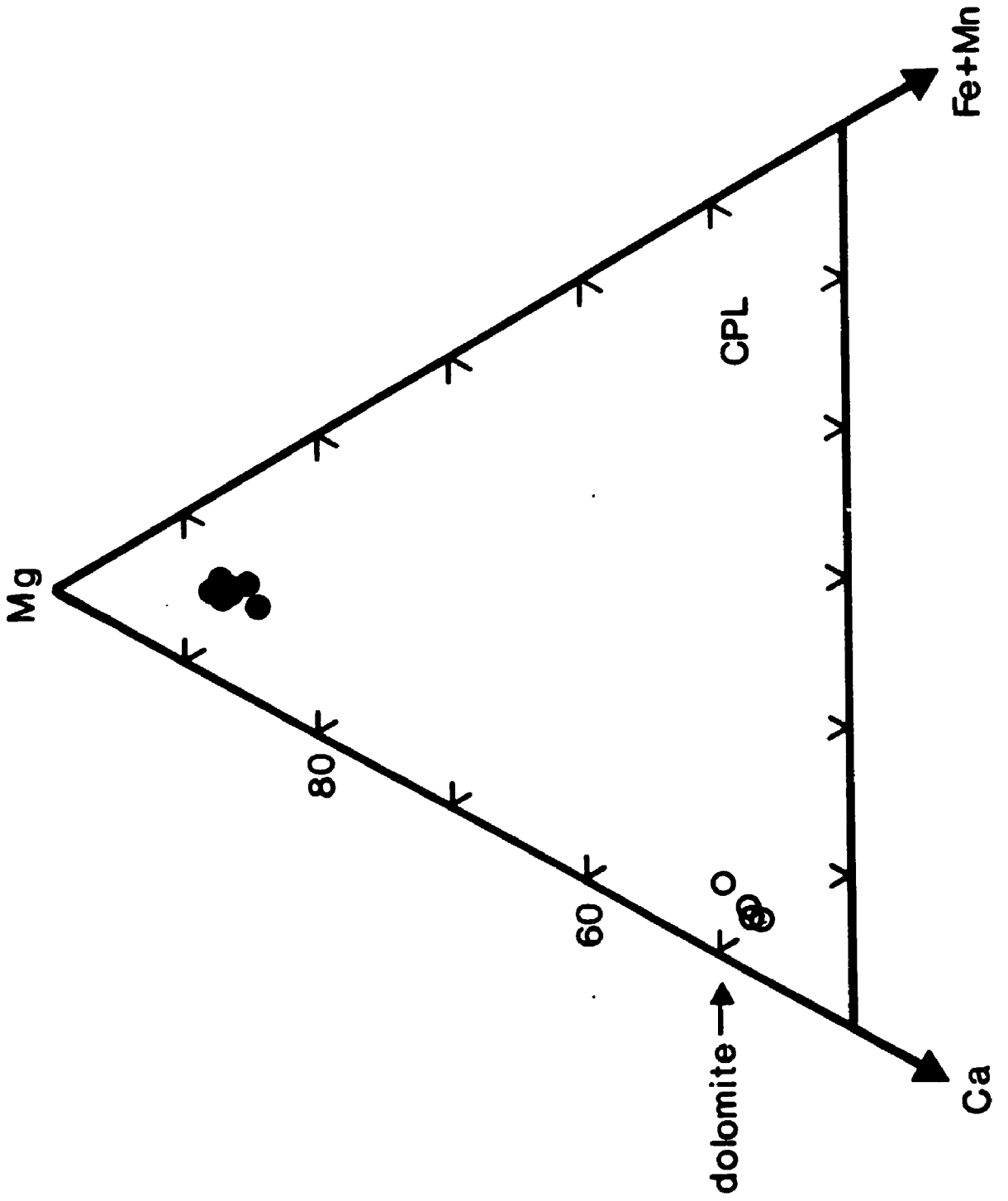
The coexistence of dolomite and magnesite at 1025°C suggests that this temperature is near the one defining the following heterogeneous equilibrium:



In their experimental investigation of this reaction, Brey et al. (1983) determined that the above transition lies at approximately 1000°C at a pressure of 3.0 GPa in the simple $\text{CaO-MgO-SiO}_2\text{-CO}_2$ system. Their suggestion, that the addition of cations like Fe, Al and Na, present in natural peridotitic systems, should not substantially influence the reaction (Brey et al., 1983, p. 71), is supported by the experimental study of Falloon and Green (1989) on the solidus of a carbonated fertile peridotite in which the transition from magnesite to dolomite also occurred at 1000°C at a pressure of 3.0 GPa. The present experimental data, suggesting that the transition occurs somewhere near 1025°C in CPL, are reasonably consistent with these previous results.

The compositional characteristics of the experimental carbonate phases can be used to divide the investigated

Figure 5.1 : (CPL standard experiments) Carbonate compositions plotted on a Mg-Ca-(Fe+Mn) ternary diagram (cationic proportions). Filled circles are carbonates analyzed at $900^{\circ}\text{C} \leq T \leq 1025^{\circ}\text{C}$. Empty circles are carbonates analyzed at $1025^{\circ}\text{C} \leq T \leq 1050^{\circ}\text{C}$.



106

temperature interval into three distinct fields: the magnesite field ($< 1025^{\circ}\text{C}$), the dolomite field ($\geq 1025^{\circ}\text{C}$ and $< 1075^{\circ}\text{C}$), and the liquid field ($\geq 1075^{\circ}\text{C}$). This nomenclature will be valid whenever these fields are referred to in the text.

5.2.2 Olivine

Olivine has an extremely constant composition throughout the entire investigated temperature interval with a value of $X_{\text{MgFe}_{\text{tot}}}$ of 0.91 in all experimental products. NiO and CaO contents range from 0.26 to 0.34 wt% and 0.08 to 0.16 wt% respectively.

5.2.3 Orthopyroxene

Orthopyroxene in the CPL series of experiments is an aluminian enstatite (Morimoto, 1988). All $X_{\text{MgFe}_{\text{tot}}}$ values fall between 0.91 and 0.92, and the proportion of Wo range from 0.95 to 1.26. Al_2O_3 contents vary from 2.89 to 3.45 wt% with no systematic correlation with temperature.

5.2.4 Clinopyroxene

All clinopyroxene grains analyzed are aluminian-chromian diopside (Morimoto, 1988) with proportions of Wo from 44.03 to 46.82, and a $X_{\text{MgFe}_{\text{tot}}}$ value of 0.91. Al_2O_3 (3.49 to 3.97

wt%), Cr_2O_3 (0.42 to 0.64 wt%), TiO_2 (0.07 to 0.14 wt%) and Na_2O (0.87 to 1.20 wt%) contents in clinopyroxene are relatively constant and do not show systematic variation with temperature. As shown in Figure 4.8, the Na content and the "Cation Excess" (total number of cations in clinopyroxene minus 4; see section 4.2.4) are generally higher than in clinopyroxene from the PLZ experiments. Therefore, the higher abundance in Na appears to be coupled with a higher Fe^{3+} content (acmite component). The higher Na content is consistent with the fact that the bulk Na_2O (0.60 wt%; Table 3.2) in CPL is significantly higher than in PLZ (Na_2O : 0.20 wt%; Table 3.2).

5.2.5 Phlogopite

As in the PLZ experiments, the SiO_2 (37.29 to 39.13 wt%) and Al_2O_3 (14.47 to 16.93 wt%) contents of phlogopite in the CPL series are such that, in the structural formula, Si is always smaller than 6 pfu/22 and the tetrahedral site can be filled completely by Si and Al ($\text{Si} + \text{Al}_{\text{tot}} > 8$ pfu/22). Cr_2O_3 contents are low, ranging from 0.06 to 0.32 wt%. TiO_2 contents vary between 3.88 and 6.73 wt%. In the interlayer site, K is the major cation (K_2O contents: 9.45 to 9.95 wt%) and the amount of Na (Na_2O contents: 0.07 to 0.49 wt%) is systematically higher than that in phlogopite found in the PLZ experiments.

The variation in Ti/K (atomic ratio) is plotted against

temperature in Figure 5.2. Because the amount of K is relatively constant in phlogopite, Ti/K reflects essentially the change in the abundance of titanium. No systematic variation is observed in the magnesite and dolomite fields where Ti/K is always lower than the value of 0.29 calculated for the bulk CPL composition (Table 3.2). However, as melting proceeds, Ti/K in phlogopite increases markedly to values in excess of 0.29 (Figure 5.2). As in the phlogopites from the PLZ experiments (section 4.2.5), these high Ti/K values observed in phlogopite at suprasolidus conditions imply that an additional K-bearing phase with a Ti/K value lower than 0.29 exists. Because no other K-bearing mineral is observed, the assumed CO₂-rich melt possibly contains a significant amount of K and has a low Ti/K value.

Variation diagrams correlating Ti content of phlogopite with the [6-OSO] and [(6-Si-Al^{VI}-Cr-Ca)/2] parameters are presented in Figure 5.3. Almost all the titanium variation in phlogopite of the CPL experiments can be accounted by a combination of the Ti-Vac ($\text{Ti}^{\text{VI}}\square^{\text{VI}} \rightleftharpoons 2[\text{Mg,Fe,Mn}]^{\text{VI}}$) and Ti-Tsch ($\text{Ti}^{\text{VI}}2\text{Al}^{\text{IV}} \rightleftharpoons [\text{Mg,Fe,Mn}]^{\text{VI}} 2\text{Si}^{\text{IV}}$) substitution mechanisms with the Ti-Vac substitution being, however, clearly dominant (Figure 5.3). The substitutions accounting for the variation in titanium are, therefore, essentially the same as those in the phlogopites found in the PLZ experiments.

Figure 5.2 : (CPL standard experiments) Variation of the Ti:K atomic ratio (Ti/K) of phlogopite against temperature (T). The dashed line represents the Ti/K value calculated for the CPL carbonated phlogopite lherzolite bulk composition. The fields defined by the stability of the different carbonate phases are indicated.

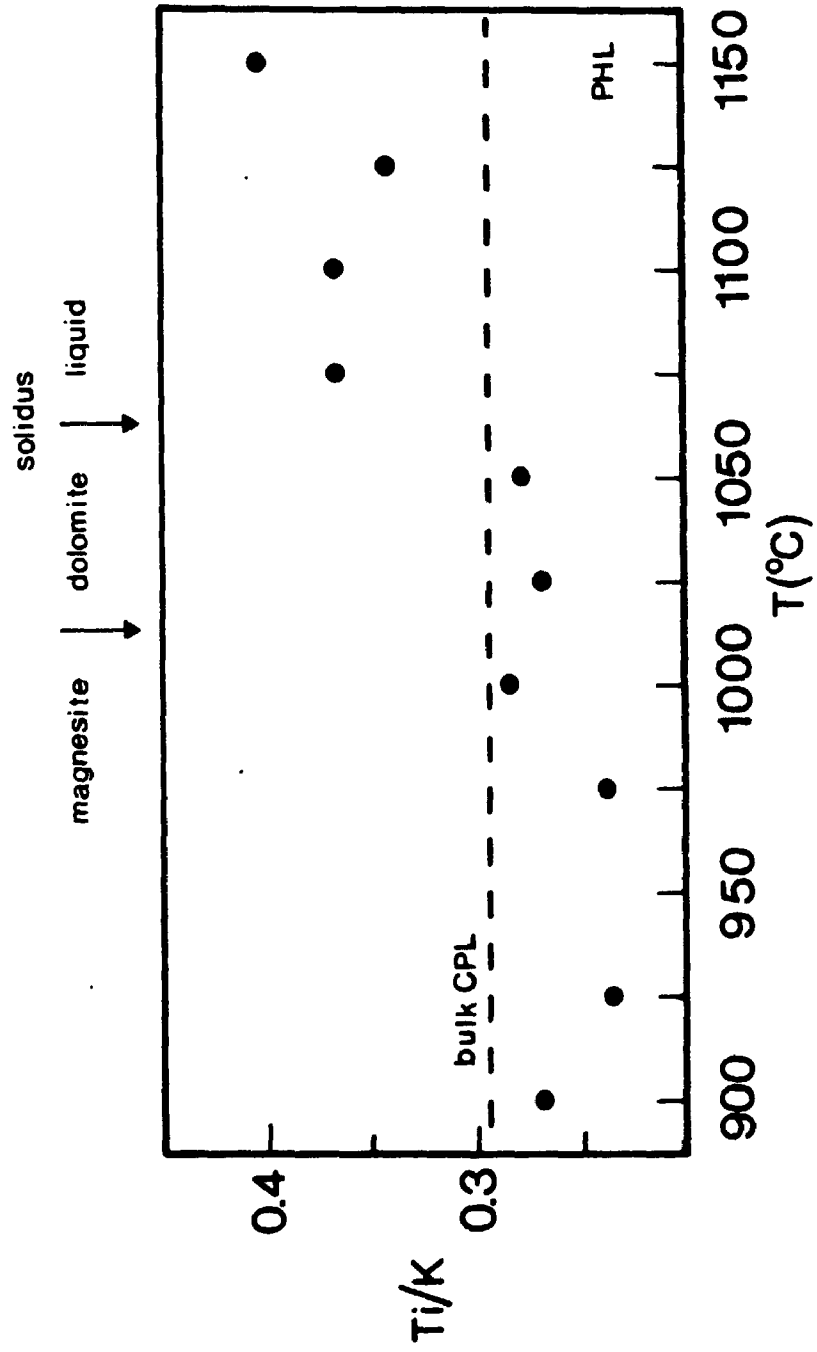
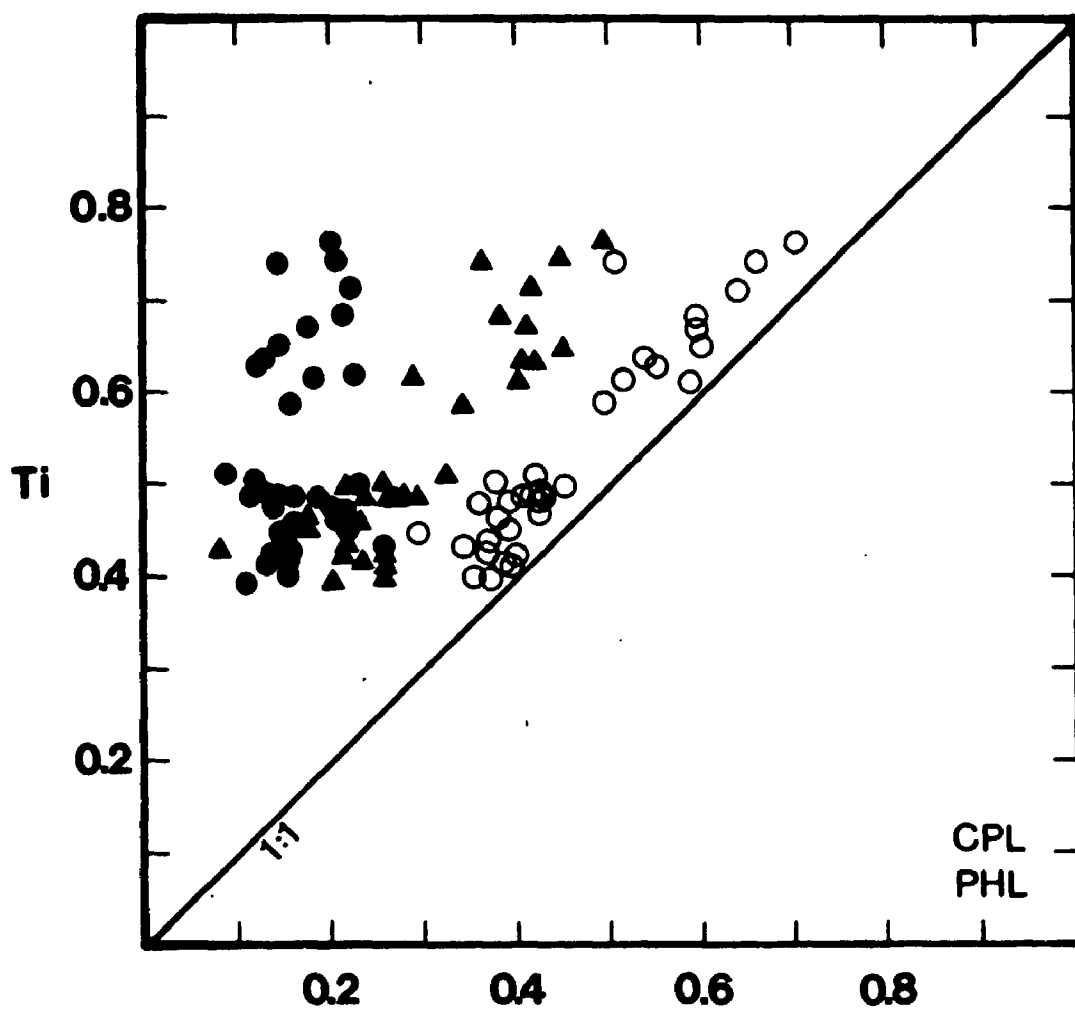


Figure 5.3 : (CPL standard experiments) Variation of Ti against $[(6\text{-Si-Al}^{\text{VI}}\text{-Cr-Ca)}/2]$ (\bullet), $[6\text{-OSO}]$ (\blacktriangle), and $[(6\text{-OSO}) + (6\text{-Si-Al}^{\text{VI}}\text{-Cr-Ca)}/2]$ (\circ) in phlogopite. OSO refers to the cations in the octahedral site ($\text{Al}^{\text{VI}} + \text{Cr} + \text{Ti} + \text{Mg} + \text{Fe} + \text{Mn}$). All cations are expressed in cations per formula unit calculated on a basis of 22 oxygens.

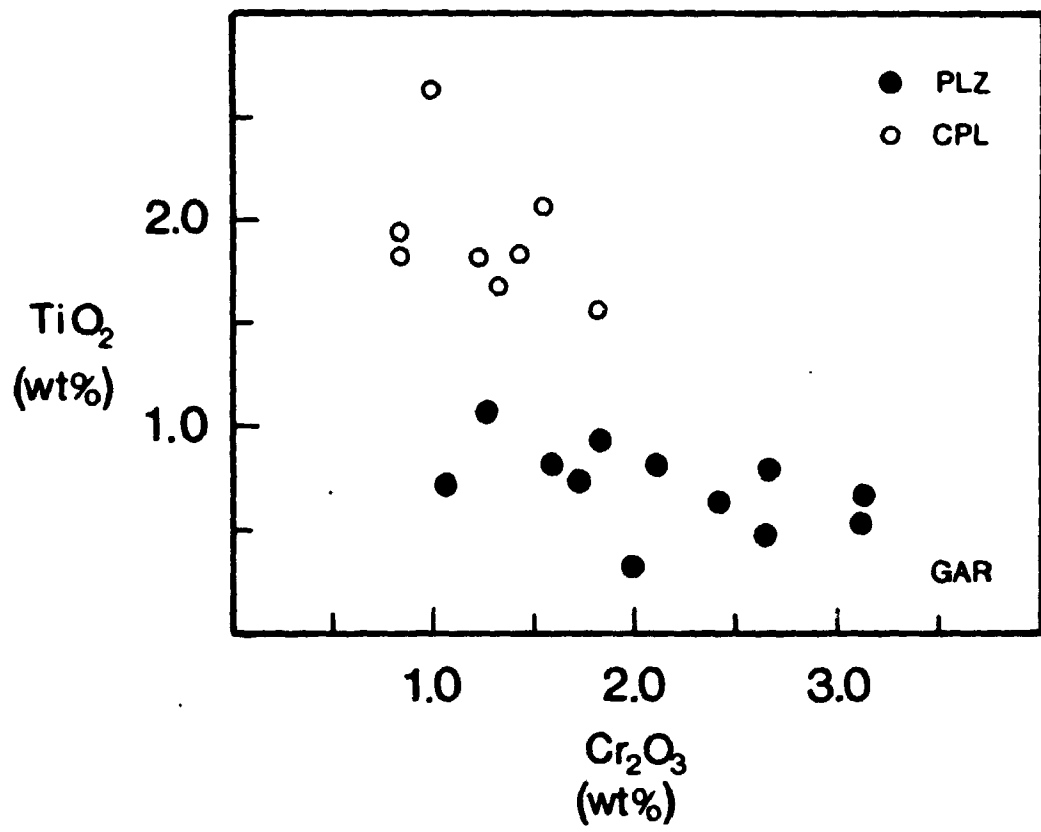


5.2.6 Garnet

As noted in section 5.1, although garnet did not nucleate in the magnesite and dolomite fields, it is nevertheless considered as a stable subsolidus phase in CPL at 3.0 GPa (cf. Takahashi and Kushiro, 1983, p. 866). However, as the solidus is crossed, garnet appears significantly more abundant than in the PLZ experimental products. This suggests that garnet is likely an additional product, together with liquid, of the melting reactions occurring in CPL between 1075° and 1150°C.

In the CPL liquid field, garnet shows a proportion of the pyrope component between 64.8 and 67.3 mol%. CaO contents are relatively constant, ranging from 7.60 to 8.38 wt%. In Figure 5.4, the TiO₂ and Cr₂O₃ contents in garnets of both the CPL and the PLZ experiments are compared. Garnet in CPL are clearly distinct being richer in TiO₂ (1.65 to 1.96 wt%) and generally poorer in Cr₂O₃ (0.82 to 1.82 wt%). Because Al/Cr, Al/Ti and Al/K have similar values in the bulk CPL and PLZ compositions (Table 3.2), there is no obvious reason why garnet compositions in PLZ and CPL should be distinct with respect to their TiO₂ and Cr₂O₃ contents. Accordingly, the distinct compositional characteristics of garnet in the investigated melting interval of CPL also suggest a significant role of garnet in the melting reactions.

Figure 5.4 : (PLZ and CPL standard experiments) Variation between TiO_2 (in wt%) and Cr_2O_3 (in wt%) in garnets. Filled circles are for the garnets found in the products of the PLZ series of experiments (Chapter 4); empty circles are for the garnets found in the products of the CPL series of experiments (Chapter 5).



5.3 Determination of melt composition in equilibrium with CPL at 1100°C: sandwich experiments

5.3.1 Details of the experimental approach

Sandwich experiments were performed at 1100°C in order to define the compositional nature of the CO₂-rich melt in equilibrium with CPL in the phlogopite-present melting interval. The experimental approach adopted is quite similar to the iterative method used with the PLZ model mantle source in that the choice of a composition for the middle layer is based on the results of the previous sandwich experiment. However, the compositions used as middle layers were prepared as simple mixtures (section 3.1.2) due to the difficulty of synthesizing CO₂-rich materials as glass.

A summary of the experimental conditions and results for the sandwich experiments performed on CPL at 1100°C are presented in Table 5.1. Chemical compositions of the analyzed minerals and melts can be found in Appendix B3.

5.3.2 Sandwich experiment on CPL using S-DOL as a middle layer

The low degree of melting, coupled with the very important quenching problem caused by the high amount of CO₂ dissolved in the liquid, have prevented any possible analysis of the interstitial melt in the standard

experiments on CPL. Consequently, the choice of a middle layer composition could not be based directly on the results of the standard experiments on CPL.

Wallace and Green (1988), in their experimental study on a carbonated amphibole peridotite, estimated that the dolomitic carbonatite magma coexisting with a pargasite-bearing lherzolithic assemblage contained a significant amount of sodium (Na_2O : 4.99 wt%, Wallace and Green, 1988, p.344, Table 1, Analysis 3). They suggested that the sodium present in the melt was probably supplied by the breakdown of the jadeite component ($\text{NaAlSi}_2\text{O}_6$) of clinopyroxene. Because it is conceivable that this melting reaction also occurs in CPL, the synthesized middle layer composition (S-DOL, Table 5.2) used in the first sandwich experiment is essentially dolomitic and contains a significant amount of Na (Na_2O : 8.19 wt%).

The residual mineral assemblage of the sandwich experiment using CPL and S-DOL in the weight proportion 88:12 consists of olivine, orthopyroxene, clinopyroxene, and garnet (Table 5.1; Experiment CPL14). However, in contrast to the standard experiment performed at the same temperature (1100°C; Table 5.1; Experiment CPL10), phlogopite is not part of the stable mineral assemblage in the product of sandwich experiment CPL14.

The S-DOL middle layer, in experiment CPL14, is not completely preserved because the melt has heavily infiltrated the CPL peridotitic material. The melt has

Table 5.2: Synthesized melt compositions used in sandwich experiments with the CPL model mantle source.

	<u>S-DOL</u>	<u>S/P-DOL</u>
	(wt%)	(wt%)
FeO*	5.61	4.54
MnO	0.13	0.11
MgO	15.40	16.38
CaO	24.95	26.53
Na ₂ O	8.19	4.10
K ₂ O	0.00	4.36
H ₂ O	0.00	1.75
CO ₂	45.72	42.23
Total	100.00	100.00
X_{MgFe[*]tot}	0.83	0.87

Notes : FeO* refers to the total Fe expressed as FeO.
X_{MgFe^{*}tot} is Mg/(Mg+Fe_{total}).

evidently not quenched to a glass but to an assemblage of large elongated, and small acicular carbonate grains (Figure 4.12b). The large elongated quench grains are of dolomitic composition, whereas the small acicular crystals are quench alkali- and calcium-rich carbonate with K₂O contents up to 11 wt% (Table 5.3). The bulk composition of the melt (quench dolomite + quench alkali-carbonate) was estimated by five microprobe analyses performed with a defocused electron beam of 10 to 25 μm diameter (Table 5.4). The analyzed melt is very poor in SiO₂ (1.02 to 1.64 wt%), TiO₂ (0.31 to 0.51 wt%) and Al₂O₃ (0.15 to 0.18 wt%), rich in alkalies (Na₂O: 6.05 to 10.00 wt%; K₂O: 3.19 to 4.78 wt%), and has a strong dolomitic affinity (CaO 21.45 to 25.14 wt%; MgO 13.86 to 15.17wt%). The very low total (55.49 to 56.94 wt%) is consistent with a very high CO₂ content (> 40 wt%).

The most striking compositional feature of the melt is its abundance in K₂O because the original S-DOL mixture did not contain any K (Table 5.2). This strongly suggests that the absence of phlogopite in the residual mineral assemblage of experiment CPL14 is due to its complete breakdown yielding potassium, and probably H₂O, to the melt. Because the melt is extremely poor in most of the other major components found in phlogopite (i.e. SiO₂, Al₂O₃, and TiO₂), it is plausible that these components, also released by the breakdown of phlogopite, are used to form garnet as an additional product (together with liquid) of the melting reaction. This suggestion is consistent with the

Table 5.3: Composition of quench carbonate analyzed in sandwich experiment CPL14 performed at 1100°C and 3.0 GPa.

<u>Quench</u> <u>alkali- and calcium-rich carbonate</u> (analysis with focused beam)			
	(wt%)		(wt%)
SiO ₂	0.56		2.46
TiO ₂	0.22		0.64
Al ₂ O ₃	0.03		0.23
FeO*	6.56		6.59
MnO	0.36		0.29
MgO	9.17		8.51
CaO	25.03		26.87
Na ₂ O	8.85		7.80
K ₂ O	10.50		11.15
Total	61.28		64.54
X_{MgFe_{tot}}	0.71		0.70

Notes : FeO* refers to the total Fe expressed as FeO. X_{MgFe_{tot}} is Mg/(Mg+Fe_{total}).

Table 5.4: Microprobe analyses of melt (quench dolomite + quench alkali-carbonate) in large melt pools of sandwich experiment CPL14 (with S-DOL middle layer) performed at 1100°C and 3.0 GPa.

	<u>Melt-1</u>	<u>Melt-2</u>	<u>Melt-3</u>	<u>Melt-4</u>	<u>Melt-5</u>
Beam diameter	10µm	15µm	20µm	20µm	25µm
SiO ₂	1.02	1.44	1.64	1.31	1.54
TiO ₂	0.44	0.51	0.48	0.36	0.51
Al ₂ O ₃	0.18	0.15	0.18	0.14	0.17
FeO*	3.45	4.12	4.39	3.70	4.19
MnO	0.15	0.16	0.20	0.18	0.13
MgO	15.17	14.33	13.86	14.97	14.96
CaO	25.14	21.47	22.11	25.59	23.39
Na ₂ O	7.87	10.00	9.75	6.05	7.65
K ₂ O	3.46	4.78	4.25	3.19	3.85
Total	56.88	56.94	56.86	55.49	56.39
X _{MgFe_{tot}}	0.89	0.86	0.85	0.88	0.86

Notes : FeO* refers to the total Fe expressed as FeO. X_{MgFe_{tot}} is Mg/(Mg+Fe_{total}).

interpretation proposed in section 5.2.6 and would explain the high modal abundance and distinct compositional characteristics of garnet found in the standard experiments on CPL at suprasolidus conditions, especially the high TiO_2 content (Figure 5.4).

In conclusion, because the sandwich experiment CPL14 did not yield the same residual mineral assemblage as that of the standard experiment CPL10, the observed melt composition in CPL14 cannot be truly representative of the ideal partial melt in equilibrium with CPL at 1100°C. However, the results strongly suggest that the ideal equilibrium partial melt composition is mainly controlled by the melting of dolomite (highly dolomitic CO_2 -rich liquid) and is characterized by a significant amount of potassium supplied by phlogopite in a reaction in which garnet is an essential product. Moreover, the absence of residual hydrous minerals in CPL14, implies that water released by phlogopite breakdown probably enters into the dolomitic melt.

5.3.3 Sandwich experiment on CPL using S/P-DOL as a middle layer

Based on the results of the previous sandwich experiment (CPL14), a significant amount of potassium (K_2O : 4.36 wt%; Table 5.2) was added to a new synthesized mixture (S/P-DOL; Table 3.1) used as a middle layer for sandwich experiment CPL16. As in the PLZ experiments (section 4.3.2), phlogopite

181

is the only supplier of potassium and water, thus the H_2O/K_2O (weight ratio) in the S/P-DOL mixture was fixed at 0.38; a value typical of a hydrous mica. The resulting composition of S/P-DOL is presented in Table 5.2.

The residual mineral assemblage of the sandwich experiment using CPL and S/P-DOL in the proportion 88:12 (Table 5.1; Experiment CPL16) consists of olivine, orthopyroxene, clinopyroxene, garnet and phlogopite and is therefore identical to that of the standard experiment also performed at 1100°C (Table 5.1; Experiment CPL10). Furthermore, there are no major differences in the chemical composition of the corresponding residual minerals between CPL16 and CPL10 (Table 5.5). The composition of the equilibrated liquid in sandwich experiment CPL16 should, therefore, be reasonably close to the ideal partial melt in equilibrium with CPL at 1100°C.

In CPL16, the melt has heavily infiltrated the CPL peridotitic material. Backscatter electron images of the largest melt pools show a quench assemblage of large elongated dolomite grains and small acicular alkali-carbonate crystals. Four defocused beam microprobe analyses (15-30 μm diameter) were done in order to estimate the melt composition (Table 5.6). The general compositional characteristics of the melt are a strong dolomitic affinity ($CaO > 20$ wt% and $MgO \approx 15$ wt%) with very low contents of SiO_2 (0.57-2.57 wt%), Al_2O_3 (0.17-0.72 wt%) and TiO_2 (0.08-0.38 wt%). The melt contains a significant amount of

Table 5.5: Comparison of the composition of the minerals in the standard experiment CPL10 and in the sandwich experiment CPL16.

	<u>Olivine</u>		<u>Orthopyroxene</u>	
	<u>CPL10</u>	<u>CPL16</u>	<u>CPL10</u>	<u>CPL16</u>
SiO ₂	40.42	40.69	55.89	56.23
TiO ₂	0.00	0.02	0.02	0.02
Al ₂ O ₃	0.00	0.03	3.03	2.91
Cr ₂ O ₃	0.05	0.03	0.32	0.27
FeO _{total}	9.02	8.72	6.09	6.00
MnO	0.04	0.20	0.02	0.19
MgO	50.25	50.16	33.77	33.80
CaO	0.09	0.14	0.59	0.60
Na ₂ O	0.00	0.00	0.00	0.00
K ₂ O	0.00	0.00	0.00	0.00
Total	99.87	99.99	99.73	100.02

	<u>Clinopyroxene</u>		<u>Phlogopite</u>	
	<u>CPL10</u>	<u>CPL16</u>	<u>CPL10</u>	<u>CPL16</u>
SiO ₂	52.59	52.95	37.29	38.18
TiO ₂	0.08	0.09	5.70	4.87
Al ₂ O ₃	3.71	3.50	16.90	17.13
Cr ₂ O ₃	0.55	0.51	0.31	0.24
FeO _{total}	2.86	2.82	4.51	4.96
MnO	0.06	0.16	0.03	0.08
MgO	16.63	16.38	19.88	20.08
CaO	22.37	22.33	0.63	0.26
Na ₂ O	0.92	0.81	0.12	0.17
K ₂ O	0.04	0.00	9.46	9.76
Total	99.81	99.55	94.83	95.73

	<u>Garnet</u>	
	<u>CPL10</u>	<u>CPL16</u>
SiO ₂	41.34	41.44
TiO ₂	1.76	1.41
Al ₂ O ₃	21.26	20.96
Cr ₂ O ₃	1.27	1.39
FeO _{total}	6.58	7.55
MnO	0.27	0.34
MgO	18.90	19.19
CaO	7.99	7.56
Na ₂ O	0.00	0.00
K ₂ O	0.00	0.00
Total	99.37	99.84

Table 5.6: Microprobe analyses of melt (quench dolomite + quench alkali-carbonate) in large melt pools of sandwich experiment CPL16 (with S/P-DOL middle layer) performed at 1100°C and 3.0 GPa.

	<u>Melt-1</u>	<u>Melt-2</u>	<u>Melt-3</u>	<u>Melt-4</u>
Beam diameter	15µm	25µm	20µm	30µm
SiO ₂	2.57	0.95	0.57	1.28
TiO ₂	0.72	0.23	0.17	0.30
Al ₂ O ₃	0.38	0.17	0.08	0.23
FeO*	4.54	3.18	3.10	3.57
MnO	0.16	0.20	0.17	0.14
MgO	15.12	14.72	15.08	14.75
CaO	21.60	28.35	27.03	27.22
Na ₂ O	4.93	2.67	3.58	3.04
K ₂ O	7.01	3.50	4.86	4.27
Total	57.03	53.97	54.64	54.80
X _{MgFe_{tot}}	0.86	0.89	0.90	0.88

Notes : FeO* refers to the total Fe expressed as FeO. X_{MgFe_{tot}} is Mg/(Mg+Fe_{total}).

304

alkalies (> 5 wt%), even though there are some variations in their abundance between different analyses. These variations are probably due to the different amount of the distinct quench products included in each microprobe analysis. The K_2O/Na_2O is, nevertheless, quite constant with values ranging from 1.31 to 1.42. The $X_{MgFe_{tot}}$ is very high (0.86-0.90). Although, this can be partially explained by iron loss to the capsule, Wallace and Green (1988) and Green and Wallace (1988) have argued that Mg/Fe fractionation between solid silicates ($X_{MgFe_{tot}} \approx 0.89$) and alkaline dolomitic carbonatite melt ($X_{MgFe_{tot}} \approx 0.85$) is significantly smaller than for silicate melt, at least in the carbonated amphibole-bearing peridotitic system that they investigated.

The estimated melt composition from CPL16 (Table 5.6) is believed to represent a relatively good approximation of the CO_2 -rich partial melt in equilibrium with the phlogopite- and garnet-bearing lherzolitic residual assemblage in the CPL system at 3.0 GPa and 1100°C.

5.4 Interaction experiments with HAR and WHR protoliths

The objective of these experiments, as was the case with SILMET (section 4.4), was to look at how reactive the partial melt composition in equilibrium with CPL at 1100°C and 3.0 GPa is towards harzburgitic and wehrlitic materials (HAR and WHR; Table 3.2) at 1000°C and 2.0 GPa. For this

purpose, a mixture (CARMET; Table 3.1) of composition representative of the estimated CPL equilibrium partial melt (Table 5.6) was synthesized and then mixed with each of the two peridotitic protoliths (HAR and WHR) in the weight proportion 10:90. The composition of CARMET and of the two mixtures (HAR-CARMET, WHR-CARMET) can be found in Table 5.7.

The two mixtures were subjected to a pressure of 2.0 GPa and a temperature of 1000°C. The experimental results, compared to those of the standard experiments on HAR and WHR, already discussed in section 4.4, are summarized in Table 5.8. The chemical composition of the mineral grains analyzed for each experiments are presented in Appendix B4.

In addition to olivine and orthopyroxene, typical of HAR, the HAR-CARMET interaction experiment shows a considerable amount of clinopyroxene distributed homogeneously throughout the charge. The clinopyroxene is an aluminian-chromian diopside (Morimoto, 1988) with a Wo proportion of 45:47 and an average Na₂O content of 0.98 wt%. Microprobe X-Ray scanning for K and Al show that these two elements are concentrated in the same very small areas. Therefore, because K and Al are major components of phlogopite and CARMET contains a significant amount of water (Table 5.7), phlogopite could be a stable phase in the assemblage, although no crystals could be unambiguously analyzed. The possibility that these small potassium- and aluminium-rich grains are quenched cannot, however, be discarded. Finally, a free CO₂ vapor phase is probably

Table 5.7: Bulk composition of CARMET, HAR+CARMET and WHR+CARMET.

	CARMET	HAR: 90wt% CARMET: 10wt%	WHR: 90wt% CARMET: 10wt%
	(wt%)	(wt%)	(wt%)
SiO ₂	1.16	43.59	38.21
TiO ₂	0.28	0.04	0.06
Al ₂ O ₃	0.21	1.39	2.15
Cr ₂ O ₃	0.00	0.14	0.59
FeO*	4.25	7.11	7.28
MnO	0.15	0.13	0.12
MgO	15.16	39.31	38.37
NiO	0.00	0.14	0.20
CaO	28.57	3.11	7.81
Na ₂ O	2.94	0.31	0.48
K ₂ O	3.99	0.40	0.40
H ₂ O	1.61	0.16	0.16
CO ₂	41.69	4.17	4.17
Total	100.01	100.00	100.00
X_{MgFe_{tot}}	0.86	0.91	0.90

Notes : The composition of CARMET was based on an average of analyses Melt-2 and Melt-4 of Table 5.6. FeO* refers to the total Fe expressed as FeO. X_{MgFe_{tot}} is Mg/(Mg+Fe_{total}).

Table 5.8: Results of standard experiments on HAR and WHR and interaction experiments with CARMET.

Run#	T (°C)	Time (hours)	Weight Prop.	Phases observed
HAR	1000	28	-----	ol,opx
HAR-CARMET	1000	20	90:10	ol,opx,cpx,phl(?),CO ₂
WHR	1000	28	-----	ol,cpx,sp
WHR-CARMET	1000	20	90:10	ol,cpx,sp,cc,phl(?),CO ₂ (?)

Notes : Weight Prop. is the respective weight proportion of the different materials used in the interaction experiments. Cryptocrystals refers to a crystalline assemblage whose specific crystals, due to their small size, could not be identified. All runs done in Ag₅₀Pd₅₀ capsules. ol: olivine; opx: orthopyroxene; cpx: clinopyroxene; sp: spinel; phl: phlogopite; cc: calcite; CO₂: free vapor.

present because no carbonates were observed.

As in the WHR standard experiment, the WHR-CARMET interaction experimental product consists essentially of olivine, clinopyroxene and spinel. However, a carbonate, rich in the calcite component (CaCO_3 : 89.80 mol%) is an additional phase in the product of the WHR-CARMET experiment. Moreover, following the same argument developed for HAR-CARMET, phlogopite is believed to be part of the stable assemblage in WHR-CARMET.

Based on these results, it can be concluded that, at the experimental conditions used (2.0 GPa, 1000°C for 20 hours), CARMET appears to be strongly reactive towards harzburgite and wehrlite. An attempt to characterize the nature of the reactions occurring between CARMET and HAR or WHR is presented in Chapter 6.

5.5 Summary

At 3.0 GPa, from 900°C up to the solidus, estimated at a temperature between 1050° and 1075°C, the stable assemblage for the CPL composition changes from a magnesite-bearing phlogopite lherzolite (< 1025°C) to a dolomite-bearing phlogopite lherzolite. From the solidus, up to at least 1150°C, a CO_2 -rich melt coexists with a residual phlogopite- and garnet-bearing lherzolitic assemblage.

At 1100°C, the equilibrium partial melt, in addition to its main dolomitic nature, contains alkalies, has a

significant but relatively low water content. K and Na are supplied by the partial breakdown of phlogopite and clinopyroxene respectively. However, because of the extremely low solubility, in the CO₂-rich melt, of the other major components released by the breakdown of phlogopite (e.g. SiO₂, Al₂O₃ and TiO₂), a titanium-rich pyrope becomes an essential constituent of the residual mineral assemblage coexisting with the dolomitic melt.

Such an alkali-bearing dolomitic melt composition (CARMET) is quite reactive towards harzburgitic and wehrlitic materials at 2.0 GPa and 1000°C. The final product of the interaction between CARMET and harzburgite appears to be a phlogopite lherzolite coexisting with free CO₂ vapor. On the other hand, the mineral assemblage resulting from the interaction of CARMET with a spinel-bearing wehrlite could be a calcite-bearing phlogopite wehrlite.

CHAPTER 6

NATURE OF THE MELTING AND METASOMATIC REACTIONS

6.1 Melting reactions in PLZ and CPL

The melting experiments performed in this study provide information on the chemical evolution of the mineral assemblages and on the composition of liquids formed in the phlogopite-present melting intervals of a phlogopite lherzolite (PLZ; Chapter 4) and a carbonated phlogopite lherzolite (CPL; Chapter 5) at 3.0 GPa. In order to characterize the nature of the reactions involved in the partial melting of these mantle sources (PLZ and CPL) the variations in the weight proportion of the phases stable throughout the investigated temperature ranges were calculated by least-squares mass balance approximations (Bryan et al., 1969).

6.1.1 Generalized melting reaction and degree of partial melting at 1225°C in the PLZ source

Two mass balance calculations were performed for the PLZ mantle source. One calculation was done using the phase assemblage observed at 1225°C, the temperature at which the

equilibrium partial melt composition (Table 4.4; analysis II) was estimated by sandwich experiments (section 4.3). The second calculation was done using the compositions of the minerals (Appendix B2) from a standard experiment on PLZ at subsolidus conditions (1125°C; Table 4.1; Experiment PLZ 31). The oxides taken into consideration were SiO₂, TiO₂, Al₂O₃, FeO_{total}, MgO, CaO, Na₂O, and K₂O. In addition to the stable phases, a pure FeO component was introduced in order to correct for iron loss to the capsule. The results of the calculations are summarized in Table 6.1 and presented in more detail in Appendix C. The low sums of least-squares (0.001 and 0.006) indicate very good solutions.

Based on the results of these calculations, PLZ yields 7 wt% of melt at 1225°C and phlogopite (1.8 wt%) is part of the residual mineral assemblage. In Figure 6.1, the percentages of the different phases at subsolidus condition (1125°C) and at 7 wt% of partial melting (1225°C), as calculated by mass balance methods, are compared. Based on the variations in the proportions of the different phases, a generalized melting reaction describing the phlogopite melting interval in PLZ would be (in weight proportion):

3.8 Phlogopite + 3.7 Clinopyroxene + 0.8 Garnet =>

1.1 Olivine + 7.1 Liquid

[6.1]

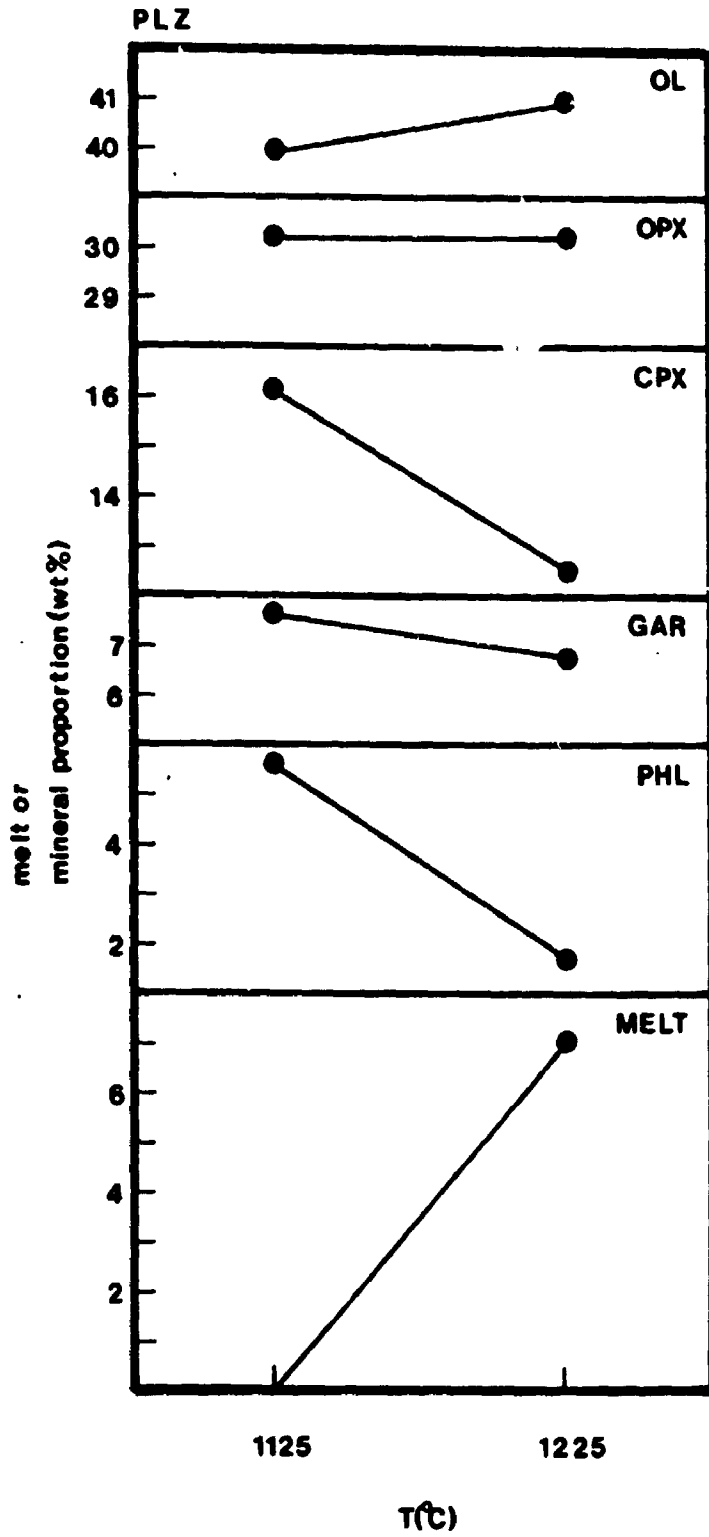
In this reaction, the major participants are phlogopite and

Table 6.1: Results of the least-squares mass balance calculations on PLZ at subsolidus and suprasolidus conditions.

	<u>PLZ31 (1125°C)</u>		<u>PLZ30 (1225°C)</u>	
	(wt%)	Rec. (wt%)	(wt%)	Rec. (wt%)
Olivine	40.0	40.2	41.0	41.3
Orthopyroxene	30.2	30.4	30.2	30.4
Clinopyroxene	16.1	16.2	12.5	12.6
Garnet	7.6	7.6	6.8	6.8
Phlogopite	5.6	5.6	1.8	1.8
Melt	0.0	0.0	7.1	7.1
FeO	0.4		0.6	
Total	99.9	100.0	100.0	100.0
Least squares	0.001		0.006	

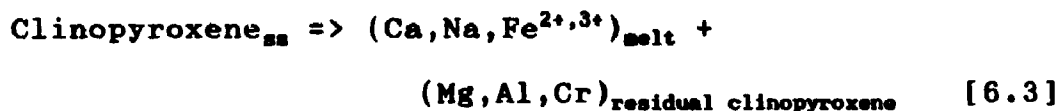
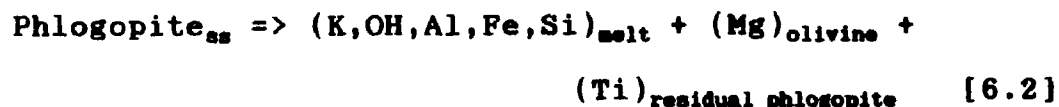
Notes : The oxides taken into consideration in the mass balance calculations are SiO₂, TiO₂, Al₂O₃, FeO_{total}, MgO, CaO, Na₂O, and K₂O. For the calculation at 1125°C, the average compositions of all the minerals analyzed in experiment PLZ31 (Appendix B2) were used. At 1225°C, the average composition of the mineral analyzed in experiment PLZ30 and the melt composition estimated in sandwich experiment PLZ40 (Table 4.4; analysis II) were used. The pure FeO component is introduced in order to correct for iron loss. Rec. is the mineral proportion recalculated to 100 weight %, without the pure FeO component. Least squares is the summation of the square of the difference for each oxide between the real composition of PLZ (Table 3.2) and the calculated one.

Figure 6.1 : Calculated phase proportions (in wt%) in the PLZ composition at subsolidus conditions (1125°C) and at 7.1 wt% of partial melting (1225°C). The lines joining the calculated proportions were drawn to emphasize the variation between the two temperatures but do not express the real intermediate proportions. OL: olivine; OPX: orthopyroxene; CPX: clinopyroxene; GAR: garnet; PHL: phlogopite.



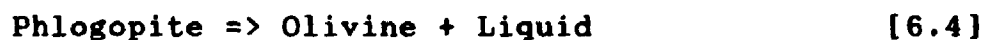
188

clinopyroxene, and the following simplified relations describe how these two minerals define the characteristic chemical nature of the melt:



where ss means solid solution and (x)_y indicates that element x is preferentially incorporated in phase y.

The formation of olivine is consistent with the simple reaction describing the incongruent melting of phlogopite (e.g. Yoder and Kushiro, 1969):



The fact that the amount of orthopyroxene is constant from 1125° to 1225°C (Figure 6.1) suggests minor participation of this mineral in the melting reaction at 3.0 GPa. This is in agreement with the experimental results of Modreski and Boettcher (1973) on the melting relationships of phlogopite in the presence of enstatite. They suggested that (p. 392): "With increasing pressure a progressively smaller proportion of enstatite participates in the [melting] reaction..."

Finally, it should be pointed out that the highest residual

value in the mass balance calculation at 1225°C lies in the amount of Na₂O (Appendix C). This possibly reflects an overestimation of the abundance of Na₂O in the melt composition obtained by sandwich experiment (Table 4.4; Analysis II).

- Some normative aspects of the equilibrium partial melt in the PLZ system at 3.0 GPa and 1225°C

The normative composition of the liquid in equilibrium with PLZ at 1225°C and 3.0 GPa was calculated and the results are presented in Table 6.2. The chemical composition used (Table 4.4, analysis II) was corrected for FeO assuming a $K_D^{olivine/liquid}(Fe/Mg)$ of 0.3 (section 4.3). Because the oxidation state of Fe has an important effect on the result of the norm calculation (e.g. Cox et al., 1979), the amount of Fe₂O₃ was approximated using the equation proposed by Kress and Carmichael (1988) allowing the estimation of the iron oxidation state of silicate melts as a function of ln fO₂, temperature and composition. The oxygen fugacity conditions estimated for the experiments using the PLZ system (section 3.4.2; log fO₂ = -7.49) were used in the calculation. The CIPW norm calculation rules were followed except that TiO₂ was allocated to both ilmenite (FeTiO₃) and ulvospinel (Fe₂TiO₄) (cf. Wallace and Carmichael, 1989). The effect of this small modification is insignificant on the amount of normative silicate minerals.

The major normative silicate minerals present in the

Table 6.2: Normative composition of the melt in equilibrium with PLZ at 3.0 GPa and 1225°C.

<u>Normative minerals</u>			
	(wt%)		(wt%)
SiO ₂	47.47	Orthoclase	1.11
TiO ₂	1.66	Anorthite	6.12
Al ₂ O ₃	10.87	Leucite	23.83
Cr ₂ O ₃	0.27	Nepheline	7.67
Fe ₂ O ₃	1.91	Diopside	40.29
FeO	6.04	Olivine	13.99
MnO	0.15	Magnetite	2.78
MgO	13.08	Ilmenite	2.11
CaO	11.48	Ulvospinel	1.55
Na ₂ O	1.73		
K ₂ O	5.34		
<hr/>			
Total	100.00		


Notes: The composition of the partial melt in equilibrium with PLZ at 3.0 GPa and 1225°C is the one given in Table 4.4 (analysis II) whose FeO content was then corrected assuming a $K_D^{\text{olivine/liquid}}(\text{Fe/Mg})$ of 0.3. The amount of Fe₂O₃ was calculated using the equation proposed by Kress and Carmichael (1988) assuming a log f_{O_2} of -7.49 and a temperature of 1225°C (see details in text), and the total was recalculated to 100 wt% on an anhydrous basis.

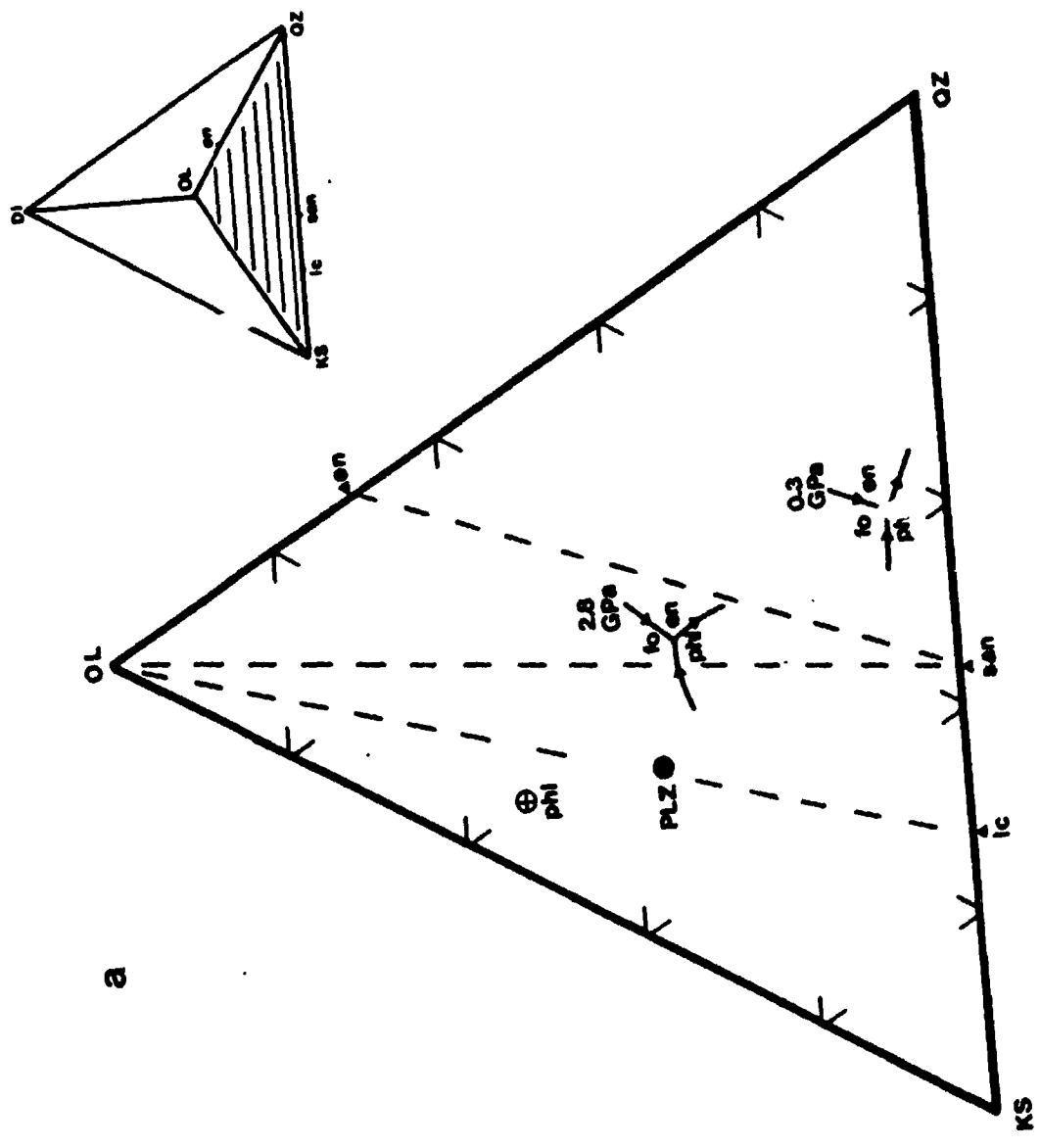
liquid in equilibrium with PLZ at 3.0 GPa and 1225°C are diopside, leucite, olivine, nepheline and anorthite (Table 6.2), reflecting the major clinopyroxene and phlogopite components of the melt (sections 6.1.1). Because the PLZ model mantle source consists essentially of olivine, orthopyroxene, clinopyroxene and phlogopite (with garnet), the quaternary system diopside-olivine-kalsilite-quartz is a reasonable analogue. Thus, the normative composition of the partial melt in equilibrium with PLZ is plotted on two projections of this quaternary in Figure 6.2: the olivine-kalsilite-quartz plane projected from diopside (Figure 6.2a), and the diopside-olivine-leucite plane projected from quartz (Figure 6.2b).

On the olivine-kalsilite-quartz plane (Figure 6.2a), the phase fields near the minimum melt composition for the simple water-saturated forsterite-kalsilite-silica (Fo-Ks-Qz) system at 0.3 GPa (Luth, 1967) and at 2.8 GPa (Gupta and Green, 1988) are shown. With increasing pressure, the major changes observed in this simple system are the important expansions of the enstatite and phlogopite fields at the expense of the olivine field (Figure 6.2a).

In comparison to the composition of the 2.8 GPa minimum in the Fo-Ks-Qz system (Gupta and Green, 1988), the equilibrium partial melt in the PLZ composition at 3.0 GPa and 1225°C (this study) is shifted towards more silica-undersaturated composition (Figure 6.2a). Nevertheless, the relative importance of the phlogopite and olivine fields

Figure 6.2 : Normative composition (wt%) of the partial melt in equilibrium with PLZ at 3.0 GPa and 1225°C in the quaternary system diopside(DI)-olivine(OL)-kalsilite(KS)-quartz(QZ).

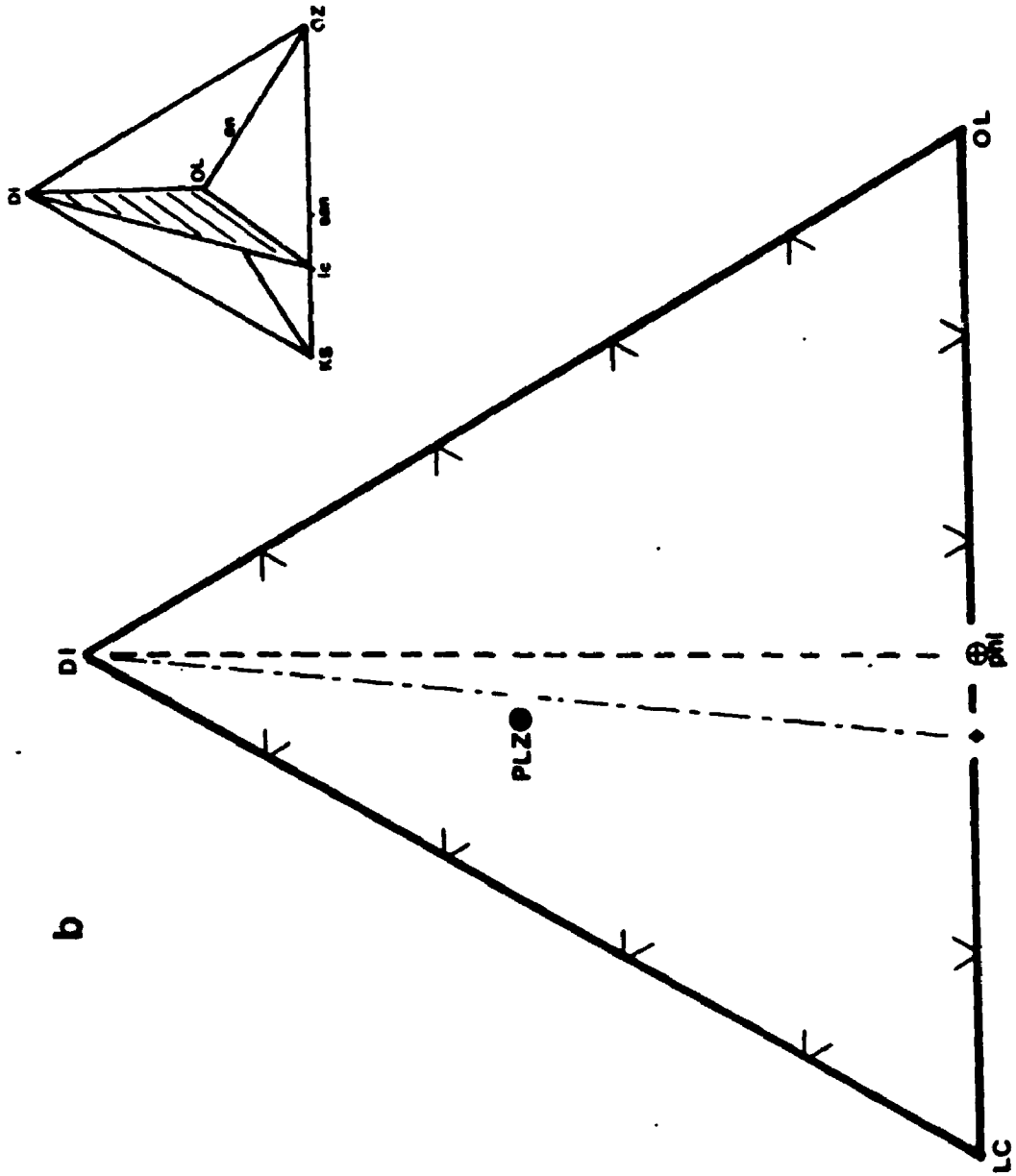
a) The equilibrium partial melt (PLZ ) is plotted on the OL-KS-QZ plane projected from DI. The phase stability fields near the minimum melt composition for the simple vapour-present forsterite-kalsilite-silica-H₂O system at 3.0 GPa (Luth, 1967) and at 2.8 GPa (Gupta and Green, 1988) are also shown. en: enstatite; lc: leucite; san: sanidine; phl: pure phlogopite end-member composition.



a

Figure 6.2 : (Continued)

b) the equilibrium partial melt (PLZ \blacksquare) is plotted on the DI-OL-LC plane projected from QZ. The filled diamond (\blacklozenge) is the minimum melt composition for the vapour-present forsterite-kalsilite-silica-H₂O system at 2.8 GPa (Gupta and Green, 1988). phl was backtrack on the OL-LC join along the phlogopite-quartz join.



b

148

appears to be quite comparable (Figures 6.2a and b), suggesting that the relation "phlogopite \rightarrow olivine + liquid" is equivalent in the two systems (PLZ and Fo-Ks-Qz-H₂O). The enstatite field seems, however, significantly more important in the PLZ composition (Figure 6.2a), reflecting the very minor participation of orthopyroxene in the reaction defining the phlogopite-present melting interval of PLZ. Although the comparison should not be taken too far because the simple Fo-Ks-Qz system does not contain diopside, the apparent difference in the size of the enstatite field could result from the fact that the experiments on the simple system were performed at vapour-present (H₂O) conditions in contrast to the experiments on the PLZ composition. H₂O is known to enlarge the stability fields of less-polymerized minerals (e.g. olivine) at the expense of more-polymerized ones (e.g. orthopyroxene) (e.g. Kushiro, 1969, 1972; Mysen, 1977).

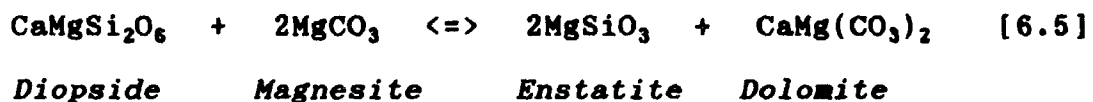
6.1.2 Generalized melting reaction and degree of partial melting at 1100°C in the CPL source

The variations in the weight proportions of the minerals and melt in the investigated temperature interval of CPL were also calculated by least-squares mass balance approximations using the phase assemblages observed at 1000°C (magnesite field), 1050°C (dolomite field), and finally 1100°C, the temperature at which the equilibrium

144

partial melt composition (Table 5.6) was estimated by sandwich experiments (section 5.3). The oxides considered were SiO₂, TiO₂, Al₂O₃, FeO_{total}, MgO, CaO, Na₂O and K₂O. The results of the calculations are summarized in Table 6.3 and shown in more detail in Appendix C. The sums of least squares are low (≥ 0.076) indicating very good solutions. Figure 6.3 illustrates the major variations in the phase proportions between each field.

From the magnesite to the dolomite field, the only significant change, besides the transition from magnesite to dolomite, is an increase in the proportion of orthopyroxene and a decrease in the amount of clinopyroxene. These variations simply reflect the following reaction:



described in section 5.2.1.

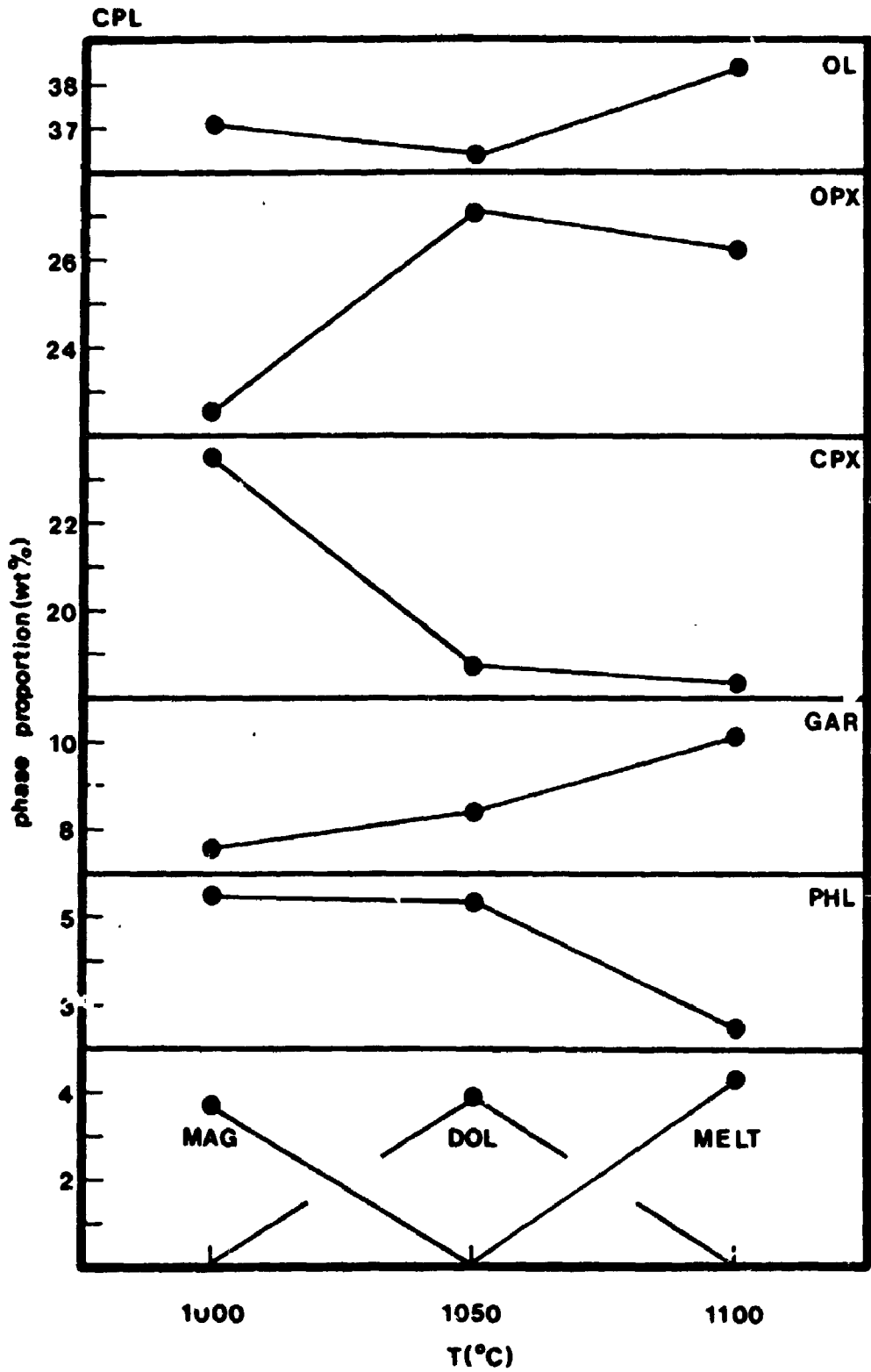
At 1100°C, in the liquid field, CPL yields 4 wt% of alkali-rich dolomitic melt (Table 6.3) and, compared to the subsolidus dolomite field, the proportions of phlogopite, clinopyroxene and orthopyroxene decrease, whereas those of garnet and olivine increase. Evidently dolomite has completely disappeared at 1100°C. Based on these varying proportions of the different phases, and on the compositional characteristics of the minerals (section 5.2) and melt (sections 5.3.2, 5.3.3), the reactions controlling

Table 6.3: Results of the least-squares mass balance calculations on CPL in the magnesite field, the dolomite field and at suprasolidus conditons.

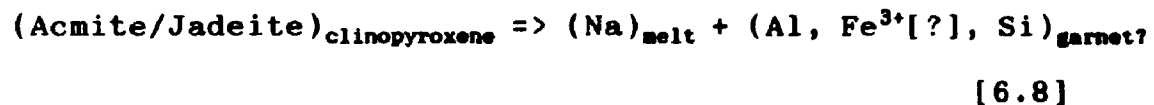
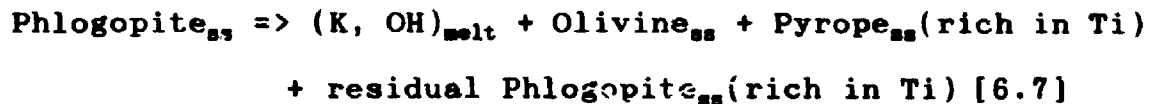
	<u>CPL11 (1000°C)</u> Magnesite field (wt%)	<u>CPL9(1050°C)</u> Dolomite field (wt%)	<u>CPL16(1100°C)</u> Liquid field (wt%)
Olivine	37.1	36.4	38.4
Orthopyroxene	22.6	27.1	26.3
Clinopyroxene	23.5	18.8	18.4
Garnet	7.6	8.4	10.1
Phlogopite	5.5	5.4	2.5
Magnesite	3.7		
Dolomite		3.9	
Melt			4.3
Total	100.0	100.0	100.0
Least squares	0.076	0.065	0.005

Notes : The oxides taken into consideration in the mass balance calculations are SiO₂, TiO₂, Al₂O₃, FeO_{total}, MgO, CaO, K₂O, CO₂. In general, the average compositions of the minerals analyzed in each of the experiment (CPL11, CPL9, CPL16) were used in the calculations. However, for the calculation of CPL11 and CPL9, because no garnet could be analyzed, the average composition of garnet in PLZ31 (1100°C) was used. For the calculation of CPL16, the melt composition used was Melt-1 (Table 5.6). Least squares is the summation of the square of the difference for each oxide between the real composition of CPL (Table 3.2) and the calculated one.

Figure 6.3 : Calculated phase proportions (in wt%) in the CPL composition for the subsolidus magnesite field (1000°C), the subsolidus dolomite field (1050°C) and at 4.3 wt% partial melting (1100°C). The lines joining the calculated proportions were drawn to emphasize the variations between the different fields but do not express the real intermediate proportions. OL: olivine; OPX: orthopyroxene; CPX: clinopyroxene; GAR: garnet; PHL: phlogopite; MAG: magnesite; DOL: dolomite.



the phlogopite-present melting interval of CPL are believed to be relatively well defined by the following simplified relations:



where ss means solid solution. These expressions are not actual reactions but simple relations describing the distribution of the components released by the partial breakdown of the major minerals participating in the melting reaction. Relation [6.6] describes simply the complete melting of dolomite at the solidus giving the strong dolomitic affinity to the carbonatitic melt. Relation [6.7] is an attempt to describe the partial breakdown of phlogopite to yield K and OH to the melt. SiO₂, Al₂O₃, MgO, FeO and TiO₂ also released from the breakdown of phlogopite, are combined according to their relative proportions to form olivine and pyrope. Finally, the residual phlogopite retains preferentially a certain amount of TiO₂. Relation [6.8] expresses the possible release of the acmite and/or jadeite

component of clinopyroxene which supplies sodium to the melt. If this is acceptable, a decrease in the sodium content of clinopyroxene should be expected when the solidus is crossed. As was discussed in section 5.2.4, no such variation was observed. Relation [6.8] is therefore highly hypothetical. However, especially at subsolidus conditions, the sodium content of clinopyroxene is too low to account for the total amount of sodium. It is consequently suspect that the total transfer of sodium, added in the form of carbonate, into the clinopyroxene structure was probably not achieved at subsolidus conditions. As briefly commented on in section 5.3.2, in their experimental determination of primary carbonatite magma composition, Wallace and Green (1988) explain the sodic dolomitic character of the carbonatite melt by an equivalent relation: "... the solidus is defined by the breakdown of dolomite and the sodium-rich jadeitic component of clinopyroxene to produce an aluminous phase plus melt" (p. 344).

6.1.3 Additional comments on the degree of partial melting

In the investigated melting intervals, olivine is always a major residual phase despite its relatively low abundance (~ 40 wt%) in the PLZ and CPL compositions. This implies that the melts are saturated in olivine. Therefore, an increase in the amount of olivine of the model mantle sources to values more comparable to those found in mantle

xenoliths (>60 vol%, e.g. Boyd, 1989, Figures 1, 2 and 4) should not greatly affect the compositional nature of the investigated melts (cf. Green and Ringwood, 1970; Jaques and Green, 1980). However, the melt fraction would be significantly lower in these more representative olivine-rich mantle sources. For example, the calculated melt fractions of 4 wt% in CPL at 1100°C, and 7 wt% in PLZ at 1225°C would represent about 2 and 3 wt% respectively in mantle sources containing 70 wt% olivine.

6.2 Metasomatic reactions in HAR and WHR

Based on the definition of Goldschmidt (1922), a process is characterized as metasomatic if an agent, be it a low-density fluid or a melt, clearly reacts with the original minerals of the solid protolith it infiltrates (section 1.1). In this context, in the interaction experiments performed in this study (sections 4.4 and 5.4), SILMET (Table 3.1) and CARMET (Table 3.1) can be seen as agents infiltrating harzburgitic (HAR) and wehrlitic (WHR) protoliths and the reactions occurring between SILMET or CARMET and HAR or WHR can be considered metasomatic.

To characterize the nature of these metasomatic reactions, least-squares mass balance methods (Bryan et al., 1969) were used to calculate the weight proportions of the different phases stable before and after each of the interaction experiments. Because phlogopite is suspected to

be a stable product of the interaction experiments with CARMET but could not be analyzed (sections 5.4 and 6.2.2), its composition was assumed. The chosen phlogopite composition is given in the footnotes of Table 6.4. The $X_{MgFe_{tot}}$ of the phlogopite was fixed to 0.90, a value equivalent to the ones for the bulk composition of the systems investigated (HAR-CARMET, WHR-CARMET; Tables 5.7). Secondly, the mica contains an equal amount of the phlogopite and eastonite end-member molecules reflecting the common cation substitution observed in trioctahedral micas: $Mg^{VI}Si^{IV} \Leftrightarrow Al^{VI}Al^{IV}$. Therefore, because a phase composition was assumed in the mass balance calculations, although the solutions yield low sums of least-squares, the results bear nevertheless greater uncertainties than those for the melting reactions.

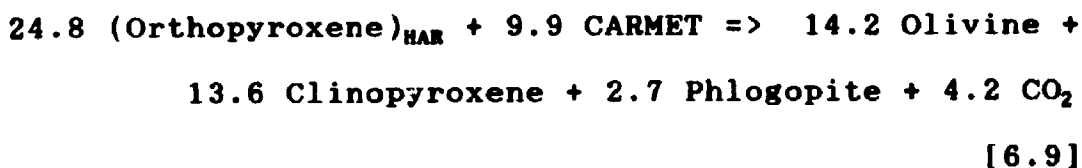
6.2.1 Metasomatic reactions involving CARMET

6.2.1.1 Metasomatic reactions between CARMET and HAR

In addition to olivine and orthopyroxene of the original harzburgitic protolith, the product of the HAR-CARMET interaction experiment contains clinopyroxene and possibly phlogopite (section 5.4). Moreover, the absence of carbonates suggests the existence of a CO_2 -rich low-density fluid.

The proportions of the different phases stable before

and after interaction, as calculated by least-squares approximations, are summarized in Table 6.4 and presented in more details in Appendix C. The solutions are very good as shown by the low sums of the squares of the residuals (0.004 and 0.079). The metasomatic reaction between CARMET and HAR, obtained from these calculations, is (in weight proportion):



This reaction expresses how CARMET can efficiently transform the harzburgite protolith at 2.0 GPa and 1000°C. For every 10 g of CARMET infiltrating an harzburgitic protolith, 24.8 g of orthopyroxene are completely consumed to form metasomatic olivine, clinopyroxene and phlogopite. This important transformation of the protolith is directly related to the destabilization, in peridotitic systems, of a dolomitic melt, at pressures lower than 2.1 GPa (e.g. Wyllie and Rutter, 1986; Wallace and Green, 1988; Falloon and Green, 1989) to form a CO₂-rich low density fluid if the temperature is sufficiently high to allow the following well-documented reaction to proceed:

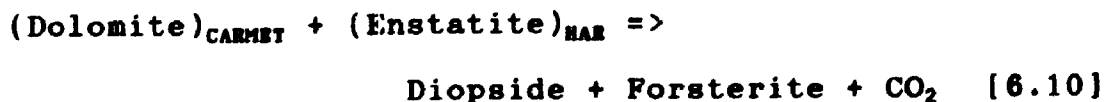


Table 6.4: Results of the least-squares mass balance calculations for the interaction experiment with HAR and CARMET

<u>HAR-CARMET</u>				
	<u>before interaction</u>		<u>after interaction</u>	
	(wt%)	Rec. (wt%)	(wt%)	Rec. (wt%)
Olivine	45.6	45.6	59.7	59.8
Orthopyroxene	44.5	44.5	19.6	19.7
Clinopyroxene			13.6	13.6
Phlogopite			2.7	2.7
CO ₂ vapor			4.2	4.2
CARMET	9.9	9.9		
FeO	0.1		0.2	
Total	100.1	100.0	100.0	100.0
Least-squares	0.004		0.079	

Notes : The oxides taken into consideration in the mass balance calculations are SiO₂, TiO₂, Al₂O₃, FeO_{total}, MgO, CaO, Na₂O, K₂O and CO₂. The composition of the minerals of the standard experiment on HAK (Appendix B4) were used together with the original composition of the CARMET mixture (Table 5.7) for the calculation of HAR-CARMET before interaction. Phlogopite has the following ideal composition (in wt%): SiO₂: 38.76; Al₂O₃: 17.33; FeO_{total}: 4.63; MgO: 23.40; K₂O: 11.05 and H₂O: 4.23. The pure FeO component is used in order to correct for iron loss. Rec. is the mineral proportion recalculated to 100 wt% without the pure FeO component. Least-squares is the summation of the squares of the differences for each oxide considered between the bulk composition of HAR-CARMET (Table 5.7) and the calculated one.

(e.g. Wyllie and Huang, 1976; Eggler, 1978; Brey et al., 1983; Wyllie et al., 1983; Wallace and Green, 1988). Because of the extremely low solubility of major elements in CO₂-rich low-density fluids (e.g. Schneider and Eggler, 1984, 1986; Eggler, 1987), CaO, MgO, K₂O, Na₂O and H₂O transported by the dolomitic melt (CARMET) are suddenly precipitated and, consequently, react strongly with the harzburgite (cf. Green and Wallace, 1988; Hunter and McKenzie, 1989; Ryabchikov et al., 1989a). The following simplified relations describe qualitatively how the components of CARMET and orthopyroxene are distributed to form the metasomatic mineral assemblage:

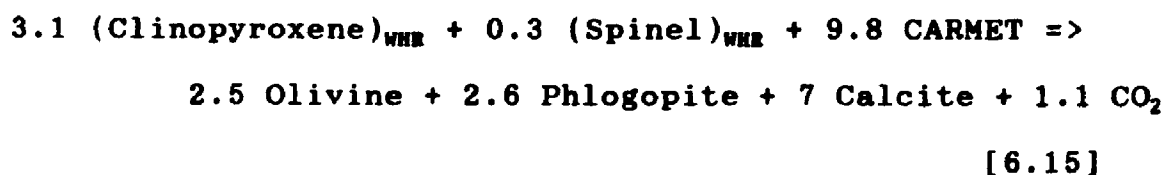


Green and Wallace (1988) have documented comparable metasomatic effects for a sodic-dolomitic melt formed in equilibrium with a pargasite-bearing lherzolite. They refer to the "ephemeral" nature of the melt to express the fact that about half of the original melt is lost as CO₂-rich fluid with the rest reacting with the solid phases of the protolith.

6.2.1.2 Metasomatic reactions between CARMET and WHR

In addition to clinopyroxene, olivine and spinel present in the original wehrlite (WHR), the resulting mineral assemblage of the WHR-CARMET interaction experiment contains a calcite solid solution ($\text{CaCO}_3 = 89.80 \text{ mol\%}$; Appendix B4) and possibly phlogopite (section 5.4).

Based on the proportions of the different phases stable before and after the experiment (Table 6.5 and Appendix C), as calculated by least-squares approximations, the estimated metasomatic reaction is (in weight proportion):

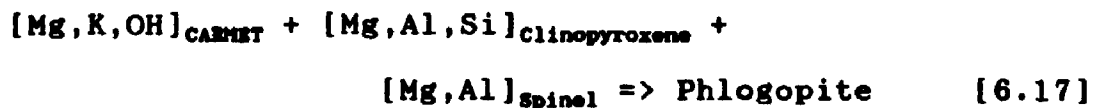


Compared with the interaction with HAR, CARMET is less efficient in transforming the mineralogy of the wehrlite protolith (WHR). Nevertheless, for every 10 g of CARMET, approximately 3.1 g of clinopyroxene and 0.3 g of spinel are consumed to form metasomatic olivine, phlogopite and calcite. The components of CARMET, clinopyroxene and spinel involved in the reaction are probably distributed following these qualitative relations:

Table 6.5: Results of the least-squares mass balance calculations for the interaction experiment with WHR and CARMET

<u>WHR-CARMET</u>				
	<u>before interaction</u>		<u>after interaction</u>	
	(wt%)	Rec. (wt%)	(wt%)	Rec. (wt%)
Olivine	65.4	65.7	67.8	68.2
Clinopyroxene	21.8	21.9	18.7	18.8
Spinel	2.6	2.6	2.3	2.3
Calcite			7.0	7.0
Phlogopite			2.6	2.6
CO ₂ vapor			1.1	1.1
CARMET	9.8	9.8		
FeO	0.4		0.5	
Total	100.0	100.0	100.0	100.0
Least-squares	0.049		0.137	

Notes : The oxides taken into consideration in the mass balance calculations are SiO₂, Al₂O₃, Cr₂O₃, FeO_{total}, MgO, CaO, Na₂O, K₂O and CO₂. The composition of the minerals of the standard experiment on WHR (Appendix B4) were used together with the original composition of the CARMET mixture (Table 5.7) for the calculation of WHR-CARMET before interaction. Phlogopite is an ideal composition presented in Table 6.4. The pure FeO component is used in order to correct for iron loss. Rec. is the mineral proportion recalculated to 100 wt% without the pure FeO component. Least-squares is the summation of the squares of the differences for each oxide considered between the bulk composition of WHR-CARMET (Table 5.7) and the calculated one.



6.2.1.3 Progressive metasomatism involving CARMET

In order to depict the progressive metasomatism caused by the infiltration of CARMET on a hypothetical mantle protolith at 2.0 GPa and 1000°C, the variations in the modal (volume) proportions of the main phases involved in the metasomatic reactions are shown on the well-known Olivine-Orthopyroxene-Clinopyroxene diagram (Streckeisen, 1973) in Figure 6.4 and on a [Olivine + Orthopyroxene]-Clinopyroxene-Phlogopite diagram in Figure 6.5. The transformation of the weight proportions, as calculated by mass balance methods (section 6.2.1.1) in volume proportions was done using the density of the magnesian end-member of olivine (Forsterite), orthopyroxene (Enstatite), clinopyroxene (Diopside) and mica (Phlogopite), and is, therefore, simply an approximation. The densities were calculated with the molar volume values given by Bermann (1988) and are presented in Table 6.6.

In Figures 6.4 and 6.5, the hypothetical protolith is an harzburgite with 70 vol% olivine and 30 vol% orthopyroxene. This is probably a realistic average of the proportions found in many mantle xenoliths of harzburgitic

001

Figure 6.4 : Effects of the progressive metasomatism of a hypothetical mantle protolith at 2.0 GPa and 1000°C caused by the infiltration of CARMET plotted in an olivine-orthopyroxene-clinopyroxene ternary diagram (in vol%). The hypothetical protolith (●) is a harzburgite with 70 vol% olivine and 30 vol% orthopyroxene. The metasomatic trend produced by the infiltration of CARMET is shown by a bold arrow graduated at intervals that indicate the amount of CARMET (in grams) per 100 g of harzburgitic protolith. When all the orthopyroxene is consumed, continued infiltration of CARMET in the olivine-rich wehrlite (Δ) causes formation of olivine, phlogopite and calcite at the expense of clinopyroxene (small bold arrow).

The thin arrows labelled with question marks (?) illustrate qualitatively the enrichment in clinopyroxene that would be produced by the infiltration of SILMET in different peridotitic rocks along the harzburgite-wehrlite trend.

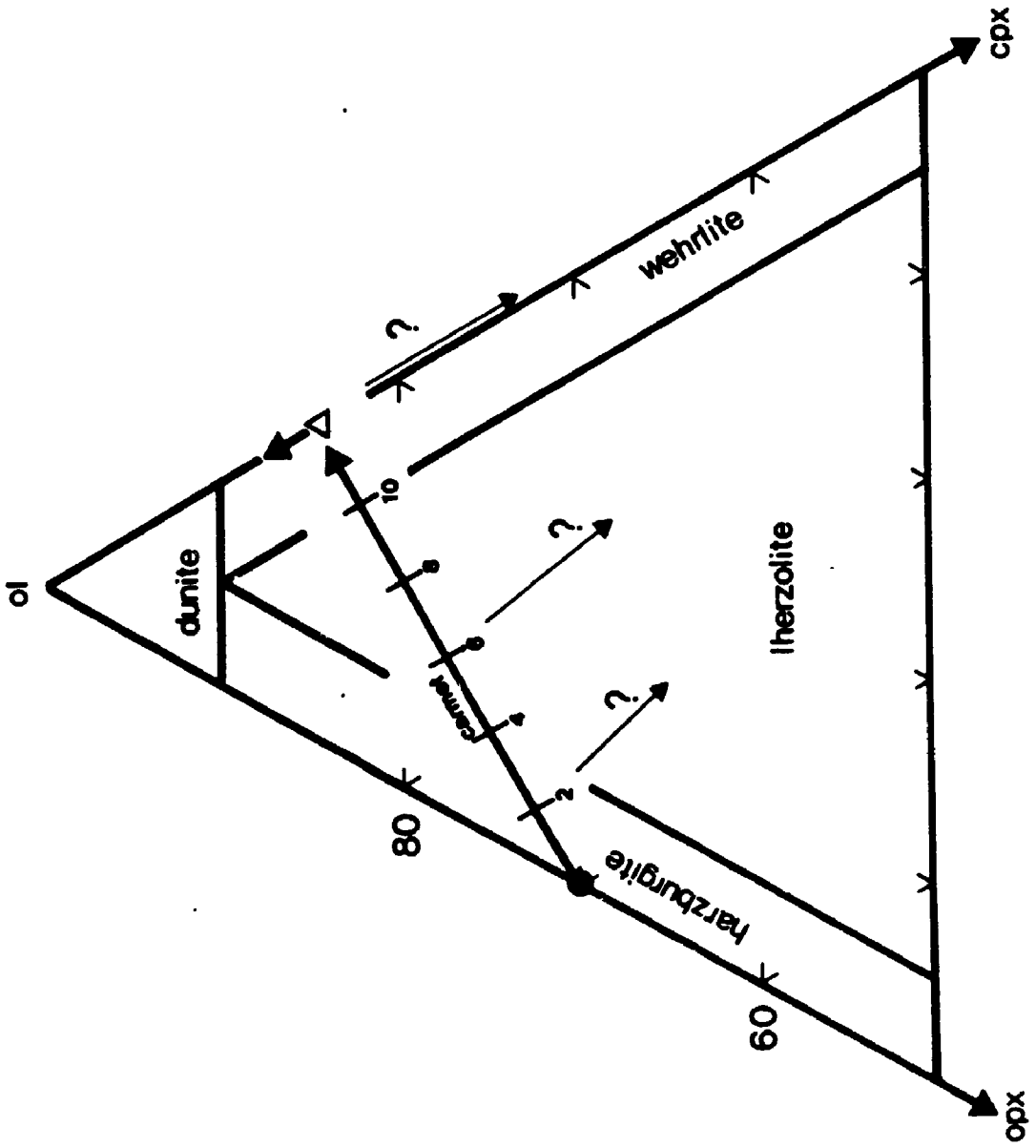


Figure 6.5 : Same as figure 6.4 but plotted on a (olivine+orthopyroxene)-clinopyroxene-phlogopite ternary diagram (in vol%) to illustrate the phlogopite enrichment in the protolith caused by the infiltration of CARMET. Symbols as in Figure 6.4.

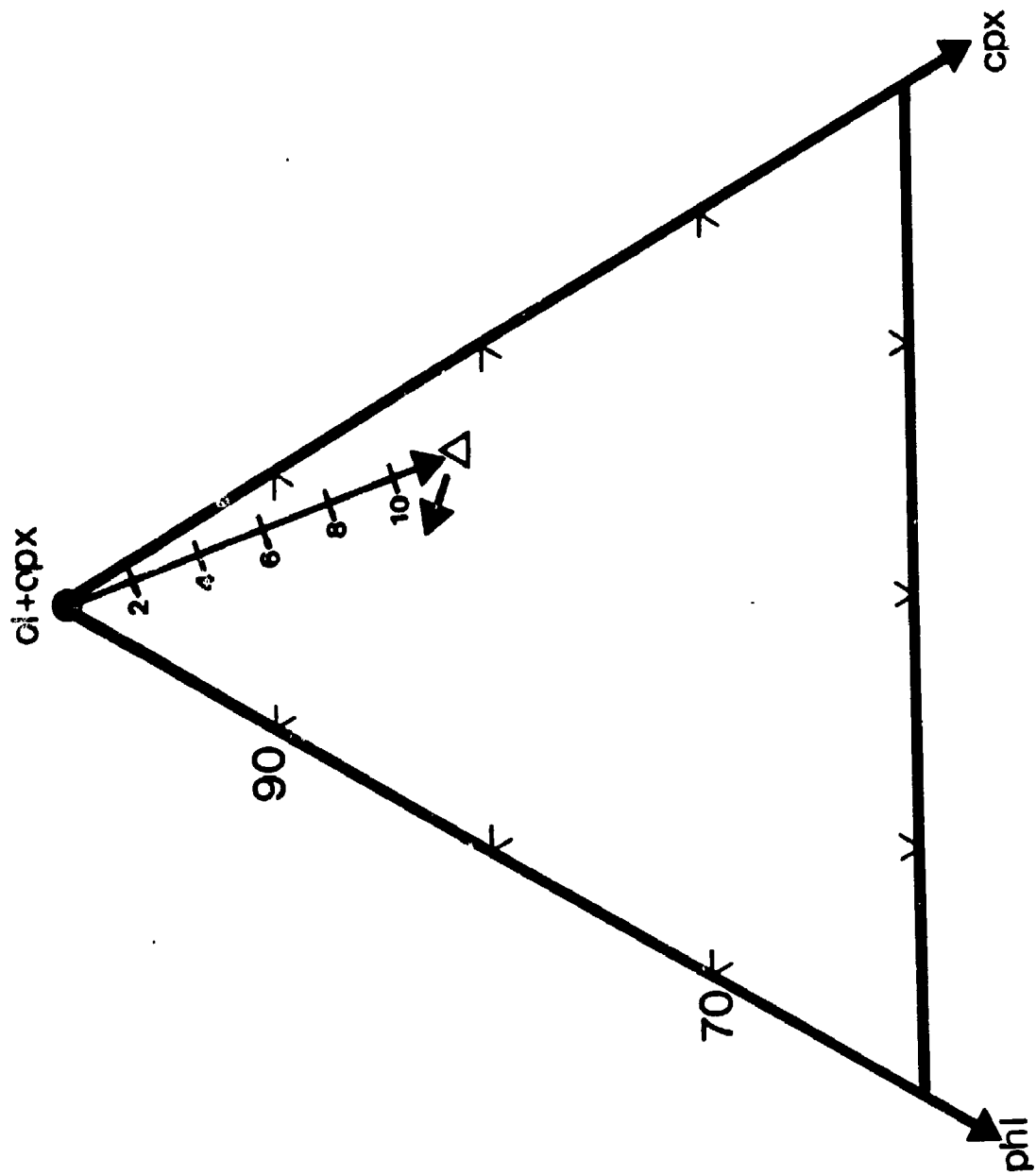


Table 6.6: Density of the silicates magnesian end members.

	Molar volume (cm ³)	Molar weight (g)	Density (g cm ⁻³)
Forsterite	43.66	140.73	3.22
Enstatite	31.33	100.41	3.20
Diopside	66.20	216.58	3.27
Phlogopite	149.77	417.32	2.79

Notes: The molar volume values are taken from Bermann (1988).

108

composition (e.g. Boyd, 1989, Figures 1, 2 and 4). The metasomatic trend produced by the infiltration of CARMET into this protolith is shown by an arrow in Figures 6.4 and 6.5. The arrow is graduated at intervals that indicate the amount of CARMET (in grams) per 100 g of harzburgitic protolith. Therefore, as shown in Figure 6.4, for 4 to 10 g of CARMET infiltrating 100 g of harzburgitic protolith, a phlogopite-bearing lherzolite is formed. With approximately 12 g of CARMET, 100 g of harzburgitic protolith are completely transformed to an olivine-rich wehrlite (Figure 6.4) with 3.3 vol% of phlogopite (Figures 6.5). If at that point, an agent of CARMET composition continues to infiltrate that portion of the mantle, olivine, calcite and phlogopite will be produced at the expense of clinopyroxene and CARMET following the trends shown in Figures 6.4 and 6.5 based on reaction [6.15].

6.2.2 Metasomatic reactions involving SILMET

In addition to olivine and orthopyroxene of the original harzburgitic protolith, the product of the HAR-SILMET(B) interaction experiment contains clinopyroxene and phlogopite (section 4.4). The proportions of the different phases stable in the protolith before and after interaction, as calculated by least-squares approximations are summarized in Table 6.7. The reaction obtained for the interaction between SILMET and HAR is in weight proportion:

Table 6.7: Results of the least-squares mass balance calculations for the interaction experiment with HAR and SILMET

<u>HAR-SILMET(B)</u>				
	<u>before interaction</u>		<u>after interaction</u>	
	(wt%)	Rec. (wt%)	(wt%)	Rec. (wt%)
Olivine	38.1	38.2	29.6	30.0
Orthopyroxene	37.2	37.2	36.5	36.9
Phlogopite(low-Ti)			10.0	10.1
Phlogopite(high-Ti)			5.0	5.1
Clinopyroxene			17.7	17.9
SILMET	24.6			
FeO	0.1		1.2	
Total	100.0	100.0	100.0	100.0
Least-squares	0.005		0.052	

Notes : The oxides taken into consideration in the mass balance calculations are SiO₂, TiO₂, Al₂O₃, FeO_{total}, MgO, CaO, Na₂O and K₂O. The composition of the minerals of the standard experiment on HAR (Appendix B4) were used together with the original composition of the SILMET glass (Table 4.7) for the calculation of HAR-SILMET(B) before interaction. The pure FeO component is used in order to correct for iron loss. Rec. is the mineral proportion recalculated to 100 wt% without the pure FeO component. Least-squares is the summation of the squares of the differences for each oxide considered between the bulk composition of HAR-SILMET(B) (Table 4.7) and the calculated one.



[6.20]

This reaction emphasizes the relative inefficiency of SILMET in transforming the minerals of the protolith: only 3.3 g of olivine are consumed in the formation of clinopyroxene and phlogopite. Therefore, most of the components required for the formation of the new minerals species come from the crystallization of the silicate melt. However, because phlogopite melts incongruently to olivine and liquid in the PLZ mantle source (section 6.1.1), SILMET likely contains an excess of H₂O, K₂O, Al₂O₃ and SiO₂ relative to that required to form phlogopite. Only these residual components, possibly released in the form of a hydrous fluid (cf. hydrous fluid composition of Schneider and Egger, 1986) could then react with the olivine of the harzburgite protolith to form metasomatic phlogopite (cf. Menzies et al., 1987, pp. 341-342). At durations beyond that of the experiment (>>23hours), it is conceivable that chemical exchange between the solidified *phlogopite clinopyroxenite* cryptocrystalline assemblage and the surrounding harzburgitic protolith might have occurred. Based on the numerous studies done on the metasomatism caused by silicate melts, the major effects of these exchanges would probably be an enrichment in Fe and Ti of the protolith (e.g. Wilshire and Shervais, 1975; Ehrenberg, 1979, 1982; Harte,

1983, 1987; Harte et al., 1987; Wilshire, 1987).

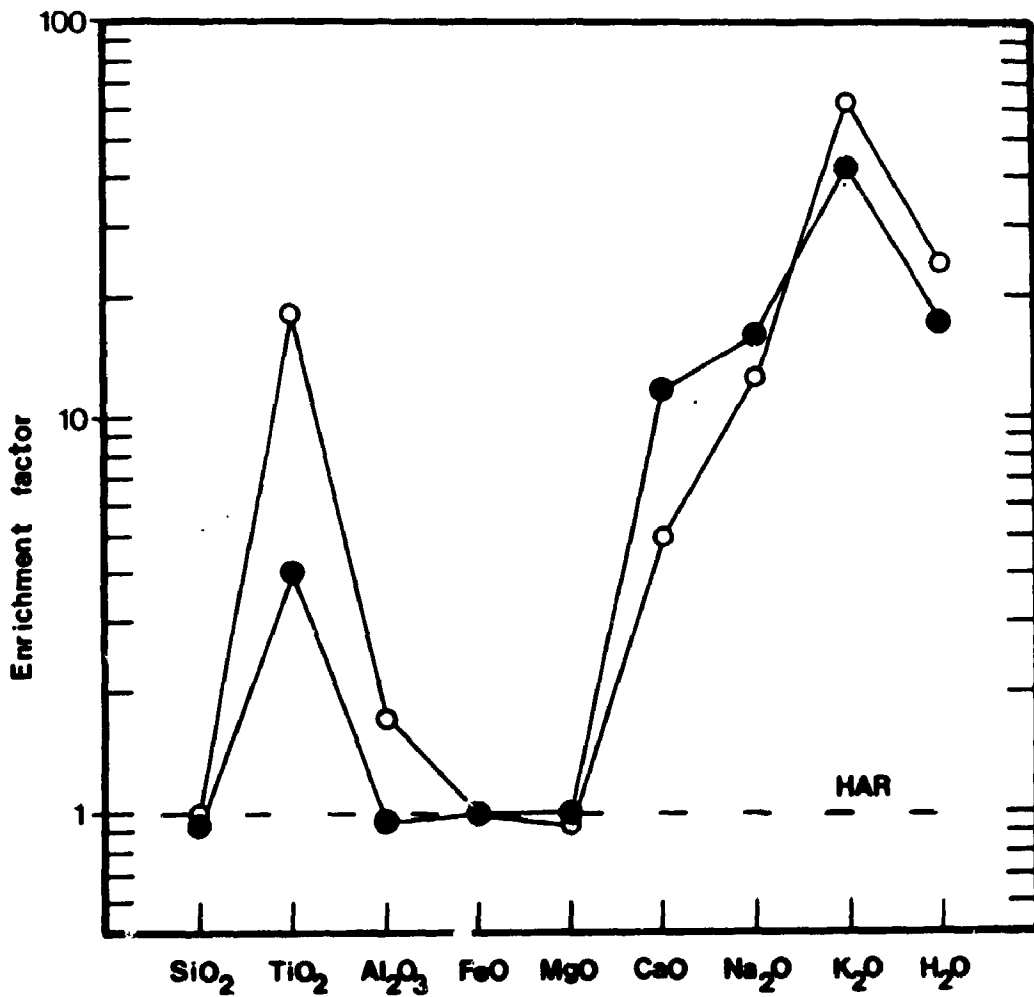
In conclusion, after complete reequilibration, the end product of an interaction like the one between SILMET and HAR (HAR-SILMET) could be a phlogopite lherzolite (Figure 6.4) with a lower $X_{MgFe_{tot}}$ than that of the original harzburgitic protolith. However, clinopyroxene and phlogopite would be the main products of the solidification of the silicate melt (SILMET) without major replacement of the original minerals of the protolith. If this interpretation is valid, SILMET infiltration is more an enrichment event rather than a metasomatic one.

Because the results of the interaction experiment in which SILMET glass was mixed with the WHR protolith (Table 4.8; WHR-SILMET) are very similar to the ones in HAR-SILMET(A), the processes involved are considered equivalent: SILMET infiltration in a wehrlite should mainly result in an enrichment in clinopyroxene and phlogopite with only minor consumption of the original minerals of the protolith (Figure 6.4).

6.2.3 Chemical modification of the protolith

The resulting chemical enrichments and depletions occurring in the harzburgitic protolith (HAR) infiltrated by 10 wt% of CARMET or SILMET are shown in Figure 6.6. CARMET will essentially enrich the mantle in CaO, alkalies (especially K_2O), and H_2O . SILMET will also enriched the

Figure 6.6 : Chemical modification occurring in the harzburgite protolith HAR by infiltration of 10 wt% of the dolomitic melt CARMET (●) or the silicate melt SILMET (○). The enrichment factor is simply the content (in wt%) in the enriched material (HAR+CARMET; HAR+SILMET) divided by the content (in wt%) in the original protolith (HAR).



mantle in alkalis (especially K_2O), H_2O and to a lesser extent CaO , but this will be coupled with a significant enrichment in TiO_2 and Al_2O_3 .

In their investigation of low-density fluids as potential metasomatic agents, Schneider and Egger (1986) determined that the solute in H_2O fluids in equilibrium with a phlogopite peridotite is rich in quartzofeldspathic components (K_2O , Al_2O_3 , SiO_2), peraluminous to metaluminous, and very poor in MgO , FeO and TiO_2 .

In conclusion, dolomitic melts (e.g. CARMET), silicate melts (e.g. SILMET) and H_2O -rich low-density fluids formed in equilibrium with a phlogopite peridotite are all efficient at enriching depleted mantle material in alkalis, especially K_2O . However, the chemical signature of each of the agents will be quite different.

6.3 Summary

At 3.0 GPa and 1225°C, the PLZ mantle source yields 7 wt% of melt coexisting with a phlogopite-bearing garnet lherzolite residual assemblage. The major participants in the melting reaction are phlogopite and clinopyroxene. The partial breakdown of phlogopite to olivine and liquid results in a silicate melt preferentially enriched in K, OH, Al and Fe, and a residual phlogopite enriched in Ti. The melt is also enriched in Ca, Na and $Fe^{3+,2+}$ by the preferential breakdown of the acmite and wollastonite

components of the clinopyroxene solid solution. The role of orthopyroxene in the melting reaction is insignificant.

The normative composition of the partial melt in equilibrium with PLZ at 3.0 GPa and 1225°C can be reasonably well defined in the diopside-olivine-kalsilite-quartz quaternary system. On the olivine-kalsilite-quartz plane projected from diopside, a comparison of the PLZ equilibrium partial melt with the 2.8 GPa minimum of the vapor-present Fo-Kz-Qz-H₂O simple system indicates that the "phlogopite - > olivine + liquid" relation is equivalent in the two systems. However, the enstatite field appears smaller in the water-saturated Fo-Ks-Qz system and this is probably related to the depolymerizing effect of H₂O in silicate melts.

The alkali-rich hydrous silicate melt (e.g. SILMET) formed in equilibrium with PLZ is considered to be a poor metasomatic agent. Nevertheless, infiltration of SILMET in harzburgitic or wehrlitic protoliths at 2.0 GPa and 1000°C may result in important enrichments in clinopyroxene and phlogopite, but without major consumption or replacement of the original mantle minerals. Chemically, the modified protolith will be richer in K, Al, Ti, Ca, OH, and Fe, causing a significant lowering of the bulk $X_{Mg/Fe_{tot}}$.

At 3.0 GPa and 1100°C, the CPL source yields 4 wt% of alkali-bearing dolomitic melt coexisting with a phlogopite-bearing garnet lherzolite mantle residuum. The strong dolomitic affinity of the melt is related to the complete breakdown of dolomite at the solidus. Phlogopite

participates in the melting reaction, but due to the low solubility of SiO_2 , TiO_2 and Al_2O_3 in the CO_2 -rich liquid, the melting behavior is quite different than in the PLZ mantle source: phlogopite partially breaks down to olivine and Ti-bearing pyrope, yielding K and OH to the carbonatite melt.

The alkali-bearing dolomitic melt (e.g. CARMET) formed in equilibrium with CPL is a very effective metasomatic agent at 2.0 GPa and 1000°C. This efficiency is directly related to a sudden destabilization of the melt resulting in the release of CO_2 -rich low-density fluid phase and the consequent precipitation of CaO, MgO, K_2O , Na_2O and H_2O transported by the melt. Infiltration of approximately 12 g of CARMET can transform 100 g of an harzburgitic protolith containing 30 vol% orthopyroxene to a phlogopite-bearing, olivine-rich wehrlite. If the infiltration of CARMET persists in the metasomatized wehrlitic assemblage, olivine, calcite, and phlogopite will be formed at the expense of clinopyroxene. Chemically, the modified mantle will essentially be enriched in CaO, alkalies and H_2O .

CHAPTER 7

PETROLOGICAL IMPLICATIONS

7.1 Multi-cycle metasomatic/enrichment process active in a continental rifting environment

The suggestion that the PLZ and CPL model compositions may represent the source of metasomatizing and enriching agents (SILMET and CARMET) can be seen as a cyclic argument (cf. Waters, 1987, p.531), since a phlogopite lherzolite (PLZ) and a carbonated phlogopite lherzolite (CPL) are certainly representative of metasomatized mantle rocks. Consequently, the main objective of the present chapter is to integrate the results of this study into a simplified petrological framework: a hypothetical *multi-cycle* metasomatic/enrichment process active in the lithospheric mantle of a continental rifting environment.

7.1.1 A basic assumption: the movement and infiltration of small melt fractions

McKenzie (1984, 1985) estimated that alkali-rich basic silicate melts can segregate from their mantle source and migrate upwards by infiltration at melt fractions of

approximately 1% (section 2.2.1). For carbonatite melts, the minimum melt fraction for segregation could be as low as 0.02% due to their very low viscosities (Hunter and McKenzie, 1989). In this context, the small dolomitic melt fraction (CARMET) formed in equilibrium with the carbonated phlogopite lherzolite (CPL) could easily segregate from its mantle residuum and extensively infiltrate the grain edges of the overlying mantle material. SILMET, the small silicate melt fraction formed in equilibrium with the phlogopite lherzolite (PLZ) could also segregate from its source. It is likely that such a silicate melt could ascend through propagating cracks (Spera, 1984, 1987). However, as pointed out by Bodinier et al. (1988, 1990), pervasive infiltration of alkali-rich silicate melt will probably be most likely in olivine-rich peridotites. This argument is based on the experimental study of Toramaru and Fujii (1986) which shows that olivine-olivine-melt dihedral angles are significantly smaller than other types of solid-solid-melt dihedral angles observed in a peridotitic rock. This observation suggests that silicate melts should preferentially infiltrate peridotitic rocks through channels completely surrounded by olivine grains.

The slow upward migration of relatively small carbonatite and silicate melt fractions by infiltration will only be possible so long as they are in thermal and chemical equilibrium with the surrounding solid material (e.g. Bailey, 1985). It is, therefore, likely that such

melts can experience heat death (i.e. solidification due to non-adiabatic ascent: Spera, 1984) and/or be consumed in metasomatic reactions during percolation in overlying colder and depleted lithospheric mantle material.

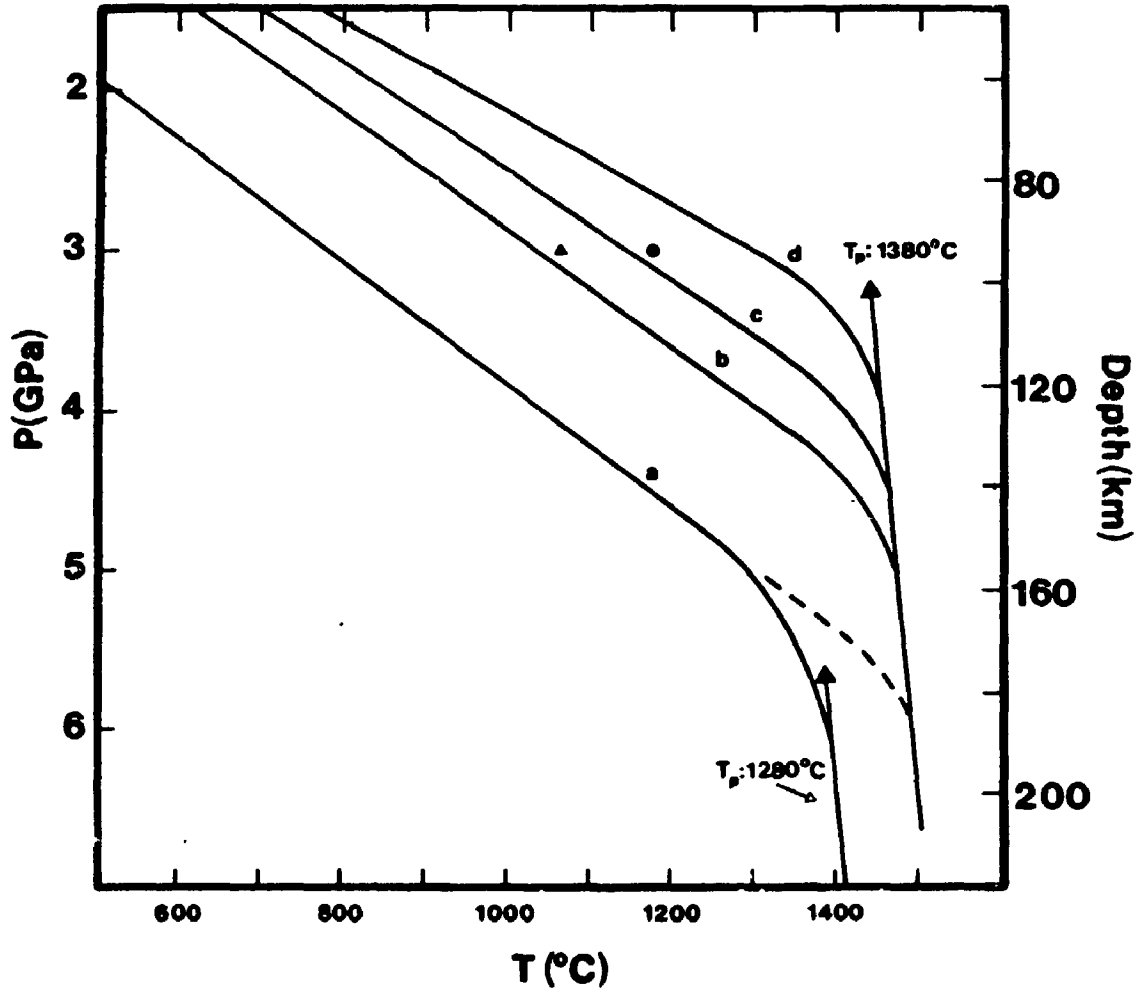
7.1.2 A thermal framework for an active continental rifting environment

The transition from the lithospheric mantle to the asthenosphere marks the passage from a stabilized region where heat is transferred essentially by conduction to a convecting one where the temperature gradient is close to adiabatic (e.g. Anderson and Bass, 1984; Anderson, 1987; McKenzie and Bickle, 1988). McKenzie and Bickle (1988) and McKenzie (1989) have proposed that, below stable continental lithospheric mantle, the *potential* temperature (T_p) of the convecting upper mantle is likely to be near 1280°C. T_p is not the real temperature but, instead, the temperature of the convecting mantle if it could rise to the earth's surface under perfect adiabatic conditions (McKenzie and Bickle, 1988).

In contrast to stable continental areas, active rifting environments are regions of extension where the lithosphere is progressively thinning and the geothermal gradient steepening. Figure 7.1 shows four hypothetical geotherms representing different stages in the thermal evolution of the upper mantle below an active continental rift. Geotherm

Figure 7.1 : Group of geotherms representing different hypothetical stages in the thermal evolution beneath a continental rift caused by the adiabatic ascent of anomalously hot asthenospheric mantle material. Geotherm "a" is considered to be characteristic of the lithospheric mantle before initiation of rifting. It is taken from McKenzie (1989; Figure 4d, p.59) and is based essentially on data from mantle nodules sampled by kimberlites free of diamond. Geotherm "b", "c" and "d" are related to the adiabatic ascent of anomalously hot asthenospheric mantle material with a potential temperature (T_p) of 1380°C. Geotherms "b" and "c" are not derived from any data or calculation but are considered reasonable intermediates between geotherm "a" and "d". The temperatures defined by geotherm "d", up to a pressure of 3.0 GPa, are comparable to the ones proposed by Seck and Wedepohl (1983) and Fuchs and Wedepohl (1983) for the Rhenish Massif, Germany.

Also shown on the pressure/depth - temperature diagram are the location of the estimated solidus, at 3.0 GPa, of the CPL (▲) and the PLZ (●) model mantle sources.



"a" is characteristic of the continental mantle before the initiation of rifting with a T_p of 1280°C in the asthenosphere. This geotherm is taken from McKenzie (1989, Figure 4d, p.59) and is based essentially on data from mantle nodules sampled by kimberlites free of diamond. Geotherm "d" is believed to be characteristic of a significantly evolved rift. The temperatures defined by geotherm "d", up to a pressure of 3.0 GPa, are comparable to the ones proposed by Seck and Wedepohl (1983) and Fuchs and Wedepohl (1983) for the Rhenish Massif, Germany, based on geothermometry calculations and geophysical modelling. Geotherms "b" and "c" are not derived from any data or calculations but may represent reasonable interpolations for intermediate stages between geotherms "a" and "d".

The initiation of rifting is seen as a consequence of the ascent of anomalously hot mantle (e.g. Wyllie, 1988, 1989a, 1989b), with a potential temperature of 1380°C, at the lithosphere-asthenosphere boundary (LAB : e.g. Haggerty, 1989a; Egger, 1989). The subsequent thinning of the lithosphere and the associated thermal disturbance is depicted as the result of the adiabatic upwelling of this hot mantle material. The slope of the 1380°C adiabat is fixed at 0.6°C km⁻¹ as estimated by McKenzie and Bickle (1988, p. 628) for the adiabatic upwelling of solid material.

Figure 7.2 shows four schematic sections with the perturbed isotherms corresponding to the four geotherms (a

Figure 7.2 : Hypothetical sections representing the thermal conditions in the lithospheric mantle beneath a continental rift zone. The sketches at the center of each section illustrate the proposed metasomatic/enrichment process in a portion of the lithospheric mantle originally harzburgitic in composition. The intersection of the isotherms with the sketch at the center of each section defines pressure/depth - temperature conditions corresponding to the geotherms of Figure 7.1. The curvature of the isotherms is purely qualitative but emphasizes the thermal disturbances accompanying the lithosphere thinning relative to the original thermal conditions shown in Figure 7.2 a. LAB refers to the lithosphere-asthenosphere boundary. See details in text.

a) Corresponds to geotherm "a" of Figure 7.1. The hot asthenospheric mantle material (large arrows; T_p : 1380°C) has reached the LAB releasing dense alkaline fluids (small arrows) at the base of the depleted lithosphere. Reaction of these fluids with the harzburgitic material has resulted in the formation of a carbonated and hydrated lherzolite horizon (patterned area).

b) Corresponds to geotherm "b" of Figure 7.1. The carbonated and hydrated lherzolite horizon (patterned area) has migrated to a depth of approximately 100 km through an unknown number of *melting-migrating-solidifying/ reacting* cycles expressed as small arrows with question marks. Based on the experimental results on the CPL mantle source, the horizon at 100 km depth could then be a dolomite-bearing phlogopite lherzolite at subsolidus conditions.

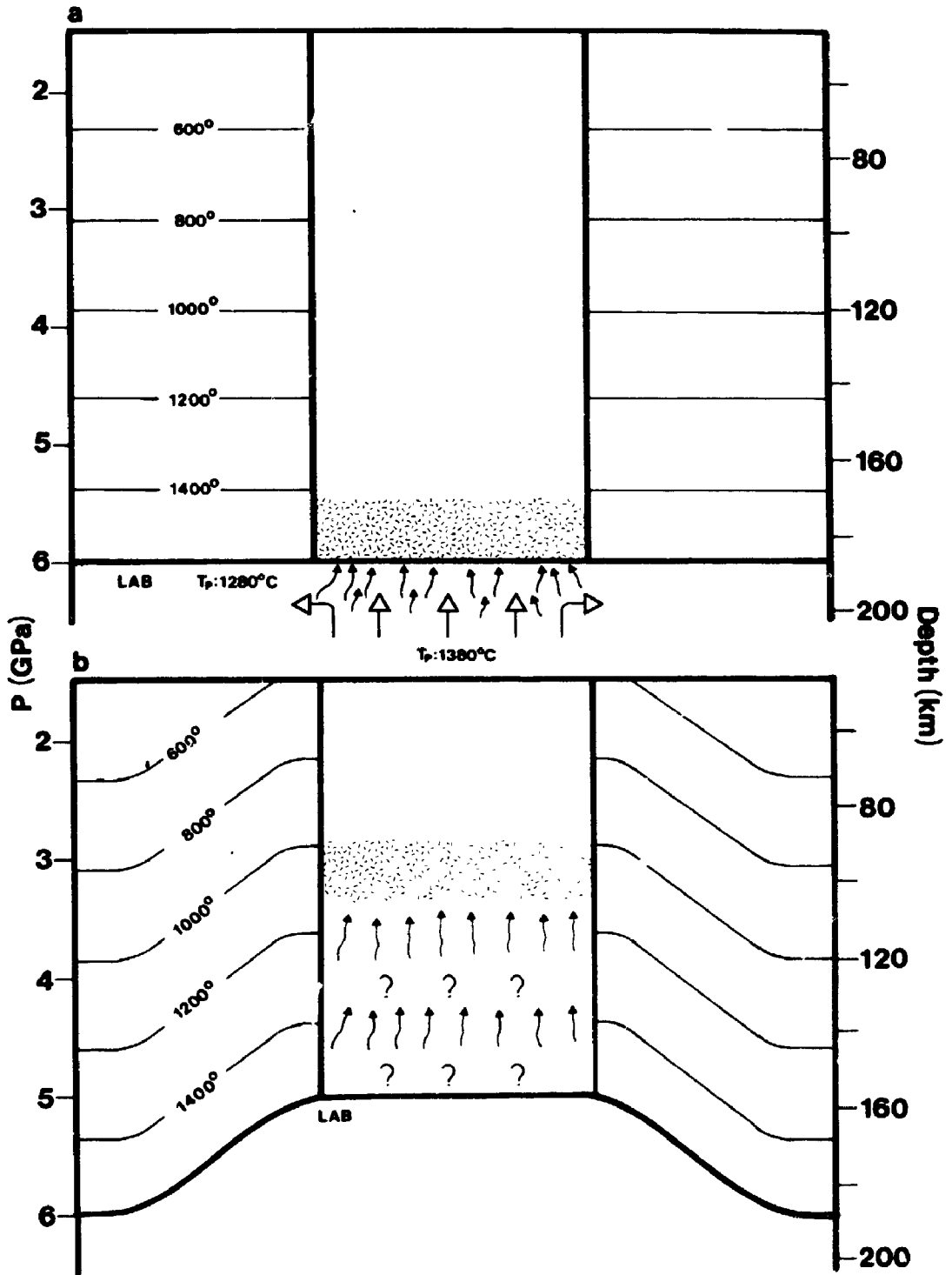
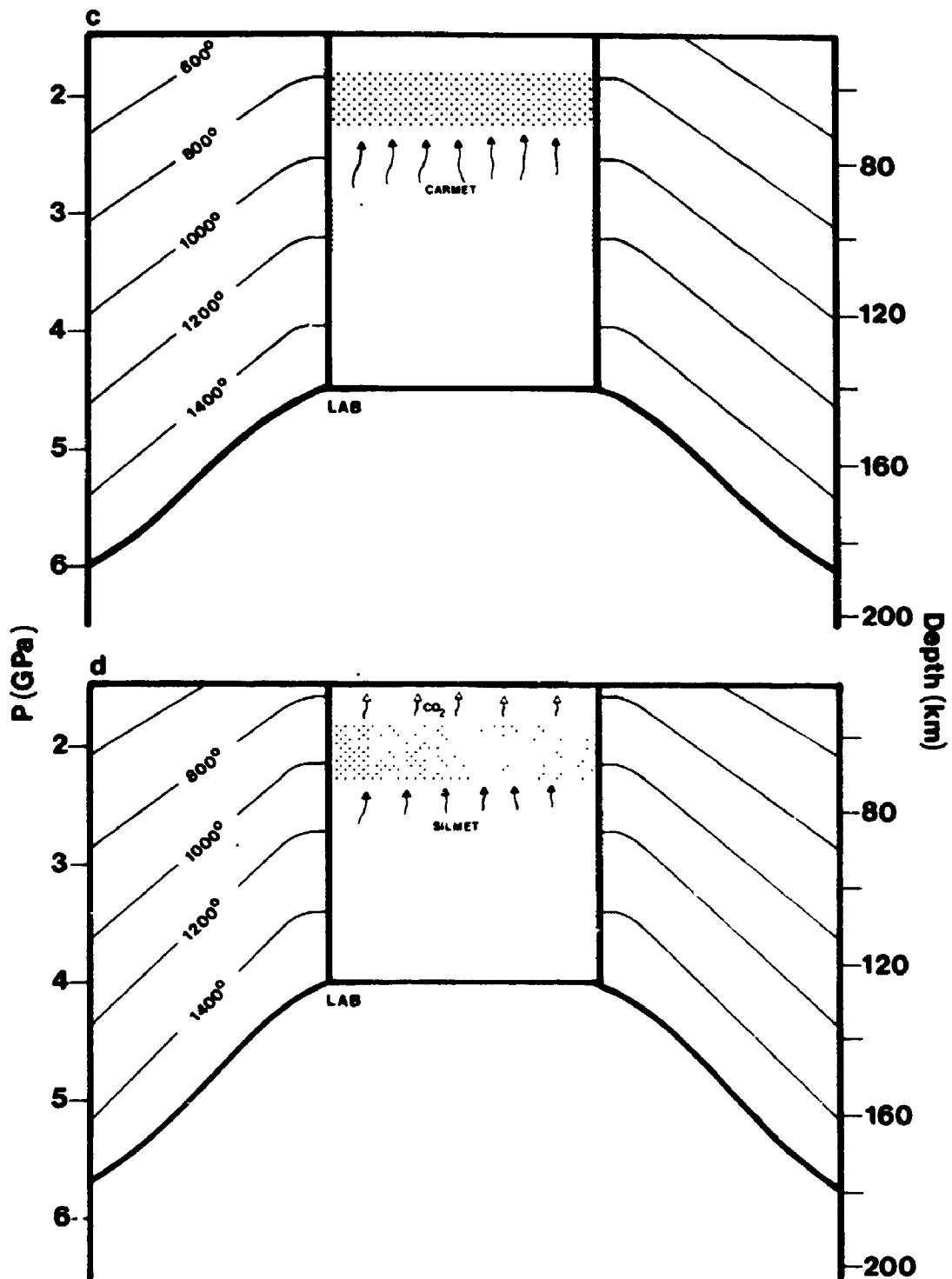


Figure 7.2 (Continued)

c) Corresponds to geotherm "c" of Figure 7.1. Partial melting of the dolomite-bearing phlogopite lherzolite horizon to form an alkali-bearing dolomitic melt (CARMET). This melt, due to its low viscosity, infiltrates the overlying depleted mantle (small arrows) leaving behind a residual garnet-bearing phlogopite lherzolite horizon at 100 km depth (lower patterned area). As the alkali-bearing dolomitic melt (CARMET) reaches depth of approximately 65 km, it solidifies to an assemblage of dolomite and phlogopite. The metasomatic/enrichment front is now decoupled in two distinct horizons: a dolomite-bearing phlogopite harzburgite horizon at 65 km depth (upper patterned area) and a CO₂-free garnet-bearing phlogopite lherzolite at 100km depth (lower patterned area).

d) Corresponds to geotherm "d" of Figure 7.1. At 65km depth, the dolomite-bearing phlogopite harzburgite is transformed to phlogopite-bearing olivin-rich lherzolite and wehrlite metasomes (patterned area) with the release of CO₂-rich low-density fluid (upper small arrows). At 100km depth, the garnet-bearing phlogopite lherzolite horizon has partially melted and an alkali-rich hydrous silicate melt (SILMET) has started to migrate upwards (lower small arrows) and will eventually reach the olivine-rich lherzolite and wehrlite metasomes at 65 km depth (patterned area) and cause enrichment in clinopyroxene and phlogopite.



to d; Figure 7.1) described above. The sketches drawn at the centre of each of the sections of Figure 7.2 depict the hypothetical processes occurring in a portion of the lithospheric mantle. It is assumed that the portion of lithospheric mantle under consideration is originally harzburgitic in composition.

7.1.3 Proposed early metasomatic/enrichment cycles

Figure 7.2a shows the lithospheric mantle before any significant thermal disturbance (Geotherm "a"). Anomalously hot mantle material ($T_p = 1380^\circ\text{C}$), consisting of undepleted and undegassed peridotite, has arisen at the LAB (≈ 190 km depth), releasing fluids at the base of the depleted lithosphere. This would correspond to the deeper level of metasomatism proposed by Wyllie (1988, 1989a, 1989b) in which asthenosphere-derived fluids would interact with harzburgitic material when entering the base of the lithosphere. The characteristics of the metasomatism should depend essentially on the compositional nature of the fluids released. No direct experimental information on the exact nature of low-density fluids or volatile-bearing melts at depths corresponding to pressures above 5 GPa are available. However diamond micro-inclusions whose compositions resemble that of potassic magmas with anomalously high volatile contents ($\approx 40\%$; essentially H_2O and CO_2) (Navon et al., 1988) could be representative of such high-pressure fluids.

008

Navon et al. (1988), referring to a suggestion of Eggler (1987), proposed that the miscibility gap between hydrous fluids and alkali-rich melts could narrow or even close at high pressure, thus allowing the existence of volatile-rich supercritical dense alkaline fluids. Because the fluid micro-inclusions are rich in SiO_2 , K_2O , CaO and FeO , in addition to H_2O and CO_2 , and poor in MgO (Navon et al., 1988, Table 1, p.786), they should be quite effective in transforming depleted harzburgitic material into carbonated and hydrated lherzolite. However, because the fraction of supercritical dense alkaline fluid released from the asthenospheric mantle is likely to be small, this process will only be effective if there is significant focusing in a narrower region of the overlying lithosphere (cf. Bailey, 1980, 1982, 1983). If such metasomatism causes significant lowering of the density at the base of the lithosphere, this could facilitate the subsequent rift-associated uplift in a manner comparable to the one proposed by Bailey (1983).

Such a deep metasomatic process could be comparable to those suggested by the nature of the mantle xenoliths sampled by the Kimberley group of kimberlites, South Africa. Erlank et al. (1987) have estimated that in the Kimberley xenolith population, the abundance of garnet phlogopite peridotites (50%) and phlogopite peridotites (30%) far exceeds the abundance of unmetasomatized garnet peridotites (10%). In this context, Waters and Erlank (1988) suggested that deep metasomatic fluids generated at the base of the

lithosphere between 200 and 150 km depth and percolating upwards could have resulted in a major upper mantle process which had a significant influence on the composition of the subcontinental lithosphere underlying the Kimberley area.

Figure 7.2b shows the same lithospheric section with thermal conditions equivalent to geotherm "b" (Figure 7.1). The LAB has risen to a depth of approximately 160km and the temperatures in the thinned lithosphere are significantly higher. Due to heat conduction from the underlying hot asthenosphere and decompression caused by uplift (e.g. McKenzie, 1989), the carbonated and hydrated lherzolite lithospheric horizon has partially melted. The low-temperature melting components (e.g. carbonates, phlogopite(?), acmite/jadeite in clinopyroxene...) are remobilized in liquid phases which migrate upwards to re-solidify and/or react as they infiltrate the overlying cold and depleted harzburgite. At these intermediate pressures (≈ 5 to 3 GPa), these hypothetical migrating agents are probably CO_2 - and H_2O -bearing melts with significantly lower volatile contents than the proposed supercritical agent responsible for the first deeper metasomatic/enrichment event. One or more of these *melting-migrating-solidifying/reacting* cycles will occur until the metasomatic/enrichment front has migrated to a depth of approximately 100 km (≈ 3.0 GPa; Figure 7.2b). The temperature at this depth is now around 1025°C and, based on the phase relationships observed in the CPL experiments

(Table 5.1), the CO₂- and H₂O-bearing migrating melts could react with the harzburgitic lithosphere to form essentially dolomite, phlogopite and clinopyroxene. This newly formed carbonated phlogopite lherzolite horizon at 100km depth would be at subsolidus conditions.

7.1.4 Late decoupled metasomatic/enrichment cycle from 100 to 65 km depth

In the lithospheric section shown in Figure 7.2c, corresponding to geotherm "c" (Figure 7.1), the dolomite-bearing phlogopite lherzolite horizon at 100 km depth (≈ 3.0 GPa) is at a temperature of approximately 1150°C. Based on the experimental data on a carbonated phlogopite lherzolite (CPL: Chapter 5), one can expect the formation of an alkali-bearing dolomitic melt such as CARMET. Due to its low viscosity, this melt will easily infiltrate the overlying depleted mantle leaving behind a residual garnet-bearing phlogopite lherzolite as suggested by the melting reactions proposed for CPL in section 6.1.2. The phlogopite lherzolite PLZ (Chapter 4) is probably a reasonable representative of such a residual CO₂-free mantle source which, at 3.0 GPa and 1150°C, should be at subsolidus conditions (Table 4.1). At 65 km (≈ 2.0 GPa), the temperature is at approximately 850°C (Figure 7.2c), and as CARMET reaches this depth it should solidify to an assemblage of dolomite and phlogopite. Consequently the metasomatic/enrichment front is now

decoupled into two distinct horizons: a dolomite-bearing phlogopite harzburgite and a CO₂-free garnet-bearing phlogopite lherzolite at 65 and 100 km depth respectively.

As rifting progresses, the lithosphere will reach the thermal conditions shown in Figure 7.2d corresponding to geotherm "d" (Figure 7.1). At 65 km depth (\approx 2.0 GPa), the temperature is now near 1000°C and the dolomite-bearing phlogopite harzburgite horizon will be transformed to phlogopite-bearing olivine-rich lherzolite and wehrlite with the release of CO₂-rich low-density fluid, following the dissociation reaction [6.9] described in section 6.2.1. At 100 km depth (\approx 3.0 GPa), based on the experimental results on PLZ (Table 4.1), the garnet-bearing phlogopite lherzolite horizon at 100 km depth is now clearly above its solidus allowing an alkali-rich hydrous silicate melt such as SILMET to form and migrate upwards. Although the silicate melt probably moves in part by propagating cracks, and may even reach the surface, some of the melt will probably have a tendency to infiltrate the more olivine-rich rocks (section 7.1.1) of the 65 km depth metasome (metasomatic horizon: cf. Haggerty, 1989a, 1989b). Based on the results (section 4.4) and interpretation (section 6.2.2) of the interaction experiments involving SILMET, this infiltration will enrich the mantle rocks (harzburgite protolith and olivine-rich lherzolic and wehrlitic metasomes) in clinopyroxene and phlogopite without significant metasomatic re-equilibration. A lowering of the bulk $X_{Mg\%_{tot}}$ should, however, be expected.

If the proposition of Bodinier et al. (1988, 1990), that silicate melts should preferentially infiltrate the rocks most enriched in olivine is acceptable (section 7.1.1), olivine-rich wehrlite should be more affected by the silicate melt enrichment than the harzburgite protolith. Moreover, because it is a progressive process in which the metasomatic/enrichment agents originate from a common source, it is probable that the infiltrating silicate melt would preferentially follow the path defined by the earlier dolomitic melt infiltration.

In conclusion, as an end product of a late *decoupled* metasomatic/enrichment cycle caused by the fractional melting of a carbonated phlogopite lherzolite horizon at 100km depth, a wide variety of rocks will occur at 65 km depth. As sketched in Figure 7.3, the major rock suites that could be encountered would be: 1) an harzburgite -> olivine-rich wehrlite suite (suite A-B-C in Figure 7.3) following the metasomatic trend caused by CARMET infiltration (section 6.2.1), 2) a clinopyroxene- and phlogopite-enriched suite (suite D-E-F in Figure 7.3) derived from SILMET infiltration in the harzburgite -> olivine-rich wehrlite suite described in 1, and finally 3) solidified SILMET veins essentially composed of varying amounts of clinopyroxene and phlogopite (alkali clinopyroxenite?: G in Figure 7.3).

Chemically, the *decoupled* metasomatic/enrichment cycle occurring at 65 km depth can be described in terms of two major events: 1) a CO₂-dominated event enriching the

Figure 7.3 : Sketch and olivine-orthopyroxene-clinopyroxene ternary diagram illustrating qualitatively the diversity of ultramafic rocks resulting from the proposed decoupled metasomatic/enrichment event occurring at 65km depth when the pressure-temperature conditions of geotherm "d" are reached.

-A represents the original harzburgite protolith that has not been infiltrated by any of the melts.

-B represents a region of the lithospheric mantle infiltrated by an intermediate amount of the alkali-bearing dolomitic melt and has, therefore, been transformed to a phlogopite-bearing olivine-rich lherzolite.

-C represents a region of the lithospheric mantle infiltrated by a large amount of the alkali-bearing dolomitic melt and has, therefore, been transformed to a phlogopite-bearing olivine-rich wehrlite.

-D represents a region of the lithospheric mantle not affected by the alkali-bearing dolomitic melt, but infiltrated by the alkali-rich hydrous silicate melt resulting in an enrichment in clinopyroxene and phlogopite without consumption of the original minerals of the harzburgite protolith.

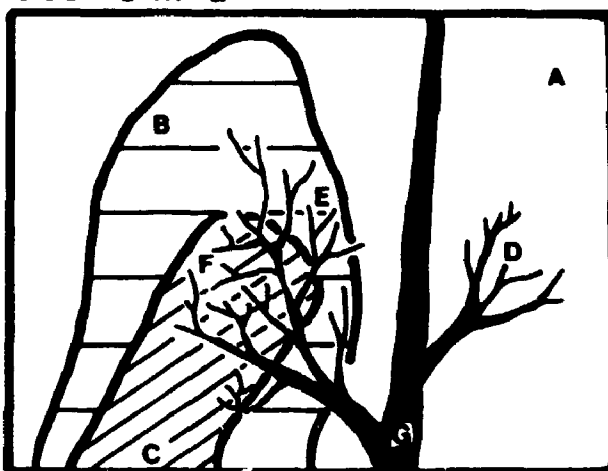
-E represents a region of the lithospheric mantle not only metasomatized to an olivine-rich phlogopite lherzolite by the infiltration of the alkali-bearing dolomitic melt (like B) but also enriched in clinopyroxene and phlogopite by infiltration of the alkali-rich hydrous silicate melt.

-F represents a region of the lithospheric mantle not only metasomatized to an olivine-rich phlogopite wehrlite by the infiltration of the alkali-bearing dolomitic melt (like C) but also enriched in clinopyroxene and phlogopite by infiltration of the alkali-rich hydrous silicate melt.

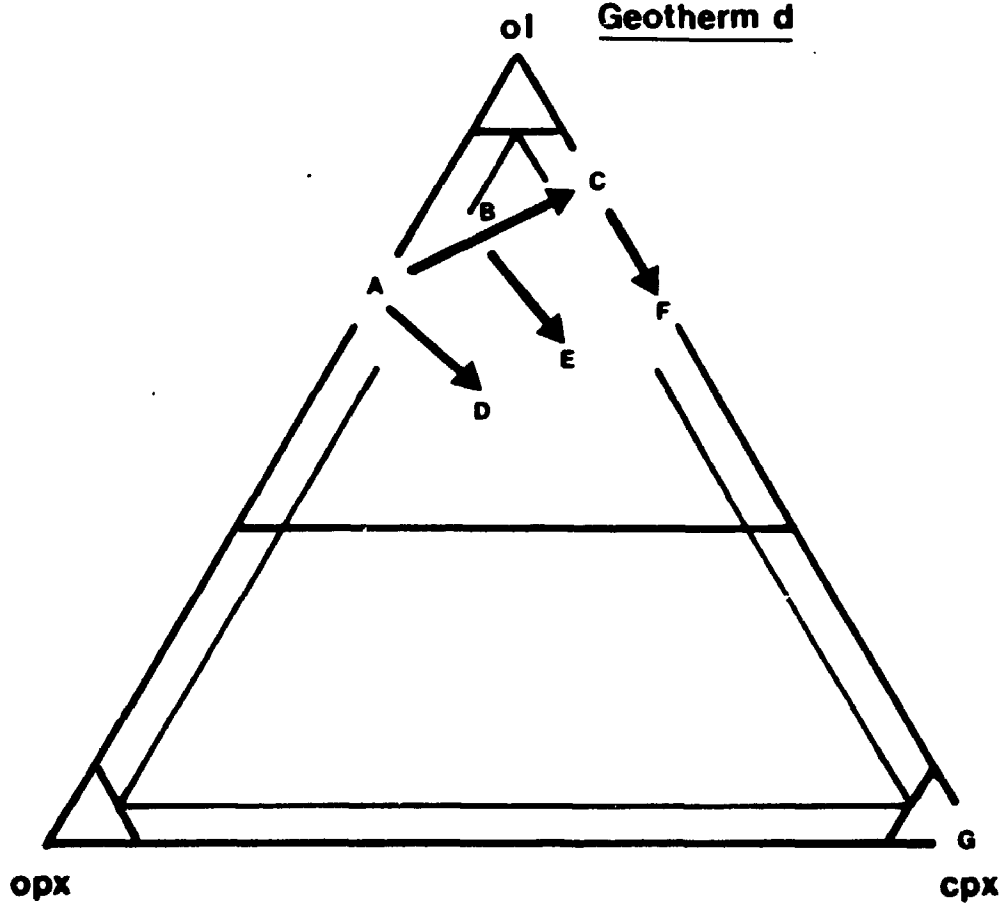
-G represents a phlogopite clinopyroxenite formed by the crystallization of a vein of alkali-rich hydrous silicate melt.

Geotherm d

DEPTH:65 km



Geotherm d



depleted mantle rocks in Ca, K, Na and H₂O, superimposed by
2) a SiO₂-, H₂O-dominated metaluminous event enriching the
rocks in K, Al, Ti, Fe, Ca and H₂O (section 6.2.3).

7.1.5 Limitations of the proposed model

The sequence of events described above, in particular the earlier metasomatic/enrichment cycles, certainly represent a simplification of the potential metasomatic and enrichment processes that could be active in the lithospheric mantle of a continental rifting environment. Consequently, although the proposed late decoupled metasomatic/enrichment event from 100 to 65 km depth is believed to be internally consistent with the experimental results presented in Chapters 4 and 5, its application to actual natural processes is only as good as the assumptions it is based on. In this context, some aspects that have not been considered in the simplified model or in the experiments and could significantly affect the metasomatic and enrichment processes are:

1) Except for the early deep metasomatic event occurring at the initiation of rifting, only lithospheric processes have been considered. However, the influence of asthenospheric melts could also be important as long as rifting progresses.

2) In the late decoupled event, the metasomatic and enrichment processes are envisioned as occurring following the proposed reactions based on the interaction experiments performed for this study (section 6.2). The reactions describing the metasomatism involving the alkali-bearing dolomitic melt are considered fairly accurate. However, the metasomatic and enrichment effects caused by alkali-rich hydrous silicate melts are likely more complex than the ones described in section 6.2.2 and based on the preliminary interaction experiments involving SILMET (section 4.4). In the interaction experiments, the influence of SILMET infiltration was investigated at a fixed pressure and temperature and in a closed system. However, it is likely that the metasomatic and enrichment phenomena caused by silicate melt infiltration should be more progressive as the melt partially crystallizes and the expelled residual liquid evolves chemically and infiltrates the overlying rocks.

3) The only hydrous phase that was considered in the experiments of this study and consequently in the proposed model is phlogopite. However, especially regarding processes occurring at depths shallower than 100 km, amphibole can be stable in the mineral assemblage. Based on the experimental results of Wallace and Green (1988), a sodic dolomitic melt can be formed in equilibrium with a residual amphibole-bearing lherzolite and Green and Wallace (1988) have documented the potential metasomatic effects of this sodic dolomitic melt. It is therefore likely that a carbonated

amphibole lherzolite horizon could, through fractional melting, be the source of distinct carbonate- and silicate-rich agents which, by infiltration in the overlying depleted mantle rocks, would result in a decoupled metasomatic/enrichment event comparable to the one proposed here. The chemical signature would, however, be significantly different. For example, the dominant alkali would be Na instead of K as is the case with phlogopite.

4) In the experiments performed for this study, the only volatiles considered are H₂O and CO₂. Although these components are probably the dominant volatiles in the upper mantle, it is likely that halogens (e.g. F and Cl) could be present in small but significant quantities. These minor volatile components could have a significant influence on the partial melting characteristics of a phlogopite lherzolite or a carbonated phlogopite lherzolite and, consequently, on the compositional nature of small melt fractions. For example, F is known to affect significantly the stability of phlogopite (e.g. Foley et al., 1986; Foley, 1989). It is also probable that F lowers the solidus and liquidus of most carbonate systems (Gittins, 1989). Another element that could have an important impact on the nature of small melt fractions is phosphorus (Ryabchikov, pers. comm.; Ryabchikov et al., 1989b).

7.2 Two well-documented occurrences of modal mantle metasomatism in continental rifting environments

7.2.1 Heterogeneous nature of the upper mantle below the West Eifel volcanic province, Germany: the possible result of a decoupled metasomatic/enrichment event?

The West Eifel sodi-potassic volcanic region is the most important of two Quaternary volcanic fields in the western part of the uplifted Rhenish Massif, Germany (e.g. Schmincke et al., 1983; Mertes and Schmincke, 1985). Many studies on the mantle xenoliths from the West Eifel have reported evidence for mantle metasomatism (e.g. Lloyd and Bailey, 1975; Stosch and Seck, 1980; Stosch et al., 1980; Stosch and Lugmair, 1986; Lloyd, 1987; Witt and Seck, 1987, 1989; Kempton et al., 1988). Recently, Edgar et al. (1989) and Lloyd et al. (1990a) reported detailed glass and mineral chemical characteristics from mantle xenoliths collected from the mafic ashes in a quarry southeast of Gees village in the West Eifel region. Here, the large majority of xenoliths (87% of a collection of 225 xenoliths as reported by Lloyd et al., 1990a) are of Group I (Frey and Prinz, 1978) and the remaining ones (13%) are of Group II (Frey and Prinz, 1978) being generally phlogopite clinopyroxenites (Edgar et al., 1989; Lloyd et al., 1990a). The glasses within the xenoliths are usually found as extensions of phlogopite-rich veins and as pools enclosing and embaying

spinel. Edgar et al. (1989) showed that these glasses likely represent migrating volatile-rich silicate melts possibly responsible for the heterogeneous mantle composition below the West Eifel.

Representative samples of the major types of xenoliths at Gees are plotted on Olivine-Orthopyroxene-Clinopyroxene and [Olivine+Orthopyroxene]-Clinopyroxene-Phlogopite diagrams in Figures 7.4 and 7.5 respectively. For each sample, the weighted average of the $X_{MgFe_{tot}}$ values of the silicate minerals is indicated. The data for the construction of these diagrams are from Lloyd et al. (1990a). Two major trends are defined by the representative samples (Figure 7.4): an harzburgite -> olivine-rich wehrlite (or clinopyroxene-bearing dunite) trend and an olivine-rich wehrlite -> phlogopite wehrlite trend.

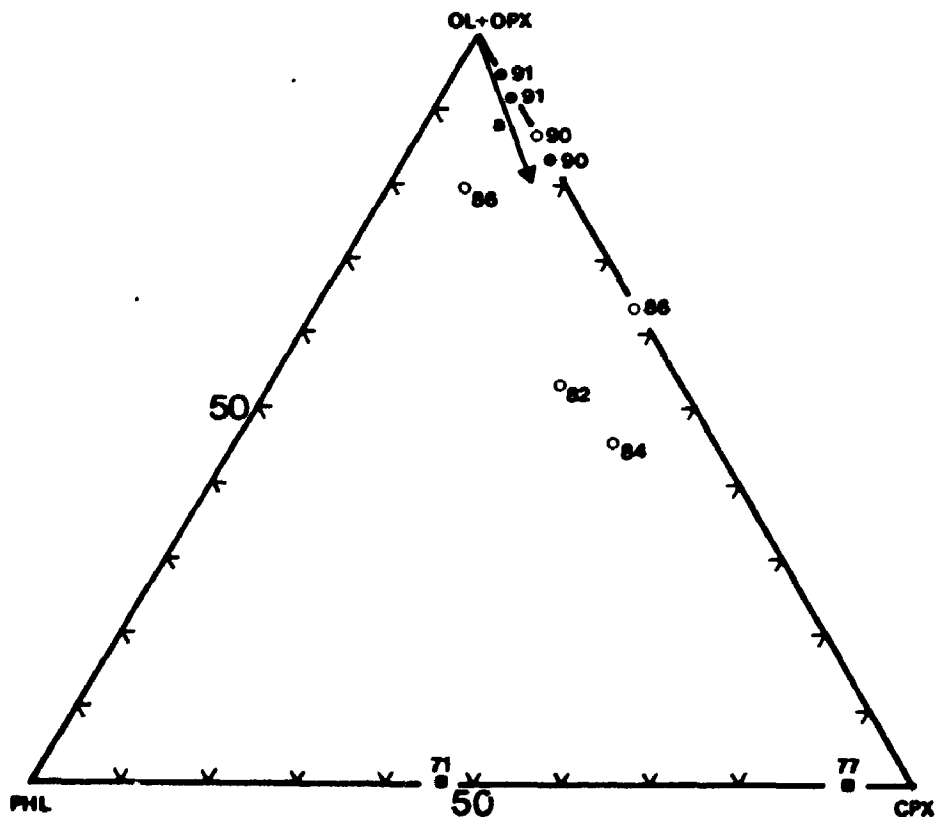
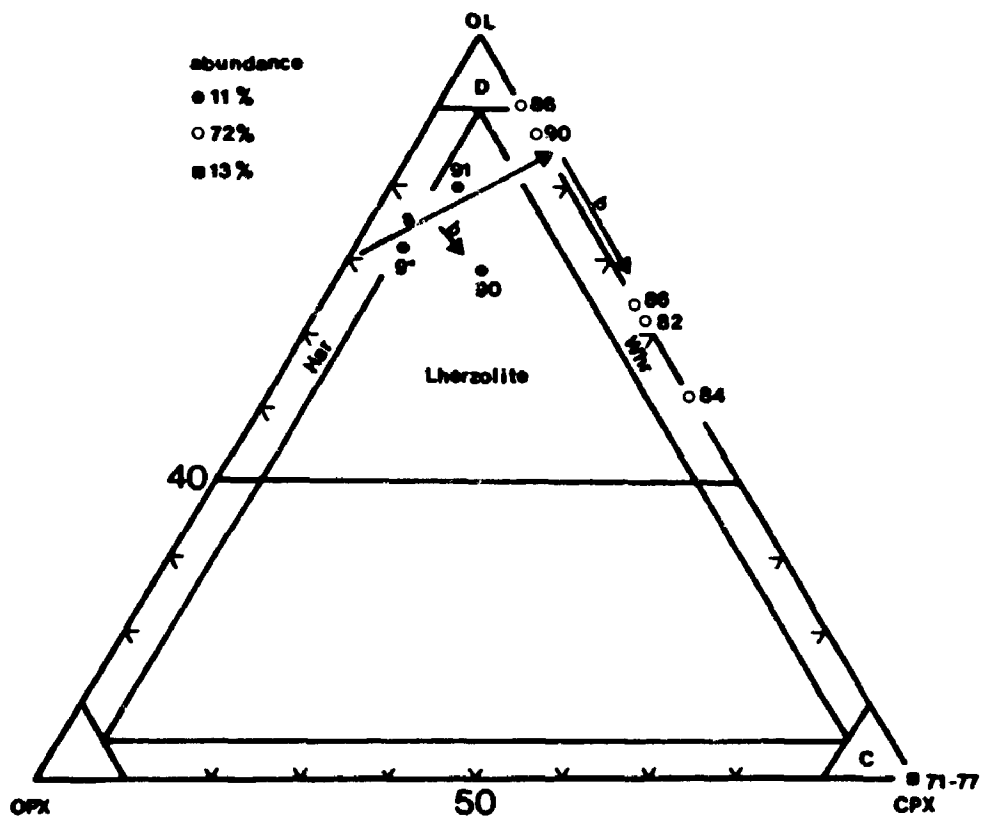
Lloyd et al. (1990a) considered that the original mantle (protolith) at Gees is harzburgite with a trace of clinopyroxene and suggested that the olivine-rich wehrlite resulted from transformation of harzburgitic material by the infiltration of Ca- and alkali-rich hydrous silicate melts. This progressive transformation is suggested by the presence of deep embayments in the enstatite grains within harzburgite xenoliths. These embayments are filled by alkali-rich silicate glass and aggregates of olivine and diopside microlites indicating reactions of the type: "enstatite + Ca-rich liquid <-> olivine + diopside + liquid" (Edgar et al., 1989). Because the transformation of

Figure 7.4 : Modal compositions of representative samples of the major types of ultramafic xenoliths collected from the mafic ashes in a quarry southeast of Gees, West Eifel, Germany, plotted in an olivine-orthopyroxene-clinopyroxene ternary diagram. Each sample is labeled by a number representing the weighted average of the $X_{MgFe_{tot}}$ values ($\times 100$) of the silicate minerals. Filled circles are Group I orthopyroxene-bearing xenoliths; empty circles are Group I orthopyroxene-free xenoliths; squares are Group II xenoliths. The relative abundances are based on a collection of 225 xenoliths, as reported by Lloyd et al. (1990a). All data for the construction of this diagram are taken from Edgar et al. (1989) and Lloyd et al. (1990a).

Also shown on the diagram, is the metasomatic trend (arrow labeled a) produced by the infiltration of an alkali-bearing dolomitic melt such as CARMET on a harzburgite protolith (cf. Figure 6.4). The arrows labeled b illustrate the enrichment in clinopyroxene believed to be produced by the infiltration of a alkali-rich hydrous silicate melt such as SILMET (cf. Figure 6.4)

Har: harzburgite field; Whr: wehrlite field; C: clinopyroxenite field

Figure 7.5 : Same as in Figure 7.4 but plotted in a (olivine+orthopyroxene)-clinopyroxene-phlogopite ternary diagram. (symbols as in Figure 7.4)



harzburgite to olivine-rich wehrlite involves the complete consumption of orthopyroxene in the protolith, the process seems clearly metasomatic.

Lloyd et al. (1990a) also proposed a progressive transformation of Gees olivine-rich wehrlite to phlogopite-bearing wehrlite. This suite of rocks is the most abundant in the collection of xenoliths (72%; Figure 7.4). In the sequence olivine-rich wehrlite \rightarrow olivine-poor wehrlite, the abundance of clinopyroxene and titaniferous phlogopite increases with clinopyroxene becoming richer in Ti, Al, and Ca as $X_{MgFe_{tot}}$ and Cr decrease (Lloyd et al, 1990a). The process envisioned by Lloyd et al. (1990a) is one where a K-, Ti-, Ca-, and Al-bearing silicate melt infiltrates olivine-rich wehrlite; the crystallization of clinopyroxene increases the activity of K, Al and Ti in the melt causing the subsequent formation of titaniferous phlogopite. Lloyd et al. (1990a) noted that: "... evidence for replacement of clinopyroxene and olivine by phlogopite is rare and introduction of this mineral is almost entirely by interpenetration". Therefore, this trend is more characteristic of an enrichment process since it appears to involve no major replacement of the original minerals.

Finally, the phlogopite clinopyroxenite xenoliths are considered by Lloyd et al. (1990a) as representing: "... a facies of Ca- and K-bearing melt activity in channel-ways lined by previously precipitated clinopyroxene and phlogopite".

It is suggested that the decoupled metasomatic/enrichment process described in section 7.1.4 is significantly compatible with the genetic relationships between the various xenoliths at Gees proposed by Edgar et al (1989) and Lloyd et al. (1990a). Similarities supporting this suggestion are:

1) The two major trends defined by the representative samples described by Edgar et al. (1989) and Lloyd et al. (1990a) are quite similar to the trends that the proposed decoupled metasomatic/enrichment process would create (Figures 7.4 and 7.5).

2) The progressive transformation of the protolith envisioned by Lloyd et al. (1990a) can be summarized by two successive infiltration events: i) the infiltration of a Ca-, alkali-rich agent which metasomatically transforms harzburgite to dunite or olivine-rich wehrlite, followed by ii) an enrichment event involving the infiltration of a K-, Al-, Ti-, Ca-, Al-bearing hydrous silicate melt which introduces clinopyroxene and phlogopite especially in the dunite and olivine-rich wehrlite. An alkali-rich hydrous silicate melt formed in equilibrium with a phlogopite lherzolite at 3.0 GPa (e.g. SILMET) would have chemical characteristics very comparable to the one required by this late enriching agent.

However, there is a significant difference regarding the

100

proposed nature of the early Ca-, alkali-rich metasomatic agent. Edgar et al. (1989) and Lloyd et al. (1990a), considering the likelihood of an ephemeral carbonatite melt (e.g. Green and Wallace, 1988) or a silicate melt, favoured the latter. On the other hand, if the decoupled metasomatic/enrichment process described in section 7.1.4 can be applicable to the Gees xenoliths, the early metasomatic agent would be a Ca-rich, alkali-bearing dolomitic melt comparable to CARMET. Some of the reasons why such a dolomitic melt is considered as a reasonable alternative candidate for the disappearance of orthopyroxene in the Gees harzburgite protolith are summarized below:

1) An alkali-bearing dolomitic melt is very efficient in consuming orthopyroxene through the dissociation reaction described in section 6.2.1 at thermal conditions represented by geotherm "d" (section 7.1) and pressures less than 2.1 GPa. These pressure-temperature conditions are probably reasonably characteristic of the mantle portion represented by the Gees xenoliths because i) geotherm "d" is based on data from the Rhenish Massif (section 7.1), and ii) the peridotitic xenoliths contain Cr-spinel and are garnet-free suggesting pressures less than 2.5 GPa (Carroll Webb and Wood, 1986).

2) The early and late infiltrating agents would originate from a common source because the proposed decoupled event results from a single progressive process:

the fractional melting of a carbonated phlogopite lherzolite horizon at 100 km depth. The existence of carbonated phlogopite-bearing peridotitic material at 100 km depth has been called upon as a likely source for some of the primitive potassic lavas erupted in the West Eifel region (Mertes and Schmincke, 1985).

3) In Figures 7.4 and 7.5, the weighted average of the $X_{MgFe_{tot}}$ of the silicates for the representative samples described by Edgar et al. (1989) and Lloyd et al. (1990a) are indicated. Except for one sample, all the olivine-rich rocks (> 65 vol% olivine; Figure 7.4) have $X_{MgFe_{tot}}$ values of 0.90 to 0.91. The only olivine-rich sample with a significantly lower $X_{MgFe_{tot}}$ (0.86; sample FL4 of Lloyd et al., 1990a) is, contrary to the others, extremely enriched in phlogopite (11.6 vol%: Lloyd et al., 1990a) as shown in Figure 7.5. This rock could, therefore, have been significantly infiltrated by the late enriching agent responsible for the addition of clinopyroxene and phlogopite (alkali-rich silicate melt or its derivatives). Concurrently, all the rocks, in which olivine represents less than 65 vol% and are probably also affected by the late silicate melt enrichment, also have significantly lower $X_{MgFe_{tot}}$ (< 0.86: Figure 7.4). In conclusion, the $X_{MgFe_{tot}}$ values of the silicate in the olivine-rich rocks that define the harzburgite -> olivine-rich wehrlite trend appears to be quite constant, which is compatible with the metasomatic effect of a primary carbonatite melt due to its higher

$X_{MgFe_{tot}}$ (≈ 0.85) relative to a primary silicate melt (< 0.80) (Green and Wallace, 1988; Edgar et al., 1989; section 5.3.3).

7.2.2 Mantle xenoliths sampled by ultrapotassic magmas in southwest Uganda: widespread metasomatism in the western branch of the East African Rift?

The southwest Uganda Quaternary to Recent volcanic fields are associated with rifted domes lying in the west branch of the East African Rift (e.g. Lloyd, 1987). The volcanic activity is highly explosive (e.g. Lloyd et al., 1990b) and the extrusives are silica-undersaturated and characterized by high K, Ti, Ca, and LILE contents (e.g. Lloyd et al., 1987). High-pressure liquidus experiments performed on some of the primitive potassium-rich magmas of the region (ugandite, katungite, mafurite) strongly suggest the existence of heterogeneous phlogopite-bearing mantle sources below the southwest Uganda volcanic fields (Edgar et al., 1976, 1980; Ryabchikov and Green, 1978; Arima and Edgar, 1983). Carbonatitic volcanic activity in the Fort Portal field, tuffs cemented by carbonate of magmatic origin, and CO_2 as the dominant volatile extracted from some of the potassic lavas (e.g. von Knorring and DuBois, 1961; Deines and Gold, 1973; Deines, 1989; Lloyd et al., 1990b) all indicate the presence of a significant amount of CO_2 in the underlying mantle material. It seems, therefore,

reasonable to infer that carbonated phlogopite-bearing peridotitic horizons are, or were, present in the subrift mantle. Some indication in the xenoliths population of processes bearing some similarities with the ones proposed in section 7.1 is therefore a possibility.

The large majority of ultramafic xenoliths brought to the surface by the southwest Ugandan volcanic activity are of Group II, as defined by Lloyd and Bailey (1975), which are clinopyroxenites rich in phlogopite, with little or no olivine and, occasionally, containing accessory titanomagnetite, titanite, and apatite. Lloyd et al. (1985) have shown that approximately 25 % partial melting of a representative of these phlogopite clinopyroxenite nodules can produce melts comparable to those of their host volcanics (katungite). Peridotitic xenoliths are rare, except in the southern field of Bufumbira where dunites and dark mica-bearing wehrlites are found together with Group II phlogopite clinopyroxenites (Lloyd et al., 1990b and references therein). As pointed out by Lloyd et al. (1987), no garnet- and/or orthopyroxene-bearing ultramafic xenoliths have been recorded from the southwest Uganda volcanic fields.

Based on textural grounds, the Group II xenoliths have been subdivided in Group II (i), (ii) and (iii) (Lloyd, 1981, 1987). Group II (ii) and (iii) xenoliths show textures of obvious igneous origin. However, Group II(i) nodules display deformation textures and replacement fabrics

suggesting a metasomatic origin. Lloyd and Bailey (1975), Lloyd (1987) and Lloyd et al. (1987) have argued that these Group II(i) nodules are in fact the end-product of extensive metasomatism of peridotitic mantle lithosphere by fluids capable of enriching "normal" mantle (lherzolite and/or harzburgite) in K, Na, Ti, Al, Fe, Mn, Ca, P, Rb, Sr, Y, Nb, Ba, H, C, F and Cl. Based on the metasomatic features and the geochemical characteristics of the xenoliths, Lloyd et al. (1987) proposed the following sequence of events:

- 1) Complete replacement of olivine, and possibly orthopyroxene, by phlogopite accompanied by crystallization of diopside-salite, due to influx of fluids adding Ti, Al, Ca, Na, K, Sr, Rb, Ba, Zr and Y to the mantle protolith;

- 2) Continued growth of titaniferous phlogopite and augite-ferroaugite at the expense of diopside-salite by infiltration of fluids rich in Ti, Al, Na, K, Rb, Ba, Fe (especially Fe^{3+});

- 3) Introduction of titanomagnetite, titanite and rarely apatite, partially replacing mica and clinopyroxene, by Ti-, Fe-, Ca- and P-bearing fluids.

It is difficult to characterize in detail the various stages of the early process responsible for the complete consumption of orthopyroxene and olivine (point 1 above), mostly because xenoliths exhibiting intermediate metasomatic features are rare. Nevertheless the only peridotitic

xenoliths that are recorded are dunites and phlogopite-bearing wehrlites. If these xenoliths are representatives of an intermediate stage prior to the complete transformation of peridotites to clinopyroxenites (cf. Lloyd, 1987), this suggests that the transformation was accomplished through at least two distinct steps: an early event causing the disappearance of orthopyroxene to form phlogopite-bearing wehrlite, followed by a later one responsible for both the consumption of olivine and the important enrichment in clinopyroxene and phlogopite. These resultant trends would have similarities to those produced by the infiltration of distinct alkali-bearing dolomitic and silicate melts originating from the fractional melting of a carbonated phlogopite lherzolite horizon (section 7.1). The existence and migration, in the underlying lithospheric mantle, of small alkali-bearing dolomitic melt fractions is considered likely because CO_2 is a dominant volatile constituent of the southwest Uganda volcanic products (see above). In addition, the migration and solidification (by heat death) of alkali-rich hydrous silicate melts in the subrift mantle is suggested by the occurrence of mantle-derived phlogopite clinopyroxenites of magmatic origin [Group II(ii) and II(iii)].

In conclusion, it is possible that distinct alkali-bearing dolomitic and silicate melts could have been involved in the early stages of the transformation of peridotite to clinopyroxenite, in a manner comparable to the

one proposed in section 7.1.4. However, the proposed decoupled metasomatic/enrichment process is far from sufficient to explain all the mineralogical and chemical characteristics of the extensive mantle metasomatism described by Lloyd and co-workers and which appears to involve a significantly greater fluid flux than would be involved in the proposed process. These characteristics emphasize the fact that the metasomatic and enrichment processes operating in the lithospheric mantle of active continental rifting environments are far more complex than in the simplified model described in section 7.1. Additional experimental work, especially on the nature and mutual solubilities of alkaline melts and low-density fluids at high pressures (>3.0 GPa), would certainly be valuable.

7.3 Summary

A hypothetical, simplified, multi-cycle metasomatic/enrichment process active in the lithospheric mantle of a continental rift has been proposed. A carbonated and hydrated lherzolite horizon, originally formed at the base of the lithosphere due to the release of supercritical dense alkaline fluids from hot asthenospheric mantle, slowly migrates upwards as rifting progresses. The migration of this carbonated and hydrated metasomatic/enrichment front proceeds through an unknown number of *melting-migrating-solidifying/reacting* cycles in which the low-temperature

melting components are each time remobilized into small volatile-rich melt fractions which infiltrate the overlying colder and depleted harzburgitic material where they suffer heat death and/or react with the surrounding solid mantle assemblage.

Based on the experimental results presented in this study, it is suggested that during the late metasomatic/enrichment cycle occurring at 65 km depth, the infiltrating agents will originate from the fractional melting of the carbonated phlogopite lherzolite horizon now at approximately 100 km depth, and this will result in the decoupling of the process into two major events: 1) an alkali- and Ca-rich metasomatic event caused by the infiltration of a dolomitic melt, creating an harzburgite -> olivine-rich wehrlite trend; 2) a later enrichment event in which the infiltration of a K-, Al-, Ti-, Ca-, Fe-, OH-bearing silicate melt introduces clinopyroxene and phlogopite into the harzburgite -> olivine-rich wehrlite suite of rocks. The suite of mantle xenoliths collected from Gees, West Eifel, Germany, and described in detail by Edgar et al. (1989) and Lloyd et al. (1990a) could represent a possible example of the variety of mantle rocks that could result from such a decoupled metasomatic/enrichment process at 65 km depth. The extensive modal metasomatism that appears to have affected the lithospheric mantle underlying the southwest Uganda volcanic fields demonstrates, however, that mantle metasomatic and enrichment processes that occur

in continental rifting environments can be far more complex than those considered in the proposed model.

CONCLUSIONS

The principal conclusions of this study are:

1) At 3.0 GPa, the PLZ phlogopite lherzolite model mantle source starts to melt partially at 1175°C and phlogopite is a residual phase up to 1275°C. At 1225°C, the fraction of melt produced is estimated at 7 wt% with phlogopite and clinopyroxene as the major participants in the melting reactions. The partial breakdown of phlogopite to olivine and liquid results in a strongly potassic ($K_2O \approx 5$ wt%) silicate melt enriched in Al, Fe, OH and a residual phlogopite enriched in Ti. The melt is also rich in Ca, Na and Fe^{3+} due to the preferential breakdown of the acmite and wollastonite components of the clinopyroxene solid solution.

The results of the interaction experiments suggest that if such a silicate melt infiltrates anhydrous peridotitic material (harzburgite or wehrlite) at 2.0 GPa and 1000°C, it will result in an enrichment in clinopyroxene and phlogopite without major consumption of the original minerals of the peridotite protolith.

2) The experiments performed on the CPL carbonated phlogopite lherzolite model mantle source indicate that at

3.0 GPa and between approximately 1060°C and 1150°C, an alkali-bearing dolomitic melt will coexist with a residual garnet- and phlogopite-bearing lherzolite assemblage. The strong dolomitic affinity of the liquid is related to the complete melting of dolomite near the solidus. The potassic affinity comes from the partial breakdown of phlogopite to olivine and pyrope yielding K and OH to the CO₂-rich melt.

Interaction of such a dolomitic melt with harzburgitic material at 2.0 GPa and 1000°C results in the consumption of orthopyroxene, the formation of metasomatic olivine, clinopyroxene and phlogopite and the release of CO₂-rich low-density fluid. Infiltration of the dolomitic melt in a spinel wehrlite at the same pressure-temperature conditions will result in the formation of metasomatic calcite, olivine and phlogopite and the partial consumption of clinopyroxene and spinel of the protolith.

3) The phase relationships observed in the investigating melting intervals of the PLZ and CPL model mantle sources suggest that, in the lithospheric mantle beneath a continental rift, fractional melting of a carbonated phlogopite lherzolite horizon at 100km depth could yield successively a alkali-bearing dolomitic melt and an alkali-rich hydrous silicate melt. Migration of these melts to a depth of 65 km could result in a metasomatic/enrichment event decoupled in two distinct steps: i) an alkali- and Ca-rich metasomatic event caused by the infiltration of the

dolomitic melt and creating an harzburgite -> phlogopite wehrlite trend followed by ii) an enrichment event in which the infiltration of a K-, Al-, Ti-, Ca-, Fe- and OH-bearing silicate melt introduces clinopyroxene and phlogopite in the harzburgite -> phlogopite wherlite suite of rocks. The variety of rocks that result from such a decoupled process bear similarities with a suite of mantle xenoliths from Gees, West Eifel, Germany.

APPENDIX A

DETAILS OF OXYGEN FUGACITY CALCULATION

-Activity-composition relationships for the silicate phases

As proposed by Wood and Virgo (1989), activity-composition relationships at 1 bar for olivine and orthopyroxene were obtained using the relations:

$$a_{\text{Fe}_2\text{SiO}_4}(\text{ol}) = X_{\text{Fe}}^2 \exp(1006 X_{\text{Mg}}^2 / T) \quad [\text{A.1}]$$

$$a_{\text{Fe}_2\text{Si}_2\text{O}_6}(\text{opx}) = X_{\text{Fe}}^{\text{M1}} \times X_{\text{Fe}}^{\text{M2}} \quad [\text{A.2}]$$

where in relation [A.1]

X_{Mg} = mole fraction of Mg_2SiO_4

X_{Fe} = mole fraction of Fe_2SiO_4

and in relation [A.2]

$X_{\text{Fe}}^{\text{M1}}$ = atomic fraction of iron in the M1 site

$X_{\text{Fe}}^{\text{M2}}$ = atomic fraction of iron in the M2 site

M1 and M2 sites are calculated following the method of Wood and Banno (1973) where Al^{VI} , Cr, Ti are in the M1 site and Na, Ca, Mn are in the M2 site. Fe and Mg are then evenly distributed in order to fill the remaining M1 and M2 positions.

-Activity-composition relationship for spinel

Based on their calibration across the $\text{MgAl}_2\text{O}_4\text{-Fe}_3\text{O}_4$ join, with correction for additional Fe^{2+} substitution in FeCr_2O_4 and FeAl_3O_4 , Mattioli and Wood (1988) give the following activity-composition relationship:

$$a_{\text{Fe}_3\text{O}_4}(\text{sp}) = [-0.0298X_{\text{mt}} + 2.878X_{\text{mt}}^2 + 206.9X_{\text{mt}}^3 - 1463X_{\text{mt}}^4 + 2843X_{\text{mt}}^5] \times (1 + 8X'_{\text{Fe}^{2+}}) \quad [\text{A.3}]$$

where

$$X_{\text{mt}} = X_{\text{Fe}_3\text{O}_4} = \text{Fe}^{3+} / (\text{Fe}^{3+} + \text{Al} + \text{Cr})$$

$$X'_{\text{Fe}^{2+}} = X_{\text{FeCr}_2\text{O}_4} + X_{\text{FeAl}_3\text{O}_4} \text{ (additional } \text{Fe}^{2+} \text{ not used in } \text{Fe}_3\text{O}_4\text{)}$$

Mattioli and Wood (1988) point out that this activity-composition relationship should be valid between 900° and 1000°C if $0.00 < X_{\text{Fe}_3\text{O}_4} < 0.15$ and $0.00 < X'_{\text{Fe}^{2+}} < 0.25$.

-Evaluation of partial molar volume

In the expression for $f\text{O}_2^{T,P}$ in equation [3.2] of section 3.4.2, the last term is used in order to correct the $f\text{O}_2$ for pressure ($P=2.0\text{GPa}$ or $20,000\text{bars}$)

The partial molar volume change (\bar{V}) is considered constant with increasing pressure and is defined by

$$\Delta\bar{V} = 6\bar{V}_{\text{Fe}_2\text{Si}_2\text{O}_4}(\text{ol}) - 3\bar{V}_{\text{Fe}_2\text{Si}_2\text{O}_6}(\text{opx}) - 2\bar{V}_{\text{Fe}_3\text{O}_4}(\text{sp}) \quad [\text{A.4}]$$

where the individual partial molar volume are given by the equation (Mattioli and Wood, 1988; see references therein):

$$\begin{aligned}\bar{V}_{\text{Fe}_{2\text{S}}\text{104}}(\text{ol}) &= 4.6262 + 0.029 [1 - X_{\text{Fe}_{2\text{S}}\text{104}}(\text{ol})] \\ \bar{V}_{\text{Fe}_{2\text{S}}\text{1206}}(\text{opx}) &= 6.5898 + 0.025 [1 - X_{\text{Fe}_{2\text{S}}\text{1206}}(\text{opx})] \\ \bar{V}_{\text{Fe}_{3\text{O}_4}}(\text{sp}) &= 4.458 + 0.126 [1 - X_{\text{Fe}_{3\text{O}_4}}(\text{sp})] \quad [\text{A.5}]\end{aligned}$$

-Results for experimental run PLZ36 (P=2.0GPa, T=1000°C)

In the calculation, all Fe in olivine and orthopyroxene is considered as ferrous (Mattioli et al., 1989). The largest source of error in this oxygen fugacity estimation is in the calculation of the ferric iron content of the spinel which was done assuming R_3O_4 stoichiometry as proposed by Mattioli et al. (1989).

The olivine and orthopyroxene compositions are averages for run PLZ36 that can be found in Appendix B1. These yield:

-For olivine:

$$\begin{aligned}X_{\text{Fe}} &= 0.0868 & X_{\text{Mg}} &= 0.9069 \\ a_{\text{Fe}_{2\text{S}}\text{104}} &= 0.0144 & V_{\text{Fe}_{2\text{S}}\text{104}} &= 4.6504\end{aligned}$$

-For orthopyroxene:

$$\begin{aligned}X_{\text{Fe}}^{\text{M1}} &= 0.0857 & X_{\text{Fe}}^{\text{M2}} &= 0.0898 \\ a_{\text{Fe}_{2\text{S}}\text{1206}} &= 0.0077 & V_{\text{Fe}_{2\text{S}}\text{1206}} &= 6.6144\end{aligned}$$

For spinel, the analyses yielding the lowest and the highest Fe_2O_3 (Appendix B1; PLZ36 SP5 and SP4 respectively) were used in order to give a range of possible $f\text{O}_2$.

-For lower Fe_2O_3 analysis:

$$X_{\text{Fe3O4}} = 0.0357 \quad X'_{\text{Fe2+}} = 0.1791$$

$$a_{\text{Fe3O4}} = 0.0238 \quad V_{\text{Fe3O4}} = 4.5752$$

-For higher Fe_2O_3 analysis:

$$X_{\text{Fe3O4}} = 0.0468 \quad X'_{\text{Fe2+}} = 0.0197$$

$$a_{\text{Fe3O4}} = 0.0450 \quad V_{\text{Fe3O4}} = 4.5725$$

Using all these data in equation [3.2] of section 3.4.2
yield a minimum and maximum $\log f\text{O}_2$ of

$$\log f\text{O}_2 = -8.03 \text{ to } -7.49.$$

The pressure-corrected fayalite-magnetite-quartz (FMQ)
buffer using the expression of Myers and Eugster (1983) and
the volume data of Berman (1988) yield:

$$\log f\text{O}_2(\text{FMQ}) = -9.17$$

APPENDIX B

MINERAL AND MELT CHEMICAL COMPOSITIONS

Nomenclature and abbreviations used:

-The structural formulae were calculated on a basis of:

4 oxygens for olivine	6 oxygens for pyroxenes
22 oxygens for phlogopite	24 oxygens for garnet
32 oxygens for spinel	

-OLIVINE

Fo :	forsterite	Fa :	fayalite
------	------------	------	----------

-PYROXENES

Wo :	wollastonite	En :	enstatite
Fs :	ferrosilite		

-PHLOGOPITE

OSO : octahedral site occupancy: $AL^{VI}+Cr+Ti+Fe+Mn+Mg$
K site : $K+Na+Ca$

-GARNET

Pyr :	pyrope	Gro :	grossular
Alm :	almandine	Spe :	spessartine
And :	andradite	Uva :	uvarovite

-GENERAL

Fe_2O_3 # and Fe^{3+} # : Calculated for perfect stoichiometry

Rec. ($H_2O/K_2O = 0.38$) : Recalculated assuming a H_2O/K_2O weight ratio of 0.38

Mg# : $-Mg/(Mg+Fe_{total})$ when all Fe is expressed as FeO
 $-Mg/(Mg+Fe^{2+})$ when Fe_2O_3 was estimated (spinel and garnet)

(c) : Analysis at the center of the grain

(b) : Analysis at the border of the grain

Beam d. : Beam diameter

Ave. : Average

A(x) : Average calculated without analysis x considered as relict composition

in SDW : For sandwich experiments, refers to analysis performed in the middle layer

in LHZ : For sandwich experiments, refers to analysis performed in the lherzolithic layers (CPL or PLZ)

APPENDIX B1

Experiment for oxygen fugacity estimation

Experiment FLE36Olivine and phlogopite analyses

P= 2.0 GPa

T= 1000 °C

time = 30 hours

	<u>Olivine</u>					<u>Phlogopite</u>		
	OL1	OL2	OL3	OL4	Ave.	PHL1	PHL2	
SiO2	40.71	40.49	40.27	40.54	40.50	SiO2	38.54	37.77
TiO2	0.03	0.01	0.01	0.02	0.02	TiO2	4.43	4.44
Al2O3	0.00	0.00	0.00	0.00	0.00	Al2O3	15.91	15.34
Cr2O3	0.06	0.00	0.06	0.02	0.04	Cr2O3	0.11	0.08
FeO*	8.60	8.25	8.60	8.84	8.57	FeO	5.97	5.97
MnO	0.14	0.19	0.13	0.11	0.14	MnO	0.05	0.1
MgO	50.76	50.28	50.11	49.95	50.27	MgO	20.95	20.46
NiO	0.36	0.35	0.33	0.30	0.34	CaO	0.15	0.2
CaO	0.06	0.08	0.10	0.09	0.08	Na2O	0.08	0.08
Na2O	0.00	0.00	0.00	0.00	0.00	K2O	9.16	9.06
K2O	0.00	0.00	0.00	0.00	0.00			
Total	100.72	99.65	99.61	99.87	99.96	Total	95.35	93.5
Si	0.9878	0.9915	0.9883	0.9924	0.9900	Si	5.4933	5.5000
Ti	0.0005	0.0002	0.0002	0.0004	0.0003	Al IV	2.5067	2.5000
Al	0.0000	0.0000	0.0000	0.0000	0.0000	Al VI	0.1668	0.1334
Cr	0.0012	0.0000	0.0012	0.0004	0.0007	Ti	0.4749	0.4862
Fe	0.1745	0.1689	0.1765	0.1810	0.1752	Cr	0.0124	0.0092
Mn	0.0029	0.0039	0.0027	0.0023	0.0030	Fe	0.7117	0.7270
Mg	1.8356	1.8348	1.8329	1.8223	1.8314	Mn	0.0060	0.0123
Ni	0.0070	0.0069	0.0065	0.0059	0.0066	Mg	4.4503	4.4402
Ca	0.0016	0.0021	0.0026	0.0024	0.0022	Ca	0.0229	0.0312
Na	0.0000	0.0000	0.0000	0.0000	0.0000	Na	0.0221	0.0226
K	0.0000	0.0000	0.0000	0.0000	0.0000	K	1.6357	1.6831
Total	3.0111	3.0084	3.0109	3.0070	3.0093	Total	15.5328	15.5453
Mg#	91.32	91.57	91.22	90.97	91.27	Mg#	86.21	85.93
Fo	91.19	91.39	91.09	90.86	91.13	OSO	5.8221	5.8084
Fa	8.81	8.61	8.91	9.14	8.87	K site	1.7107	1.7369

Experiment PL136**Pyroxenes analyses****P= 2.0 GPa****T= 1000 °C****time = 30 hours**

	<u>Orthopyroxene</u>					<u>Clinopyroxene</u>	
	OPX1	OPX2	OPX3	OPX4	Ave.	CPX1	CPX2
SiO2	56.59	56.22	56.29	56.13	56.31	52.86	52.94
TiO2	0.00	0.03	0.00	0.01	0.01	0.07	0.08
Al2O3	3.20	3.16	3.35	3.04	3.19	3.72	3.81
Cr2O3	0.31	0.29	0.43	0.30	0.33	0.54	0.45
FeO*	5.89	6.30	6.12	6.02	6.11	3.01	3.07
MnO	0.11	0.11	0.14	0.21	0.14	0.10	0.09
MgO	33.84	33.85	33.74	33.61	33.76	17.06	16.79
CaO	0.57	0.59	0.65	0.56	0.59	22.11	22.27
Na2O	0.00	0.00	0.00	0.00	0.00	0.83	0.87
K2O	0.00	0.00	0.00	0.00	0.00	0.00	0.00
Total	100.61	100.55	100.72	99.88	100.44	100.30	100.37
Si	1.9363	1.9291	1.9274	1.9365	1.9323	1.9156	1.9176
Al IV	0.0637	0.0709	0.0726	0.0635	0.0677	0.0844	0.0824
Al VI	0.0654	0.0569	0.0626	0.0602	0.0613	0.0745	0.0803
Ti	0.0000	0.0008	0.0000	0.0003	0.0003	0.0019	0.0022
Cr	0.0084	0.0079	0.0116	0.0082	0.0090	0.0155	0.0129
Fe	0.1714	0.1808	0.1753	0.1737	0.1753	0.0912	0.0930
Mn	0.0032	0.0032	0.0041	0.0061	0.0041	0.0031	0.0028
Mg	1.7256	1.7310	1.7217	1.7261	1.7266	0.9214	0.9064
Ca	0.0209	0.0217	0.0238	0.0207	0.0218	0.8585	0.8644
Na	0.0000	0.0000	0.0000	0.0000	0.0000	0.0583	0.0611
K	0.0000	0.0000	0.0000	0.0000	0.0000	0.0000	0.0000
Total	3.9949	4.0023	3.9992	3.9973	3.9984	4.0244	4.0230
Mg#	90.96	90.54	90.76	90.87	90.76	90.99	90.69
Wo	1.09	1.12	1.24	1.07	1.13	45.81	46.31
En	89.82	89.38	89.45	89.60	89.56	49.16	48.56
Fs	9.09	9.50	9.32	9.32	9.31	5.03	5.13

Experiment FLE36**Spinel analysis**

P= 2.0 GPa

T= 1000 °C

time = 30 hours

Spinel						
	SP1	SP2	SP3	SP4	SP5	Ave.
TiO2	0.07	0.07	0.08	0.05	0.06	0.07
Al2O3	50.75	50.54	50.52	49.55	50.82	50.44
Cr2O3	15.41	15.37	15.75	15.75	15.56	15.57
Fe2O3 ‡	3.92	4.33	4.50	4.62	3.55	4.18
FeO	9.55	9.58	9.31	9.22	9.64	9.46
MnO	0.06	0.02	0.06	0.05	0.02	0.04
MgO	19.83	19.84	20.12	19.79	19.77	19.87
Total	99.59	99.75	100.34	99.03	99.42	99.63
Ti	0.0112	0.0112	0.0127	0.0081	0.0096	0.0106
Al	12.7517	12.6946	12.6186	12.5592	12.7851	12.6818
Cr	2.5964	2.5888	2.6380	2.6770	2.6250	2.6250
Fe3+ ‡	0.6287	0.6942	0.7175	0.7475	0.5701	0.6716
Fe2+	1.7027	1.7077	1.6498	1.6583	1.7198	1.6876
Mn	0.0108	0.0036	0.0108	0.0091	0.0036	0.0076
Mg	6.2987	6.2987	6.3529	6.3410	6.2874	6.3159
Total	24.0003	23.9999	24.0002	24.0001	24.0003	24.0002
Mg#	78.72	78.67	79.38	79.27	78.52	78.91
Cr#	16.92	16.94	17.29	17.57	17.03	17.15
Y Al	79.81	79.45	78.99	78.58	80.01	79.37
Y Cr	16.25	16.20	16.51	16.75	16.43	16.43
Y Fe3+	3.94	4.35	4.49	4.68	3.57	4.20

APPENDIX B2

Experiments on PLZ

Olivine analyses

Melting experiments at 3.00Pa

PLZ series

	PLZ31 (1125 °C, 28hrs)				PLZ37 (1150 °C, 28hrs)				
	OL1	OL2	OL3	Ave.	OL1	OL2	OL3	OL4	Ave.
SiO ₂	41.01	41.38	40.47	40.95	41.00	40.34	40.87	41.20	40.85
TiO ₂	0.01	0.00	0.03	0.01	0.00	0.01	0.00	0.00	0.00
Al ₂ O ₃	0.02	0.12	0.00	0.05	0.00	0.08	0.01	0.00	0.02
Cr ₂ O ₃	0.05	0.00	0.00	0.02	0.04	0.02	0.04	0.05	0.04
FeO*	8.38	8.60	8.90	8.63	8.57	8.96	7.94	8.71	8.55
MnO	0.04	0.05	0.01	0.03	0.07	0.13	0.08	0.11	0.10
MgO	50.13	49.00	49.84	49.66	49.47	50.24	50.57	49.73	50.00
NiO	0.18	0.21	0.24	0.21	0.33	0.31	0.33	0.27	0.31
CaO	0.14	0.16	0.08	0.13	0.13	0.12	0.16	0.13	0.14
Na ₂ O	0.00	0.00	0.00	0.00	0.00	0.05	0.00	0.00	0.01
K ₂ O	0.00	0.00	0.00	0.00	0.00	0.04	0.00	0.00	0.01
Total	99.96	99.52	99.57	99.68	99.61	100.30	100.00	100.20	100.03
Si	0.9992	1.0119	0.9932	1.0014	1.0036	0.9852	0.9949	1.0030	0.9967
Ti	0.0002	0.0000	0.0006	0.0002	0.0000	0.0002	0.0000	0.0000	0.0000
Al	0.0006	0.0035	0.0000	0.0013	0.0000	0.0023	0.0003	0.0000	0.0006
Cr	0.0010	0.0000	0.0000	0.0003	0.0008	0.0004	0.0008	0.0010	0.0007
Fe	0.1708	0.1759	0.1827	0.1764	0.1754	0.1830	0.1617	0.1773	0.1744
Mn	0.0008	0.0010	0.0002	0.0007	0.0015	0.0027	0.0016	0.0023	0.0020
Mg	1.8202	1.7858	1.8228	1.8096	1.8048	1.8285	1.8347	1.8043	1.8181
Ni	0.0035	0.0041	0.0047	0.0041	0.0065	0.0061	0.0065	0.0053	0.0061
Ca	0.0037	0.0042	0.0021	0.0033	0.0034	0.0031	0.0042	0.0034	0.0035
Na	0.0000	0.0000	0.0000	0.0000	0.0000	0.0024	0.0000	0.0000	0.0006
K	0.0000	0.0000	0.0000	0.0000	0.0000	0.0012	0.0000	0.0000	0.0003
Total	2.9999	2.9864	3.0063	2.9975	2.9960	3.0151	3.0046	2.9965	3.0030
Mg#	91.42	91.03	90.89	91.12	91.14	90.90	91.90	91.05	91.25
Fo	91.39	90.99	90.88	91.09	91.07	90.78	91.83	90.95	91.16
Fa	8.61	9.01	9.12	8.91	8.93	9.22	8.17	9.05	8.84

Olivine analyses

Melting experiments at 3.0GPa

PLZ series

	PLZ21 (1175 °C, 20hrs)					PLZ22 (1200 °C, 20hrs)				
	OL1	OL2	OL3	OL4	Ave.	OL1	OL2	OL3	OL4	Ave.
SiO2	41.35	41.36	40.15	40.28	40.79	40.97	41.36	40.28	40.02	40.66
TiO2	0.00	0.02	0.00	0.03	0.01	0.05	0.01	0.07	0.02	0.04
Al2O3	0.07	0.08	0.05	0.05	0.06	0.11	0.13	0.03	0.00	0.07
Cr2O3	0.09	0.12	0.05	0.03	0.07	0.14	0.08	0.02	0.06	0.08
FeO*	7.56	7.67	9.24	9.12	8.40	9.00	8.77	8.22	8.55	8.64
MnO	0.06	0.13	0.15	0.12	0.12	0.06	0.04	0.10	0.13	0.08
MgO	50.80	50.70	49.48	50.07	50.26	49.59	50.44	51.03	50.80	50.47
NiO	0.34	0.34	0.33	0.32	0.33	0.37	0.29	0.28	0.34	0.32
CaO	0.13	0.16	0.09	0.13	0.13	0.15	0.22	0.12	0.14	0.16
Na2O	0.04	0.01	0.00	0.01	0.02	0.04	0.01	0.09	0.03	0.04
K2O	0.00	0.00	0.00	0.00	0.00	0.00	0.00	0.09	0.00	0.02
Total	100.44	100.59	99.54	100.16	100.18	100.48	101.35	100.33	100.09	100.56
Si	0.9996	0.9992	0.9889	0.9855	0.9934	0.9971	0.9962	0.9809	0.9787	0.9883
Ti	0.0000	0.0004	0.0000	0.0006	0.0002	0.0009	0.0002	0.0013	0.0004	0.0007
Al	0.0020	0.0023	0.0015	0.0014	0.0016	0.0032	0.0037	0.0009	0.0000	0.0019
Cr	0.0017	0.0023	0.0010	0.0006	0.0014	0.0027	0.0015	0.0004	0.0012	0.0014
Fe	0.1528	0.1550	0.1903	0.1866	0.1711	0.1832	0.1767	0.1674	0.1749	0.1755
Mn	0.0012	0.0027	0.0031	0.0025	0.0024	0.0012	0.0008	0.0021	0.0027	0.0017
Mg	1.8302	1.8254	1.8162	1.8257	1.8244	1.7987	1.8105	1.8521	1.8515	1.8281
Ni	0.0066	0.0066	0.0065	0.0063	0.0065	0.0072	0.0056	0.0055	0.0067	0.0063
Ca	0.0034	0.0041	0.0024	0.0034	0.0033	0.0039	0.0057	0.0031	0.0037	0.0041
Na	0.0019	0.0005	0.0000	0.0005	0.0007	0.0019	0.0005	0.0042	0.0014	0.0020
K	0.0000	0.0000	0.0000	0.0000	0.0000	0.0000	0.0000	0.0028	0.0000	0.0007
Total	2.9995	2.9984	3.0099	3.0131	3.0052	3.0000	3.0013	3.0207	3.0211	3.0107
Mg#	92.29	92.17	90.51	90.73	91.43	90.76	91.11	91.71	91.37	91.24
Fo	92.24	92.05	90.37	90.61	91.32	90.70	91.07	91.62	91.25	91.16
Fa	7.76	7.95	9.63	9.39	8.68	9.30	8.93	8.38	8.75	8.84

Olivine analyses

Melting experiments at 3.0GPa

PLZ series

	PLZ30 (1225 °C, 19hrs)				PLZ23 (1235 °C, 20hrs)			
	OL1	OL2	OL3	Ave.	OL1	OL2	OL3	Ave.
SiO2	40.72	41.06	40.94	40.91	40.90	40.84	40.41	40.72
TiO2	0.02	0.00	0.00	0.01	0.00	0.00	0.00	0.00
Al2O3	0.33	0.16	0.03	0.17	0.00	0.00	0.02	0.01
Cr2O3	0.07	0.00	0.10	0.06	0.07	0.07	0.09	0.08
FeO*	8.52	6.97	8.56	8.02	6.99	7.42	7.70	7.37
MnO	0.08	0.06	0.07	0.07	0.17	0.12	0.13	0.14
MgO	48.88	50.46	50.39	49.91	52.15	51.55	51.56	51.75
NiO	0.20	0.20	0.21	0.20	0.28	0.32	0.27	0.29
CaO	0.34	0.24	0.18	0.25	0.13	0.13	0.16	0.14
Na2O	0.03	0.01	0.01	0.02	0.00	0.05	0.00	0.02
K2O	0.04	0.00	0.00	0.01	0.00	0.00	0.00	0.00
Total	99.23	99.16	100.49	99.63	100.69	100.50	100.34	100.51
Si	1.0008	1.0020	0.9941	0.9989	0.9858	0.9880	0.9812	0.9850
Ti	0.0004	0.0000	0.0000	0.0001	0.0000	0.0000	0.0000	0.0000
Al	0.0096	0.0046	0.0009	0.0050	0.0000	0.0000	0.0006	0.0002
Cr	0.0014	0.0000	0.0019	0.0011	0.0013	0.0013	0.0017	0.0015
Fe	0.1751	0.1423	0.1738	0.1637	0.1409	0.1501	0.1564	0.1491
Mn	0.0017	0.0012	0.0014	0.0014	0.0035	0.0025	0.0027	0.0029
Mg	1.7903	1.8352	1.8234	1.8164	1.8733	1.8586	1.8657	1.8659
Ni	0.0040	0.0039	0.0041	0.0040	0.0054	0.0062	0.0053	0.0056
Ca	0.0090	0.0063	0.0047	0.0066	0.0034	0.0034	0.0042	0.0036
Na	0.0014	0.0005	0.0005	0.0008	0.0000	0.0023	0.0000	0.0008
K	0.0013	0.0000	0.0000	0.0004	0.0000	0.0000	0.0000	0.0000
Total	2.9948	2.9959	3.0048	2.9985	3.0135	3.0125	3.0177	3.0146
Mg#	91.09	92.81	91.30	91.73	93.00	92.53	92.27	92.60
Fo	91.01	92.75	91.23	91.66	92.84	92.41	92.15	92.47
Fa	8.99	7.25	8.77	8.34	7.16	7.59	7.85	7.53

Olivine analyses

Melting experiments at 3.0GPa

PLZ series

	PLZ32 (1250 °C, 10hrs)				PLZ29 (1275 °C, 6hrs)				
	OL1	OL2	OL3	Ave.	OL1	OL2	OL3	OL4	Ave.
SiO2	40.91	40.84	40.82	40.86	41.11	42.02	41.49	42.15	41.69
TiO2	0.01	0.00	0.00	0.00	0.00	0.01	0.03	0.00	0.01
Al2O3	0.08	0.02	0.00	0.03	0.02	0.00	0.00	0.09	0.03
Cr2O3	0.08	0.06	0.00	0.05	0.07	0.15	0.15	0.12	0.12
FeO*	8.55	8.41	7.97	8.31	3.45	2.48	2.30	2.61	2.71
MnO	0.09	0.09	0.05	0.08	0.08	0.09	0.02	0.08	0.07
MgO	49.44	49.80	50.36	49.87	54.52	55.50	54.90	55.31	55.06
NiO	0.23	0.21	0.18	0.21	0.16	0.20	0.21	0.21	0.20
CaO	0.20	0.13	0.15	0.16	0.16	0.16	0.11	0.20	0.16
Na2O	0.03	0.00	0.01	0.01	0.02	0.00	0.00	0.00	0.01
K2O	0.00	0.00	0.00	0.00	0.00	0.00	0.00	0.05	0.01
Total	99.82	99.56	99.54	99.57	99.59	100.61	99.21	100.82	100.06
Si	1.0014	0.9996	0.9973	0.9995	0.9855	0.9920	0.9923	0.9935	0.9909
Ti	0.0002	0.0000	0.0000	0.0001	0.0000	0.0002	0.0005	0.0000	0.0002
Al	0.0023	0.0006	0.0000	0.0010	0.0006	0.0000	0.0000	0.0025	0.0008
Cr	0.0015	0.0012	0.0000	0.0009	0.0013	0.0028	0.0028	0.0022	0.0023
Fe	0.1750	0.1722	0.1629	0.1700	0.0692	0.0490	0.0460	0.0515	0.0539
Mn	0.0019	0.0019	0.0010	0.0016	0.0016	0.0018	0.0004	0.0016	0.0014
Mg	1.8036	1.8166	1.8337	1.8180	1.9478	1.9528	1.9568	1.9430	1.9501
Ni	0.0045	0.0041	0.0035	0.0041	0.0031	0.0038	0.0040	0.0040	0.0037
Ca	0.0052	0.0034	0.0039	0.0042	0.0041	0.0040	0.0028	0.0051	0.0040
Na	0.0014	0.0000	0.0005	0.0006	0.0009	0.0000	0.0000	0.0000	0.0002
K	0.0000	0.0000	0.0000	0.0000	0.0000	0.0000	0.0000	0.0015	0.0004
Total	2.9972	2.9995	3.0029	2.9999	3.0140	3.0064	3.0058	3.0048	3.0077
Mg#	91.15	91.34	91.84	91.45	96.57	97.55	97.70	97.42	97.31
Fe	91.07	91.26	91.80	91.38	96.49	97.47	97.68	97.34	97.25
Fa	8.93	8.74	8.20	8.62	3.51	2.53	2.32	2.66	2.75

Olivine analyses

Melting experiments at 3.0GPa

PLI series

PLI35 (1300 °C, 5hrs)

	OL1	OL2	OL3	OL4	Ave.
SiO2	42.31	42.56	42.34	41.99	42.30
TiO2	0.00	0.00	0.00	0.01	0.00
Al2O3	0.01	0.00	0.06	0.08	0.04
Cr2O3	0.08	0.09	0.13	0.09	0.10
FeO*	1.67	1.13	1.36	1.86	1.51
MnO	0.11	0.15	0.12	0.17	0.14
MgO	55.94	56.85	56.43	55.79	56.25
NiO	0.15	0.03	0.08	0.14	0.10
CaO	0.22	0.17	0.19	0.16	0.19
Na2O	0.00	0.00	0.03	0.07	0.03
K2O	0.00	0.01	0.00	0.05	0.02
Total	100.49	100.99	100.74	100.41	100.66
Si	0.9958	0.9942	0.9929	0.9911	0.9935
Ti	0.0000	0.0000	0.0000	0.0002	0.0000
Al	0.0003	0.0000	0.0017	0.0022	0.0010
Cr	0.0015	0.0017	0.0024	0.0017	0.0018
Fe	0.0329	0.0221	0.0267	0.0367	0.0296
Mn	0.0022	0.0030	0.0024	0.0034	0.0027
Mg	1.9622	1.9791	1.9721	1.9625	1.9690
Ni	0.0028	0.0006	0.0015	0.0027	0.0019
Ca	0.0055	0.0043	0.0048	0.0040	0.0047
Na	0.0000	0.0000	0.0014	0.0032	0.0011
K	0.0000	0.0003	0.0000	0.0015	0.0004
Total	3.0033	3.0051	3.0058	3.0091	3.0058
Mg#	98.35	98.90	98.67	98.16	98.52
Fe	98.24	98.75	98.55	98.00	98.39
Fa	1.76	1.25	1.45	2.00	1.61

Olivine analyses

Melting experiments at 3.0GPa

PLI series (sandwich experiments)

	PLI33 (1225 °C, 8hrs)				PLI38 (1225 °C, 10hrs)			
	OL1	OL2	OL3	Ave.	OL1	OL2	OL3	Ave.
SiO2	40.84	40.56	41.04	40.81	39.86	40.45	40.65	40.32
TiO2	0.02	0.05	0.02	0.03	0.00	0.00	0.00	0.00
Al2O3	0.00	0.00	0.00	0.00	0.00	0.00	0.00	0.00
Cr2O3	0.04	0.14	0.09	0.09	0.04	0.02	0.01	0.02
FeO*	7.68	8.05	7.87	7.87	9.17	8.98	8.26	8.80
MnO	0.18	0.06	0.06	0.10	0.15	0.21	0.10	0.15
MgO	49.88	49.80	50.19	49.96	49.67	49.79	50.47	49.98
NiO	0.25	0.32	0.31	0.29	0.31	0.33	0.33	0.32
CaO	0.10	0.10	0.12	0.11	0.14	0.17	0.17	0.16
Na2O	0.00	0.00	0.00	0.00	0.00	0.00	0.00	0.00
K2O	0.14	0.00	0.00	0.05	0.01	0.00	0.00	0.00
Total	99.13	99.08	99.70	99.30	99.35	99.95	99.99	99.76
Si	1.0018	0.9970	1.0008	0.9999	0.9842	0.9910	0.9917	0.9890
Ti	0.0004	0.0009	0.0004	0.0006	0.0000	0.0000	0.0000	0.0000
Al	0.0000	0.0000	0.0000	0.0000	0.0000	0.0000	0.0000	0.0000
Cr	0.0008	0.0027	0.0017	0.0017	0.0008	0.0004	0.0002	0.0005
Fe	0.1576	0.1655	0.1605	0.1612	0.1894	0.1840	0.1685	0.1806
Mn	0.0037	0.0012	0.0012	0.0021	0.0031	0.0044	0.0021	0.0032
Mg	1.8235	1.8244	1.8241	1.8240	1.8278	1.8180	1.8349	1.8269
Ni	0.0049	0.0063	0.0061	0.0058	0.0062	0.0065	0.0065	0.0064
Ca	0.0026	0.0026	0.0031	0.0028	0.0037	0.0045	0.0044	0.0042
Na	0.0000	0.0000	0.0000	0.0000	0.0000	0.0000	0.0000	0.0000
K	0.0044	0.0000	0.0000	0.0015	0.0003	0.0000	0.0000	0.0001
Total	2.9996	3.0007	2.9980	2.9994	3.0155	3.0088	3.0083	3.0108
Mg#	92.05	91.68	91.91	91.88	90.61	90.81	91.59	91.00
Fe	91.87	91.63	91.85	91.78	90.47	90.61	91.49	90.86
Fa	8.13	8.37	8.15	8.22	9.53	9.39	8.51	9.14

Olivine analyses

Melting experiments at 3.0GPa

PLZ series (sandwich experiments)

PLZ40 (1225 °C, 1hr)

	OL1	OL2	OL3	OL4	Ave.
SiO2	40.96	40.91	41.10	41.02	41.00
TiO2	0.02	0.00	0.01	0.02	0.01
Al2O3	0.00	0.00	0.00	0.00	0.00
Cr2O3	0.09	0.09	0.03	0.07	0.07
FeO*	8.68	8.99	9.67	9.36	9.18
MnO	0.13	0.12	0.10	0.15	0.13
MgO	50.30	49.67	49.54	49.58	49.77
NiO	0.25	0.26	0.29	0.28	0.27
CaO	0.13	0.10	0.12	0.15	0.13
Na2O	0.00	0.00	0.00	0.00	0.00
K2O	0.01	0.00	0.00	0.00	0.00
Total	100.57	100.14	100.86	100.63	100.55
Si	0.9946	0.9985	0.9987	0.9981	0.9975
Ti	0.0004	0.0000	0.0002	0.0004	0.0002
Al	0.0000	0.0000	0.0000	0.0000	0.0000
Cr	0.0017	0.0017	0.0006	0.0013	0.0013
Fe	0.1763	0.1835	0.1965	0.1905	0.1867
Mn	0.0027	0.0025	0.0021	0.0031	0.0026
Mg	1.8202	1.8067	1.7940	1.7980	1.8047
Ni	0.0049	0.0051	0.0057	0.0055	0.0053
Ca	0.0034	0.0026	0.0031	0.0039	0.0033
Na	0.0000	0.0000	0.0000	0.0000	0.0000
K	0.0003	0.0000	0.0000	0.0000	0.0001
Total	3.0044	3.0006	3.0008	3.0008	3.0017
Mg#	91.17	90.78	90.13	90.42	90.63
Fo	91.05	90.67	90.03	90.28	90.51
Fa	8.95	9.33	9.97	9.72	9.49

Orthopyroxene analyses

Melting experiments at 3.0GPa

PLX series

	<u>PLX3</u> (1125 °C, 28hrs)					<u>PLX7</u> (1150 °C, 28hrs)				
	OPX1	OPX2	OPX3	OPX4	Ave.	OPX1	OPX2	OPX3	OPX4	Ave.
SiO2	56.02	56.54	55.83	55.89	56.07	55.76	56.29	55.80	56.19	56.04
TiO2	0.02	0.00	0.00	0.00	0.01	0.00	0.00	0.01	0.02	0.01
Al2O3	3.20	3.20	3.34	3.02	3.19	3.17	3.05	3.15	3.07	3.11
Cr2O3	0.29	0.23	0.27	0.18	0.24	0.29	0.2	0.27	0.31	0.29
FeO*	5.54	5.74	5.59	5.78	5.66	5.80	5.92	5.91	5.81	5.86
MnO	0.03	0.08	0.06	0.09	0.07	0.15	0.09	0.09	0.14	0.12
MgO	33.81	34.45	34.10	34.16	34.13	33.63	33.63	33.53	33.43	33.56
CaO	0.59	0.62	0.58	0.55	0.59	0.52	0.58	0.64	0.58	0.58
Na2O	0.06	0.07	0.05	0.05	0.06	0.05	0.00	0.00	0.00	0.01
K2O	0.00	0.00	0.00	0.00	0.00	0.01	0.01	0.00	0.00	0.01
Total	99.56	100.93	99.82	99.72	100.01	99.38	99.84	99.50	99.55	99.57
Si	1.9338	1.9280	1.9240	1.9296	1.9289	1.9319	1.9403	1.9345	1.9417	1.9371
Al IV	0.0662	0.0720	0.0760	0.0704	0.0711	0.0681	0.0597	0.0655	0.0583	0.0629
Al VI	0.0641	0.0566	0.0597	0.0525	0.0582	0.0614	0.0642	0.0630	0.0668	0.0638
Ti	0.0005	0.0000	0.0000	0.0000	0.0001	0.0000	0.0000	0.0003	0.0005	0.0002
Cr	0.0079	0.0062	0.0074	0.0049	0.0066	0.0079	0.0074	0.0074	0.0085	0.0078
Fe	0.1599	0.1637	0.1611	0.1669	0.1629	0.1681	0.1707	0.1710	0.1679	0.1694
Mn	0.0009	0.0023	0.0018	0.0026	0.0019	0.0044	0.0026	0.0026	0.0041	0.0034
Mg	1.7394	1.7507	1.7514	1.7576	1.7498	1.7365	1.7276	1.7293	1.7217	1.7287
Ca	0.0218	0.0227	0.0214	0.0203	0.0216	0.0193	0.0214	0.0237	0.0215	0.0215
Na	0.0040	0.0046	0.0033	0.0033	0.0038	0.0034	0.0000	0.0000	0.0000	0.0008
K	0.0000	0.0000	0.0000	0.0000	0.0000	0.0004	0.0004	0.0000	0.0000	0.0002
Total	3.9986	4.0069	4.0061	4.0082	4.0049	4.0013	3.9943	3.9973	3.9910	3.9960
Mg#	91.58	91.45	91.58	91.33	91.48	91.18	91.01	91.00	91.11	91.07
Wo	1.14	1.17	1.11	1.04	1.11	1.00	1.11	1.23	1.12	1.12
En	90.50	90.27	90.48	90.25	90.37	90.05	89.87	89.75	89.90	89.89
Fs	8.37	8.56	8.41	8.70	8.51	8.94	9.01	9.01	8.98	8.99

Orthopyroxene analyses

Melting experiments at 3.0GPa

PLI series

	PLI21 (1175 °C, 20hrs)					PLI22 (1200 °C, 20hrs)				
	OPX1	OPX2	OPX3	OPX4	Ave.	OPX1	OPX2	OPX3	OPX4	Ave.
SiO2	55.95	56.02	56.22	55.84	56.01	56.09	55.88	56.49	56.71	56.29
TiO2	0.00	0.04	0.05	0.03	0.03	0.05	0.02	0.04	0.05	0.04
Al2O3	3.48	3.42	3.19	3.22	3.33	3.07	3.23	3.20	3.30	3.20
Cr2O3	0.34	0.35	0.29	0.23	0.30	0.37	0.37	0.29	0.34	0.34
FeO*	5.86	6.10	6.01	6.01	6.00	6.05	5.95	6.07	5.86	5.98
MnO	0.12	0.10	0.10	0.11	0.11	0.13	0.09	0.13	0.11	0.12
MgO	34.13	33.32	34.17	33.85	33.87	33.85	34.16	33.61	33.40	33.76
CaO	0.63	0.63	0.60	0.63	0.62	0.54	0.47	0.59	0.62	0.58
Na2O	0.06	0.02	0.05	0.04	0.04	0.03	0.05	0.06	0.05	0.05
K2O	0.00	0.00	0.00	0.00	0.00	0.00	0.00	0.00	0.00	0.00
Total	100.57	100.00	100.68	99.96	100.30	100.18	100.22	100.46	100.44	100.33
Si	1.9177	1.9306	1.9250	1.9258	1.9248	1.9303	1.9219	1.9367	1.9419	1.9327
Al IV	0.0823	0.0694	0.0750	0.0742	0.0752	0.0697	0.0781	0.0633	0.0581	0.0673
Al VI	0.0583	0.0695	0.0538	0.0567	0.0596	0.0548	0.0528	0.0660	0.0751	0.0622
Ti	0.0000	0.0010	0.0013	0.0008	0.0008	0.0013	0.0005	0.0010	0.0013	0.0010
Cr	0.0092	0.0095	0.0079	0.0063	0.0082	0.0101	0.0101	0.0070	0.0092	0.0093
Fe	0.1680	0.1758	0.1721	0.1733	0.1723	0.1741	0.1711	0.1740	0.1678	0.1718
Mn	0.0035	0.0029	0.0029	0.0032	0.0031	0.0038	0.0026	0.0038	0.0032	0.0033
Mg	1.7434	1.7113	1.7437	1.7398	1.7346	1.7361	1.7509	1.7173	1.7045	1.7272
Ca	0.0231	0.0233	0.0220	0.0233	0.0229	0.0199	0.0173	0.0217	0.0227	0.0204
Na	0.0040	0.0013	0.0033	0.0027	0.0028	0.0020	0.0033	0.0040	0.0033	0.0032
K	0.0000	0.0000	0.0000	0.0000	0.0000	0.0000	0.0000	0.0000	0.0000	0.0000
Total	4.0094	3.9948	4.0070	4.0061	4.0044	4.0021	4.0086	3.9957	3.9872	3.9984
Mg#	91.21	90.68	91.02	90.94	90.96	90.86	91.10	90.60	91.04	90.95
Wo	1.19	1.22	1.13	1.20	1.19	1.03	0.89	1.13	1.20	1.06
En	89.96	89.44	89.85	89.70	89.74	89.77	90.16	89.59	89.79	89.83
Fs	8.85	9.34	9.02	9.10	9.08	9.20	8.95	9.28	9.01	9.11

Orthopyroxene analyses

Melting experiments at 3.0GPa

PLZ series

	PLZ30 (1225 °C, 19hrs)					PLZ23 (1235 °C, 20hrs)		
	OPX1	OPX2	OPX3	OPX4	Ave.	OPX1	OPX2	Ave.
SiO2	55.92	54.62	55.34	55.97	55.46	55.39	55.87	55.63
TiO2	0.00	0.17	0.02	0.00	0.05	0.01	0.00	0.01
Al2O3	3.41	4.73	3.66	3.28	3.77	3.30	2.91	3.11
Cr2O3	0.32	0.72	0.34	0.34	0.43	0.42	0.31	0.37
FeO*	5.70	5.33	5.74	5.67	5.61	6.02	5.81	5.92
MnO	0.07	0.04	0.05	0.00	0.04	0.12	0.12	0.12
MgO	33.72	33.04	33.59	34.04	33.60	33.84	34.08	33.96
CaO	0.66	1.67	0.78	0.61	0.93	0.66	0.60	0.63
Na2O	0.07	0.11	0.06	0.06	0.08	0.05	0.03	0.04
K2O	0.00	0.00	0.00	0.00	0.00	0.00	0.00	0.00
Total	99.87	100.43	99.58	99.97	99.96	99.81	99.73	99.77
Si	1.9271	1.8798	1.9151	1.9264	1.9121	1.9160	1.9301	1.9231
Al IV	0.0729	0.1202	0.0849	0.0736	0.0879	0.0840	0.0699	0.0769
Al VI	0.0657	0.0717	0.0644	0.0595	0.0653	0.0506	0.0487	0.0490
Ti	0.0000	0.0044	0.0005	0.0000	0.0012	0.0003	0.0000	0.0001
Cr	0.0087	0.0196	0.0093	0.0093	0.0117	0.0115	0.0085	0.0100
Fe	0.1643	0.1534	0.1661	0.1632	0.1617	0.1742	0.1679	0.1710
Mn	0.0020	0.0012	0.0015	0.0000	0.0012	0.0035	0.0035	0.0035
Mg	1.7318	1.6946	1.7324	1.7460	1.7262	1.7445	1.7547	1.7496
Ca	0.0244	0.0616	0.0289	0.0225	0.0344	0.0245	0.0222	0.0233
Na	0.0047	0.0073	0.0040	0.0040	0.0050	0.0034	0.0020	0.0027
K	0.0000	0.0000	0.0000	0.0000	0.0000	0.0000	0.0000	0.0000
Total	4.0016	4.0138	4.0071	4.0045	4.0067	4.0124	4.0074	4.0099
Mg#	91.34	91.70	91.25	91.45	91.43	90.92	91.27	91.10
Wo	1.27	3.22	1.50	1.16	1.79	1.26	1.14	1.20
En	90.08	88.69	89.81	90.39	89.74	89.62	90.06	89.84
Fs	8.65	8.09	8.69	8.45	8.47	9.13	8.80	8.96

Orthopyroxene analysis

Melting experiments at 3.0GPa

FLI series

	FLX32 (1250 °C, 10hrs)					FLX29 (1275 °C, 6hrs)				
	OPX1	OPX2	OPX3	OPX4	Ave.	OPX1	OPX2	OPX3	OPX4	Ave.
SiO2	56.55	54.42	55.75	56.39	55.78	55.72	56.63	55.93	54.97	55.81
TiO2	0.06	0.19	0.00	0.06	0.08	0.08	0.02	0.08	0.13	0.08
Al2O3	3.22	4.04	3.21	3.09	3.39	3.40	3.32	3.24	5.28	3.81
Cr2O3	0.22	0.58	0.22	0.20	0.31	0.28	0.35	0.45	1.30	0.60
FeO*	6.07	5.41	5.96	5.70	5.79	4.53	5.15	3.87	2.30	3.96
MnO	0.09	0.08	0.05	0.12	0.09	0.08	0.09	0.14	0.10	0.10
MgO	34.02	33.11	33.80	4.13	33.77	34.30	34.26	34.76	33.94	34.32
CaO	0.52	1.84	0.57	0.66	0.92	0.79	0.66	1.17	1.92	1.14
Na2O	0.00	0.06	0.00	0.03	0.02	0.03	0.00	0.03	0.08	0.04
K2O	0.00	0.00	0.00	0.00	0.00	0.00	0.00	0.02	0.02	0.01
Total	100.85	99.73	99.56	100.38	100.13	99.21	100.48	99.69	100.04	99.86
Si	1.9315	1.8862	1.9285	1.9329	1.9204	1.9241	1.9336	1.9209	1.8766	1.9138
Al IV	0.0685	0.1118	0.0715	0.0671	0.0796	0.0759	0.0664	0.0791	0.1234	0.0862
Al VI	0.0612	0.0535	0.0594	0.0578	0.0580	0.0625	0.0672	0.0521	0.0891	0.0678
Ti	0.0015	0.0050	0.0000	0.0015	0.0020	0.0021	0.0005	0.0021	0.0033	0.0020
Cr	0.0059	0.0159	0.0060	0.0054	0.0083	0.0076	0.0094	0.0122	0.0351	0.0161
Fe	0.1734	0.1570	0.1724	0.1634	0.1666	0.1308	0.1471	0.1112	0.0657	0.1136
Mn	0.0026	0.0024	0.0015	0.0035	0.0025	0.0023	0.0026	0.0041	0.0029	0.0030
Mg	1.7318	1.7121	1.7425	1.7435	1.7325	1.7652	1.7434	1.7792	1.7268	1.7536
Ca	0.0227	0.0684	0.0211	0.0242	0.0340	0.0292	0.0241	0.0431	0.0702	0.0417
Na	0.0000	0.0040	0.0000	0.0020	0.0015	0.0020	0.0000	0.0020	0.0053	0.0023
K	0.0000	0.0000	0.0000	0.0000	0.0000	0.0000	0.0000	0.0009	0.0009	0.0004
Total	3.9991	4.0183	4.0030	4.0014	4.0054	4.0018	3.9944	4.0068	3.9993	4.0005
Mg*	90.90	91.60	91.00	91.43	91.23	93.10	92.22	94.12	96.34	93.91
Wo	1.18	3.53	1.09	1.25	1.76	1.52	1.26	2.22	3.76	2.18
En	89.71	88.26	89.93	90.12	89.51	91.58	9	91.83	92.56	91.72
Fs	9.12	8.21	8.97	8.63	8.73	6.91	7.81	5.95	3.67	6.10

Orthopyroxene analyses

Melting experiments at 3.0GPa

PLZ series

PLZ35 (1300 °C, 5hrs)

	OPX1	OPX2	OPX3	OPX4	Ave.
SiO2	55.24	55.13	55.35	54.49	55.05
TiO2	0.06	0.08	0.23	0.20	0.14
Al2O3	3.38	3.76	3.92	5.01	4.02
Cr2O3	0.46	1.04	0.86	1.37	0.93
FeO*	4.73	2.08	4.16	2.36	3.33
MnO	0.14	0.14	0.11	0.07	0.12
MgO	34.72	35.93	34.23	33.64	34.63
CaO	0.90	1.71	1.52	2.10	1.56
Na2O	0.00	0.00	0.00	0.08	0.02
K2O	0.00	0.00	0.00	0.03	0.01
Total	99.63	99.87	100.38	99.35	99.81
Si	1.8062	1.8848	1.8954	1.8760	1.8906
Al IV	0.0938	0.1152	0.1046	0.1240	0.1094
Al VI	0.0437	0.0363	0.0537	0.0793	0.0532
Ti	0.0016	0.0021	0.0059	0.0052	0.0037
Cr	0.0125	0.0281	0.0233	0.0373	0.0253
Fe	0.1365	0.0595	0.1191	0.0680	0.0957
Mn	0.0041	0.0041	0.0032	0.0020	0.0033
Mg	1.7856	1.8307	1.7469	1.7260	1.7724
Ca	0.0333	0.0626	0.0558	0.0775	0.0573
Na	0.0000	0.0000	0.0000	0.0053	0.0013
K	0.0000	0.0000	0.0000	0.0013	0.0003
Total	4.0172	4.0233	4.0079	4.0019	4.0126
Mg#	92.90	96.85	93.62	96.21	94.86
Wo	1.70	3.20	2.90	4.13	2.97
En	91.13	93.55	90.75	92.13	91.89
Fs	7.18	3.25	6.35	3.74	5.14

Orthopyroxene analyses

Melting experiments at 3.0GPa

PLZ series (sandwich experiments)

	PLZ33 (1225 °C, 8hrs)					PLZ38 (1225 °C, 10hrs)				
	OPX1	OPX2	OPX3	OPX4	Ave.	OPX1	OPX2	OPX3	OPX4	Ave.
SiO2	56.17	55.66	56.51	55.49	55.96	56.04	56.19	54.31	56.44	55.75
TiO2	0.07	0.08	0.03	0.05	0.06	0.04	0.03	0.17	0.02	0.07
Al2O3	3.22	3.02	2.95	3.19	3.10	3.05	3.32	4.98	2.89	3.56
Cr2O3	0.38	0.32	0.33	0.28	0.33	0.33	0.36	1.17	0.28	0.54
FeO*	5.49	5.45	5.61	5.64	5.55	5.76	5.92	5.44	5.74	5.72
MnO	0.07	0.11	0.11	0.11	0.10	0.15	0.10	0.18	0.10	0.13
MgO	34.54	34.25	34.54	34.21	34.39	33.41	33.30	32.01	33.83	33.14
CaO	0.66	0.72	0.54	0.52	0.61	0.52	0.94	1.76	0.55	0.94
Na2O	0.07	0.00	0.00	0.00	0.02	0.00	0.00	0.00	0.00	0.00
K2O	0.01	0.00	0.00	0.00	0.00	0.00	0.00	0.00	0.00	0.00
Total	100.68	99.61	100.62	99.49	100.10	99.30	100.16	100.02	99.85	99.83
Si	1.9204	1.9234	1.9318	1.9203	1.9240	1.9411	1.9332	1.8796	1.9435	1.9244
Al IV	0.0796	0.0766	0.0682	0.0797	0.0760	0.0589	0.0668	0.1204	0.0565	0.0756
Al VI	0.0501	0.0465	0.0507	0.0504	0.0494	0.0657	0.0679	0.0828	0.0608	0.0693
Ti	0.0018	0.0021	0.0008	0.0013	0.0015	0.0010	0.0008	0.0044	0.0005	0.0017
Cr	0.0103	0.0087	0.0089	0.0077	0.0089	0.0090	0.0098	0.0320	0.0076	0.0146
Fe	0.1570	0.1575	0.1604	0.1632	0.1595	0.1669	0.1703	0.1575	0.1653	0.1650
Mn	0.0020	0.0032	0.0032	0.0032	0.0029	0.0044	0.0029	0.0053	0.0029	0.0039
Mg	1.7599	1.7639	1.7597	1.7644	1.7620	1.7247	1.7074	1.6511	1.7361	1.7049
Ca	0.0242	0.0267	0.0198	0.0193	0.0225	0.0193	0.0347	0.0653	0.0203	0.0349
Na	0.0046	0.0000	0.0000	0.0000	0.0012	0.0000	0.0000	0.0000	0.0000	0.0000
K	0.0004	0.0000	0.0000	0.0000	0.0001	0.0000	0.0000	0.0000	0.0000	0.0000
Total	4.0103	4.0086	4.0035	4.0095	4.0080	3.9910	3.9938	3.9983	3.9935	3.9942
Mg#	91.81	91.80	91.65	91.53	91.70	91.18	90.93	91.29	91.31	91.18
Wo	1.24	1.37	1.02	0.99	1.15	1.01	1.81	3.47	1.05	1.83
En	90.57	90.40	90.56	90.48	90.50	90.05	89.15	87.87	90.21	89.33
Fs	8.18	8.24	8.42	8.54	8.34	8.94	9.05	8.66	8.74	8.85

Orthopyroxene analyses

Melting experiments at 3.00Pa

PLZ series (sandwich experiments)

PLZ10 (1225 °C, 1hr)

	OPX1	OPX2	OPX3	OPX4	Ave.
SiO2	55.70	55.98	55.39	55.57	55.66
TiO2	0.00	0.00	0.00	0.02	0.01
Al2O3	3.06	3.25	2.96	3.19	3.12
Cr2O3	0.24	0.33	0.25	0.34	0.29
FeO*	5.82	6.13	6.27	5.82	6.01
MnO	0.10	0.09	0.13	0.10	0.11
MgO	33.63	33.86	33.58	33.48	33.64
CaO	0.48	0.64	0.45	0.71	0.57
Na2O	0.00	0.01	0.01	0.00	0.01
K2O	0.00	0.01	0.00	0.00	0.00
Total	99.03	100.30	99.04	99.23	99.40
Si	1.9353	1.9252	1.9299	1.9293	1.9299
Al IV	0.0647	0.0748	0.0701	0.0707	0.0701
Al VI	0.0607	0.2570	0.0515	0.0598	0.0573
Ti	0.0000	0.0000	0.0000	0.0005	0.0001
Cr	0.0066	0.0090	0.0069	0.0093	0.0079
Fe	0.1691	0.1763	0.1827	0.1690	0.1743
Mn	0.0029	0.0026	0.0038	0.0029	0.0031
Mg	1.7415	1.7354	1.7437	1.7323	1.7382
Ca	0.0179	0.0236	0.0168	0.0264	0.0212
Na	0.0000	0.0007	0.0007	0.0000	0.0003
K	0.0000	0.0004	0.0000	0.0000	0.0001
Total	3.9987	4.0050	4.0062	4.0003	4.0025
Mg#	91.15	90.78	90.52	91.11	90.89
Wo	0.93	1.22	0.86	1.37	1.09
En	90.17	89.55	89.58	89.73	89.75
Fs	8.91	9.23	9.58	8.91	9.16

Clinopyroxene analyses

Melting experiments at 3.0GPa

FLK series

	FLK31 (1125 °C, 28hrs)					FLK37 (1150 °C, 28hrs)				
	CPX1	CPX2	CPX3	CPX4	Ave.	CPX1	CPX2	CPX3	CPX4	Ave.
SiO2	52.80	53.08	52.93	53.43	53.06	53.27	52.31	53.20	53.30	53.02
TiO2	0.10	0.13	0.08	0.08	0.10	0.05	0.19	0.11	0.09	0.11
Al2O3	3.87	3.89	3.91	3.98	3.91	3.78	4.57	3.85	3.71	3.93
Cr2O3	0.51	0.52	0.46	0.58	0.52	0.54	0.73	0.77	0.84	0.67
FeO*	3.11	2.73	2.72	2.73	2.82	2.95	3.03	2.72	3.04	2.84
MnO	0.08	0.05	0.05	0.03	0.05	0.08	0.13	0.08	0.06	0.08
MgO	16.43	17.10	16.46	16.82	16.70	16.88	16.97	16.76	16.95	16.89
CaO	22.28	21.93	22.52	21.88	22.15	22.26	21.20	22.49	22.19	22.04
Na2O	0.93	0.88	0.89	0.97	0.92	0.85	0.82	0.83	0.80	0.83
K2O	0.00	0.00	0.00	0.00	0.00	0.02	0.07	0.08	0.04	0.05
Total	100.09	100.31	100.02	100.50	100.23	100.68	100.02	100.67	100.82	100.55
Si	1.9187	1.9184	1.9215	1.9258	1.9211	1.9217	1.8982	1.9207	1.9209	1.9154
Al IV	0.0813	0.0816	0.0785	0.0742	0.0789	0.0783	0.1018	0.0793	0.0791	0.0846
Al VI	0.0845	0.0842	0.0888	0.0949	0.0881	0.0825	0.0937	0.0760	0.0785	0.0827
Ti	0.0027	0.0035	0.0022	0.0022	0.0027	0.0014	0.0052	0.0030	0.0024	0.0030
Cr	0.0147	0.0149	0.0132	0.0165	0.0148	0.0154	0.0209	0.0220	0.0182	0.0191
Fe	0.0945	0.0825	0.0826	0.0823	0.0855	0.0890	0.0920	0.0821	0.0916	0.0887
Mn	0.0018	0.0015	0.0015	0.0009	0.0015	0.0024	0.0040	0.0018	0.0018	0.0025
Mg	0.8898	0.9211	0.8905	0.9035	0.9012	0.9075	0.9178	0.9018	0.9104	0.9094
Ca	0.8675	0.8493	0.8760	0.8450	0.8594	0.8604	0.8243	0.8700	0.8569	0.8530
Na	0.0655	0.0617	0.0626	0.0678	0.0644	0.0595	0.0577	0.0581	0.0559	0.0578
K	0.0000	0.0000	0.0000	0.0000	0.0000	0.0009	0.0032	0.0037	0.0018	0.0024
Total	4.0211	4.0186	4.0174	4.0131	4.0175	4.0190	4.0188	4.0186	4.0176	4.0185
Mg#	90.40	91.78	91.51	91.65	91.34	91.07	90.89	91.65	90.86	91.11
Wo	46.80	45.80	47.33	46.13	46.52	46.28	44.85	46.88	46.05	46.02
En	48.00	49.67	48.12	49.33	48.78	48.81	49.93	48.59	48.93	49.06
Fs	5.20	4.53	4.55	4.54	4.70	4.92	5.22	4.52	5.02	4.92

Glinovrovskans analyses

Melting experiments at 3.0GPa

PLI series

	PLK21 (1175 °C, 20hrs)					PLK22 (1200 °C, 20hrs)				
	CPX1	CPX2	CPX3	CPX4	Ave.	CPX1	CPX2	CPX3	CPX4	Ave.
SiO2	52.33	52.80	53.51	53.03	52.92	52.03	52.53	53.47	53.53	52.89
TiO2	0.09	0.14	0.09	0.12	0.11	0.42	0.10	0.12	0.14	0.20
Al2O3	3.86	4.22	3.56	3.84	3.87	4.81	3.94	3.58	3.65	4.00
Cr2O3	0.50	0.60	0.75	0.68	0.63	0.90	0.73	0.72	0.60	0.74
FeO*	2.87	2.97	2.97	3.01	2.96	3.37	2.78	2.84	3.00	3.00
MnO	0.04	0.06	0.11	0.09	0.08	0.11	0.06	0.06	0.06	0.07
MgO	17.11	16.50	16.56	16.43	16.65	18.03	16.64	16.76	16.86	17.07
CaO	21.64	22.49	22.51	22.73	22.34	19.99	22.22	22.40	22.30	21.73
Na2O	0.80	0.82	0.82	0.82	0.82	0.74	0.78	0.82	0.78	0.78
K2O	0.10	0.00	0.00	0.00	0.03	0.06	0.00	0.00	0.00	0.02
Total	99.34	100.60	100.88	100.75	100.39	100.46	99.78	100.77	100.92	100.48
Si	1.9125	1.9084	1.9282	1.9160	1.9163	1.8781	1.9127	1.9268	1.9258	1.9109
Al IV	0.0875	0.0916	0.0718	0.0840	0.0837	0.1219	0.0873	0.0732	0.0742	0.0891
Al VI	0.0788	0.0882	0.0794	0.0795	0.0815	0.0828	0.0818	0.0789	0.0806	0.0810
Ti	0.0025	0.0038	0.0024	0.0033	0.0030	0.0114	0.0027	0.0033	0.0038	0.0053
Cr	0.0144	0.0171	0.0214	0.0194	0.0181	0.0257	0.0210	0.0205	0.0171	0.0211
Fe	0.0877	0.0898	0.0895	0.0910	0.0895	0.1017	0.0847	0.0856	0.0903	0.0906
Mn	0.0012	0.0018	0.0034	0.0028	0.0023	0.0034	0.0019	0.0018	0.0018	0.0022
Mg	0.9319	0.8888	0.8893	0.8847	0.8956	0.9699	0.9030	0.9001	0.9040	0.9193
Ca	0.8474	0.8710	0.8691	0.8800	0.8669	0.7732	0.8669	0.8649	0.8596	0.8411
Na	0.0567	0.0575	0.0573	0.0574	0.0572	0.0518	0.0551	0.0573	0.0544	0.0546
K	0.0047	0.0000	0.0000	0.0000	0.0012	0.0028	0.0000	0.0000	0.0000	0.0007
Total	4.0253	4.0180	4.0118	4.0180	4.0183	4.0226	4.0170	4.0123	4.0116	4.0159
Mg#	91.40	90.83	90.86	90.68	90.94	90.51	91.43	91.32	90.92	91.03
Wo	45.36	47.05	46.95	47.35	46.68	41.83	46.70	46.69	46.32	45.39
En	49.88	48.01	48.04	47.61	48.38	52.48	48.64	48.59	48.71	49.60
Fs	4.76	4.95	5.02	5.04	4.94	5.69	4.66	4.72	4.96	5.01

Clinopyroxene analyses

Melting experiments at 3.0GPa

PLX series

	PLX30 (1225 °C, 19hrs)					PLX23 (1235 °C, 20hrs)				
	CPX1	CPX2	CPX3	CPX4	Ave.	CPX1	CPX2	CPX3	CPX4	A(1,2)
SiO2	53.13	52.69	52.26	52.67	52.69	53.39	53.28	53.23	52.96	53.10
TiO2	0.18	0.24	0.14	0.04	0.15	0.08	0.14	0.18	0.31	0.25
Al2O3	4.25	4.37	4.48	3.50	4.15	3.74	3.56	4.12	4.38	4.28
Cr2O3	0.62	0.64	0.63	0.56	0.61	0.56	0.69	0.71	1.05	0.88
FeO*	3.15	3.22	2.92	3.01	3.08	2.83	2.96	2.73	3.33	3.03
MnO	0.08	0.00	0.11	0.05	0.06	0.09	0.09	0.08	0.11	0.10
MgO	17.42	18.64	17.21	16.77	17.51	16.32	16.59	17.06	18.41	17.74
CaO	21.34	19.21	20.90	21.92	20.84	21.85	21.67	20.96	18.80	19.88
Na2O	0.77	0.71	0.73	0.84	0.76	0.87	0.89	0.73	0.64	0.69
K2O	0.00	0.03	0.00	0.00	0.01	0.00	0.00	0.00	0.00	0.00
Total	100.94	99.75	99.38	99.36	99.86	99.73	99.87	99.80	99.99	99.90
Si	1.9082	1.9046	1.9040	1.9257	1.9106	1.9391	1.9346	1.9263	1.9090	1.9176
Al IV	0.0918	0.0954	0.0960	0.0743	0.0894	0.0609	0.0654	0.0737	0.0910	0.0824
Al VI	0.0882	0.0908	0.0964	0.0765	0.0880	0.0993	0.0870	0.1021	0.0951	0.0986
Ti	0.0049	0.0065	0.0038	0.0011	0.0041	0.0022	0.0038	0.0049	0.0064	0.0067
Cr	0.0176	0.0183	0.0181	0.0162	0.0176	0.0161	0.0198	0.0203	0.0299	0.0251
Fe	0.0946	0.0973	0.0890	0.0920	0.0933	0.0860	0.0899	0.0826	0.1004	0.0915
Mn	0.0024	0.0000	0.0034	0.0015	0.0018	0.0028	0.0028	0.0025	0.0034	0.0029
Mg	0.9324	1.0041	0.9345	0.9138	0.9463	0.8834	0.8978	0.9201	0.9890	0.9546
Ca	0.8212	0.7440	0.8159	0.8587	0.8098	0.8503	0.8431	0.8127	0.7261	0.7693
Na	0.0536	0.0498	0.0516	0.0595	0.0536	0.0613	0.0627	0.0512	0.0447	0.0480
K	0.0000	0.0014	0.0000	0.0000	0.0003	0.0000	0.0000	0.0000	0.0000	0.0000
Total	4.0150	4.0122	4.0127	4.0195	4.0148	4.0012	4.0068	3.9964	3.9970	3.9967
Mg#	90.79	91.16	91.31	90.85	91.03	91.13	90.90	91.76	90.78	91.25
Wo	44.37	40.32	44.28	46.02	43.75	46.66	45.98	44.71	39.92	42.31
En	50.38	54.41	50.71	48.97	51.12	48.47	48.96	50.61	54.37	52.50
Fs	5.24	5.27	5.01	5.02	5.14	4.87	5.05	4.68	5.70	5.19

Clinopyroxene analyses

Melting experiments at 3.0GPa

FLZ series

	FLZ32 (1250 °C, 10hrs)					FLZ29 (1275 °C, 6hrs)				
	CPX1	CPX2	CPX3	CPX4	Ave.	CPX1	CPX2	CPX3	CPX4	Ave.
SiO2	51.99	52.61	52.04	52.30	52.24	51.98	51.81	53.30	52.91	52.50
TiO2	0.38	0.28	0.15	0.42	0.31	0.27	0.25	0.23	0.24	0.25
Al2O3	5.30	4.58	4.25	5.18	4.83	5.40	5.34	4.47	4.81	5.01
Cr2O3	1.14	0.55	0.53	0.76	0.75	1.56	1.53	1.20	1.43	1.43
FeO*	3.48	3.25	3.12	3.51	3.34	1.51	2.32	1.81	2.35	2.00
MnO	0.11	0.00	0.06	0.00	0.04	0.04	0.06	0.09	0.08	0.07
MgO	19.03	18.10	18.94	21.77	19.46	19.69	19.73	18.80	20.85	19.77
CaO	18.30	20.11	19.96	14.45	18.21	19.20	18.24	19.97	17.28	18.67
Na2O	0.52	0.62	0.72	0.49	0.59	0.45	0.38	0.42	0.36	0.40
K2O	0.01	0.10	0.03	0.11	0.06	0.01	0.02	0.00	0.04	0.02
Total	100.26	100.20	99.80	98.99	99.81	100.11	99.68	100.29	100.35	100.11
Si	1.8706	1.8982	1.8873	1.8824	1.8846	1.8628	1.8662	1.9071	1.8854	1.8804
Al IV	0.1294	0.1018	0.1127	0.1176	0.1154	0.1372	0.1338	0.0929	0.1146	0.1196
Al VI	0.0954	0.0930	0.0890	0.1022	0.0899	0.0910	0.0930	0.0957	0.0875	0.0918
Ti	0.0103	0.0076	0.0041	0.0114	0.0083	0.0073	0.0068	0.0062	0.0064	0.0067
Cr	0.0324	0.0157	0.0152	0.0216	0.0212	0.0442	0.0436	0.0339	0.0403	0.0405
Fe	0.1047	0.0981	0.0946	0.1057	0.1008	0.0453	0.0699	0.0542	0.0700	0.0598
Mn	0.0034	0.0000	0.0018	0.0000	0.0013	0.0012	0.0018	0.0027	0.0024	0.0020
Mg	1.0204	0.9732	1.0237	1.1678	1.0464	1.0516	1.0591	1.0025	1.1073	1.0552
Ca	0.7055	0.7774	0.7756	0.5573	0.7038	0.7373	0.7040	0.7656	0.6598	0.7166
Na	0.0363	0.0434	0.0506	0.0342	0.0411	0.0313	0.0265	0.0291	0.0249	0.0280
K	0.0005	0.0046	0.0014	0.0051	0.0029	0.0005	0.0009	0.0000	0.0018	0.0008
Total	4.0089	4.0130	4.0361	4.0051	4.0157	4.0096	4.0056	3.9900	4.0004	4.0014
Mg#	90.69	90.85	91.54	91.70	91.21	95.87	93.81	94.87	94.05	94.63
Wo	38.47	42.05	40.91	30.44	38.00	40.17	38.37	41.95	35.87	39.08
En	55.64	52.64	54.00	63.79	56.49	57.30	57.72	54.93	60.19	57.54
Fs	5.89	5.30	5.09	5.77	5.51	2.53	3.91	3.12	3.94	3.37

Clinopyroxene analyses

Melting experiments at 3.0GPa

PLZ series

PLZ35 (1300 °C, 5hrs)					
	CPX1	CPX2	CPX3	CPX4	Ave.
SiO2	52.68	52.41	52.86	53.07	52.78
TiO2	0.15	0.20	0.24	0.20	0.20
Al2O3	3.89	3.98	4.23	4.18	4.07
Cr2O3	1.12	1.51	1.53	1.56	1.43
FeO*	1.30	1.74	2.28	1.74	1.76
MnO	0.09	0.16	0.10	0.05	0.10
MgO	19.91	20.34	20.41	20.33	20.25
CaO	19.63	18.77	17.74	18.57	18.68
Na2O	0.45	0.38	0.35	0.33	0.38
K2O	0.05	0.02	0.03	0.03	0.03
Total	99.27	99.51	99.75	100.04	99.64
Si	1.9026	1.8904	1.8976	1.8990	1.8974
Al IV	0.0974	0.1096	0.1024	0.1010	0.1026
Al VI	0.0682	0.0596	0.0767	0.0745	0.0698
Ti	0.0041	0.0054	0.0065	0.0054	0.0053
Cr	0.0320	0.0431	0.0434	0.0441	0.0407
Fe	0.0393	0.0525	0.0679	0.0521	0.0529
Mn	0.0028	0.0049	0.0030	0.0015	0.0030
Mg	1.0717	1.0934	1.0920	1.0841	1.0853
Ca	0.7597	0.7254	0.6824	0.7120	0.7198
Na	0.0315	0.0266	0.0244	0.0229	0.0263
K	0.0023	0.0009	0.0014	0.0014	0.0015
Total	4.0114	4.0118	3.9975	3.9980	4.0047
Mg#	96.47	95.42	94.15	95.42	95.35
Wo	40.55	38.67	36.98	38.49	38.68
En	57.21	58.28	59.18	58.61	58.32
Fs	2.24	3.06	3.84	2.90	3.01

Clinopyroxene analyses

Melting experiments at 3.0GPa

FL3 series (sandwich experiments)

	FL333 (1225 °C, 8hrs)					FL338 (1225 °C, 10hrs)				
	CPX1 in LHZ	CPX2 in LHZ	CPX3 in LHZ	CPX4 in LHZ	Ave.	CPX1 in LHZ	CPX2 in LHZ	CPX3 in LHZ	CPX4 in LHZ	Ave.
SiO2	53.41	53.31	53.82	54.06	53.65	52.82	52.17	53.07	51.82	52.47
TiO2	0.14	0.11	0.16	0.08	0.12	0.06	0.27	0.08	0.26	0.17
Al2O3	3.63	3.66	3.29	3.43	3.50	3.59	4.50	3.98	5.17	4.31
Cr2O3	0.66	0.57	0.57	0.56	0.59	0.54	1.16	0.58	1.49	0.94
FeO*	2.69	2.73	3.00	2.74	2.79	2.89	3.49	3.00	3.23	3.15
MnO	0.03	0.06	0.03	0.08	0.05	0.12	0.14	0.10	0.07	0.11
MgO	16.66	16.95	17.13	16.91	16.91	16.65	19.59	16.79	18.38	17.85
CaO	22.34	21.61	21.75	22.37	22.02	22.24	18.41	22.50	19.64	20.70
Na2O	0.72	0.73	0.72	0.73	0.73	0.78	0.63	0.83	0.58	0.71
K2O	0.07	0.00	0.00	0.00	0.02	0.15	0.04	0.01	0.00	0.05
Total	100.35	99.73	100.47	100.96	100.38	99.84	100.40	100.94	100.64	100.45
Si	1.9303	1.9340	1.9401	1.9399	1.9361	1.9238	1.8780	1.9122	1.8651	1.8947
Al IV	0.0697	0.0660	0.0599	0.0601	0.0639	0.0762	0.1220	0.0878	0.1349	0.1053
Al VI	0.0850	0.0905	0.0800	0.0850	0.0851	0.0780	0.0690	0.0812	0.0845	0.0782
Ti	0.0038	0.0030	0.0043	0.0022	0.0033	0.0016	0.0073	0.0022	0.0070	0.0045
Cr	0.0189	0.0163	0.0162	0.0159	0.0168	0.0155	0.0330	0.0165	0.0424	0.0269
Fe	0.0813	0.0828	0.0904	0.0822	0.0842	0.0880	0.1051	0.0904	0.0972	0.0952
Mn	0.0009	0.0018	0.0009	0.0024	0.0015	0.0037	0.0043	0.0031	0.0021	0.0033
Mg	0.8973	0.9164	0.9203	0.9043	0.9096	0.9038	1.0510	0.9016	0.9859	0.9608
Ca	0.8651	0.8400	0.8401	0.8601	0.8514	0.8680	0.7101	0.8687	0.7574	0.8008
Na	0.0505	0.0513	0.0503	0.0508	0.0507	0.0551	0.0440	0.0580	0.0405	0.0494
K	0.0032	0.0000	0.0000	0.0000	0.0008	0.0070	0.0018	0.0005	0.0000	0.0023
Total	4.0060	4.0023	4.0027	4.0029	4.0034	4.0207	4.0256	4.0221	4.0172	4.0214
Mg#	91.69	91.71	91.05	91.67	91.53	91.12	90.91	90.89	91.02	90.98
Wo	46.90	45.63	45.37	46.52	46.10	46.58	37.97	46.61	41.10	43.05
En	48.64	49.78	49.70	48.91	49.26	48.50	56.19	48.38	53.50	51.65
Fs	4.46	4.60	4.93	4.58	4.64	4.92	5.85	5.01	5.39	5.30

Glinopyroxene analyses

Melting experiments at 3.0GPa

PLX series (sandwich experiments)

PLX40 (1225 °C, 1hr)

	CPX1 in LHZ	CPX2 in LHZ	CPX3 in LHZ	CPX4 in LHZ	Ave.	Quench in SDW	Quench in SDW
SiO ₂	53.03	52.63	52.93	51.29	52.47	51.25	49.03
TiO ₂	0.09	0.15	0.12	0.15	0.13	0.95	1.28
Al ₂ O ₃	3.52	4.20	3.52	4.12	3.84	6.63	7.27
Cr ₂ O ₃	0.19	0.98	0.59	0.80	0.64	0.04	0.00
FeO*	2.91	2.94	2.91	3.58	3.09	5.02	5.61
MnO	0.10	0.08	0.03	0.08	0.07	0.19	0.14
MgO	16.94	17.20	16.90	19.93	17.74	17.42	14.45
CaO	21.91	20.89	21.97	18.69	20.87	15.16	15.97
Na ₂ O	0.81	0.83	0.79	0.79	0.81	1.05	0.84
K ₂ O	0.04	0.03	0.05	0.03	0.04	1.01	1.14
Total	99.54	99.91	99.81	99.46	99.68	98.72	95.73
Si	1.9319	1.9089	1.9253	1.8694	1.9089	1.8758	1.8638
Al IV	0.0881	0.0911	0.0747	0.1306	0.0911	0.1242	0.1362
Al VI	0.0831	0.0885	0.0763	0.0465	0.0736	0.1619	0.1896
Ti	0.0025	0.0041	0.0033	0.0041	0.0035	0.0262	0.0366
Cr	0.0055	0.0281	0.0170	0.0231	0.0184	0.0012	0.0000
Fe	0.0887	0.0892	0.0885	0.1091	0.0939	0.1537	0.1783
Mn	0.0031	0.0018	0.0009	0.0025	0.0021	0.0059	0.0045
Mg	0.9197	0.9297	0.9162	1.0826	0.9620	0.9502	0.8186
Ca	0.8553	0.8119	0.8563	0.7299	0.8134	0.5946	0.6505
Na	0.0572	0.0584	0.0557	0.0558	0.0568	0.0745	0.0619
K	0.0019	0.0014	0.0023	0.0014	0.0017	0.0472	0.0553
Total	4.0168	4.0130	4.0165	4.0550	4.0253	4.0152	3.9953
Mg#	91.21	91.25	91.19	90.84	91.11	86.08	82.11
Wo	45.82	44.30	45.99	37.94	43.47	34.88	39.38
En	49.27	50.73	49.21	56.26	51.41	55.75	49.55
Fs	4.91	4.97	4.80	5.80	5.13	9.36	11.07

Phlogopite analyses

Melting experiments at 3.0GPa

PLK series

	PLK31 (1125 °C, 28hrs)					PLK37 (1150 °C, 28hrs)				
	PHL 1	PHL 2	PHL 3	PHL 4	Ave.	PHL 1	PHL 2	PHL 3	PHL 4	Ave.
SiO2	37.40	38.90	38.61	39.53	38.61	37.57	38.98	38.32	38.07	38.23
TiO2	3.45	3.59	3.37	3.32	3.43	4.41	3.53	4.55	3.93	4.11
Al2O3	18.59	18.18	17.17	17.76	17.93	16.19	15.89	15.30	15.79	15.79
Cr2O3	2.03	0.79	1.13	0.72	1.17	1.08	1.34	1.31	1.55	1.32
FeO*	3.91	4.30	4.08	3.96	4.06	4.28	4.04	4.23	4.04	4.14
MnO	0.08	0.04	0.00	0.00	0.03	0.06	0.08	0.00	0.02	0.04
MgO	20.38	20.64	20.67	21.01	20.69	19.80	21.10	21.15	21.91	20.94
CaO	0.08	0.00	0.16	0.21	0.11	0.16	0.19	0.32	0.13	0.20
Na2O	0.04	0.04	0.00	0.04	0.03	0.00	0.00	0.00	0.00	0.00
K2O	10.78	10.68	10.47	10.38	10.58	9.96	9.54	9.31	9.68	9.62
Total	96.74	97.16	95.66	96.93	96.62	93.79	94.67	94.49	95.12	94.39
Si	5.2749	5.4327	5.4700	5.5104	5.4242	5.4726	5.5621	5.4945	5.4324	5.4905
Al IV	2.7251	2.5673	2.5220	2.4896	2.5758	2.5274	2.4379	2.5055	2.5676	2.5095
Al VI	0.3660	0.4260	0.3500	0.4290	0.3930	0.2528	0.2365	0.0808	0.0887	0.1644
Ti	0.3659	0.3771	0.3596	0.3481	0.3627	0.4631	0.3790	0.4906	0.4218	0.4434
Cr	0.2263	0.0872	0.1267	0.0793	0.1297	0.1244	0.1512	0.1485	0.1749	0.1489
Fe	0.4612	0.5022	0.4641	0.4617	0.4773	0.5190	0.4624	0.5072	0.4821	0.4976
Mn	0.0096	0.0047	0.0000	0.0000	0.0036	0.0074	0.0097	0.0000	0.0024	0.0049
Mg	4.2838	4.2959	4.3706	4.3648	4.3288	4.2549	4.4894	4.5195	4.6594	4.4819
Ca	0.0121	0.0000	0.0243	0.0314	0.0169	0.0250	0.0291	0.0492	0.0199	0.0308
Na	0.0109	0.0108	0.0000	0.0108	0.0082	0.0000	0.0000	0.0000	0.0000	0.0000
K	1.9398	1.9029	1.8952	1.8460	1.8958	1.8509	1.7376	1.7031	1.7622	1.7631
Total	15.6757	15.6069	15.6106	15.5710	15.6159	15.5175	15.5149	15.4990	15.6114	15.5356
Mg#	90.28	89.53	90.03	90.43	90.07	89.13	90.30	89.91	90.62	90.01
OSO	5.7129	5.6931	5.6911	5.6828	5.6950	5.6416	5.7482	5.7467	5.8293	5.7419
K site	1.9628	1.9137	1.9195	1.8882	1.9209	1.8759	1.7867	1.7522	1.7821	1.7939

Phlogopite analyses**Melting experiments at 3.0GPa****PLI series**

	PLI21 (1175 °C, 20hrs)				PLI22 (1200 °C, 20hrs)				
	PHL 1	PHL2	PHL3	Ave.	PHL 1	PHL2	PHL3	PHL4	Ave.
SiO2	37.31	37.98	38.05	37.78	38.42	38.61	38.72	38.21	38.49
TiO2	5.05	3.57	5.00	4.54	4.59	4.42	5.31	4.84	4.79
Al2O3	16.11	16.95	17.05	16.70	15.65	17.06	16.43	16.46	16.40
Cr2O3	1.68	1.32	1.64	1.55	2.01	1.99	2.17	2.33	2.13
FeO*	4.02	3.33	3.88	3.74	3.89	3.61	4.04	4.08	3.91
MnO	0.00	0.04	0.02	0.02	0.00	0.05	0.05	0.05	0.04
MgO	20.66	21.12	19.66	20.48	21.19	19.79	19.22	20.05	20.06
CaO	0.08	0.02	0.20	0.10	0.82	0.12	0.15	0.19	0.32
Na2O	0.08	0.05	0.04	0.06	0.05	0.04	0.05	0.03	0.04
K2O	9.98	10.51	9.96	10.15	9.36	10.40	10.28	9.81	9.96
Total	94.97	94.89	95.50	95.12	95.98	96.09	96.42	96.05	96.14
Si	5.3516	5.4279	5.4047	5.3948	5.4344	5.4536	5.4645	5.4095	5.4405
Al IV	2.6484	2.5721	2.5953	2.6052	2.5656	2.5464	2.5355	2.5905	2.5595
Al VI	0.0758	0.2837	0.2598	0.2067	0.0442	0.2945	0.1981	0.1568	0.1734
Ti	0.5448	0.3837	0.5341	0.4876	0.4883	0.4695	0.5636	0.5153	0.5092
Cr	0.1905	0.1491	0.1842	0.1746	0.2248	0.2222	0.2421	0.2608	0.2375
Fe	0.4822	0.3980	0.4609	0.4470	0.4602	0.4264	0.4768	0.4831	0.4616
Mn	0.0000	0.0048	0.0024	0.0024	0.0000	0.0060	0.0060	0.0060	0.0045
Mg	4.4164	4.4983	4.1618	4.3584	4.4669	4.1659	4.0425	4.2304	4.2263
Ca	0.0123	0.0031	0.0304	0.0153	0.1243	0.0182	0.0227	0.0288	0.0485
Na	0.0222	0.0139	0.0110	0.0157	0.0137	0.0110	0.0137	0.0082	0.0116
K	1.8263	1.9163	1.8049	1.8491	1.6891	1.8741	1.8509	1.7719	1.7966
Total	15.5706	15.6510	15.4495	15.5568	15.5114	15.4879	15.4164	15.4612	15.4692
Mg#	90.16	91.87	90.03	90.70	90.66	90.71	89.45	89.75	90.15
OSO	5.7097	5.7178	5.6032	5.6767	5.6843	5.5846	5.5291	5.6523	5.6125
K site	1.8608	1.9332	1.8464	1.8801	1.8271	1.9032	1.8873	1.8089	1.8587

Phosonite analyses

Melting experiments at 3.0GPa

PLZ series

	PLZ30 (1225 °C, 19hrs)					PLZ23 (1235 °C, 20hrs)				
	PHL 1	PHL2	PHL3	PHL4	Ave.	PHL 1	PHL2	PHL3	PHL4	Ave.
SiO2	37.60	37.67	37.82	38.14	37.81	37.70	38.07	38.36	37.59	37.93
TiO2	7.13	7.46	6.84	6.73	7.04	6.05	5.61	5.99	6.07	5.83
Al2O3	16.79	15.83	15.89	15.98	16.12	15.50	16.44	16.47	16.34	16.19
Cr2O3	1.58	1.56	1.62	1.41	1.54	2.36	2.29	2.58	2.74	2.49
FeO*	3.90	4.11	3.95	4.19	4.04	3.78	3.30	3.30	3.03	3.35
MnO	0.07	0.05	0.07	0.06	0.06	0.05	0.07	0.06	0.05	0.06
MgO	18.34	18.24	19.81	19.73	19.03	19.32	19.70	19.46	19.16	19.41
CaO	0.09	0.48	0.13	0.15	0.21	0.32	0.09	0.17	0.17	0.17
Na2O	0.00	0.04	0.04	0.04	0.03	0.05	0.09	0.07	0.04	0.08
K2O	16.98	10.39	10.31	10.05	10.43	9.54	9.97	9.83	10.09	9.86
Total	96.48	95.83	96.48	96.48	96.32	94.67	95.63	96.29	95.27	95.47
Si	5.3284	5.3728	5.3476	5.3821	5.3577	5.4145	5.4004	5.4012	5.3621	5.3945
Al IV	2.6716	2.6272	2.6488	2.6179	2.6423	2.5855	2.5996	2.5988	2.6379	2.6055
Al VI	0.1335	0.0345	0.0000	0.0405	0.0512	0.0384	0.1498	0.1351	0.1100	0.1087
Ti	0.7599	0.8002	0.7274	0.7142	0.7503	0.6535	0.5985	0.6343	0.6512	0.6343
Cr	0.1770	0.1759	0.1811	0.1573	0.1728	0.2680	0.2568	0.2872	0.3090	0.2802
Fe	0.4622	0.4903	0.4671	0.4945	0.4785	0.4540	0.3915	0.3886	0.3615	0.3948
Mn	0.0084	0.0060	0.0084	0.0072	0.0075	0.0061	0.0084	0.0072	0.0060	0.0069
Mg	3.8734	3.8771	4.1745	4.1493	4.0190	4.1353	4.1648	4.0835	4.0732	4.1141
Ca	0.0137	0.0734	0.0197	0.0227	0.0323	0.0492	0.0137	0.0256	0.0168	0.0263
Na	0.0000	0.0111	0.0110	0.0109	0.0082	0.0139	0.0248	0.0191	0.0249	0.0207
K	1.8854	1.8906	1.8599	1.8093	1.8861	1.7480	1.8043	1.7658	1.8363	1.7886
Total	15.4132	15.3590	15.4454	15.4060	15.4060	15.3688	15.4126	15.3464	15.3889	15.3786
Mg#	89.34	88.77	89.94	89.35	89.36	90.11	91.41	91.31	91.85	91.16
OSO	5.4144	5.3840	5.5585	5.5630	5.4794	5.5557	5.5698	5.5359	5.5109	5.5430
K	1.9988	1.9750	1.8905	1.8429	1.9268	1.8112	1.8428	1.8106	1.8780	1.8356

Phlogopite analyses

Melting experiments at 3.0GPa

PLZ series

	PLZ32 (1250 °C, 10hrs)					PLZ29 (1275 °C, 6hrs)			
	PHL 1	PHL2	PHL3	PHL4	Ave.	PHL 1	PHL2	PHL3	Ave.
SiO2	37.84	38.89	38.92	38.09	38.44	41.19	39.63	41.42	40.75
TiO2	5.54	6.71	6.29	6.64	6.30	2.34	2.61	2.06	2.34
Al2O3	15.62	15.38	15.65	17.10	15.94	17.01	17.84	15.83	16.89
Cr2O3	1.71	1.60	1.80	1.75	1.72	0.16	0.10	0.12	0.13
FeO*	3.96	4.23	4.24	3.68	4.03	1.72	1.91	2.01	1.88
MnO	0.00	0.06	0.05	0.04	0.04	0.00	0.10	0.01	0.04
MgO	19.34	19.71	19.24	18.77	19.27	23.80	22.33	23.81	23.31
CaO	0.15	0.21	0.19	0.21	0.19	0.73	0.42	0.54	0.56
Na2O	0.02	0.04	0.00	0.05	0.03	0.12	0.10	0.10	0.11
K2O	10.50	10.42	10.64	10.53	10.52	9.05	9.59	8.89	9.18
Total	94.68	97.25	97.02	96.06	96.45	96.12	94.63	94.79	95.18
Si	5.4526	5.4551	5.4759	5.3525	5.4339	5.6725	5.5718	5.7822	5.6757
Al IV	2.5474	2.5433	2.5241	2.6475	2.5661	2.3275	2.4282	2.2178	2.3243
Al VI	0.1061	0.0000	0.0718	0.1854	0.0903	0.4342	0.5288	0.3874	0.4499
Ti	0.0004	0.7078	0.6658	0.7017	0.6693	0.2424	0.2760	0.2163	0.2448
Cr	0.1948	0.1774	0.2002	0.1944	0.1917	0.0174	0.0111	0.0132	0.0139
Fe	0.4772	0.4962	0.4989	0.4325	0.4762	0.1981	0.2246	0.2347	0.2190
Mn	0.0000	0.0071	0.0060	0.0048	0.0045	0.0000	0.0119	0.0012	0.0043
Mg	4.1533	4.1203	4.0343	3.9309	4.0592	4.8847	4.6789	4.9536	4.8397
Ca	0.0232	0.0316	0.0286	0.0316	0.0288	0.1077	0.0633	0.0808	0.0841
Na	0.0056	0.0109	0.0000	0.0136	0.0075	0.0320	0.0273	0.0271	0.0288
K	1.9303	1.8647	1.9099	1.8878	1.8980	1.5901	1.7202	1.5833	1.6308
Total	15.4908	15.4144	15.4154	15.3828	15.4255	15.5066	15.5419	15.4975	15.5152
Mg#	89.69	89.25	88.99	90.09	89.50	96.10	95.42	95.45	95.67
OSO	5.5318	5.5089	5.4763	5.4497	5.4912	5.7768	5.7312	5.8064	5.7716
K site	1.9590	1.9071	1.9365	1.9331	1.9343	1.7298	1.8107	1.6911	1.7437

Phlocozite analyses

Melting experiments at 3.0GPa

PLZ series (sandwich experiments)

	PLZ33 (1225 °C, 8hrs)					PLZ38 (1225 °C, 10hrs)				
	PHL 1 in SDW	PHL2 in SDW	PHL3 in SDW	PHL4 in LHZ	Ave.	PHL1 in LHZ	PHL2 in LHZ	PHL3 in LHZ	PHL4 in LHZ	Ave.
SiO2	40.49	39.39	39.06	37.58	39.13	39.14	38.75	38.60	39.58	39.02
TiO2	5.39	5.55	4.82	4.12	4.97	4.93	4.70	4.89	4.25	4.69
Al2O3	15.33	16.78	17.62	16.30	16.51	16.80	17.23	16.43	16.34	16.72
Cr2O3	0.05	0.09	0.06	2.18	0.60	0.92	1.26	1.70	2.04	1.23
FeO*	4.75	4.92	4.34	4.09	4.53	5.20	4.85	21	3.78	4.76
MnO	0.03	0.00	0.01	0.00	0.01	0.06	0.05	0.07	0.03	0.05
MgO	19.44	20.33	20.67	19.61	20.01	19.28	19.48	20.20	19.78	19.69
CaO	1.31	0.45	0.16	0.09	0.50	0.08	0.07	0.08	0.30	0.13
Na2O	0.10	0.07	0.07	0.10	0.09	0.01	0.01	0.05	0.00	0.02
K2O	9.46	10.33	10.32	10.16	10.07	10.02	10.32	10.13	8.78	9.81
Total	96.35	97.91	97.13	94.23	96.41	96.53	96.72	96.36	94.88	96.12
Si	5.6824	5.4687	5.4434	5.4361	5.5080	5.5100	5.4532	5.4591	5.6014	5.5058
Al IV	2.3176	2.5313	2.5566	2.5639	2.4920	2.4900	2.5468	2.5409	2.3986	2.4942
Al VI	0.2188	0.2152	0.3382	0.2158	0.2473	0.3132	0.3118	0.1985	0.3276	0.2878
Ti	0.5689	0.5795	0.5052	0.4482	0.5261	0.5220	0.4974	0.5201	0.4523	0.4980
Cr	0.0055	0.0099	0.0066	0.2493	0.0662	0.1024	0.1402	0.0783	0.2282	0.1372
Fe	0.5575	0.5713	0.5058	0.4948	0.5327	0.6122	0.5708	0.6162	0.4474	0.5618
Mn	0.0036	0.0000	0.0012	0.0000	0.0012	0.0072	0.0060	0.0084	0.0036	0.0063
Mg	4.0680	4.2065	4.2930	4.2276	4.1982	4.0450	4.0855	4.2576	4.1718	4.1398
Ca	0.1470	0.0669	0.0239	0.0139	0.0758	0.0121	0.0106	0.0121	0.0455	0.0200
Na	0.0272	0.0188	0.0189	0.0280	0.0232	0.0027	0.0027	0.0137	0.0000	0.0048
K	1.6938	1.8297	1.8348	1.8750	1.8079	1.7996	1.8528	1.8278	1.5852	1.7865
Total	15.3382	15.4979	15.5276	15.5527	15.4787	15.4164	15.4778	15.5327	15.2617	15.4222
Mg#	87.94	88.04	89.46	89.52	89.74	86.85	87.74	87.36	90.31	88.05
OSO	5.4203	5.5824	5.6500	5.6357	5.5718	5.6020	5.6117	5.6791	5.6310	5.6309
K site	1.9180	1.9155	1.8776	1.9170	1.9069	1.8144	1.8661	1.8536	1.6307	1.7914

Phlogopite analyses

Melting experiments at 3.0GPa

PLZ series (sandwich experiments)

PLZ10 (1225 °C, 1hr)

	PHL 1 in LHZ	PHL2 in LHZ	PHL3 in LHZ	PHL4 in LHZ	PHL5 in LHZ	A(5)
SiO2	39.62	38.67	38.97	40.37	38.75	39.41
TiO2	4.13	4.49	4.61	4.16	6.56	4.35
Al2O3	16.09	16.71	17.43	15.74	16.93	16.49
Cr2O3	0.59	0.47	0.49	0.49	0.39	0.51
FeO*	3.98	4.61	4.68	4.51	5.22	4.45
MnO	0.02	0.03	0.03	0.02	0.05	0.03
MgO	20.92	19.32	19.26	20.38	18.87	19.97
CaO	0.11	0.16	0.09	0.59	0.04	0.24
Na2O	0.12	0.19	0.11	0.12	0.10	0.14
K2O	9.69	10.29	10.19	9.02	10.44	9.80
Total	95.27	94.94	95.86	95.40	97.35	95.37
Si	5.6038	5.5317	5.5090	5.6904	5.4265	5.5840
Al IV	2.3962	2.4683	2.4910	2.3096	2.5735	2.4160
Al VI	0.2868	0.3497	0.4139	0.3060	0.2216	0.3391
Ti	0.4393	0.4830	0.4901	0.4410	0.6909	0.4633
Cr	0.0660	0.0532	0.0548	0.0546	0.0432	0.0571
Fe	0.4708	0.5515	0.5533	0.5317	0.6114	0.5268
Mn	0.0024	0.0036	0.0036	0.0024	0.0059	0.0030
Mg	4.4097	4.1188	4.0577	4.2812	3.9383	4.2172
Ca	0.0167	0.0245	0.0136	0.0591	0.0060	0.0361
Na	0.0329	0.0527	0.0302	0.0328	0.0272	0.0371
K	1.7485	1.8779	1.8378	1.6221	1.8652	1.7712
Total	15.4731	15.5150	15.4550	15.3609	15.4096	15.4508
Mg#	90.35	88.19	88.00	88.95	86.56	88.90
OSO	5.6750	5.5599	5.5734	5.6169	5.5112	5.6064
K site	1.7981	1.9552	1.8816	1.7440	1.8984	1.8443

Garnet analyses

Melting experiments at 3.4 kPa

PLZ series

	PLZ31 (1125 °C, 28hrs)			PLZ37 (1150 °C, 28hrs)			PLZ21 (1175 °C, 20hrs)		
	GAR1	GAR2	Ave.	GAR1	GAR2	Ave.	GAR1	GAR2	Ave.
SiO2	42.00	42.25	42.13	41.59	42.55	42.35	42.45		
TiO2	0.84	0.48	0.66	1.10	0.33	0.65	0.49		
Al2O3	20.73	20.33	20.53	22.03	21.99	20.82	21.41		
Cr2O3	2.10	2.64	2.37	1.24	1.97	2.39	2.18		
Fe2O3#	0.97	0.94	0.96	0.17	0.75	1.48	1.12		
FeO	5.33	5.34	5.34	5.87	4.66	4.60	4.63		
MnO	0.29	0.30	0.30	0.26	0.28	0.20	0.24		
MgO	20.42	20.41	20.42	19.62	21.62	20.79	21.21		
CaO	7.00	6.97	6.99	7.51	6.02	7.32	6.87		
Na2O	0.00	0.00	0.00	0.00	0.00	0.00	0.00		
K2O	0.00	0.00	0.00	0.00	0.00	0.00	0.00		
Total	99.68	99.66	99.67	99.39	100.17	100.60	100.38		
Si	5.9950	6.0366	6.0158	5.9461	5.9906	5.9844	5.9875		
Al IV	0.0050	0.0000	0.0000	0.0539	0.0094	0.0156	0.0125		
Al VI	3.4833	3.4245	3.4564	3.6582	3.6405	3.4528	3.5468		
Ti	0.0902	0.0516	0.0709	0.1183	0.0349	0.0691	0.0520		
Cr	0.2370	0.2982	0.2676	0.1402	0.2193	0.2670	0.2431		
Fe3+ #	0.1042	0.1011	0.1026	0.0183	0.0795	0.1574	0.1183		
Fe2+	0.6359	0.6386	0.6373	0.7015	0.5481	0.5434	0.5458		
Mn	0.0351	0.0363	0.0357	0.0315	0.0334	0.0239	0.0287		
Mg	4.3438	4.3460	4.3449	4.1804	4.5363	4.3782	4.4574		
Ca	1.0706	1.0671	1.0688	1.1505	0.9082	1.1083	1.0081		
Na	0.0000	0.0000	0.0000	0.0000	0.0000	0.0000	0.0000		
K	0.0000	0.0000	0.0000	0.0000	0.0000	0.0000	0.0000		
Total	16.0001	16.0000	16.0000	15.9999	16.0002	16.0002	16.0002		
Mgf	87.23	87.19	87.21	85.63	89.22	88.96	89.09		
Pyr	71.4	71.4	71.4	68.9	75.3	72.3	73.8		
Gro	6.2	6.0	6.1	11.2	6.5	5.5	6.0		
Alm	10.5	10.5	10.5	11.6	9.1	9.0	9.0		
Spe	0.6	0.6	0.6	0.5	0.6	0.4	0.5		
And	5.5	4.2	4.9	4.4	3.1	6.2	4.7		
Uva	5.8	7.3	6.6	3.5	5.5	6.6	6.0		

Melting experiments at 3.0GPa

PLX series

	PLX22 (1200 °C, 20hrs)			PLX30 (1225 °C, 19hrs)			PLX23 (1235 °C, 20hrs)
	GAR1	GAR2	Ave.	GAR1	GAR2	Ave.	GAR1
SiO2	42.33	41.86	42.10	42.30	42.49	42.40	42.24
TiO2	0.83	0.73	0.78	0.69	0.54	0.62	0.81
Al2O3	21.66	21.01	21.34	20.44	20.10	20.27	21.33
Cr2O3	1.59	2.80	2.20	3.12	3.10	3.11	2.66
Fe2O3 \ddagger	0.74	1.03	0.89	0.48	0.00	0.24	0.13
FeO	5.61	5.35	5.48	4.73	4.69	4.71	5.61
MnO	0.16	0.22	0.19	0.25	0.17	0.21	0.24
MgO	20.10	19.72	19.91	20.81	20.89	20.85	20.38
CaO	7.62	7.80	7.71	7.13	7.14	7.14	7.07
Na2O	0.00	0.00	0.00	0.00	0.00	0.00	0.00
K2O	0.00	0.00	0.00	0.00	0.00	0.00	0.00
Total	100.64	100.52	100.58	99.95	99.12	99.53	100.47
Si	5.9801	5.9494	5.9648	6.0126	6.0750	6.0437	5.9786
Al IV	0.0199	0.0506	0.0352	0.0000	0.0000	0.0000	0.0214
Al VI	3.5876	3.4697	3.5288	3.4252	3.3880	3.4067	3.5378
Ti	0.0882	0.0780	0.0831	0.0738	0.0581	0.0659	0.0862
Cr	0.1776	0.3146	0.2459	0.3506	0.3504	0.3505	0.2976
Fe3+ \ddagger	0.0787	0.1102	0.0944	0.0513	0.0000	0.0257	0.0138
Fe2+	0.6633	0.6363	0.6498	0.5621	0.5608	0.5614	0.6644
Mn	0.0191	0.0265	0.0228	0.0301	0.0206	0.0254	0.0288
Mg	4.2319	4.1770	4.2045	4.4084	4.4512	4.4297	4.2989
Ca	1.1535	1.1878	1.1706	1.0859	1.0938	1.0899	1.0722
Na	0.0000	0.0000	0.0000	0.0000	0.0000	0.0000	0.0000
K	0.0000	0.0000	0.0000	0.0000	0.0000	0.0000	0.0000
Total	15.9999	16.0001	16.0000	16.0000	15.9978	15.9990	15.9999
Mg \ddagger	86.45	86.78	86.61	88.69	88.81	88.75	86.61
Pyr	69.7	69.3	69.5	72.4	72.7	72.5	70.9
Gro	9.8	8.5	8.2	5.5	7.4	6.4	7.1
Alm	10.9	10.6	10.7	9.2	9.2	9.2	11.0
Spe	0.3	0.4	0.4	0.5	0.3	0.4	0.5
And	4.9	5.3	5.1	3.7	1.9	2.8	3.2
Uva	4.4	7.8	6.1	8.6	8.6	8.6	7.4

Garnet analyses

250

Melting experiments at 3.0GPa

PLI series

PLE32 (1250 °C, 10hrs)			
	GAR1	GAR2	Ave.
SiO2	42.53	41.98	42.26
TiO2	0.74	0.94	0.84
Al2O3	21.13	20.84	20.99
Cr2O3	1.71	1.80	1.76
Fe2O3 [§]	0.00	0.64	0.29
FeO	6.05	5.17	5.64
MnO	0.29	0.25	0.27
MgO	20.32	20.62	20.47
CaO	6.96	6.92	6.94
Na2O	0.00	0.00	0.00
K2O	0.00	0.00	0.00
Total	99.73	99.16	99.44
Si	6.0536	6.0054	6.0300
Al IV	0.0000	0.0000	0.0000
Al VI	3.5457	3.5147	3.5305
Ti	0.0792	0.1011	0.0902
Cr	0.1924	0.2036	0.1980
Fe3+ [§]	0.0000	0.0689	0.0311
Fe2+	0.7202	0.6190	0.6730
Mn	0.0350	0.0303	0.0326
Mg	4.3105	4.3961	4.3535
Ca	1.0615	1.0607	1.0612
Na	0.0000	0.0000	0.0000
K	0.0000	0.0000	0.0000
Total	15.9981	15.9999	16.0001
Mgf	85.68	87.66	86.61
Pyr	70.4	72.0	71.1
Gro	10.0	7.4	8.8
Alm	11.8	10.1	11.0
Spe	0.6	0.5	0.5
And	2.6	5.0	3.7
Uva	4.7	5.0	4.9

Garnet analyses

Melting experiments at 3.0GPa

PLI series (sandwich experiments)

PLI33 (1225 °C, 8hrs)

	GAR1(c) in SDW	GAR1(b) in SDW	GAR2(c) in SDW	GAR2(b) in SDW	GAR1 in LHZ	GAR2 in LHZ	Ave.
SiO2	40.31	41.42	40.40	41.37	42.20	42.50	42.35
TiO2	1.11	0.62	1.39	0.59	0.79	0.62	0.81
Al2O3	22.24	23.21	21.82	22.99	19.75	19.31	19.53
Cr2O3	0.00	0.00	0.00	0.03	3.03	2.43	2.73
Fe2O3#	1.79	1.76	1.00	1.12	1.54	1.52	1.53
FeO	9.98	8.47	10.35	8.46	4.56	5.21	4.89
MnO	0.47	0.24	0.49	0.25	0.27	0.24	0.26
MgO	15.38	18.86	15.16	18.75	20.86	20.85	20.86
CaO	8.85	6.06	9.13	6.14	7.15	6.98	7.07
Na2O	0.00	0.00	0.00	0.00	0.00	0.00	0.00
K2O	0.00	0.00	0.00	0.00	0.00	0.00	0.00
Total	100.13	100.64	99.74	99.70	100.15	99.86	100.01
Si	5.8708	5.8930	5.9103	5.9314	6.0057	6.0981	6.0368
Al IV	0.1292	0.1070	0.0897	0.0686	0.0000	0.0000	0.0000
Al VI	3.6895	3.7860	3.6736	3.8173	3.3136	3.2504	3.2820
Ti	0.1216	0.0663	0.1529	0.0636	0.0846	0.0881	0.0863
Cr	0.0000	0.0000	0.0000	0.0034	0.3409	0.2743	0.3076
Fe3+ ‡	0.1962	0.1854	0.1101	0.1208	0.1649	0.1633	0.1641
Fe2+	1.2155	1.0074	1.2663	1.0147	0.5432	0.6224	0.5828
Mn	0.0580	0.0289	0.0607	0.0304	0.0325	0.0290	0.0308
Mg	3.3383	3.9990	3.3053	4.0064	4.4243	4.4366	4.4304
Ca	1.3811	0.9238	1.4312	0.9433	1.0903	1.0679	1.0791
Na	0.0000	0.0000	0.0000	0.0000	0.0000	0.0000	0.0000
K	0.0000	0.0000	0.0000	0.0000	0.0000	0.0000	0.0000
Total	16.0002	15.9999	16.0001	15.9999	16.0000	16.0000	15.9999
Mg#	73.31	79.88	72.30	79.79	89.06	87.70	88.38
Pyr	55.7	67.1	54.5	66.8	72.6	72.1	72.4
Gro	14.1	8.5	15.8	10.5	2.7	3.8	3.2
Alm	20.3	16.9	20.9	16.9	8.9	10.1	9.5
Spe	1.0	0.5	1.0	0.5	0.5	0.5	0.5
And	9.0	7.0	7.8	5.1	6.8	6.8	6.8
Uva	0.0	0.0	0.0	0.1	8.4	6.7	7.5

Garnet analyses

Melting experiments at 3.0GPa

FLX series (sandwich experiments)

	FLX38 (1225 °C, 10hrs)			FLX40 (1225 °C, 1hr)
	GAR1 in LHZ	GAR2 in LHZ	Ave.	GAR1 in LHZ
SiO2	42.12	41.77	41.95	41.66
TiO2	0.56	0.59	0.58	1.11
Al2O3	21.51	21.35	21.43	21.25
Cr2O3	2.49	2.50	2.50	1.13
Fe2O3	0.00	0.85	0.43	2.19
FeO	5.93	5.54	5.73	4.24
MnO	0.26	0.20	0.23	0.28
MgO	19.97	19.90	19.94	20.98
CaO	6.98	7.24	7.10	6.95
Na2O	0.00	0.00	0.00	0.00
K2O	0.00	0.00	0.00	0.00
Total	99.80	99.94	99.87	99.79
Si	6.0003	5.9558	5.9780	5.9205
Al IV	0.0000	0.0442	0.0220	0.0795
Al VI	3.6125	3.5447	3.5787	3.4808
Ti	0.0600	0.0633	0.0616	0.1186
Cr	0.2804	0.2818	0.2811	0.1270
Fe3+	0.0000	0.0912	0.0456	0.2342
Fe2+	0.7065	0.6601	0.6833	0.5039
Mn	0.0314	0.0242	0.0278	0.0337
Mg	4.2398	4.2287	4.2342	4.4435
Ca	1.0624	1.1061	1.0843	1.0583
Na	0.0000	0.0000	0.0000	0.0000
K	0.0000	0.0000	0.0000	0.0000
Total	15.9932	16.0000	15.9966	16.0001
Mg#	85.72	86.50	86.11	89.82
Pyr	70.2	70.3	70.2	73.6
Gro	8.6	7.0	7.8	4.6
Alm	11.7	11.0	11.3	8.3
Spe	0.5	0.4	0.5	0.6
And	2.0	4.4	3.2	9.7
Uva	7.0	7.0	7.0	3.2

Melt analyses

Melting experiments at 3.0GPa

PLZ series

	PLZ30 (1225 °C, 19hrs)		PLZ23 (1235 °C, 20hrs)	Ave. (PLZ30 + PLZ23)	Rec. (H2O/K2O=0.38)
	Melt-1	Melt-2	Melt-1		
SiO2	37.62	39.40	35.35	37.46	43.28
TiO2	3.02	2.33	1.73	2.36	2.73
Al2O3	15.57	14.23	13.22	14.34	16.57
Cr2O3	0.00	0.00	0.11	0.04	0.04
FeO*	5.01	4.95	4.51	4.82	5.57
MnO	0.06	0.10	0.09	0.08	0.10
MgO	8.73	14.05	10.82	11.20	12.94
CaO	6.66	6.94	6.61	6.80	7.86
Na2O	0.80	0.62	0.80	0.74	0.86
K2O	7.41	5.68	5.81	6.30	7.28
H2O‡					2.77
Total	85.08	88.30	79.05	84.14	100.00
Mg‡	75.64	83.49	81.04	80.54	80.54

Remarks :

The average is done in order to include
the analyses for PLZ30 and PLZ23 together.

Melt analyses

Melting experiments at 3.0GPa

PLS series (sandwich experiments)

PLS33 (1225 °C, 8hrs) with SDW2

<u>Elem. d.</u>									<u>Rec.</u>	
	<u>Melt-1</u> (10µm)	<u>Melt-2</u> (10µm)	<u>Melt-3</u> (10µm)	<u>Melt-4</u> (5µm)	<u>Melt-5</u> (10µm)	<u>Melt-6</u> (5µm)	<u>Melt-7</u> (10µm)	<u>Melt-8</u> (5µm)	<u>Ave. (H2O/K2O</u> =0.38)	
SiO2	44.32	46.91	47.31	48.68	48.54	47.72	47.52	47.10	47.26	47.64
TiO2	2.56	2.13	1.42	0.57	1.49	1.50	1.52	0.67	1.48	1.49
Al2O3	13.68	12.82	11.80	10.41	11.07	11.79	11.72	11.67	11.87	11.98
Cr2O3	0.01	0.03	0.05	0.01	0.14	0.07	0.01	0.00	0.04	0.04
FeO*	4.38	4.71	4.44	4.80	4.57	4.32	4.36	4.29	4.48	4.52
MnO	0.08	0.05	0.11	0.11	0.07	0.12	0.14	0.07	0.09	0.09
MgO	13.22	14.20	12.65	11.93	13.94	13.41	12.93	9.49	12.72	12.82
CaO	6.42	9.53	11.10	13.28	10.05	11.03	11.19	10.22	10.35	10.44
Na2O	1.02	1.03	1.27	1.43	1.30	1.21	1.28	1.89	1.30	1.31
K2O	8.89	6.98	6.80	5.18	6.70	5.33	6.36	9.42	6.96	7.01
H2O†										2.68
Total	94.58	98.39	96.95	96.38	97.87	96.50	97.03	94.82	96.57	100.00
Mg‡	84.32	84.31	83.54	81.58	84.46	84.69	84.09	79.77	83.49	83.49

PLS49 (1225 °C, 1hr) with SDW3

<u>Elem. d.</u>									<u>Rec.</u>	
	<u>Melt-1</u> (20µm)	<u>Melt-2</u> (20µm)	<u>Melt-3</u> (10µm)	<u>Melt-4</u> (10µm)	<u>Melt-5</u> (30µm)	<u>Melt-6</u> (15µm)	<u>Melt-7</u> (10µm)	<u>Melt-8</u> (20µm)	<u>Ave. (H2O/K2O</u> =0.38)	
SiO2	45.88	47.27	45.71	44.08	47.44	47.48	45.96	46.71	46.32	47.63
TiO2	1.83	1.57	1.62	1.66	1.62	1.59	1.67	1.63	1.62	1.67
Al2O3	10.77	10.06	10.58	11.40	10.15	10.37	10.96	10.46	10.59	10.90
Cr2O3	1.73	0.00	0.00	0.00	0.02	0.20	0.17	0.08	0.28	0.28
FeO*	5.49	5.35	5.53	5.62	5.44	5.55	5.47	5.24	5.46	5.62
MnO	0.17	0.12	0.16	0.08	0.16	0.13	0.17	0.16	0.14	0.15
MgO	12.75	13.26	12.71	11.31	13.68	12.94	12.73	12.65	12.75	13.12
CaO	11.01	11.69	11.49	10.26	11.59	11.35	11.09	11.04	11.19	11.51
Na2O	1.73	1.50	1.66	2.08	1.52	1.74	1.62	1.69	1.69	1.74
K2O	5.36	4.67	5.17	6.29	4.77	4.73	5.29	5.36	5.21	5.35
H2O†										2.03
Total	96.52	95.49	94.63	92.78	96.39	96.08	95.13	95.02	95.25	100.00
Mg‡	80.54	81.54	80.38	78.20	81.76	80.60	80.57	81.14	80.63	80.63

Spinel analysis**Melting experiments at 3.0GPa****PLX series**

	PLX31	PLX37	PLX21	PLX22	PLX30	PLX23	PLX32
	1125 °C	1150 °C	1175 °C	1200 °C	1225 °C	1235 °C	1250 °C
TiO2	0.09	0.07	0.09	0.06	0.07	0.07	0.08
Al2O3	51.94	52.02	52.81	52.85	53.60	53.34	52.23
Cr2O3	16.00	15.64	16.04	15.76	16.11	15.66	16.36
Fe2O3 #	2.67	2.24	1.73	1.62	1.54	2.09	1.83
FeO	8.60	8.92	9.00	8.26	7.67	7.61	6.80
MnO	0.12	0.00	0.12	0.17	0.05	0.14	0.04
MgO	20.66	20.35	20.55	20.82	21.60	21.50	21.70
Total	100.08	99.24	100.34	99.54	100.64	100.41	99.04
Al	0.0142	0.0112	0.0142	0.0095	0.0109	0.0109	0.0127
Ti	12.8866	12.9997	13.0424	13.1042	13.0978	13.0766	12.9621
Cr	2.6620	2.6209	2.6564	2.6204	2.6398	2.5744	2.7226
Fe3+ #	0.4229	0.3573	0.2727	0.2564	0.2402	0.3271	0.2899
Fe2+	1.5132	1.5821	1.5774	1.4533	1.3303	1.3234	1.1978
Mn	0.0214	0.0000	0.0213	0.0303	0.0088	0.0247	0.0071
Mg	6.4798	6.4287	6.4157	6.5259	6.6724	6.6631	6.8079
Total	24.0000	23.9999	24.0001	24.0000	24.0002	24.0000	24.0000
Mg#	81.07	80.25	80.27	81.79	83.38	83.43	85.04
Cr#	17.12	16.78	16.92	16.66	16.77	16.45	17.36
Y Al	80.69	81.36	81.66	82.00	81.97	81.84	81.14
Y Cr	16.67	16.40	16.63	16.40	16.52	16.11	17.04
Y Fe3+	2.65	2.24	1.71	1.60	1.50	2.05	1.81

Spinel analyses

Melting experiments at 3.0GPa

PLE series (sandwich experiments)

	PLE33	PLE38	PLE40
	1225 °C	1225 °C	1225 °C
TiO ₂	0.15	0.15	0.18
Al ₂ O ₃	50.76	52.66	52.95
Cr ₂ O ₃	16.00	16.04	15.48
Fe ₂ O ₃ ‡	4.35	1.26	2.28
FeO	8.70	8.06	9.46
MnO	0.12	0.16	0.15
MgO	20.62	20.94	20.41
Total	100.70	99.27	100.91
Al	0.0238	0.0238	0.0283
Ti	12.6003	13.0809	13.0311
Cr	2.6633	2.6718	2.5547
Fe ³⁺ ‡	0.6693	0.1998	0.3582
Fe ²⁺	1.5313	1.4196	1.6513
Mn	0.0214	0.0286	0.0265
Mg	6.4705	6.5755	6.3497
Total	23.9998	24.0000	23.9998
Mg‡	80.86	82.24	79.36
Cr‡	17.45	16.96	16.39
Y Al	78.98	82.00	81.73
Y Cr	16.69	16.75	16.02
Y Fe ³⁺	4.32	1.25	2.25

APPENDIX B3

Experiments on CPL

Carbonate analyses

Melting experiments at 3.0GPa

CPL series

	CPL4 (925 °C, 18hrs)			CPL (975 °C, 20hrs)			CPL11 (1000 °C, 28hrs)		
	MAG1	MAG2	Ave.	MAG1	MAG2	Ave.	MAG1	MAG2	Ave.
FeO*	5.07	4.99	5.03	4.93	4.91	4.92	4.73	4.77	4.75
MnO	0.16	0.18	0.17	0.12	0.13	0.13	0.23	0.17	0.20
MgO	39.41	41.82	40.62	38.14	37.50	37.82	40.83	40.95	40.89
CaO	4.30	4.74	4.37	4.90	5.74	5.32	4.76	4.77	4.77
Total	48.64	51.73	50.19	48.09	48.28	48.19	50.55	50.66	50.61
Fe	0.1258	0.1164	0.1209	0.1243	0.1240	0.1242	0.1129	0.1135	0.1132
Mn	0.0040	0.0043	0.0041	0.0031	0.0033	0.0032	0.0056	0.0041	0.0048
Mg	1.7430	1.7378	1.7403	1.7142	1.6871	1.7007	1.7361	1.7369	1.7365
Ca	0.1272	0.1416	0.1346	0.1583	0.1857	0.1720	0.1455	0.1455	0.1455
C #	2.0000	2.0000	2.0000	2.0000	2.0000	2.0000	2.0000	2.0000	2.0000
Total	4.0000	4.0000	4.0000	4.0000	4.0000	4.0000	4.0000	4.0000	4.0000
FeCO3	6.29	5.82	6.05	6.22	6.20	6.21	5.64	5.68	5.66
MnCO3	0.20	0.21	0.21	0.15	0.17	0.16	0.28	0.20	0.24
MgCO3	87.15	86.89	87.01	85.71	84.35	85.03	86.80	86.85	86.82
CaCO3	6.36	7.08	6.73	7.92	9.28	8.60	7.28	7.27	7.27

Carbonate analyses

Melting experiments at 3.0GPa

CPL series

	CPL8 (950° → 1025° C 21 → 5hrs)			CPL9 (950° → 1050° C 20 → 5hrs)					
	MAG1	MAG2	Ave.	DOL1	DOL2	Ave.	DOL1	DOL2	Ave.
FeO*	5.01	5.09	5.05	3.61	2.74	3.18	2.94	2.67	2.81
MnO	0.09	0.17	0.13	0.19	0.19	0.19	0.15	0.15	0.15
MgO	40.46	39.34	39.90	22.40	20.87	21.64	20.95	21.19	21.07
CaO	4.00	5.01	4.51	28.61	29.18	28.90	30.46	29.86	30.16
Total	49.56	49.61	49.59	54.81	52.98	53.90	54.50	53.87	54.19
Fe	0.1217	0.1245	0.1231	0.0898	0.0707	0.0804	0.0740	0.0677	0.0709
Mn	0.0022	0.0042	0.0032	0.0048	0.0050	0.0049	0.0038	0.0039	0.0038
Mg	1.7516	1.7143	1.7330	0.9933	0.9596	0.9766	0.9398	0.9579	0.9488
Ca	0.1245	0.1570	0.1407	0.9121	0.9647	0.9379	0.9824	0.9705	0.9765
C #	2.0000	2.0000	2.0000	2.0000	2.0000	2.0000	2.0000	2.0000	2.0000
Total	4.0000	4.0000	4.0000	4.0000	4.0000	4.0000	4.0000	4.0000	4.0000
FeCO3	6.09	6.22	6.15	1.49	3.54	4.02	3.70	3.39	3.54
MnCO3	0.11	0.21	0.16	0.24	0.25	0.24	0.19	0.19	0.19
MgCO3	87.58	85.72	86.65	49.66	47.98	48.84	46.99	47.90	47.44
CaCO3	6.23	7.85	7.03	45.61	48.23	46.90	49.12	48.53	48.82

Olivine analyses

Melting experiments at 3.0GPa

CFL series

	CFL 2 (900 °C, 28hrs)					CFL 4 (925 °C, 28hrs)				
	OL1	OL2	OL3	OL4	Ave.	OL1	OL2	OL3	OL4	Ave.
SiO2	39.91	40.04	40.24	39.98	40.04	40.68	40.51	40.73	40.66	40.65
TiO2	0.00	0.04	0.02	0.00	0.02	0.00	0.02	0.03	0.00	0.01
Al2O3	0.00	0.00	0.00	0.00	0.00	0.00	0.00	0.02	0.00	0.01
Cr2O3	0.09	0.00	0.04	0.05	0.05	0.00	0.00	0.02	0.00	0.01
FeO*	8.54	8.82	8.87	8.46	8.62	9.27	9.27	9.03	9.32	9.22
MnO	0.12	0.12	0.12	0.14	0.13	0.09	0.14	0.13	0.16	0.13
MgO	50.30	50.33	50.40	50.12	50.29	49.57	50.20	49.89	49.81	49.87
NiO	0.32	0.34	0.36	0.32	0.34	0.27	0.29	0.31	0.29	0.29
CaO	0.10	0.07	0.08	0.11	0.09	0.09	0.08	0.08	0.08	0.08
Na2O	0.00	0.03	0.04	0.01	0.02	0.00	0.00	0.00	0.00	0.00
K2O	0.00	0.00	0.00	0.00	0.00	0.00	0.00	0.00	0.00	0.00
Total	99.38	99.79	99.97	99.19	99.58	99.97	100.51	100.24	100.32	100.26
Si	0.9824	0.9826	0.9848	0.9854	0.9838	0.9860	0.9877	0.9939	0.9921	0.9926
Ti	0.0000	0.0007	0.0004	0.0000	0.0003	0.0000	0.0004	0.0006	0.0000	0.0002
Al	0.0000	0.0000	0.0000	0.0000	0.0000	0.0000	0.0000	0.0006	0.0000	0.0001
Cr	0.0018	0.0000	0.0008	0.0010	0.0009	0.0000	0.0000	0.0004	0.0000	0.0001
Fe	0.1758	0.1810	0.1775	0.1744	0.1772	0.1898	0.1890	0.1843	0.1903	0.1884
Mn	0.0025	0.0025	0.0025	0.0029	0.0026	0.0019	0.0029	0.0027	0.0033	0.0027
Mg	1.8453	1.8406	1.8383	1.8410	1.8413	1.8087	1.8241	1.8144	1.8128	1.8150
Ni	0.0063	0.0067	0.0071	0.0063	0.0066	0.0053	0.0057	0.0061	0.0057	0.0057
Ca	0.0026	0.0018	0.0021	0.0029	0.0024	0.0024	0.0021	0.0021	0.0021	0.0022
Na	0.0000	0.0014	0.0019	0.0005	0.0010	0.0000	0.0000	0.0000	0.0000	0.0000
K	0.0000	0.0000	0.0000	0.0000	0.0000	0.0000	0.0000	0.0000	0.0000	0.0000
Total	3.0167	3.0174	3.0153	3.0144	3.0160	3.0040	3.0119	3.0050	3.0071	3.0070
Mg#	91.30	91.05	91.20	91.35	91.22	90.50	90.61	90.78	90.50	90.60
Fe	91.19	90.93	91.08	91.22	91.11	90.42	90.48	90.66	90.35	90.48
Fa	8.81	9.07	8.92	8.78	8.89	9.58	9.52	9.34	9.65	9.52

Olivine analyses

Melting experiments at 3.0GPa

CPL series

	CPL5 (975 °C, 20hrs)					CPL11 (1000 °C, 26hrs)			
	OL1	OL2	OL3	OL4	Ave.	OL1	OL2	OL3	Ave.
SiO2	40.88	40.66	40.37	40.51	40.61	40.31	40.20	40.25	40.25
TiO2	0.01	0.04	0.00	0.00	0.01	0.00	0.00	0.01	0.00
Al2O3	0.01	0.00	0.00	0.00	0.00	0.00	0.00	0.00	0.00
Cr2O3	0.00	0.00	0.05	0.04	0.02	0.03	0.00	0.03	0.02
FeO*	9.43	9.19	8.45	9.34	9.10	8.95	9.05	8.79	8.83
MnO	0.13	0.15	0.11	0.17	0.14	0.03	0.01	0.00	0.01
MgO	49.94	49.83	49.81	50.20	49.95	49.79	50.18	50.50	50.16
NiO	0.31	0.30	0.32	0.31	0.31	0.27	0.30	0.27	0.28
CaO	0.09	0.13	0.15	0.15	0.13	0.13	0.09	0.07	0.10
Na2O	0.00	0.00	0.00	0.01	0.00	0.00	0.00	0.00	0.00
K2O	0.00	0.00	0.00	0.00	0.00	0.00	0.00	0.00	0.00
Total	100.80	100.30	99.26	100.73	100.27	99.51	99.83	99.92	99.75
Si	0.9937	0.9927	0.9930	0.9865	0.9915	0.9909	0.9859	0.9850	0.9872
Ti	0.0002	0.0007	0.0000	0.0000	0.0002	0.0000	0.0000	0.0002	0.0001
Al	0.0003	0.0000	0.0000	0.0000	0.0001	0.0000	0.0000	0.0000	0.0000
Cr	0.0000	0.0000	0.0010	0.0008	0.0004	0.0006	0.0000	0.0006	0.0004
Fe	0.1917	0.1876	0.1738	0.1902	0.1859	0.1840	0.1856	0.1799	0.1832
Mn	0.0027	0.0031	0.0023	0.0035	0.0029	0.0006	0.0002	0.0000	0.0003
Mg	1.8091	1.8131	1.8260	1.8219	1.8175	1.8240	1.8341	1.8418	1.8333
Ni	0.0061	0.0059	0.0063	0.0061	0.0061	0.0053	0.0059	0.0053	0.0055
Ca	0.0023	0.0034	0.0040	0.0039	0.0034	0.0034	0.0024	0.0018	0.0025
Na	0.0000	0.0000	0.0000	0.0005	0.0001	0.0000	0.0000	0.0000	0.0000
K	0.0000	0.0000	0.0000	0.0000	0.0000	0.0000	0.0000	0.0000	0.0000
Total	3.0060	3.0066	3.0065	3.0133	3.0081	3.0088	3.0141	3.0145	3.0125
Mg#	90.42	90.62	91.31	90.55	90.72	90.84	90.81	91.10	90.92
Fo	90.30	90.48	91.20	90.39	90.59	90.81	90.80	91.10	90.90
Fa	9.70	9.52	8.80	9.61	9.41	9.19	9.20	8.90	9.10

Olivine analyses

Melting experiments at 3.0GPa

CFL series

	CFL8 (950°→1025°C, 21→5hrs)			CFL9 (950°→1050°C, 20→5hrs)			
	OL1	OL2	Ave.	OL1	OL2	OL3	Ave.
SiO2	39.56	40.62	40.09	40.52	40.54	40.55	40.54
TiO2	0.01	0.01	0.01	0.00	0.00	0.00	0.00
Al2O3	0.00	0.00	0.00	0.00	0.00	0.00	0.00
Cr2O3	0.06	0.06	0.06	0.05	0.05	0.00	0.03
FeO*	8.90	8.68	8.79	9.22	8.98	8.79	9.00
MnO	0.11	0.12	0.12	0.00	0.04	0.00	0.01
MgO	50.23	50.10	50.17	50.27	50.46	50.31	50.35
NiO	0.31	0.31	0.31	0.28	0.28	0.26	0.27
CaO	0.09	0.07	0.08	0.13	0.09	0.09	0.10
Na2O	0.00	0.00	0.00	0.00	0.00	0.00	0.00
K2O	0.00	0.00	0.00	0.00	0.00	0.00	0.00
Total	99.27	99.97	99.62	100.47	100.44	100.00	100.30
Si	0.9771	0.9927	0.9849	0.9877	0.9875	0.9906	0.9866
Ti	0.0002	0.0002	0.0002	0.0000	0.0000	0.0000	0.0000
Al	0.0000	0.0000	0.0000	0.0000	0.0000	0.0000	0.0000
Cr	0.0012	0.0012	0.0012	0.0010	0.0010	0.0000	0.0006
Fe	0.1838	0.1774	0.1806	0.1880	0.1829	0.1796	0.1835
Mn	0.0023	0.0025	0.0024	0.0000	0.0008	0.0000	0.0003
Mg	1.8490	1.8247	1.8368	1.8262	1.8319	1.8317	1.8299
Ni	0.0062	0.0061	0.0061	0.0055	0.0055	0.0051	0.0054
Ca	0.0024	0.0018	0.0021	0.0034	0.0023	0.0024	0.0027
Na	0.0000	0.0000	0.0000	0.0000	0.0000	0.0000	0.0000
K	0.0000	0.0000	0.0000	0.0000	0.0000	0.0000	0.0000
Total	3.0221	3.0065	3.0143	3.0118	3.0120	3.0094	3.0111
Mg#	90.96	91.14	91.05	90.67	90.92	91.07	90.89
Fe	90.85	91.03	90.94	90.67	90.88	91.07	90.87
Fa	9.15	8.97	9.06	9.33	9.12	8.93	9.13

Wet chemistry analyses

Melting experiments at 3.0GPa

CPL series

	CPL7 (950°→1075°C, 21→4hrs30min)				CPL10 (950°→1100°C, 20→5hrs)			
	OL1	OL2	OL3	Ave.	OL1	OL2	OL3	Ave.
SiO2	40.09	39.98	40.04	40.04	40.56	40.30	40.40	40.42
TiO2	0.00	0.02	0.00	0.01	0.00	0.00	0.00	0.00
Al2O3	0.00	0.00	0.00	0.00	0.00	0.00	0.00	0.00
Cr2O3	0.05	0.04	0.06	0.05	0.05	0.06	0.03	0.05
FeO*	8.49	8.55	8.83	8.62	8.96	9.06	9.04	9.02
MnO	0.17	0.11	0.10	0.13	0.02	0.05	0.04	0.04
MgO	49.91	49.92	50.18	50.00	50.34	50.12	50.30	50.25
NiO	0.27	0.32	0.31	0.30	0.25	0.25	0.27	0.26
CaO	0.08	0.09	0.12	0.10	0.07	0.09	0.10	0.09
Na2O	0.00	0.00	0.06	0.02	0.00	0.00	0.00	0.00
K2O	0.00	0.04	0.08	0.04	0.00	0.00	0.00	0.00
Total	99.06	99.07	99.78	99.30	100.25	99.93	100.18	100.12
Si	0.9868	0.9868	0.9832	0.9863	0.9893	0.9872	0.9871	0.9879
Ti	0.0000	0.0004	0.0000	0.0001	0.0000	0.0000	0.0000	0.0000
Al	0.0000	0.0000	0.0000	0.0000	0.0000	0.0000	0.0000	0.0000
Cr	0.0010	0.0008	0.0012	0.0010	0.0010	0.0012	0.0006	0.0009
Fe	0.1751	0.1765	0.1813	0.1777	0.1828	0.1856	0.1847	0.1844
Mn	0.0036	0.0023	0.0021	0.0026	0.0004	0.0010	0.0008	0.0008
Mg	1.8347	1.8363	1.8364	1.8358	1.8300	1.8298	1.8315	1.8304
Ni	0.0054	0.0064	0.0061	0.0059	0.0049	0.0049	0.0053	0.0050
Ca	0.0021	0.0024	0.0032	0.0026	0.0018	0.0024	0.0026	0.0023
Na	0.0000	0.0000	0.0029	0.0010	0.0000	0.0000	0.0000	0.0000
K	0.0000	0.0013	0.0025	0.0013	0.0000	0.0000	0.0000	0.0000
Total	3.0107	3.0131	3.0189	3.0142	3.0102	3.0122	3.0126	3.0117
Mg#	91.29	91.23	91.01	91.18	90.92	90.79	90.84	90.85
Fe	91.12	91.13	90.92	91.06	90.90	90.74	90.80	90.82
Fa	8.88	8.87	9.08	8.94	9.10	9.26	9.20	9.18

Olivine analyses

Melting experiments at 3.0GPa

CPL series

	<u>CPL13</u> (950°→1125°C, 20→4hrs)				<u>CPL12</u> (950°→1150°C, 20→4hrs)			
	OL1	OL2	OL3	Ave.	OL1	OL2	OL3	Ave.
SiO2	40.38	39.94	39.92	40.08	40.24	40.36	40.29	40.30
TiO2	0.00	0.00	0.00	0.00	0.01	0.01	0.02	0.01
Al2O3	0.00	0.00	0.00	0.00	0.00	0.00	0.00	0.00
Cr2O3	0.03	0.07	0.02	0.04	0.05	0.06	0.07	0.06
FeO*	9.40	9.22	9.07	9.23	9.24	8.89	8.87	9.00
MnO	0.04	0.00	0.03	0.02	0.00	0.05	0.00	0.02
MgO	50.53	49.85	49.91	50.10	49.98	50.26	50.05	50.10
NiO	0.31	0.27	0.35	0.31	0.26	0.30	0.25	0.27
CaO	0.14	0.24	0.10	0.16	0.15	0.10	0.18	0.14
Na2O	0.00	0.00	0.00	0.00	0.00	0.00	0.00	0.00
K2O	0.00	0.00	0.00	0.00	0.00		0.00	0.00
Total	100.83	99.59	99.40	99.94	99.9	100.03	99.73	99.90
Si	0.9825	0.9835	0.9842	0.9834	0.9866	0.9872	0.9881	0.9873
Ti	0.0000	0.0000	0.0000	0.0000	0.0002	0.0002	0.0004	0.0002
Al	0.0000	0.0000	0.0000	0.0000	0.0000	0.0000	0.0000	0.0000
Cr	0.0006	0.0014	0.0004	0.0008	0.0010	0.0012	0.0014	0.0012
Fe	0.1913	0.1899	0.1870	0.1894	0.1895	0.1819	0.1819	0.1844
Mn	0.0008	0.0000	0.0006	0.0005	0.0000	0.0010	0.0000	0.0003
Mg	1.8323	1.8294	1.8338	1.8318	1.8263	1.8321	1.8294	1.8293
Ni	0.0061	0.0053	0.0069	0.0061	0.0051	0.0059	0.0049	0.0053
Ca	0.0036	0.0063	0.0026	0.0042	0.0039	0.0026	0.0047	0.0038
Na	0.0000	0.0000	0.0000	0.0000	0.0000	0.0000	0.0000	0.0000
K	0.0000	0.0000	0.0000	0.0000	0.0000	0.0000	0.0000	0.0000
Total	3.0172	3.0156	3.0156	3.0162	3.0127	3.0121	3.0108	3.0119
Mg#	90.55	90.60	90.75	90.63	90.60	90.97	90.95	90.84
Fe	90.51	90.60	90.72	90.61	90.60	90.92	90.95	90.83
Fa	9.49	9.40	9.28	9.39	9.40	9.08	9.05	9.17

Olivine analyses

Melting experiments at 3.0GPa

CPL series (sandwich experiments)

	CPL14 (1100 °C, 9hrs30min)					CPL15 (1100 °C, 9hrs30min)				
	OL1	OL2	OL3	OL4	Ave.	OL1	OL2	OL3	OL4	Ave.
SiO2	40.68	40.86	41.01	40.81	40.84	40.64	40.37	40.96	40.78	40.69
TiO2	0.03	0.01	0.01	0.01	0.02	0.02	0.00	0.01	0.00	0.01
Al2O3	0.00	0.07	0.00	0.00	0.02	0.00	0.00	0.00	0.00	0.00
Cr2O3	0.00	0.00	0.03	0.00	0.01	0.00	0.00	0.00	0.00	0.00
FeO*	8.53	8.88	9.00	8.96	8.84	8.91	8.69	8.56	8.34	8.63
MnO	0.11	0.18	0.16	0.20	0.16	0.13	0.18	0.16	0.17	0.16
MgO	49.57	50.02	49.54	49.99	49.78	49.43	49.61	49.95	50.28	49.82
NiO	0.44	0.43	0.40	0.34	0.40	0.37	0.41	0.43	0.36	0.39
CaO	0.12	0.16	0.16	0.13	0.14	0.12	0.23	0.10	0.11	0.14
Na2O	0.07	0.15	0.00	0.00	0.06	0.00	0.00	0.00	0.00	0.00
K2O	0.04	0.13	0.00	0.00	0.06	0.00	0.00	0.00	0.00	0.00
Total	99.54	100.95	100.31	100.44	100.32	98.62	99.49	100.17	100.04	99.83
Si	0.9978	0.9919	0.9999	0.9941	0.9959	0.9975	0.9927	0.9983	0.9945	0.9957
Ti	0.0006	0.0002	0.0002	0.0002	0.0003	0.0004	0.0000	0.0002	0.0000	0.0001
Al	0.0000	0.0020	0.0000	0.0000	0.0005	0.0000	0.0000	0.0000	0.0000	0.0000
Cr	0.0000	0.0000	0.0006	0.0000	0.0001	0.0000	0.0000	0.0000	0.0000	0.0000
Fe	0.1756	0.1803	0.1835	0.1825	0.1803	0.1829	0.1787	0.1745	0.1701	0.1765
Mn	0.0023	0.0037	0.0033	0.0041	0.0034	0.0027	0.0037	0.0033	0.0035	0.0033
Mg	1.8120	1.8097	1.8001	1.8148	1.8091	1.8082	1.8180	1.8143	1.8274	1.8170
Ni	0.0087	0.0084	0.0078	0.0067	0.0079	0.0073	0.0081	0.0084	0.0071	0.0077
Ca	0.0032	0.0042	0.0042	0.0034	0.0037	0.0032	0.0061	0.0026	0.0029	0.0037
Na	0.0033	0.0071	0.0000	0.0000	0.0026	0.0000	0.0000	0.0000	0.0000	0.0000
K	0.0013	0.0059	0.0000	0.0000	0.0018	0.0000	0.0000	0.0000	0.0000	0.0000
Total	3.0040	3.0133	2.9996	3.0057	3.0057	3.0021	3.0073	3.0015	3.0055	3.0041
Mg#	91.19	90.94	90.75	90.86	90.94	90.81	91.05	91.23	91.48	91.14
Fe	91.09	90.77	90.60	90.67	90.78	90.69	90.88	91.08	91.32	90.99
Fa	8.91	9.23	9.40	9.33	9.22	9.31	9.12	8.92	8.68	9.01

Olivine analyses

Melting experiments at 3.0GPa

CPL series (marzich experiments)

CPL16 (1100 °C, 9hrs30min)

	OL1	OL2	OL3	OL4	Ave.
SiO2	40.79	40.43	40.50	41.05	40.69
TiO2	0.03	0.03	0.00	0.01	0.02
Al2O3	0.00	0.11	0.00	0.00	0.03
Cr2O3	0.01	0.11	0.00	0.00	0.03
FeO*	8.58	8.88	8.98	8.44	8.72
MnO	0.21	0.18	0.18	0.23	0.20
MgO	50.30	50.00	49.99	50.34	50.16
NiO	0.39	0.39	0.40	0.41	0.40
CaO	0.09	0.17	0.19	0.11	0.14
Na2O	0.00	0.00	0.00	0.00	0.00
K2O	0.00	0.00	0.00	0.00	0.00
Total	100.40	100.30	100.24	100.59	100.38
Si	0.9927	0.9872	0.9897	0.9961	0.9914
Ti	0.0005	0.0006	0.0000	0.0002	0.0003
Al	0.0000	0.0032	0.0000	0.0000	0.0008
Cr	0.0002	0.0021	0.0000	0.0000	0.0006
Fe	0.1746	0.1813	0.1835	0.1713	0.1777
Mn	0.0043	0.0037	0.0037	0.0047	0.0041
Mg	1.8243	1.8195	1.8206	1.8205	1.8212
Ni	0.0076	0.0077	0.0079	0.0080	0.0078
Ca	0.0023	0.0044	0.0050	0.0029	0.0037
Na	0.0000	0.0000	0.0000	0.0000	0.0000
K	0.0000	0.0000	0.0000	0.0000	0.0000
Total	3.0067	3.0096	3.0103	3.0037	3.0076
Mg#	91.26	90.94	90.84	91.40	91.11
Fo	91.07	90.77	90.67	91.18	90.92
Fa	8.93	9.23	9.33	8.82	8.08

Orthopyroxene analyses

Melting experiments at 3.0GPa

CPL series

	CPL2 (900 °C, 28hrs)					CPL4 (925 °C, 28hrs)				
	OPX1	OPX2	OPX3	OPX4	Ave.	OPX1	OPX2	OPX3	OPX4	Ave.
SiO2	55.50	55.78	55.60	55.78	55.67	56.66	55.91	56.33	56.74	56.41
TiO2	0.01	0.01	0.00	0.05	0.02	0.03	0.05	0.01	0.06	0.04
Al2O3	3.15	3.42	3.57	3.07	3.30	2.94	2.91	2.83	2.88	2.89
Cr2O3	0.28	0.46	0.42	0.30	0.37	0.22	0.24	0.26	0.22	0.24
FeO*	5.98	5.91	5.80	5.71	5.85	5.83	5.85	5.95	5.67	5.83
MnO	0.13	0.12	0.11	0.15	0.13	0.12	0.13	0.14	0.06	0.11
MgO	33.83	33.71	33.93	33.81	33.82	34.59	34.43	34.30	34.43	34.44
CaO	0.52	0.68	0.64	0.69	0.66	0.46	0.57	0.50	0.61	0.54
Na2O	0.06	0.04	0.06	0.11	0.07	0.02	0.01	0.00	0.04	0.02
K2O	0.00	0.00	0.00	0.00	0.00	0.00	0.00	0.00	0.00	0.00
Total	99.50	100.13	100.13	99.67	99.87	100.87	100.10	100.32	100.71	100.50
Si	1.9230	1.9210	1.9143	1.9284	1.9217	1.9331	1.9250	1.9342	1.9374	1.9324
Al IV	0.0770	0.0790	0.0857	0.0716	0.0783	0.0669	0.0750	0.0658	0.0626	0.0676
Al VI	0.0516	0.0599	0.0592	0.0535	0.0561	0.0513	0.0432	0.0488	0.0533	0.0492
Ti	0.0003	0.0003	0.0000	0.0013	0.0005	0.0008	0.0013	0.0003	0.0015	0.0010
Cr	0.0077	0.0125	0.0114	0.0082	0.0100	0.0059	0.0065	0.0071	0.0059	0.0064
Fe	0.1733	0.1702	0.1670	0.1651	0.1689	0.1663	0.1685	0.1709	0.1619	0.1669
Mn	0.0038	0.0035	0.0032	0.0044	0.0037	0.0035	0.0038	0.0041	0.0017	0.0033
Mg	1.7469	1.7302	1.7410	1.7420	1.7400	1.7587	1.7667	1.7553	1.7520	1.7582
Ca	0.0230	0.0251	0.0236	0.0256	0.0243	0.0168	0.0210	0.0184	0.0223	0.0196
Na	0.0040	0.0027	0.0040	0.0074	0.0045	0.0013	0.0007	0.0000	0.0026	0.0012
K	0.0000	0.0000	0.0000	0.0000	0.0000	0.0000	0.0000	0.0000	0.0000	0.0000
Total	4.0106	4.0044	4.0095	4.0074	4.0080	4.0047	4.0117	4.0047	4.0015	4.0056
Mg#	90.98	91.04	91.25	91.34	91.15	91.36	91.30	91.13	91.54	91.33
Wo	1.18	1.30	1.22	1.32	1.26	0.86	1.07	0.94	1.15	1.01
En	89.72	89.69	89.98	89.93	89.83	90.41	90.14	90.08	90.40	90.26
Fs	9.10	9.01	8.80	8.75	8.91	8.73	8.79	8.98	8.44	8.73

Orthopyroxene analyses

Melting experiments at 3.0GPa

CFL series

	<u>CFL5</u> (975 °C, 20hrs)					<u>CFL11</u> (1000 °C, 28hrs)				
	OPX1	OPX2	OPX3	OPX4	Ave.	OPX1	OPX2	OPX3	OPX4	Ave.
SiO2	56.87	56.17	56.31	55.86	56.30	56.01	55.51	55.62	56.19	55.82
TiO2	0.03	0.02	0.03	0.05	0.03	0.03	0.00	0.00	0.01	0.01
Al2O3	2.99	2.86	2.96	3.03	2.97	3.45	3.36	3.15	3.09	3.26
Cr2O3	0.32	0.35	0.31	0.33	0.33	0.31	0.26	0.26	0.26	0.27
FeO*	5.69	5.53	5.59	5.76	5.64	5.75	6.16	5.94	6.05	5.98
MnO	0.14	0.15	0.11	0.11	0.13	0.01	0.06	0.02	0.00	0.02
MgO	34.27	34.51	34.01	34.28	34.27	33.49	33.62	33.70	33.74	33.64
CaO	0.55	0.64	0.60	0.66	0.61	0.59	0.68	0.61	0.59	0.62
Na2O	0.02	0.00	0.03	0.08	0.03	0.01	0.01	0.00	0.00	0.01
K2O	0.00	0.00	0.00	0.00	0.00	0.00	0.00	0.00	0.00	0.00
Total	100.88	100.25	99.95	100.16	100.31	99.65	99.66	99.30	99.93	99.64
Si	1.9386	1.9286	1.9373	1.9226	1.9318	1.9324	1.9217	1.9292	1.9360	1.9298
Al IV	0.0614	0.0714	0.0627	0.0774	0.0682	0.0676	0.0783	0.0708	0.0640	0.0702
Al VI	0.0588	0.0452	0.0574	0.0455	0.0517	0.0728	0.0588	0.0580	0.0615	0.0628
Ti	0.0008	0.0005	0.0008	0.0013	0.0008	0.0008	0.0000	0.0000	0.0003	0.0003
Cr	0.0086	0.0095	0.0084	0.0090	0.0089	0.0085	0.0071	0.0071	0.0071	0.0074
Fe	0.1622	0.1588	0.1608	0.1658	0.1619	0.1659	0.1783	0.1723	0.1743	0.1727
Mn	0.0040	0.0044	0.0032	0.0032	0.0037	0.0003	0.0018	0.0006	0.0000	0.0007
Mg	1.7410	1.7659	1.7439	1.7584	1.7523	1.7220	1.7346	1.7421	1.7325	1.7328
Ca	0.0201	0.0235	0.0221	0.0243	0.0225	0.0218	0.0252	0.0227	0.0218	0.0229
Na	0.0013	0.0000	0.0020	0.0053	0.0022	0.0007	0.0007	0.0000	0.0000	0.0003
K	0.0000	0.0000	0.0000	0.0000	0.0000	0.0000	0.0000	0.0000	0.0000	0.0000
Total	3.9969	4.0078	3.9986	4.0128	4.0040	3.9927	4.0065	4.0028	3.9975	3.9999
Mg#	91.48	91.75	91.56	91.36	91.54	91.21	90.68	91.00	90.86	90.94
Wo	1.04	1.21	1.15	1.25	1.16	1.14	1.30	1.17	1.13	1.19
En	90.33	90.44	90.35	90.09	90.30	90.16	89.42	89.91	89.83	89.83
Fs	8.63	8.36	8.50	8.66	8.54	8.70	9.28	8.92	9.04	8.99

Orthopyroxene analyses

Melting experiments at 3.0GPa

CPL series

	CPL8 (950° -> 1025°C, 21->5hrs)			CPL9 (950° -> 1050°C, 20->5hrs)				
	OPX1	OPX2	Ave.	OPX1	OPX2	OPX3	OPX4	Ave.
SiO2	55.28	55.64	55.46	56.05	56.00	55.44	55.34	55.71
TiO2	0.04	0.01	0.03	0.00	0.00	0.02	0.04	0.02
Al2O3	3.29	3.09	3.19	2.78	2.64	2.98	3.19	2.80
Cr2O3	0.31	0.40	0.36	0.22	0.29	0.21	0.31	0.26
FeO*	5.84	5.89	5.87	5.92	5.84	5.98	6.03	5.94
MnO	0.09	0.17	0.13	0.01	0.20	0.04	0.03	0.02
MgO	33.56	33.68	33.62	34.28	34.03	33.91	33.61	33.96
CaO	0.60	0.49	0.55	0.51	0.51	0.56	0.60	0.55
Na2O	0.00	0.00	0.00	0.00	0.00	0.00	0.04	0.01
K2O	0.00	0.00	0.00	0.00	0.00	0.00	0.00	0.00
Total	99.01	99.37	99.19	99.77	99.31	99.14	99.19	99.35
Si	1.9236	1.9295	1.9265	1.9342	1.9404	1.9272	1.9239	1.9314
Al IV	0.0764	0.0705	0.0735	0.0658	0.0596	0.0728	0.0761	0.0686
Al VI	0.0586	0.0558	0.0572	0.0473	0.0483	0.0493	0.0546	0.0499
Ti	0.0010	0.0003	0.0007	0.0000	0.0000	0.0005	0.0010	0.0004
Cr	0.0085	0.0110	0.0097	0.0060	0.0079	0.0058	0.0085	0.0071
Fe	0.1700	0.1708	0.1704	0.1709	0.1692	0.1739	0.1753	0.1723
Mn	0.0027	0.0050	0.0038	0.0003	0.0000	0.0012	0.0009	0.0006
Mg	1.7404	1.7406	1.7405	1.7630	1.7573	1.7568	1.7414	1.7546
Ca	0.0224	0.0182	0.0203	0.0189	0.0189	0.0209	0.0224	0.0202
Na	0.0000	0.0000	0.0000	0.0000	0.0000	0.0000	0.0027	0.0007
K	0.0000	0.0000	0.0000	0.0000	0.0000	0.0000	0.0000	0.0000
Total	4.0036	4.0016	4.0026	4.0063	4.0017	4.0083	4.0068	4.0058
Mg#	91.10	91.06	91.08	91.17	91.22	90.99	90.85	91.08
Wo	1.16	0.94	1.05	0.97	0.97	1.07	1.15	1.04
En	89.93	89.97	89.95	90.27	90.33	89.97	89.76	90.08
Fs	8.92	9.09	9.00	8.76	8.70	8.96	9.08	8.88

Orthopyroxene analyses

Melting experiments at 3.0GPa

CPL series

	CPLI (950°→1075°C, 21→4hrs30min)					CPLIQ (950°→1100°C, 20→5hrs)				
	OPX1	OPX2	OPX3	OPX4	Ave.	OPX1	OPX2	OPX3	OPX4	Ave.
SiO2	55.64	55.64	55.59	55.67	55.64	55.60	56.18	56.02	55.74	55.89
TiO2	0.00	0.02	0.02	0.01	0.01	0.00	0.04	0.01	0.02	0.02
Al2O3	3.05	3.18	3.07	2.87	3.04	2.95	3.01	3.06	3.10	3.03
Cr2O3	0.37	0.30	0.28	0.36	0.33	0.27	0.31	0.33	0.35	0.32
FeO*	5.93	6.15	6.07	6.04	6.05	6.15	6.01	5.76	6.42	6.09
MnO	0.10	0.17	0.12	0.15	0.14	0.01	0.03	0.00	0.03	0.02
MgO	33.89	33.56	33.96	33.62	33.76	34.09	33.81	33.63	33.56	33.77
CaO	0.51	0.47	0.49	0.51	0.50	0.65	0.52	0.53	0.66	0.59
Na2O	0.04	0.06	0.00	0.00	0.03	0.00	0.00	0.00	0.00	0.00
K2O	0.00	0.02	0.00	0.00	0.01	0.00	0.00	0.00	0.00	0.00
Total	99.53	99.57	99.60	99.23	99.48	99.72	99.91	99.34	99.88	99.71
Si	1.9269	1.9279	1.9248	1.9343	1.9285	1.9240	1.9360	1.9388	1.9273	1.9316
Al IV	0.0731	0.0721	0.0752	0.0657	0.0715	0.0760	0.0640	0.0612	0.0727	0.0684
Al VI	0.0515	0.0578	0.0501	0.0518	0.0528	0.0443	0.0589	0.0637	0.0537	0.0550
Ti	0.0000	0.0005	0.0005	0.0003	0.0003	0.0000	0.0010	0.0003	0.0005	0.0005
Cr	0.0101	0.0082	0.0077	0.0099	0.0090	0.0074	0.0084	0.0090	0.0096	0.0086
Fe	0.1718	0.1782	0.1758	0.1755	0.1753	0.1780	0.1732	0.1667	0.1857	0.1759
Mn	0.0029	0.0050	0.0035	0.0044	0.0040	0.0003	0.0009	0.0000	0.0009	0.0005
Mg	1.7492	1.7330	1.7524	1.7409	1.7439	1.7581	1.7334	1.7346	1.7294	1.7396
Ca	0.0189	0.0174	0.0182	0.0190	0.0184	0.0241	0.0192	0.0197	0.0245	0.0219
Na	0.0027	0.0040	0.0000	0.0000	0.0017	0.0000	0.0000	0.0000	0.0000	0.0000
K	0.0000	0.0009	0.0000	0.0000	0.0002	0.0000	0.0000	0.0000	0.0000	0.0000
Total	4.0071	4.0050	4.0082	4.0018	4.0055	4.0122	3.9976	3.9940	4.0042	4.0020
Mg#	91.06	90.68	90.88	90.84	90.87	90.81	90.93	91.23	90.31	90.82
Wo	0.97	0.90	0.93	0.98	0.95	1.23	1.00	1.02	1.28	1.13
En	90.03	89.62	89.87	89.75	89.82	89.68	89.98	90.30	89.13	89.77
Fs	8.99	9.47	9.20	9.28	9.23	9.09	9.02	8.68	9.61	9.10

Orthopyroxene analyses

Melting experiments at 3.0GPa

CPL series

	CPL13 (950°→1125°C, 20→4hrs)					CPL12 (950°→1150°C, 20→4hrs)				
	OPX1	OPX2	OPX3	OPX4	Ave.	OPX1	OPX2	OPX3	OPX4	Ave.
SiO2	55.54	55.25	55.81	55.43	55.51	55.82	55.80	55.48	55.62	55.68
TiO2	0.02	0.01	0.00	0.02	0.01	0.00	0.03	0.03	0.04	0.03
Al2O3	3.08	2.99	2.98	3.4	3.13	2.96	2.95	3.38	2.94	3.06
Cr2O3	0.22	0.34	0.36	0.34	0.32	0.24	0.26	0.28	0.37	0.29
FeO*	5.98	5.78	5.62	5.97	5.84	5.81	5.98	6.06	5.88	5.93
MnO	0.04	0.04	0.04	0.00	0.03	0.01	0.00	0.00	0.07	0.02
MgO	34.11	34.11	33.67	33.46	33.84	33.95	33.88	33.64	33.95	33.86
CaO	0.52	0.49	0.51	0.72	0.56	0.61	0.63	0.64	0.54	0.61
Na2O	0.00	0.00	0.01	0.00	0.00	0.00	0.00	0.00	0.00	0.00
K2O	0.00	0.00	0.00	0.00	0.00	0.00	0.00	0.00	0.00	0.00
Total	99.51	99.01	99.00	99.39	99.23	99.40	99.53	99.51	99.41	99.46
Si	1.9235	1.9225	1.9380	1.9222	1.9265	1.9329	1.9315	1.9219	1.9280	1.9286
Al IV	0.0765	0.0775	0.0620	0.0778	0.0735	0.0671	0.0685	0.0781	0.0720	0.0714
Al VI	0.0493	0.0451	0.0600	0.0632	0.0544	0.0537	0.0519	0.0599	0.0482	0.0534
Ti	0.0005	0.0003	0.0000	0.0005	0.0003	0.0000	0.0008	0.0008	0.0010	0.0007
Cr	0.0060	0.0094	0.0099	0.0093	0.0086	0.0086	0.0071	0.0077	0.0101	0.0079
Fe	0.1732	0.1682	0.1632	0.1731	0.1694	0.1683	0.1731	0.1756	0.1705	0.1718
Mn	0.0012	0.0012	0.0012	0.0000	0.0009	0.0003	0.0000	0.0000	0.0021	0.0008
Mg	1.7606	1.7689	1.7425	1.7292	1.7503	1.7520	1.7478	1.7367	1.7539	1.7476
Ca	0.0193	0.0183	0.0190	0.0268	0.0208	0.0226	0.0234	0.0238	0.0201	0.0225
Na	0.0000	0.0000	0.0007	0.0000	0.0002	0.0000	0.0000	0.0000	0.0000	0.0000
K	0.0000	0.0000	0.0000	0.0000	0.0000	0.0000	0.0000	0.0000	0.0000	0.0000
Total	4.0101	4.0113	3.9964	4.0021	4.0050	4.0034	4.0040	4.0045	4.0058	4.0041
Mg#	91.04	91.32	91.44	90.90	91.17	91.24	90.99	90.62	91.14	91.05
Wo	0.99	0.93	0.99	1.39	1.07	1.16	1.20	1.23	1.03	1.16
En	90.0	90.41	90.48	89.64	90.15	90.16	89.89	89.70	90.11	89.97
Fs	8.92	8.66	8.54	8.98	8.77	8.67	8.90	9.07	8.86	8.88

Orthopyroxene analyses

Melting experiments at 3.0GPa

CPL series (sandwich experiments)

	CPL14 (1100 °C, 21->9hrs30min)					CPL15 (1100 °C, 21->9hrs30min)				
	OPX1	OPX2	OPX3	OPX4	Ave.	OPX1	OPX2	OPX3	OPX4	Ave.
SiO2	56.50	55.68	55.88	55.97	56.01	56.11	55.68	55.93	56.74	56.12
TiO2	0.03	0.00	0.00	0.01	0.01	0.01	0.00	0.04	0.01	0.02
Al2O3	2.78	2.85	3.03	2.99	2.91	3.06	3.07	2.90	2.88	2.98
Cr2O3	0.36	0.38	0.21	0.24	0.30	0.15	0.27	0.22	0.20	0.21
FeO*	6.05	6.01	5.94	5.80	5.95	5.71	5.94	6.10	5.78	5.88
MnO	0.07	0.08	0.16	0.18	0.12	0.14	0.21	0.24	0.18	0.19
MgO	34.50	34.16	34.32	34.14	34.28	33.74	33.57	34.03	33.98	33.83
CaO	0.54	0.58	0.71	0.78	0.65	0.76	0.71	0.53	0.62	0.66
Na2O	0.07	0.10	0.00	0.00	0.04	0.00	0.00	0.00	0.00	0.00
K2O	0.00	0.04	0.00	0.00	0.01	0.00	0.00	0.00	0.00	0.00
Total	100.90	99.88	100.25	100.11	100.29	99.68	99.45	99.99	100.39	99.88
Si	1.9309	1.9244	1.9227	1.9273	1.9263	1.9369	1.9306	1.9298	1.9441	1.9353
Al IV	0.0691	0.0756	0.0773	0.0727	0.0737	0.0631	0.0694	0.0702	0.0559	0.0647
Al VI	0.0429	0.0406	0.0456	0.0487	0.0444	0.0614	0.0561	0.0477	0.0604	0.0564
Ti	0.0008	0.0000	0.0000	0.0003	0.0003	0.0003	0.0000	0.0010	0.0003	0.0004
Cr	0.0097	0.0104	0.0057	0.0065	0.0081	0.0041	0.0074	0.0060	0.0054	0.0057
Fe	0.1729	0.1737	0.1709	0.1670	0.1711	0.1648	0.1722	0.1760	0.1656	0.1697
Mn	0.0020	0.0023	0.0047	0.0053	0.0036	0.0041	0.0062	0.0070	0.0052	0.0056
Mg	1.7571	1.7596	1.7599	1.7520	1.7571	1.7358	1.7347	1.7498	1.7351	1.7389
Ca	0.0198	0.0215	0.0262	0.0288	0.0240	0.0281	0.0264	0.0196	0.0228	0.0242
Na	0.0046	0.0067	0.0000	0.0000	0.0028	0.0000	0.0000	0.0000	0.0000	0.0000
K	0.0000	0.0018	0.0000	0.0000	0.0004	0.0000	0.0000	0.0000	0.0000	0.0000
Total	4.0098	4.0165	4.0130	4.0085	4.0120	3.9986	4.0030	4.0072	3.9948	4.0009
Mg#	91.04	91.01	91.15	91.30	91.12	91.33	90.97	90.86	91.29	91.11
Wo	1.01	1.10	1.33	1.47	1.23	1.45	1.36	1.00	1.18	1.25
En	90.02	89.91	89.71	89.71	89.84	89.81	89.44	89.62	89.96	89.71
Fs	8.96	9.00	8.95	8.82	8.93	8.74	9.20	9.37	8.86	9.04

Orthopyroxene analyses

Melting experiments at 3.0GPa

CPL series (sandwich experiments)

CPL16 (1100 °C, 21->9hrs30min)

	OPX1	OPX2	OPX3	OPX4	Ave.
SiO2	56.24	56.41	56.13	56.13	56.23
TiO2	0.01	0.04	0.02	0.02	0.02
Al2O3	3.08	2.73	2.68	3.14	2.91
Cr2O3	0.31	0.20	0.32	0.25	0.27
FeO*	6.04	6.03	5.81	6.10	6.00
MnO	0.15	0.20	0.21	0.21	0.19
MgO	33.81	33.90	33.81	33.69	33.80
CaO	0.66	0.46	0.55	0.72	0.60
Na2O	0.00	0.00	0.00	0.00	0.00
K2O	0.00	0.00	0.00	0.00	0.00
Total	100.30	99.97	99.53	100.26	100.02
Si	1.9328	1.9432	1.9420	1.9311	1.9373
Al IV	0.0672	0.0568	0.0580	0.0689	0.0627
Al VI	0.0576	0.0541	0.0513	0.0584	0.0554
Ti	0.0003	0.0010	0.0005	0.0005	0.0006
Cr	0.0084	0.0054	0.0088	0.0068	0.0074
Fe	0.1736	0.1737	0.1681	0.1755	0.1727
Mn	0.0044	0.0058	0.0062	0.0061	0.0058
Mg	1.7317	1.7404	1.7433	1.7274	1.7357
Ca	0.0243	0.0170	0.0204	0.0265	0.0221
Na	0.0000	0.0000	0.0000	0.0000	0.0000
K	0.0000	0.0000	0.0000	0.0000	0.0000
Total	4.0003	3.9976	3.9985	4.0013	3.9994
Mg#	90.89	90.92	91.20	90.78	90.95
Wo	1.26	0.88	1.05	1.37	1.14
En	89.54	89.85	89.96	89.24	89.65
Fs	9.20	9.27	8.99	9.38	9.21

Clinopyroxene analyses

Melting experiments at 3.0GPa

CPL series

	GPL2 (900 °C, 28hrs)					CPL4 (925 °C, 28hrs)				
	CPX1	CPX2	CPX3	CPX4	Ave.	CPX1	CPX2	CPX3	CPX4	Ave.
SiO2	53.60	53.70	53.31	52.77	53.35	52.73	52.82	52.96	53.59	53.03
TiO2	0.05	0.10	0.18	0.13	0.12	0.18	0.19	0.09	0.09	0.14
Al2O3	3.89	3.58	4.46	3.95	3.97	4.03	3.79	3.72	3.40	3.74
Cr2O3	0.51	0.62	0.75	0.64	0.63	0.68	0.59	0.54	0.65	0.62
FeO*	2.94	2.84	3.21	2.89	2.97	3.09	2.76	3.02	2.90	2.94
MnO	0.10	0.07	0.09	0.08	0.09	0.13	0.08	0.06	0.10	0.09
MgO	16.59	16.45	18.17	17.21	17.11	16.97	16.98	16.70	16.87	16.88
CaO	21.68	21.85	17.92	20.93	20.60	20.23	21.70	22.15	22.18	21.57
Na2O	1.13	1.02	1.50	1.15	1.20	1.47	1.22	0.97	0.91	1.14
K2O	0.00	0.00	0.08	0.00	0.02	0.04	0.00	0.00	0.00	0.01
Total	100.49	100.23	99.67	99.75	100.04	99.55	100.13	100.21	100.69	100.15
Si	1.9332	1.9413	1.9244	1.9171	1.9290	1.9201	1.9156	1.9210	1.9323	1.9223
Al IV	0.0668	0.0587	0.0756	0.0829	0.0710	0.0799	0.0844	0.0790	0.0677	0.0777
Al VI	0.0986	0.0939	0.1142	0.0863	0.0983	0.0931	0.0776	0.0801	0.0769	0.0819
Ti	0.0014	0.0027	0.0049	0.0036	0.0031	0.0049	0.0052	0.0025	0.0024	0.0037
Cr	0.0145	0.0177	0.0214	0.0184	0.0180	0.0196	0.0169	0.0155	0.0185	0.0176
Fe	0.0887	0.0859	0.0969	0.0878	0.0898	0.0941	0.0837	0.0916	0.0875	0.0892
Mn	0.0031	0.0021	0.0028	0.0025	0.0026	0.0040	0.0025	0.0018	0.0031	0.0028
Mg	0.8918	0.8863	0.9775	0.9318	0.9218	0.9209	0.9177	0.9028	0.9066	0.9120
Ca	0.8379	0.8464	0.6931	0.8148	0.7980	0.7893	0.8432	0.8609	0.8570	0.8377
Na	0.0790	0.0715	0.1050	0.0810	0.0841	0.1038	0.0858	0.0682	0.0638	0.0803
K	0.0000	0.0000	0.0037	0.0000	0.0009	0.0019	0.0000	0.0000	0.0000	0.0005
Total	4.0149	4.0065	4.0195	4.0261	4.0167	4.0315	4.0327	4.0234	4.0155	4.0257
Mg#	90.95	91.17	90.98	91.39	91.12	90.73	91.64	90.79	91.20	91.09
Wo	46.00	46.49	39.15	44.36	44.03	43.65	45.65	46.36	46.22	45.48
En	48.96	48.68	55.22	50.73	50.87	50.93	49.68	48.61	48.90	49.52
Fs	5.04	4.83	5.63	4.91	5.10	5.43	4.66	5.03	4.88	5.00

Clinopyroxene analyses

Melting experiments at 3.0GPa

CPL series

	<u>CPL5</u> (975 °C, 20hrs)					<u>CPL11</u> (1000 °C, 28hrs)				
	CPX1	CPX2	CPX3	CPX4	Ave.	CPX1	CPX2	CPX3	CPX4	Ave.
SiO2	52.71	52.91	52.24	52.57	52.61	52.35	52.41	52.71	52.95	52.61
TiO2	0.10	0.09	0.14	0.15	0.12	0.06	0.10	0.10	0.05	0.08
Al2O3	3.59	3.45	3.51	3.50	3.51	4.08	4.14	3.87	3.45	3.89
Cr2O3	0.58	0.62	0.49	0.69	0.60	0.51	0.54	0.54	0.41	0.50
FeO*	2.56	2.88	2.88	3.12	2.86	3.00	2.90	2.68	2.86	2.86
MnO	0.13	0.03	0.11	0.09	0.09	0.08	0.07	0.03	0.07	0.06
MgO	16.91	16.82	17.29	18.34	17.34	16.50	16.25	16.59	16.67	16.50
CaO	22.33	22.31	21.56	20.37	21.64	21.54	21.65	22.24	22.45	21.97
Na2O	0.88	0.93	1.18	1.10	1.02	1.08	1.13	0.89	0.81	0.98
K2O	0.00	0.00	0.05	0.00	0.01	0.03	0.01	0.01	0.01	0.02
Total	99.79	100.04	99.45	99.93	99.80	99.23	99.20	99.66	99.73	99.46
Si	1.9186	1.9228	1.9109	1.9083	1.9152	1.9161	1.9182	1.9197	1.9289	1.9207
Al IV	0.0814	0.0772	0.0891	0.0917	0.0848	0.0839	0.0818	0.0803	0.0711	0.0793
Al VI	0.0727	0.0706	0.0623	0.0581	0.0659	0.0922	0.0968	0.0859	0.0771	0.0850
Ti	0.0027	0.0025	0.0039	0.0041	0.0033	0.0017	0.0028	0.0027	0.0014	0.0021
Cr	0.0167	0.0178	0.0142	0.0198	0.0171	0.0148	0.0156	0.0155	0.0118	0.0144
Fe	0.0779	0.0875	0.0881	0.0947	0.0871	0.0918	0.0888	0.0816	0.0871	0.0873
Mn	0.0040	0.0009	0.0034	0.0028	0.0028	0.0025	0.0022	0.0009	0.0022	0.0019
Mg	0.9173	0.9110	0.9426	0.9922	0.9403	0.9001	0.8864	0.9005	0.9050	0.8980
Ca	0.8709	0.8688	0.8450	0.7923	0.8442	0.8448	0.8491	0.8679	0.8763	0.8595
Na	0.0621	0.0655	0.0837	0.0774	0.0722	0.0766	0.0802	0.0628	0.0572	0.0692
K	0.0000	0.0000	0.0023	0.0000	0.0006	0.0014	0.0005	0.0005	0.0005	0.0007
Total	4.0243	4.0247	4.0455	4.0415	4.0340	4.0258	4.0222	4.0184	4.0186	4.0212
Mg#	92.17	91.23	91.45	91.29	91.53	90.74	90.90	91.69	91.22	91.14
Wo	46.57	46.50	44.97	42.10	45.03	45.93	46.49	46.89	46.85	46.54
En	49.05	48.76	50.16	52.72	50.18	48.94	48.53	48.65	48.36	48.62
Fs	4.36	4.73	4.87	5.18	4.79	5.13	4.98	4.46	4.77	4.83

Clinopyroxene analyses

Melting experiments at 3.0GPa

GPL series

	GPL8 (950°→1025°C, 21→5hrs)					GPL9 (950°→1050°C, 20→5hrs)				
	CPX1	CPX2	CPX3	CPX4	Ave.	CPX1	CPX2	CPX3	CPX4	Ave.
SiO2	53.26	52.58	52.64	52.36	52.71	52.75	52.87	52.25	52.29	52.54
TiO2	0.05	0.08	0.06	0.10	0.07	0.12	0.05	0.07	0.06	0.08
Al2O3	3.67	4.18	4.33	3.47	3.91	3.60	3.34	3.87	4.01	3.71
Cr2O3	0.58	0.64	0.69	0.63	0.64	0.50	0.48	0.52	0.52	0.51
FeO*	2.78	3.06	2.93	2.88	2.91	2.82	2.95	2.76	2.83	2.84
MnO	0.06	0.09	0.13	0.06	0.09	0.09	0.01	0.10	0.10	0.08
MgO	16.55	16.15	16.20	16.76	16.42	16.89	17.03	16.48	16.55	16.74
CaO	22.69	21.71	21.71	22.53	22.16	22.17	22.55	22.32	21.65	22.17
Na2O	0.81	0.97	0.96	0.82	0.89	0.84	0.84	0.86	1.03	0.89
K2O	0.00	0.00	0.00	0.00	0.00	0.00	0.00	0.02	0.03	0.01
Total	100.45	99.46	99.65	99.61	99.79	99.78	100.12	99.25	99.07	99.56
Si	1.9261	1.9197	1.9172	1.9141	1.9193	1.9203	1.9211	1.9141	1.9164	1.9180
Al IV	0.0739	0.0803	0.0828	0.0859	0.0807	0.0797	0.0789	0.0859	0.0836	0.0820
Al VI	0.0826	0.0996	0.1031	0.0637	0.0872	0.0748	0.0642	0.0813	0.0897	0.0775
Ti	0.0014	0.0022	0.0016	0.0027	0.0020	0.0033	0.0014	0.0019	0.0017	0.0021
Cr	0.0166	0.0185	0.0199	0.0182	0.0183	0.0144	0.0138	0.0151	0.0151	0.0146
Fe	0.0841	0.0934	0.0892	0.0881	0.0887	0.0859	0.0896	0.0846	0.0867	0.0867
Mn	0.0018	0.0028	0.0040	0.0019	0.0026	0.0028	0.0003	0.0031	0.0031	0.0023
Mg	0.8920	0.8788	0.8793	0.9131	0.8908	0.9164	0.9222	0.8998	0.9040	0.9106
Ca	0.8792	0.8493	0.8472	0.8825	0.8646	0.8648	0.8780	0.8761	0.8502	0.8673
Na	0.0568	0.0687	0.0678	0.0581	0.0628	0.0593	0.0592	0.0611	0.0732	0.0632
K	0.0000	0.0000	0.0000	0.0000	0.0000	0.0000	0.0000	0.0009	0.0014	0.0006
Total	4.0144	4.0132	4.0122	4.0283	4.0170	4.0216	4.0247	4.0238	4.0250	4.0248
Mg#	91.39	90.39	90.79	91.21	90.94	91.43	91.14	91.41	91.24	91.31
Wo	47.34	46.56	46.56	46.80	46.82	46.25	46.45	47.01	46.11	46.46
En	48.03	48.17	48.32	48.43	48.24	49.01	48.79	48.28	49.02	48.78
Fs	4.63	5.27	5.12	4.77	4.94	4.74	4.76	4.70	4.87	4.77

Glinopyroxene analyses

Melting experiments at 3.0GPa

CPL series

	CPL7 (950°→1075°C, 21→4hrs30min)					CPL10 (950°→1100°C, 20→5hrs)				
	CPX1	CPX2	CPX3	CPX4	Ave.	CPX1	CPX2	CPX3	CPX4	Ave.
SiO2	52.71	52.57	52.32	52.62	52.56	52.91	53.35	51.98	52.12	52.59
TiO2	0.08	0.07	0.07	0.04	0.07	0.09	0.06	0.05	0.10	0.08
Al2O3	3.32	3.19	3.67	3.77	3.49	3.74	3.50	3.93	3.66	3.71
Cr2O3	0.63	0.57	0.50	0.74	0.61	0.46	0.49	0.62	0.63	0.55
FeO*	3.15	2.87	2.94	3.06	3.01	2.97	2.77	2.91	2.80	2.86
MnO	0.14	0.08	0.11	0.11	0.11	0.08	0.00	0.07	0.09	0.06
MgO	16.71	16.99	16.66	16.38	16.69	16.72	16.73	16.35	16.72	16.63
CaO	22.03	22.38	21.98	21.97	22.09	22.26	22.94	22.42	21.87	22.37
Na2O	0.78	0.84	0.95	0.90	0.87	0.85	0.88	0.91	1.02	0.92
K2O	0.00	0.00	0.00	0.00	0.00	0.00	0.01	0.03	0.13	0.04
Total	99.55	99.56	99.20	99.59	99.48	100.08	100.73	99.27	99.14	99.81
Si	1.9263	1.9216	1.9179	1.9214	1.9218	1.9210	1.9254	1.9075	1.9132	1.9168
Al IV	0.0737	0.0784	0.0821	0.0786	0.0782	0.0790	0.0746	0.0925	0.0868	0.0832
Al VI	0.0694	0.0591	0.0765	0.0836	0.0721	0.0811	0.0743	0.0775	0.0716	0.0761
Ti	0.0022	0.0019	0.0019	0.0011	0.0018	0.0025	0.0016	0.0014	0.0028	0.0021
Cr	0.0182	0.0165	0.0145	0.0214	0.0176	0.0132	0.0140	0.0180	0.0183	0.0158
Fe	0.0063	0.0877	0.0901	0.0934	0.0919	0.0902	0.0836	0.0893	0.0860	0.0873
Mn	0.0043	0.0025	0.0034	0.0034	0.0034	0.0025	0.0000	0.0022	0.0028	0.0019
Mg	0.9101	0.9255	0.9101	0.8914	0.9093	0.9047	0.8998	0.8942	0.9147	0.9033
Ca	0.8627	0.8785	0.8633	0.8596	0.8655	0.8660	0.8871	0.8816	0.8602	0.8737
Na	0.0553	0.0595	0.0675	0.0637	0.0615	0.0598	0.0616	0.0647	0.0726	0.0647
K	0.0000	0.0000	0.0000	0.0000	0.0000	0.0000	0.0005	0.0014	0.0061	0.0020
Total	4.0185	4.0293	4.0274	4.0176	4.0232	4.0198	4.0225	4.0302	4.0350	4.0269
Mg#	90.43	91.34	90.99	90.51	90.82	90.94	91.50	90.92	91.41	91.19
Wo	46.05	46.32	46.24	46.52	46.28	46.47	47.42	47.21	46.16	46.82
En	48.58	48.91	48.75	48.24	48.62	48.55	48.11	47.89	49.08	48.41
Fs	5.37	4.77	5.01	5.24	5.10	4.97	4.47	4.90	4.76	4.77

Clinopyroxene analyses

Melting experiments at 3.0GPa

CPL series

	CPL13 (950°→1125°C, 20→4hrs)					CPL12 (950°→1150°C, 20→4hrs)				
	CPX1	CPX2	CPX3	CPX4	Ave.	CPX1	CPX2	CPX3	CPX4	Ave.
SiO2	53.04	53.04	52.67	52.99	52.94	53.03	52.76	52.58	52.34	52.75
TiO2	0.09	0.08	0.09	0.05	0.08	0.08	0.10	0.06	0.07	0.08
Al2O3	3.61	3.38	3.92	3.59	3.63	3.58	3.50	3.82	3.82	3.68
Cr2O3	0.39	0.36	0.41	0.52	0.42	0.49	0.44	0.50	0.55	0.50
FeO*	3.03	2.90	2.82	2.86	2.90	2.82	2.95	2.75	2.88	2.85
MnO	0.07	0.08	0.05	0.07	0.07	0.05	0.05	0.00	0.07	0.04
MgO	16.55	16.74	16.60	16.88	16.69	16.90	17.04	16.65	16.43	16.76
CaO	21.52	22.02	21.80	22.20	21.89	22.25	22.09	21.81	22.00	22.04
Na2O	1.10	0.90	0.94	0.83	0.94	0.91	0.86	1.01	0.96	0.94
K2O	0.02	0.02	0.02	0.01	0.02	0.03	0.01	0.03	0.02	0.03
Total	99.42	99.52	99.32	100.00	99.57	100.14	99.85	99.51	99.14	99.66
Si	1.9351	1.9343	1.9232	1.9243	1.9292	1.9234	1.9205	1.9266	1.9188	1.9224
Al IV	0.0649	0.0657	0.0768	0.0757	0.0708	0.0766	0.0795	0.0734	0.0812	0.0776
Al VI	0.0904	0.0796	0.0920	0.0780	0.0850	0.0765	0.0707	0.0907	0.0839	0.0804
Ti	0.0025	0.0022	0.0025	0.0014	0.0021	0.0022	0.0027	0.0018	0.0019	0.0021
Cr	0.0112	0.0104	0.0118	0.0149	0.0121	0.0141	0.0127	0.0144	0.0159	0.0143
Fe	0.0925	0.0884	0.0861	0.0869	0.0885	0.0855	0.0898	0.0838	0.0883	0.0869
Mn	0.0022	0.0025	0.0015	0.0022	0.0021	0.0015	0.0015	0.0000	0.0022	0.0013
Mg	0.8999	0.9098	0.9034	0.9135	0.9067	0.9135	0.9244	0.9041	0.8977	0.9099
Ca	0.8413	0.8605	0.8529	0.8638	0.8546	0.8647	0.8616	0.8515	0.8642	0.8605
Na	0.0778	0.0636	0.0666	0.0584	0.0666	0.0640	0.0621	0.0714	0.0682	0.0664
K	0.0009	0.0009	0.0009	0.0005	0.0008	0.0014	0.0019	0.0014	0.0009	0.0014
Total	4.0186	4.0180	4.0177	4.0195	4.0184	4.0235	4.0273	4.0188	4.0233	4.0233
Mg#	90.68	91.14	91.30	91.32	91.11	91.44	91.15	91.52	91.04	91.29
Wo	45.83	46.23	46.26	46.28	46.15	46.36	45.89	46.29	46.65	46.30
En	49.02	48.88	48.99	48.95	48.96	48.97	49.24	48.15	48.46	48.96
Fs	5.15	4.89	4.75	4.77	4.89	4.67	4.87	4.56	4.88	4.74

Clinopyroxene analyses

Melting experiments at 3.0GPa

CPL series (sandwich experiments)

	CPL14 (1100 °C, 9hrs30min)					CPL15 (1100 °C, 9hrs30min)			
	CPX1	CPX2	CPX3	CPX4	Ave.	CPX1	CPX2	CPX3	Ave.
SiO2	53.42	52.32	53.11	52.67	52.88	53.46	53.44	53.56	53.49
TiO2	0.10	0.13	0.11	0.04	0.10	0.07	0.06	0.12	0.08
Al2O3	3.26	3.28	3.38	3.25	3.29	3.30	3.44	3.40	3.38
Cr2O3	0.50	0.55	0.55	0.77	0.59	0.53	0.62	0.56	0.57
FeO*	2.96	2.76	2.89	2.67	2.87	2.91	2.86	2.94	2.90
MnO	0.12	0.08	0.08	0.08	0.09	0.13	0.11	0.14	0.13
MgO	16.63	16.52	16.58	16.46	16.55	16.63	16.46	16.85	16.65
CaO	22.39	22.64	22.19	22.24	22.37	21.95	22.41	22.62	22.33
Na2O	0.96	0.97	0.95	0.99	0.97	0.74	0.71	0.69	0.71
K2O	0.03	0.05	0.04	0.00	0.03	0.00	0.00	0.00	0.00
Total	100.37	99.30	99.88	99.39	99.74	99.72	100.11	100.83	100.24
Si	1.9349	1.9198	1.9321	1.9284	1.9288	1.9434	1.9373	1.9292	1.9366
Al IV	0.0651	0.0802	0.0679	0.0716	0.0712	0.0566	0.0627	0.0708	0.0634
Al VI	0.0741	0.0617	0.0770	0.0687	0.0704	0.0848	0.0844	0.0736	0.0809
Ti	0.0027	0.0036	0.0030	0.0011	0.0026	0.0019	0.0016	0.0033	0.0023
Cr	0.0143	0.0160	0.0158	0.0223	0.0171	0.0152	0.0178	0.0159	0.0163
Fe	0.0897	0.0847	0.0879	0.0879	0.0876	0.0885	0.0867	0.0886	0.0879
Mn	0.0037	0.0025	0.0025	0.0025	0.0028	0.0040	0.0034	0.0043	0.0039
Mg	0.8977	0.9034	0.8989	0.8992	0.8998	0.9009	0.8893	0.9045	0.8983
Ca	0.8690	0.8901	0.8650	0.8725	0.8741	0.8550	0.8705	0.8730	0.8682
Na	0.0674	0.0690	0.0670	0.0703	0.0684	0.0522	0.0499	0.0482	0.0501
K	0.0014	0.0023	0.0019	0.0000	0.0014	0.0000	0.0000	0.0000	0.0000
Total	4.0260	4.0333	4.0190	4.0244	4.0242	4.0025	4.0036	4.0114	4.0058
Mg#	90.92	91.43	91.09	91.10	91.13	91.06	91.12	91.08	91.09
Wo	46.72	47.33	46.65	46.86	46.89	46.26	47.06	46.68	46.66
En	48.26	48.03	48.48	48.29	48.27	48.74	48.07	48.36	48.39
Fs	5.02	4.64	4.87	4.85	4.85	5.00	4.87	4.96	4.95

Clinopyroxene analyses

Melting experiments at 3.0GPa

CPL series (sandwich experiments)

CPL16 (1100°C, 9hrs30min)

	CPX1	CPX2	CPX3	CPX4	Ave.
SiO2	53.10	52.69	53.10	52.90	52.95
TiO2	0.09	0.08	0.08	0.09	0.09
Al2O3	3.38	3.44	3.41	3.77	3.50
Cr2O3	0.50	0.52	0.53	0.47	0.51
FeO ^w	2.63	2.78	3.03	2.82	2.82
MnO	0.16	0.17	0.18	0.12	0.16
MgO	16.33	16.34	16.44	16.39	16.38
CaO	22.86	22.40	22.07	21.99	22.33
Na2O	0.85	0.77	0.80	0.81	0.81
K2O	0.00	0.00	0.00	0.00	0.00
Total	99.90	99.19	99.64	99.36	99.52
Si	1.9321	1.9304	1.9357	1.9307	1.9322
Al IV	0.0679	0.0696	0.0643	0.0693	0.0678
Al VI	0.0771	0.0790	0.0823	0.0929	0.0828
Ti	0.0025	0.0022	0.0022	0.0025	0.0023
Cr	0.0144	0.0151	0.0153	0.0136	0.0146
Fe	0.0800	0.0852	0.0924	0.0861	0.0859
Mn	0.0049	0.0053	0.0056	0.0037	0.0049
Mg	0.8855	0.8922	0.8932	0.8915	0.8906
Ca	0.8913	0.8793	0.8621	0.8600	0.8732
Na	0.0600	0.0547	0.0585	0.0573	0.0571
K	0.0000	0.0000	0.0000	0.0000	0.0000
Total	4.0157	4.0129	4.0095	4.0076	4.0114
Mg#	91.71	91.28	90.63	91.19	91.20
Wo	47.87	47.23	46.52	46.71	47.08
En	47.56	47.92	48.20	48.42	48.02
Fs	4.56	4.86	5.28	4.88	4.90

Phononite analyses

Melting experiments at 3.0GPa

CPL series

	<u>GPL 2 (900 °C, 28hrs)</u>					<u>GPL4 (925 °C, 28hrs)</u>				
	<u>PHL 1</u>	<u>PHL2</u>	<u>PHL3</u>	<u>PHL4</u>	<u>Ave.</u>	<u>PHL1</u>	<u>PHL2</u>	<u>PHL3</u>	<u>PHL4</u>	<u>Ave.</u>
SiO2	38.60	37.99	38.99	37.95	38.38	39.14	37.80	38.47	38.83	38.56
TiO2	4.14	4.42	4.34	4.68	4.40	3.72	3.93	3.87	4.01	3.88
Al2O3	16.83	16.67	16.59	16.93	16.76	16.04	16.64	16.22	16.95	16.46
Cr2O3	0.14	0.09	0.00	0.00	0.06	0.06	0.16	0.10	0.00	0.08
FeO*	5.12	5.88	4.24	6.39	5.41	4.43	4.28	4.08	4.28	4.26
MnO	0.02	0.02	0.05	0.06	0.04	0.04	0.02	0.00	0.00	0.02
MgO	21.39	21.09	22.18	20.73	21.35	21.85	21.48	21.99	22.19	21.88
CaO	0.08	0.06	0.27	0.08	0.12	0.31	0.58	0.51	0.09	0.37
Na2O	0.46	0.38	0.73	0.39	0.49	0.46	0.52	0.58	0.40	0.49
K2O	9.59	9.87	9.13	9.94	9.63	9.86	9.43	9.47	9.88	9.66
Total	96.37	96.47	96.52	97.15	96.63	95.91	94.84	95.27	96.61	95.66
Si	5.4373	5.3814	5.4528	5.3528	5.4062	5.5310	5.4043	5.4645	5.4382	5.4596
Al IV	2.5627	2.6186	2.5472	2.6471	2.5938	2.4690	2.5957	2.5355	2.5618	2.5404
Al VI	0.2322	0.1653	0.1880	0.1681	0.1885	0.2033	0.2091	0.1807	0.2368	0.2076
Ti	0.4386	0.4709	0.4565	0.4965	0.4656	0.3954	0.4226	0.4134	0.4224	0.4134
Cr	0.0156	0.0101	0.0000	0.0000	0.0064	0.0067	0.0181	0.0112	0.0000	0.0090
Fe	0.6032	0.6966	0.4959	0.7538	0.6370	0.5236	0.5118	0.4823	0.4990	0.5041
Mn	0.0024	0.0024	0.0059	0.0072	0.0045	0.0048	0.0024	0.0000	0.0000	0.0018
Mg	4.4904	4.4523	4.6228	4.3577	4.4812	4.6017	4.5768	4.6551	4.6315	4.6164
Ca	0.0121	0.0091	0.0405	0.0121	0.0185	0.0469	0.0889	0.0776	0.0135	0.0565
Na	0.1256	0.1044	0.1979	0.1067	0.1338	0.1260	0.1442	0.1597	0.1086	0.1345
K	1.7234	1.7837	1.6290	1.7887	1.7309	1.7776	1.7201	1.7162	1.7653	1.7449
Total	15.6434	15.6948	15.6366	15.6907	15.6663	15.6860	15.6938	15.6963	15.8771	15.6883
Mg#	88.16	86.47	90.31	85.25	87.55	89.78	89.94	90.61	90.27	90.15
OSO	5.7823	5.7976	5.7692	5.7833	5.7830	5.7354	5.7407	5.7428	5.7897	5.7523
K site	1.8611	1.8972	1.8674	1.9075	1.8832	1.9506	1.9531	1.9535	1.8875	1.9360

Phlogonite analyses

Melting experiments at 3.0GPa

CPL series

	<u>CPL 5 (975 °C, 20hrs)</u>					<u>CPL 11 (1650 °C, 28hrs)</u>				
	PML 1	PML2	PML3	PML4	Ave.	PML 1	PML2	PML3	PML4	Ave.
SiO2	38.50	38.35	37.91	38.77	38.38	37.97	38.20	38.84	38.18	38.32
TiO2	4.31	4.10	3.93	3.72	4.02	4.72	4.70	4.23	4.54	4.55
Al2O3	16.68	16.77	17.58	15.55	16.65	16.55	17.12	15.95	16.51	16.53
Cr2O3	0.09	0.07	0.22	0.09	0.12	0.83	0.28	0.22	0.05	0.35
FeO*	4.89	4.18	4.21	4.24	4.38	4.59	4.77	4.88	5.74	5.00
MnO	0.00	0.00	0.00	0.00	0.00	0.00	0.00	0.00	0.00	0.00
MgO	22.28	23.49	21.48	22.32	22.39	20.11	20.53	22.23	20.83	20.93
CaO	0.12	0.09	0.06	0.06	0.08	0.42	0.10	0.33	0.11	0.24
Na2O	0.33	0.28	0.30	0.40	0.33	0.07	0.12	0.09	0.19	0.12
K2O	9.89	9.77	10.25	9.88	9.95	9.51	9.38	8.93	9.99	9.45
Total	97.09	97.10	95.94	95.03	96.29	94.77	95.20	95.80	96.14	95.48
Si	5.3902	5.3497	5.3632	5.5276	5.4072	5.4354	5.4265	5.4895	5.4204	5.4431
Al IV	2.6098	2.6503	2.6368	2.4724	2.5928	2.5646	2.5735	2.5105	2.5796	2.5569
Al VI	0.1433	0.1076	0.2953	0.1413	0.1717	0.2285	0.2937	0.1404	0.1837	0.2114
Ti	0.4538	0.4301	0.4181	0.3989	0.4254	0.5081	0.5021	0.4485	0.4847	0.4858
Cr	0.0100	0.0077	0.0246	0.0101	0.0131	0.0939	0.0314	0.0245	0.0056	0.0387
Fe	0.5726	0.4877	0.4981	0.5056	0.5160	0.5495	0.5667	0.5754	0.6815	0.5933
Mn	0.0000	0.0000	0.0000	0.0000	0.0000	0.0000	0.0000	0.0000	0.0000	0.0000
Mg	4.6488	4.8835	4.5289	4.7426	4.7014	4.2903	4.3464	4.6704	4.4072	4.4293
Ca	0.0180	0.0135	0.0091	0.0092	0.0125	0.0644	0.0152	0.0498	0.0167	0.0365
Na	0.0896	0.0757	0.0823	0.1106	0.0895	0.0194	0.0331	0.0246	0.0523	0.0324
K	1.7865	1.7388	1.8500	1.7971	1.7879	1.7368	1.7000	1.6061	1.8094	1.7128
Total	15.7025	15.7446	15.7064	15.7154	15.7173	15.4911	15.4886	15.5397	15.0413	15.5403
Mg#	89.03	90.92	90.09	90.37	90.11	88.65	88.47	89.03	86.61	88.19
OSO	5.8284	5.9166	5.7650	5.7986	5.8275	5.6704	5.7403	5.8591	5.7628	5.7585
K site	1.8741	1.8279	1.9414	1.9169	1.8898	1.8207	1.7482	1.6805	1.8785	1.7817

Phononite analyses

Melting experiments at 3.0GPa

CPL series

	CPL 8 (950 °C → 1025 °C, 21 → 5hrs)					CPL 9 (950 °C → 1050 °C, 20 → 5hrs)				
	PHL 1	PHL 2	PHL 3	PHL 4	A(4)	PHL 1	PHL 2	PHL 3	PHL 4	A(4)
SiO ₂	38.05	38.33	38.15	38.31	38.18	37.73	37.74	38.28	37.41	37.92
TiO ₂	4.48	4.47	4.33	4.41	4.43	4.51	4.51	4.48	4.55	4.50
Al ₂ O ₃	15.62	14.91	15.85	15.34	15.46	16.84	17.13	16.83	16.33	16.93
Cr ₂ O ₃	0.28	0.16	0.08	0.00	0.17	0.35	0.11	0.32	0.05	0.28
FeO*	4.40	4.90	5.32	6.48	4.87	4.33	4.56	4.56	6.40	4.48
MnO	0.03	0.03	0.00	0.08	0.02	0.07	0.01	0.03	0.06	0.04
MgO	20.85	21.79	21.85	20.35	21.43	20.42	20.60	21.21	20.29	20.74
CaO	0.10	0.22	0.13	0.19	0.15	0.23	0.12	0.11	0.18	0.15
Na ₂ O	0.05	0.15	0.06	0.10	0.09	0.21	0.32	0.23	0.24	0.25
K ₂ O	9.77	9.48	9.86	9.79	9.70	9.58	9.62	9.29	9.74	9.50
Total	93.63	94.44	95.43	95.05	94.50	94.27	94.72	95.34	95.25	94.78
Si	5.5087	5.5127	5.4451	5.5180	5.4887	5.4212	5.3990	5.4278	5.3834	5.4160
Al IV	2.4913	2.4873	2.5549	2.4820	2.5113	2.5788	2.6010	2.5722	2.6166	2.5840
Al VI	0.1747	0.0408	0.1121	0.1228	0.1091	0.2738	0.2880	0.2412	0.1538	0.2676
Ti	0.4878	0.4835	0.4648	0.4777	0.4786	0.4874	0.4852	0.4777	0.4824	0.4834
Cr	0.0320	0.0182	0.0090	0.0000	0.0197	0.0398	0.0124	0.0350	0.0057	0.0294
Fe	0.5328	0.5894	0.6350	0.7806	0.5860	0.5203	0.5456	0.5407	0.7702	0.5356
Mn	0.0037	0.0037	0.0000	0.0098	0.0024	0.0085	0.0012	0.0036	0.0073	0.0044
Mg	4.4987	4.6705	4.6052	4.3683	4.5917	4.3727	4.3920	4.4821	4.3514	4.4158
Ca	0.0155	0.0339	0.0199	0.0293	0.0231	0.0354	0.0184	0.0167	0.0278	0.0235
Na	0.0140	0.0418	0.0166	0.0279	0.0242	0.0585	0.0888	0.0632	0.0670	0.0702
K	1.8046	1.7395	1.7954	1.7990	1.7798	1.7561	1.7558	1.6806	1.7882	1.7306
Total	15.5638	15.6213	15.6581	15.6154	15.6146	15.5525	15.5873	15.5417	15.6637	15.5605
Mg#	89.41	88.79	87.88	84.84	88.68	89.37	89.95	89.23	84.96	89.18
OSO	5.7297	5.8061	5.8262	5.7591	5.7875	5.7025	5.7244	5.7812	5.7808	5.7362
K site	1.8341	1.8152	1.8319	1.8562	1.8271	1.8501	1.8629	1.7805	1.8829	1.8243

Phlogopite analyses

Melting experiments at 3.0GPa

CPL series

	<u>CPL 7</u> (950° → 1075°C, 21 → 4hrs 30min)					<u>CPL 10</u> (950° → 1100°C, 20 → 5hrs)				
	PHL 1	PHL2	PHL3	PHL4	A(3,4)	PHL 1	PHL2	PHL3	PHL4	A(1)
SiO2	38.20	38.67	37.94	38.69	38.44	37.11	37.45	37.16	37.42	37.34
TiO2	6.30	5.96	4.93	4.37	6.13	4.97	5.52	6.00	6.31	5.94
Al2O3	16.34	16.86	17.01	16.08	16.60	16.95	17.71	16.75	16.18	16.88
Cr2O3	0.41	0.37	0.13	0.19	0.39	0.24	0.34	0.25	0.42	0.34
FeO*	4.35	4.52	4.24	4.67	4.44	4.72	4.54	4.21	4.57	4.44
MnO	0.03	0.06	0.00	0.03	0.05	0.06	0.04	0.00	0.00	0.01
MgO	19.88	19.92	19.98	19.84	19.90	20.25	20.02	19.54	19.71	19.76
CaO	0.21	0.60	0.25	1.94	0.41	0.85	0.54	0.98	0.14	0.55
Na2O	0.03	0.07	0.07	0.20	0.05	0.20	0.10	0.07	0.10	0.09
K2O	9.98	9.71	10.15	9.18	9.85	9.26	9.43	9.45	9.69	9.52
Total	95.73	96.74	94.70	95.19	96.24	94.61	95.69	94.41	94.54	94.88
Si	5.4160	5.4194	5.4319	5.5185	5.4177	5.3311	5.3056	5.3415	5.3763	5.3417
Al IV	2.5840	2.5806	2.5681	2.4815	2.5823	2.6689	2.6942	2.6585	2.6217	2.6583
Al VI	0.1472	0.2050	0.3030	0.2224	0.1763	0.2017	0.2639	0.1801	0.1200	0.1863
Ti	0.6718	0.6282	0.5308	0.4688	0.6498	0.5370	0.5882	0.6486	0.6821	0.6394
Cr	0.0460	0.0410	0.0147	0.0214	0.0435	0.0273	0.0381	0.0284	0.0477	0.0381
Fe	0.5158	0.5298	0.5077	0.5571	0.5228	0.5671	0.5379	0.5061	0.5493	0.5312
Mn	0.0036	0.0071	0.0000	0.0036	0.0054	0.0073	0.0048	0.0070	0.0000	0.0016
Mg	4.2006	4.1605	4.2631	4.2174	4.1804	4.3354	4.2271	4.1860	4.2219	4.2118
Ca	0.0319	0.0901	0.0384	0.2965	0.0612	0.1308	0.0820	0.1509	0.0216	0.0648
Na	0.0082	0.0190	0.0194	0.0553	0.0137	0.0557	0.0275	0.0195	0.0279	0.0250
K	1.8052	1.7361	1.8540	1.6705	1.7705	1.6971	1.7045	1.7330	1.7768	1.7380
Total	15.4304	15.4167	15.5311	15.5130	15.4235	15.5594	15.4739	15.4526	15.4473	15.4580
Mg#	89.06	88.70	89.36	88.33	88.88	88.43	88.71	89.21	88.49	88.80
OSO	5.5850	5.5715	5.6193	5.4907	5.5787	5.6757	5.6600	5.5492	5.6210	5.6103
K site	1.8454	1.8452	1.9117	2.0223	1.8453	1.8837	1.8139	1.9035	1.8263	1.8477

Phlogopite analyses

Melting experiments at 3.0GPa

CPL series

	CPL 13 (950° → 1125°C, 20 → 4hrs)					CPL 12 (950° → 1150°C, 20 → 4hrs)				
	PHL 1	PHL 2	PHL 3	PHL 4	Ave.	PHL 1	PHL 2	PHL 3	PHL 4	Ave.
SiO ₂	37.70	37.01	37.74	37.96	37.60	39.75	39.34	38.68	38.74	39.13
TiO ₂	6.65	5.59	5.70	4.52	5.62	5.92	6.91	6.94	7.13	6.73
Al ₂ O ₃	16.47	16.03	15.68	16.44	16.16	14.11	13.72	14.83	15.20	14.47
Cr ₂ O ₃	0.48	0.25	0.41	0.10	0.31	0.16	0.60	0.38	0.13	0.32
FeO*	4.54	4.38	4.62	5.27	4.70	4.28	4.22	4.41	4.24	4.29
MnO	0.00	0.00	0.00	0.00	0.00	0.00	0.00	0.00	0.00	0.00
MgO	19.69	19.96	20.92	20.62	20.30	20.64	20.35	19.89	19.68	20.14
CaO	0.24	0.77	0.37	0.13	0.38	0.10	0.22	0.15	0.14	0.15
Na ₂ O	0.13	0.19	0.07	0.23	0.16	0.06	0.08	0.09	0.05	0.07
K ₂ O	9.84	9.62	9.48	9.79	9.68	9.77	9.45	9.81	10.19	9.81
Total	95.74	93.80	94.99	95.06	94.90	94.79	94.89	95.18	95.50	95.09
Si	5.3545	5.3699	5.3977	5.4350	5.3893	5.6681	5.6110	5.5146	5.5052	5.5747
Al IV	2.6455	2.6301	2.6023	2.5650	2.6107	2.3319	2.3070	2.4854	2.4948	2.4253
Al VI	0.1122	0.1118	0.0416	0.2101	0.1189	0.0401	0.0000	0.0072	0.0518	0.0043
Ti	0.7103	0.6100	0.6131	0.4867	0.6052	0.6349	0.7412	0.7441	0.7620	0.7206
Cr	0.0539	0.0287	0.0464	0.0113	0.0351	0.0180	0.0677	0.0428	0.0146	0.0358
Fe	0.5393	0.5315	0.5526	0.6310	0.5637	0.5104	0.5034	0.5258	0.5039	0.5109
Mn	0.0000	0.0000	0.0000	0.0000	0.0000	0.0000	0.0000	0.0000	0.0000	0.0000
Mg	4.1678	4.3160	4.4591	4.3999	4.3355	4.3863	4.3257	4.2261	4.1680	4.2764
Ca	0.0365	0.1197	0.0567	0.0199	0.0580	0.0153	0.0336	0.0229	0.0213	0.0233
Na	0.0358	0.0535	0.0194	0.0639	0.0431	0.0166	0.0221	0.0249	0.0138	0.0193
K	1.7830	1.7807	1.7298	1.7883	1.7704	1.7774	1.7196	1.7843	1.8474	1.7822
Total	15.4388	15.5519	15.5187	15.6112	15.5299	15.3990	15.3313	15.3782	15.3828	15.3728
Mg#	88.54	89.04	88.97	87.46	88.49	89.58	89.58	88.93	89.21	89.33
OSO	5.5835	5.5980	5.7128	5.7391	5.6584	5.5897	5.6379	5.5461	5.5003	5.5480
K site	1.8553	1.9539	1.8059	1.8721	1.8715	1.8092	1.7753	1.8321	1.8825	1.8249

Phlogonite analyses**Melting experiments at 3.0GPa****CPL series (sandwich experiments)**

	CPL 15 (1100 °C, 9hrs30min)					CPL 16 (1100 °C, 9hrs30min)				
	PHL 1	PHL2	PHL3	PHL4	Ave.	PHL 1	PHL2	PHL3	PHL4	Ave.
SiO2	38.36	38.23	38.94	38.10	38.41	37.76	38.10	38.26	38.58	38.18
TiO2	3.99	3.76	3.61	4.39	3.94	4.95	4.46	4.60	5.45	4.87
Al2O3	16.92	17.35	16.60	16.91	16.95	16.92	17.39	16.83	17.37	17.13
Cr2O3	0.38	0.46	0.82	0.23	0.47	0.19	0.01	0.14	0.61	0.24
FeO*	4.57	4.68	4.68	5.04	4.74	4.57	5.09	5.35	4.82	4.96
MnO	0.08	0.08	0.11	0.10	0.09	0.05	0.08	0.07	0.10	0.08
MgO	20.60	20.61	20.21	20.82	20.56	19.93	20.33	20.30	19.74	20.08
CaO	0.32	0.18	1.14	0.50	0.54	0.24	0.21	0.23	0.35	0.26
Na2O	0.00	0.00	0.00	0.00	0.00	0.13	0.15	0.25	0.13	0.17
K2O	10.05	10.29	9.68	9.77	9.95	9.93	9.59	9.71	9.82	9.76
Total	95.27	95.64	95.79	95.86	95.64	94.67	95.41	95.74	96.87	95.70
Si	5.4645	5.4333	5.5212	5.4051	5.4560	5.4155	5.4153	5.4362	5.4027	5.4174
Al IV	2.5355	2.5667	2.4788	2.5949	2.5440	2.5845	2.5847	2.5638	2.5973	2.5826
Al VI	0.3060	0.3403	0.2961	0.2333	0.2939	0.2764	0.3293	0.2553	0.2705	0.2828
Ti	0.4275	0.4019	0.3849	0.4684	0.4207	0.5339	0.4767	0.4915	0.5740	0.5192
Cr	0.0428	0.0517	0.0919	0.0258	0.0531	0.0215	0.0011	0.0157	0.0675	0.0266
Fe	0.5445	0.5563	0.5550	0.5980	0.5634	0.5482	0.6050	0.6357	0.5645	0.5884
Mn	0.0097	0.0096	0.0132	0.0120	0.0111	0.0061	0.0096	0.0084	0.0119	0.0090
Mg	4.3734	4.3654	4.2706	4.4019	4.3528	4.2599	4.3084	4.2986	4.1198	4.2457
Ca	0.0488	0.0274	0.1732	0.0760	0.0814	0.0369	0.0320	0.0350	0.0525	0.0392
Na	0.0000	0.0000	0.0000	0.0000	0.0000	0.0362	0.0413	0.0689	0.0353	0.0454
K	1.8265	1.8658	1.7510	1.7683	1.8028	1.8169	1.7390	1.7601	1.7545	1.7675
Total	15.5791	15.6183	15.5360	15.5837	15.5792	15.5359	15.5406	15.5694	15.4505	15.5238
Mg#	88.93	88.70	88.50	88.04	88.54	88.60	87.68	87.12	87.95	87.83
OSO	5.7038	5.7252	5.6117	5.7394	5.6950	5.6459	5.7283	5.7053	5.6082	5.6718
K site	1.8753	1.8932	1.9242	1.8443	1.8843	1.8900	1.8123	1.8640	1.8423	1.8520

Garnet analyses

Melting experiments at 3.0GPa

CPL series

	<u>CPL7</u> (950°→1075 °C, 21→4.5hrs)			<u>CPL10</u> (950°→1100 °C, 20→5hrs)			<u>CPL13</u> (950°→1125 °C, 20→4hrs)		
	GAR1	GAR2	Ave.	GAR1	GAR2	Ave.	GAR1	GAR2	Ave.
SiO2	41.39	41.31	41.35	41.38	41.37	41.38	41.11	41.56	41.34
TiO2	1.96	1.85	1.91	1.59	1.85	1.72	1.84	1.68	1.76
Al2O3	20.95	20.57	20.76	21.08	21.73	21.41	21.08	21.44	21.26
Cr2O3	0.82	1.41	1.12	1.82	0.82	1.32	1.22	1.32	1.27
Fe2O3#	0.13	0.05	0.09	0.48	0.78	0.63	0.00	0.00	0.00
FeO	7.06	6.97	7.01	6.54	6.72	6.63	6.56	6.60	6.58
MnO	0.25	0.24	0.25	0.36	0.29	0.33	0.27	0.27	0.27
MgO	18.50	18.72	18.61	19.31	19.22	19.27	18.58	19.22	18.90
CaO	8.56	8.19	8.38	7.49	7.70	7.60	8.22	7.76	7.99
Na2O	0.00	0.00	0.00	0.00	0.00	0.00	0.00	0.00	0.00
K2O	0.00	0.00	0.00	0.00	0.00	0.00	0.00	0.00	0.00
Total	99.62	99.31	99.46	100.05	100.48	100.26	98.88	99.85	99.36
Si	5.9569	5.9650	5.9610	5.9218	5.8903	5.9060	5.9463	5.9430	5.9446
Al IV	0.0431	0.0350	0.0390	0.0782	0.1097	0.0940	0.0537	0.0570	0.0554
Al VI	3.5116	3.4667	3.4892	3.4783	3.5379	3.5081	3.5410	3.5575	3.5493
Ti	0.2121	0.2009	0.2065	0.1711	0.1981	0.1846	0.2002	0.1807	0.1904
Cr	0.0933	0.1610	0.1271	0.2059	0.0923	0.1490	0.1395	0.1492	0.1444
Fe3+ #	0.0141	0.0054	0.0098	0.0517	0.0836	0.0677	0.0000	0.0000	0.0000
Fe2+	0.8501	0.8411	0.8456	0.7825	0.8000	0.7913	0.7936	0.7893	0.7914
Mn	0.0305	0.0294	0.0299	0.0436	0.0350	0.0393	0.0331	0.0327	0.0329
Mg	3.9681	4.0285	3.9982	4.1184	4.0784	4.0983	4.0052	4.0961	4.0509
Ca	1.3201	1.2672	1.2937	1.1485	1.1747	1.1617	1.2740	1.1890	1.2313
Na	0.0000	0.0000	0.0000	0.0000	0.0000	0.0000	0.0000	0.0000	0.0000
K	0.0000	0.0000	0.0000	0.0000	0.0000	0.0000	0.0000	0.0000	0.0000
Total	15.9989	16.0001	16.0000	16.0000	15.9989	16.0000	15.9865	15.9945	15.9905
Mg#	82.36	82.73	82.54	84.03	83.60	83.82	83.46	83.84	83.66
Pyr	64.3	65.3	64.8	67.6	67.0	67.3	65.6	67.1	66.3
Gro	11.9	10.0	11.0	6.9	8.5	7.7	10.9	9.9	10.4
Alm	13.8	13.6	13.7	12.8	13.1	13.0	13.0	12.9	13.0
Spe	0.5	0.5	0.5	0.7	0.6	0.6	0.5	0.5	0.5
And	7.2	6.6	6.9	6.9	8.6	7.7	6.6	5.9	6.2
Uva	2.3	3.9	3.1	5.1	2.3	3.7	3.4	3.7	3.5

Garnet analyses

Melting experiments at 3.0GPa

	CPL series			CPL series (sandwich experiments)					
	CPL12 (950 ^o ->1150 ^o C, 20->4hrs)			CPL14 (1100 ^o C,9.5hrs)			CPL16 (1100 ^o C,9.5hrs)		
	GAR1	GAR2	Ave.	GAR1	GAR2	Ave.	GAR1	GAR2	Ave.
SiO2	40.64	40.97	40.81	41.30	41.26	41.28	41.53	41.35	41.44
TiO2	2.65	2.09	2.37	1.66	1.74	1.70	1.37	1.45	1.41
Al2O3	20.84	20.97	20.91	20.48	20.45	20.47	21.25	20.66	20.96
Cr2O3	0.97	1.53	1.25	1.76	1.43	1.60	1.29	1.49	1.39
Fe2O3#	0.00	0.00	0.00	0.84	0.35	0.80	1.35	0.78	1.07
FeO	6.65	6.53	6.59	6.58	7.24	6.91	6.42	6.77	6.59
MnO	0.27	0.21	0.24	0.39	0.33	0.36	0.37	0.31	0.34
MgO	18.66	18.88	18.77	19.61	19.34	19.48	19.32	19.06	19.19
CaO	8.43	8.14	8.29	6.99	6.92	6.96	7.55	7.57	7.56
Na2O	0.00	0.00	0.00	0.00	0.00	0.00	0.00	0.00	0.00
K2O	0.00	0.00	0.00	0.00	0.00	0.00	0.00	0.00	0.00
Total	99.11	99.32	99.22	99.61	99.06	99.33	100.45	99.44	99.94
Si	5.8791	5.9063	5.8927	5.9389	5.9667	5.9528	5.9218	5.9602	5.9409
Al IV	0.1209	0.0937	0.1073	0.0611	0.0333	0.0472	0.0782	0.0398	0.0591
Al VI	3.4334	3.4703	3.4519	3.4108	3.4532	3.4320	3.4940	3.4710	3.4826
Ti	0.2883	0.2266	0.2574	0.1795	0.1892	0.1844	0.1469	0.1572	0.1520
Cr	0.1109	0.1744	0.1427	0.2001	0.1635	0.1818	0.1454	0.1698	0.1575
Fe3+ #	0.0000	0.0000	0.0000	0.0909	0.0381	0.0646	0.1449	0.0846	0.1149
Fe2+	0.8046	0.7873	0.7959	0.7918	0.8750	0.8333	0.7650	0.8159	0.7903
Mn	0.0331	0.0256	0.0294	0.0475	0.0404	0.0440	0.0447	0.0378	0.0413
Mg	4.0230	4.0563	4.0397	4.2025	4.1682	4.1854	4.1056	4.0944	4.1001
Ca	1.3067	1.2574	1.2820	1.0770	1.0723	1.0747	1.1535	1.1692	1.1613
Na	0.0000	0.0000	0.0000	0.0000	0.0000	0.0000	0.0000	0.0000	0.0000
K	0.0000	0.0000	0.0000	0.0000	0.0000	0.0000	0.0000	0.0000	0.0000
Total	16.0000	15.9979	15.9989	16.0002	16.0000	16.0001	16.0001	16.0000	16.0000
Mg#	83.33	83.75	83.54	84.15	82.65	83.40	84.29	83.38	83.84
Pyr	65.2	66.2	65.7	68.7	67.7	68.2	67.7	66.9	67.3
Gro	9.1	8.9	9.0	4.6	6.4	5.5	7.0	7.7	7.4
Alm	13.0	12.9	12.9	12.9	14.2	13.6	12.6	13.3	13.0
Spe	0.5	0.4	0.5	0.8	0.7	0.7	0.7	0.6	0.7
And	9.3	7.4	8.4	8.1	7.1	7.6	8.4	7.2	7.8
Uva	2.7	4.3	3.5	4.9	4.0	4.4	3.6	4.2	3.9

Melt analyses

Melting experiments at 3.0GPa

CPL series (sandwich experiments)

CPL14 (1100 °C, 9.5hrs)		(with S-DOL as a middle layer)					
Beam d.	Melt-1 (10µm)	Melt-2 (15µm)	Melt-3 (20µm)	Melt-4 (20µm)	Melt-5 (25µm)	"Individual quench grains of alkali-rich carbonates"	
SiO ₂	1.02	1.44	1.64	1.31	1.54	0.56	2.46
TiO ₂	0.44	0.51	0.48	0.36	0.51	0.22	0.64
Al ₂ O ₃	0.18	0.15	0.18	0.14	0.17	0.03	0.23
Cr ₂ O ₃	0.00	0.00	0.00	0.00	0.00	0.00	0.00
FeO*	3.45	4.12	4.39	3.70	4.19	6.56	6.59
MnO	0.15	0.16	0.20	0.18	0.13	0.36	0.29
MgO	15.17	14.33	13.86	14.97	14.96	9.17	8.51
CaO	25.14	21.45	22.11	25.59	23.39	25.03	26.87
Na ₂ O	7.87	10.00	9.75	6.05	7.65	8.85	7.80
K ₂ O	3.46	4.78	4.25	3.19	3.85	10.50	11.15
Total	56.88	56.94	56.86	55.49	56.39	61.28	64.54
Mg#	88.68	86.11	84.91	87.82	86.42	71.35	69.71

CPL16 (1100 °C, 9.5hrs)		(with S/P-DOL as middle layer)		
Beam d.	Melt-1 (15µm)	Melt-2 (25µm)	Melt-3 (20µm)	Melt-4 (30µm)
SiO ₂	2.57	0.95	0.57	1.28
TiO ₂	0.72	0.23	0.17	0.30
Al ₂ O ₃	0.38	0.17	0.08	0.23
Cr ₂ O ₃	0.00	0.00	0.00	0.00
FeO*	4.54	3.18	3.10	3.57
MnO	0.16	0.20	0.17	0.14
MgO	15.12	14.72	15.08	14.75
CaO	21.60	28.35	27.03	27.22
Na ₂ O	4.93	2.67	3.58	3.04
K ₂ O	7.01	3.50	4.86	4.27
Total	57.03	53.97	54.64	54.80
Mg#	85.58	89.19	89.66	88.04

Spinel analyses

Melting experiments at 3.0GPa

CPL series

	CPL2	CPL4	CPL5	CPL11	CPL8
	900 °C	925 °C	975 °C	1000 °C	950 °-> 1025 °C
TiO2	0.04	0.08	0.04	0.08	0.08
Al2O3	50.72	49.62	50.38	49.80	50.26
Cr2O3	15.70	15.96	15.50	16.09	15.28
Fe2O3 ‡	4.74	4.63	4.79	4.06	4.24
FeO	9.19	8.96	8.91	9.77	9.22
MnO	0.11	0.18	0.12	0.04	0.00
MgO	20.24	19.98	20.22	19.57	19.91
Total	100.74	99.41	99.96	99.41	98.99
Al	0.0063	0.0129	0.0064	0.0129	0.0129
Ti	12.6160	12.5259	12.6181	12.5907	12.7005
Cr	2.6187	2.7017	2.6032	2.7278	2.5892
Fe3+ ‡	0.7526	0.7461	0.7658	0.6552	0.6839
Fe2+	1.6225	1.6052	1.5831	1.7517	1.6536
Mn	0.0197	0.0326	0.0216	0.0073	0.0000
Mg	6.3642	6.3759	6.4019	6.2547	6.3601
Total	24.0000	24.0003	24.0001	24.0002	24.0003
Mg‡	79.69	79.89	80.17	78.12	79.36
Cr‡	17.19	17.74	17.10	17.81	16.93
Y Al	78.91	78.42	78.93	78.82	79.51
Y Cr	16.38	16.91	16.28	17.08	16.21
Y Fe3+	4.71	4.67	4.79	4.10	4.28

Spinel analyses

Melting experiments at 3.00Pa

CPL series

	CPL9	CPL7	CPL10	CPL13	CPL12
	950 °-> 1050 °C	950 °-> 1075 °C	950 °-> 1100 °C	950 °-> 1125 °C	950 °-> 1150 °C
TiO2	0.06	0.05	0.08	0.06	0.09
Al2O3	50.20	50.53	50.24	50.15	50.38
Cr2O3	15.56	15.43	16.51	15.90	15.80
Fe2O3 #	4.49	3.99	4.10	4.53	4.46
FeO	9.35	9.41	9.66	9.60	9.14
MnO	0.03	0.05	0.12	0.02	0.07
MgO	19.91	19.83	19.88	19.86	20.17
Total	99.60	99.29	100.59	100.12	100.13
Al	0.0096	0.0080	0.0128	0.0096	0.0144
Ti	12.6339	12.7341	12.5536	12.5802	12.6051
Cr	2.6260	2.6075	2.7664	2.6746	2.6509
Fe3+ #	0.7213	0.6418	0.6539	0.7254	0.7155
Fe2+	1.6693	1.6822	1.7125	1.7090	1.6221
Mn	0.0054	0.0091	0.0215	0.0036	0.0126
Mg	6.3343	6.3174	6.2796	6.2978	6.3795
Total	23.9998	24.0002	24.0003	24.0003	23.9999
Mg#	79.14	78.97	78.57	78.66	79.73
Cr#	17.21	17.00	18.06	17.53	17.38
Y Al	79.05	79.67	78.59	78.72	78.92
Y Cr	16.43	16.31	17.32	16.74	16.60
Y Fe3+	4.51	4.02	4.09	4.54	4.48

Spinel analyses**Melting experiments at 3.0GPa****CPL series (sandwich experiments)**

	CPL14	CPL15	CPL16
	1100 °C	1100 °C	1100 °C
TiO2	0.02	0.04	0.07
Al2O3	51.05	50.78	50.57
Cr2O3	15.37	15.23	16.47
Fe2O3 ‡	5.02	4.98	4.41
FeO	9.27	8.75	9.84
MnO	0.11	0.13	0.09
MgO	20.29	20.44	19.98
Total	101.13	100.35	101.43
Al	0.0032	0.0064	0.0111
Ti	12.6465	12.6508	12.5409
Cr	2.5533	2.5443	2.7389
Fe3+ ‡	0.7938	0.7919	0.6981
Fe2+	1.6296	1.5462	1.7314
Mn	0.0196	0.0233	0.0160
Mg	6.3541	6.4372	6.2636
Total	24.0000	24.0001	24.0000
Mg‡	79.59	80.63	78.34
Cr‡	16.80	16.74	17.92
Y Al	79.07	79.13	78.49
Y Cr	15.96	15.91	17.14
Y Fe3+	4.96	4.95	4.37

APPENDIX B4

Interaction experiments

Olivine analyses

Interaction experiments at 2.0GPa

MAR series

MAR	MAR					MAR-SILMET(A)				
	OL1	OL2	OL3	OL4	Ave.	OL1	OL2	OL3	OL4	Ave.
SiO2	40.91	40.92	41.27	40.79	40.97	40.86	40.94	41.37	40.75	40.98
TiO2	0.00	0.00	0.00	0.00	0.00	0.00	0.00	0.00	0.01	0.00
Al2O3	0.00	0.00	0.00	0.00	0.00	0.00	0.00	0.00	0.00	0.00
Cr2O3	0.02	0.03	0.00	0.05	0.03	0.04	0.01	0.05	0.00	0.03
FeO*	8.64	8.79	8.89	8.63	8.74	8.73	8.85	8.81	9.08	8.87
MnO	0.13	0.13	0.13	0.10	0.12	0.00	0.00	0.00	0.00	0.00
MgO	50.08	50.19	50.25	50.07	50.14	49.65	49.93	50.13	49.79	49.88
NiO	0.33	0.30	0.31	0.31	0.31	0.34	0.32	0.33	0.32	0.33
CaO	0.02	0.05	0.04	0.03	0.04	0.08	0.04	0.06	0.06	0.06
Na2O	0.00	0.00	0.00	0.00	0.00	0.00	0.00	0.03	0.00	0.01
K2O	0.00	0.00	0.00	0.00	0.00	0.00	0.00	0.00	0.00	0.00
Total	100.11	100.41	100.89	99.98	100.35	99.70	100.09	100.78	100.01	100.15
Si	0.9974	0.9954	0.9989	0.9958	0.9969	1.0001	0.9985	1.0015	0.9961	0.9991
Ti	0.0000	0.0000	0.0000	0.0000	0.0000	0.0000	0.0000	0.0000	0.0002	0.0000
Al	0.0000	0.0000	0.0000	0.0000	0.0000	0.0000	0.0000	0.0000	0.0000	0.0000
Cr	0.0004	0.0006	0.0000	0.0010	0.0005	0.0008	0.0002	0.0010	0.0000	0.0005
Fe	0.1762	0.1788	0.1800	0.1762	0.1778	0.1787	0.1805	0.1784	0.1856	0.1808
Mn	0.0027	0.0027	0.0027	0.0021	0.0025	0.0000	0.0000	0.0000	0.0000	0.0000
Mg	1.8189	1.8196	1.8126	1.8218	1.8182	1.8111	1.8149	1.8086	1.8139	1.8121
Ni	0.0065	0.0059	0.0060	0.0061	0.0061	0.0067	0.0063	0.0064	0.0063	0.0064
Ca	0.0005	0.0013	0.0010	0.0008	0.0009	0.0021	0.0010	0.0016	0.0016	0.0016
Na	0.0000	0.0000	0.0000	0.0000	0.0000	0.0000	0.0000	0.0014	0.0000	0.0004
K	0.0000	0.0000	0.0000	0.0000	0.0000	0.0000	0.0000	0.0000	0.0000	0.0000
Total	3.0024	3.0043	3.0011	3.0037	3.0029	2.9995	3.0014	2.9988	3.0037	3.0008
Mg#	91.17	91.05	90.97	91.18	91.09	91.02	90.95	91.02	90.72	90.93
Fo	91.05	90.93	90.85	91.09	90.98	91.02	90.95	91.02	90.72	90.93
Fa	8.95	9.07	9.15	8.91	9.02	8.98	9.05	8.98	9.28	9.07

Olivine analyses

Interaction experiments at 2.0GPa

HAR series

	<u>HAR-SILMEL(B)</u>				<u>HAR-GARRET</u>				
	OL1	OL2	OL3	Ave.	OL1	OL2	OL3	OL4	Ave.
SiO2	41.15	40.78	41.26	41.06	40.88	40.38	40.73	41.54	40.88
TiO2	0.02	0.01	0.05	0.03	0.00	0.00	0.03	0.01	0.01
Al2O3	0.01	0.02	0.00	0.01	0.00	0.00	0.00	0.00	0.00
Cr2O3	0.02	0.02	0.03	0.02	0.05	0.07	0.02	0.00	0.04
FeO*	8.98	8.95	8.77	8.90	8.72	8.99	8.87	8.72	8.78
MnO	0.15	0.13	0.06	0.11	0.00	0.00	0.00	0.01	0.00
MgO	50.18	49.08	49.16	49.47	50.27	49.65	49.54	50.21	49.92
NiO	0.00	0.00	0.00	0.00	0.30	0.36	0.32	0.33	0.33
CaO	0.15	0.15	0.17	0.16	0.09	0.07	0.10	0.09	0.09
Na2O	0.00	0.00	0.00	0.00	0.16	0.00	0.00	0.00	0.04
K2O	0.00	0.00	0.00	0.00	0.01	0.00	0.02	0.00	0.01
Total	100.66	99.14	99.50	99.77	100.48	99.52	99.43	100.91	100.09
Si	0.9979	1.0036	1.0096	1.0037	0.9939	0.9926	0.9996	1.0035	0.9974
Ti	0.0004	0.0002	0.0009	0.0005	0.0000	0.0000	0.0006	0.0002	0.0002
Al	0.0003	0.0006	0.0000	0.0003	0.0000	0.0000	0.0000	0.0000	0.0000
Cr	0.0004	0.0004	0.0006	0.0005	0.0010	0.0014	0.0004	0.0000	0.0007
Fe	0.1821	0.1842	0.1795	0.1819	0.1773	0.1848	0.1780	0.1762	0.1790
Mn	0.0031	0.0027	0.0012	0.0023	0.0000	0.0000	0.0000	0.0002	0.0001
Mg	1.8135	1.8001	1.7928	1.8022	1.8214	1.8189	1.8119	1.8076	1.8150
Ni	0.0000	0.0000	0.0000	0.0000	0.0059	0.0071	0.0063	0.0064	0.0064
Ca	0.0039	0.0040	0.0045	0.0041	0.0023	0.0018	0.0026	0.0023	0.0023
Na	0.0000	0.0000	0.0000	0.0000	0.0075	0.0000	0.0000	0.0000	0.0019
K	0.0000	0.0000	0.0000	0.0000	0.0003	0.0000	0.0006	0.0000	0.0002
Total	3.0014	2.9957	2.9891	2.9955	3.0096	3.0067	3.0000	2.9964	3.0031
Mg#	90.87	90.72	90.90	90.83	91.13	90.78	91.06	91.12	91.02
Fo	90.73	90.59	90.84	90.72	91.13	90.78	91.06	91.11	91.02
Fa	9.27	9.41	9.16	9.28	8.87	9.22	8.94	8.89	8.98

Orthopyroxene analyses

Interaction experiments at 2.0GPa

HAR series

HAR	HAR-SILMET(A)									
	OPX1	OPX2	OPX3	OPX4	Ave.	OPX1	OPX2	OPX3	OPX4	Ave.
SiO2	55.71	56.37	55.55	55.98	55.80	55.29	54.73	55.54	54.77	55.08
TiO2	0.00	0.00	0.00	0.00	0.00	0.02	0.05	0.04	0.01	0.03
Al2O3	2.90	2.90	3.05	2.89	2.84	3.33	3.37	3.01	3.16	3.22
Cr2O3	0.31	0.21	0.25	0.28	0.26	0.32	0.36	0.27	0.38	0.33
FeO*	5.72	5.91	5.91	6.05	5.90	5.69	5.72	5.59	5.57	5.64
MnO	0.19	0.08	0.12	0.07	0.12	0.00	0.00	0.00	0.00	0.00
MgO	33.77	33.68	34.35	33.48	33.82	34.49	34.28	34.80	34.64	34.55
CaO	0.45	0.58	0.60	0.59	0.56	0.63	0.65	0.41	0.62	0.58
Na2O	0.00	0.01	0.00	0.02	0.01	0.03	0.00	0.00	0.00	0.01
K2O	0.00	0.00	0.00	0.00	0.00	0.00	0.00	0.00	0.00	0.00
Total	99.05	99.74	99.83	99.36	99.50	99.80	99.16	99.66	99.15	99.44
Si	1.9358	1.9443	1.9192	1.9407	1.9350	1.9094	1.9038	1.9178	1.9046	1.9089
Al IV	0.0642	0.0557	0.0808	0.0593	0.0650	0.0906	0.0962	0.0822	0.0954	0.0911
Al VI	0.0546	0.0622	0.0434	0.0588	0.0548	0.0450	0.0420	0.0403	0.0341	0.0404
Ti	0.0000	0.0000	0.0000	0.0000	0.0000	0.0005	0.0013	0.0010	0.0003	0.0008
Cr	0.0085	0.0057	0.0068	0.0077	0.0072	0.0087	0.0099	0.0074	0.0104	0.0091
Fe	0.1662	0.1705	0.1708	0.1754	0.1707	0.1643	0.1664	0.1614	0.1620	0.1635
Mn	0.0058	0.0023	0.0035	0.0021	0.0034	0.0000	0.0000	0.0000	0.0000	0.0000
Mg	1.7488	1.7313	1.7686	1.7298	1.7446	1.7751	1.7771	1.7909	1.7952	1.7846
Ca	0.0168	0.0214	0.0222	0.0219	0.0206	0.0233	0.0242	0.0152	0.0231	0.0214
Na	0.0000	0.0007	0.0000	0.0013	0.0005	0.0020	0.0000	0.0000	0.0000	0.0005
K	0.0000	0.0000	0.0000	0.0000	0.0000	0.0000	0.0000	0.0000	0.0000	0.0000
Total	4.0005	3.9942	4.0153	3.9971	4.0018	4.0190	4.0209	4.0162	4.0252	4.0203
Mgf	91.32	91.04	91.20	90.79	91.09	91.53	91.44	91.73	91.72	91.61
Wo	0.66	1.11	1.13	1.14	1.06	1.19	1.23	0.77	1.17	1.09
En	90.27	89.91	90.00	89.66	89.96	90.44	90.31	91.02	90.65	90.61
Fs	8.87	8.96	8.87	9.20	8.98	8.37	8.46	8.21	8.16	8.30

Orthopyroxene analyses

Interaction experiments at 2.0GPa

NAR series

	<u>NAR-SILSIT(B)</u>					<u>NAR-CAMT</u>				
	OPX1	OPX2	OPX3	OPX4	Ave.	OPX1	OPX2	OPX3	OPX4	Ave.
SiO2	55.70	55.60	56.49	55.43	55.81	55.39	56.31	55.66	55.98	55.84
TiO2	0.01	0.05	0.12	0.05	0.06	0.04	0.03	0.03	0.00	0.03
Al2O3	2.98	2.84	1.48	3.16	2.62	3.00	2.95	2.94	2.89	2.95
Cr2O3	0.30	0.32	0.29	0.29	0.30	0.23	0.20	0.22	0.28	0.23
FeO*	5.43	5.64	5.04	5.71	5.46	5.92	5.85	5.91	6.05	5.93
MnO	0.11	0.16	0.08	0.11	0.12	0.01	0.05	0.00	0.07	0.03
MgO	34.82	34.79	34.08	34.05	34.44	34.03	34.44	33.94	33.48	33.97
CaO	0.68	0.55	1.87	0.45	0.89	0.54	0.60	0.64	0.59	0.59
Na2O	0.07	0.09	0.09	0.05	0.08	0.00	0.03	0.00	0.02	0.01
K2O	0.01	0.02	0.00	0.02	0.01	0.00	0.00	0.00	0.00	0.00
Total	100.11	100.06	99.54	99.32	99.76	99.16	100.46	99.34	99.36	99.58
Si	1.9166	1.9165	1.9560	1.9222	1.9278	1.9247	1.9300	1.9300	1.9407	1.9314
Al IV	0.0834	0.0835	0.0440	0.0778	0.0722	0.0753	0.0700	0.0700	0.0593	0.0686
Al VI	0.0375	0.0319	0.0164	0.0513	0.0343	0.0476	0.0493	0.0502	0.0588	0.0515
Ti	0.0003	0.0013	0.0031	0.0013	0.0015	0.0010	0.0008	0.0008	0.0000	0.0007
Cr	0.0082	0.0087	0.0079	0.0080	0.0082	0.0063	0.0054	0.0060	0.0077	0.0064
Fe	0.1563	0.1626	0.1459	0.1656	0.1576	0.1720	0.1677	0.1714	0.1754	0.1716
Mn	0.0032	0.0047	0.0023	0.0032	0.0034	0.0003	0.0015	0.0000	0.0021	0.0010
Mg	1.7856	1.7872	1.7586	1.7597	1.7728	1.7623	1.7592	1.7539	1.7298	1.7513
Ca	0.0251	0.0203	0.0694	0.0167	0.0329	0.0201	0.0220	0.0236	0.0219	0.0220
Na	0.0047	0.0060	0.0060	0.0034	0.0050	0.0000	0.0020	0.0000	0.0013	0.0008
K	0.0004	0.0009	0.0000	0.0009	0.0006	0.0000	0.0000	0.0000	0.0000	0.0000
Total	4.0212	4.0236	4.0098	4.0101	4.0162	4.0097	4.0079	4.0061	3.9971	4.0052
Mg#	91.95	91.66	92.34	91.40	91.84	91.11	91.30	91.10	90.79	91.08
Wo	1.27	1.03	3.51	0.86	1.67	1.03	1.13	1.22	1.14	1.13
En	90.63	90.50	88.99	90.46	90.14	90.16	90.20	89.99	89.66	90.00
Fs	8.09	8.47	7.50	8.68	8.18	8.82	8.67	8.79	9.20	8.87

Clinopyroxene analyses

Interaction experiments at 2.0GPa

HAR series

	<u>HAR-SILMEX(B)</u>			<u>HAR-CARMET</u>			
	CPX1	CPX2	Ave.	CPX1	CPX2	CPX3	Ave.
SiO2	52.58	52.94	52.76	53.55	52.88	52.70	53.04
TiO2	0.54	0.42	0.48	0.08	0.10	0.08	0.09
Al2O3	4.15	4.30	4.23	3.70	4.24	3.53	3.82
Cr2O3	0.19	0.44	0.32	0.48	0.69	0.48	0.55
FeO*	4.38	3.87	4.13	2.97	2.99	3.07	3.01
MnO	0.11	0.15	0.13	0.00	0.00	0.02	0.01
MgO	21.06	20.88	20.97	16.65	16.33	18.08	17.02
CaO	15.16	16.20	15.68	22.00	22.09	21.01	21.70
Na2O	0.73	0.61	0.67	0.96	0.98	1.01	0.98
K2O	0.05	0.04	0.05	0.03	0.02	0.00	0.02
Total	98.95	99.85	99.40	100.42	100.32	99.98	100.24
Si	1.9044	1.9010	1.9026	1.9338	1.9148	1.9123	1.9203
Al IV	0.0956	0.0990	0.0974	0.0662	0.0852	0.0877	0.0797
Al VI	0.0816	0.0830	0.0823	0.0913	0.0958	0.0633	0.0835
Ti	0.0147	0.0113	0.0130	0.0022	0.0027	0.0022	0.0024
Cr	0.0054	0.0125	0.0090	0.0137	0.0198	0.0138	0.0157
Fe	0.1327	0.1162	0.1244	0.0897	0.0905	0.0932	0.0911
Mn	0.0034	0.0046	0.0040	0.0000	0.0000	0.0006	0.0002
Mg	1.1368	1.1174	1.1270	0.8961	0.8813	0.9777	0.9183
Ca	0.5883	0.6233	0.6059	0.8513	0.8571	0.8169	0.8418
Na	0.0513	0.0425	0.0468	0.0672	0.0688	0.0711	0.0690
K	0.0023	0.0018	0.0021	0.0014	0.0009	0.0000	0.0008
Total	4.0164	4.0128	4.0145	4.0128	4.0169	4.0387	4.0228
Mg#	89.55	90.58	90.06	90.90	90.68	91.30	90.97
Wo	31.61	33.48	32.55	46.34	46.86	43.26	45.47
En	61.08	60.03	60.55	48.78	48.19	51.78	49.60
Fs	7.31	6.49	6.90	4.88	4.95	4.97	4.93

Phlogopite analyses

Interaction experiments at 2.0GP

HAR seriesHAR-SILMET(B)

	PHL1	PHL2	PHL3
SiO2	38.67	40.14	38.52
TiO2	5.66	0.34	6.07
Al2O3	15.70	16.10	16.42
Cr2O3	0.00	0.06	0.00
FeO*	4.67	4.16	4.54
MnO	0.07	0.02	0.01
MgO	20.55	23.36	20.26
CaO	0.70	0.26	0.02
Na2O	0.35	0.31	0.29
K2O	9.55	9.55	10.19
Total	95.92	94.30	96.32
Si	5.4749	5.7226	5.4318
Al IV	2.5251	2.2774	2.5682
Al VI	0.0954	0.4286	0.1616
Ti	0.6027	0.0385	0.6437
Cr	0.0000	0.0088	0.0000
Fe	0.5530	0.4960	0.5354
Mn	0.0084	0.0024	0.0012
Mg	4.3360	4.9633	4.2584
Ca	0.1062	0.0397	0.0030
Na	0.0961	0.0857	0.0793
K	1.7250	1.7370	1.8332
Total	15.5227	15.7959	15.5158
Si	88.69	90.91	88.83
OSO	5.5955	5.9335	5.6003
K site	1.9273	1.8624	1.9155

Olivine analyses

Interaction experiments at 2.0GPa

WHR series

	WHR				(1000 °C, 28hrs)					WHR-SILMET					(1000 °C, 20hrs)				
	OL1	OL2	OL3	OL4	Ave.	OL1	OL2	OL3	OL4	Ave.	OL1	OL2	OL3	OL4	Ave.				
SiO2	40.22	40.90	40.79	40.08	40.50	41.02	40.64	40.55	41.37	40.90									
TiO2	0.00	0.00	0.00	0.00	0.00	0.00	0.01	0.03	0.04	0.02									
Al2O3	0.00	0.00	0.97	0.00	0.24	0.00	0.00	0.00	0.00	0.00									
Cr2O3	0.05	0.04	0.09	0.02	0.05	0.03	0.10	0.02	0.00	0.04									
FeO*	8.38	8.88	8.30	8.22	8.45	8.55	8.72	8.59	9.26	8.78									
MnO	0.04	0.11	0.05	0.09	0.07	0.00	0.00	0.00	0.02	0.01									
MgO	50.45	50.59	49.26	50.45	50.19	49.73	49.58	49.56	49.29	49.54									
NiO	0.30	0.30	0.32	0.35	0.32	0.33	0.35	0.29	0.31	0.32									
CaO	0.12	0.10	0.23	0.11	0.14	0.13	0.13	0.12	0.29	0.17									
Na2O	0.00	0.00	0.02	0.00	0.01	0.00	0.00	0.00	0.00	0.00									
K2O	0.00	0.00	0.00	0.00	0.00	0.01	0.00	0.00	0.00	0.00									
Total	99.56	100.92	100.03	99.32	99.96	99.80	99.53	99.16	100.58	99.77									
Si	0.9864	0.9908	0.9929	0.9852	0.9889	1.0020	0.9972	0.9977	1.0055	1.0006									
Ti	0.0000	0.0000	0.0000	0.0000	0.0000	0.0000	0.0002	0.0006	0.0007	0.0004									
Al	0.0000	0.0000	0.0278	0.0000	0.0070	0.0000	0.0000	0.0000	0.0000	0.0000									
Cr	0.0010	0.0008	0.0017	0.0004	0.0010	0.0006	0.0019	0.0004	0.0000	0.0007									
Fe	0.1719	0.1799	0.1690	0.1690	0.1725	0.1747	0.1789	0.1768	0.1882	0.1797									
Mn	0.0008	0.0023	0.0010	0.0019	0.0015	0.0000	0.0000	0.0000	0.0004	0.0001									
Mg	1.8440	1.8265	1.7871	1.8482	1.8264	1.8104	1.8131	1.8173	1.7854	1.8065									
Ni	0.0059	0.0058	0.0063	0.0069	0.0062	0.0065	0.0069	0.0057	0.0061	0.0063									
Ca	0.0032	0.0028	0.0060	0.0029	0.0037	0.0034	0.0034	0.0032	0.0078	0.0044									
Na	0.0000	0.0000	0.0009	0.0000	0.0002	0.0000	0.0000	0.0000	0.0000	0.0000									
K	0.0000	0.0000	0.0000	0.0000	0.0000	0.0003	0.0000	0.0000	0.0000	0.0001									
Total	3.0131	3.0088	2.9928	3.0148	3.0073	2.9979	3.0017	3.0016	2.9938	2.9987									
Mg#	91.47	91.03	91.36	91.62	91.37	91.20	91.02	91.14	90.46	90.95									
Fe	91.44	90.93	91.31	91.54	91.30	91.20	91.02	91.14	90.44	90.95									
Fa	8.56	9.07	8.69	8.46	8.70	8.80	8.98	8.86	9.58	9.05									

Olivine analyses

Interaction experiments at 2.0GPa

WHE series

	<u>WHE-CARMET</u> (1000 °C, 20hrs)			
	OL1	OL2	OL3	Ave.
SiO2	41.18	40.33	40.39	40.63
TiO2	0.00	0.00	0.00	0.00
Al2O3	0.00	0.00	0.00	0.00
Cr2O3	0.06	0.01	0.00	0.02
FeO*	8.50	8.59	8.67	8.58
MnO	0.00	0.06	0.00	0.02
MgO	50.68	50.24	50.39	50.44
NiO	0.26	0.30	0.31	0.29
CaO	0.17	0.18	0.17	0.17
Na2O	0.00	0.00	0.00	0.00
K2O	0.00	0.00	0.06	0.02
Total	100.85	99.71	99.99	100.18
Si	0.9955	0.9884	0.9875	0.9905
Ti	0.0000	0.0000	0.0000	0.0000
Al	0.0000	0.0000	0.0000	0.0000
Cr	0.0011	0.0002	0.0000	0.0004
Fe	0.1719	0.1761	0.1773	0.1751
Mn	0.0000	0.0012	0.0000	0.0004
Mg	1.8259	1.8350	1.8361	1.8323
Ni	0.0051	0.0059	0.0061	0.0057
Ca	0.0044	0.0047	0.0045	0.0045
Na	0.0000	0.0000	0.0000	0.0000
K	0.0000	0.0000	0.0019	0.0006
Total	3.0039	3.0115	3.0134	3.0096
Mg#	91.40	91.25	91.19	91.28
Fo	91.40	91.19	91.19	91.26
Fa	8.60	8.81	8.81	8.74

Clinopyroxene analyses

Interaction experiments at 2.0GPa

WHR series

	WHR					WHR-SILMET				
	(1000 °C, 28hrs)					(1000 °C, 20hrs)				
	CPX1	CPX2	CPX3	CPX4	Ave.	CPX1	CPX2	CPX3	CPX4	Ave.
SiO ₂	52.62	53.21	52.84	53.08	52.94	52.07	52.32	52.51	51.95	52.21
TiO ₂	0.04	0.07	0.09	0.06	0.07	0.07	0.09	0.10	0.09	0.09
Al ₂ O ₃	3.53	3.53	3.35	3.61	3.51	3.72	3.62	3.30	3.92	3.64
Cr ₂ O ₃	0.22	0.24	0.23	0.27	0.24	0.48	0.59	0.50	0.57	0.54
FeO*	3.07	2.64	2.91	2.90	2.88	2.82	2.79	2.82	2.88	2.83
MnO	0.03	0.11	0.04	0.14	0.08	0.00	0.00	0.00	0.00	0.00
MgO	16.67	16.89	16.45	16.48	16.62	16.80	16.67	16.86	16.68	16.75
CaO	22.13	22.79	22.83	22.44	22.55	22.17	22.54	22.68	22.29	22.42
Na ₂ O	0.88	0.84	0.88	0.90	0.88	0.86	0.88	0.85	0.96	0.89
K ₂ O	0.00	0.00	0.00	0.00	0.00	0.03	0.00	0.01	0.00	0.01
Total	99.19	100.32	99.62	99.88	99.75	99.02	99.50	99.63	99	99.37
Si	1.9274	1.9260	1.9295	1.9305	1.9284	1.9120	1.9135	1.9186	1.9038	1.9120
Al IV	0.0726	0.0740	0.0705	0.0695	0.0716	0.0880	0.0865	0.0814	0.0962	0.0880
Al VI	0.0798	0.0767	0.0737	0.0852	0.0789	0.0731	0.0695	0.0607	0.0732	0.0691
Ti	0.0011	0.0019	0.0025	0.0016	0.0018	0.0019	0.0025	0.0027	0.0025	0.0024
Cr	0.0064	0.0069	0.0066	0.0078	0.0069	0.0139	0.0171	0.0144	0.0165	0.0155
Fe	0.0940	0.0799	0.0889	0.0882	0.0877	0.0866	0.0853	0.0862	0.0883	0.0866
Mn	0.0009	0.0034	0.0012	0.0043	0.0025	0.0000	0.0000	0.0000	0.0000	0.0000
Mg	0.9100	0.9111	0.8952	0.8932	0.9024	0.9194	0.9086	0.9181	0.9110	0.9143
Ca	0.8686	0.8639	0.8933	0.8745	0.8801	0.8723	0.8833	0.8879	0.8753	0.8797
Na	0.0625	0.0590	0.0623	0.0635	0.0618	0.0612	0.0624	0.0602	0.0682	0.0630
K	0.0000	0.0000	0.0000	0.0000	0.0000	0.0014	0.0000	0.0005	0.0000	0.0005
Total	4.0233	4.0228	4.0237	4.0194	4.0220	4.0299	4.0287	4.0307	4.0349	4.0310
Mg#	90.63	91.94	90.97	91.01	91.14	91.39	91.41	91.42	91.17	91.35
Wo	46.36	47.06	47.55	47.01	47.00	46.44	47.05	46.93	46.69	46.78
En	48.57	48.51	47.65	48.02	48.19	48.95	48.40	48.52	48.60	48.62
Fs	5.07	4.43	4.80	4.97	4.82	4.61	4.55	4.55	4.71	4.60

Clinopyroxene analyses

Interaction experiments at 2.0GPa

WHR series

	<u>WHR-CARMEI</u> (1000 °C, 20hrs)				
	CPX1	CPX2	CPX3	CPX4	Ave.
SiO2	53.42	52.64	52.99	52.92	52.99
TiO2	0.08	0.11	0.03	0.06	0.07
Al2O3	3.57	3.48	3.36	3.78	3.55
Cr2O3	0.60	0.48	0.59	0.59	0.57
FeO*	2.79	2.84	2.86	2.89	2.85
MnO	0.00	0.03	0.02	0.00	0.01
MgO	16.80	16.40	16.41	16.79	16.60
CaO	22.59	22.47	22.74	21.99	22.45
Na2O	0.89	0.88	0.90	0.89	0.89
K2O	0.06	0.06	0.12	0.05	0.08
Total	100.80	99.41	100.02	99.96	100.05
Si	1.9255	1.9260	1.9287	1.9219	1.9255
Al IV	0.0745	0.0740	0.0713	0.0781	0.0745
Al VI	0.0772	0.0761	0.0729	0.0837	0.0775
Ti	0.0022	0.0030	0.0008	0.0016	0.0019
Cr	0.0171	0.0139	0.0170	0.0169	0.0162
Fe	0.0841	0.0869	0.0871	0.0878	0.0865
Mn	0.0000	0.0009	0.0006	0.0000	0.0004
Mg	0.9025	0.8942	0.8901	0.9087	0.8989
Ca	0.8725	0.8809	0.8869	0.8557	0.8740
Na	0.0622	0.0624	0.0635	0.0627	0.0627
K	0.0028	0.0037	0.0056	0.0023	0.0036
Total	4.0204	4.0221	4.0244	4.0196	4.0216
Mg#	91.46	91.14	91.09	91.19	91.23
Wo	46.93	47.28	47.56	46.20	46.99
En	48.54	48.00	47.74	49.06	48.34
Fs	4.52	4.71	4.70	4.74	4.67

Spinel analyses

Interaction experiments at 2.0GPa

WHR series

	<u>WHR</u> (1000 °C, 28hrs)			<u>WHR-SILMST</u> (1000 °C, 20hrs)			<u>WHR-CARMET</u> (1000 °C, 20hrs)		
	SP1	SP2	Ave.	SP1	SP2	Ave.	SP1	SP2	Ave.
TiO2	0.05	0.03	0.04	0.04	0.03	0.04	0.00	0.01	0.01
Al2O3	52.40	50.99	51.70	50.59	50.02	50.31	50.55	50.92	50.74
Cr2O3	14.90	14.65	14.78	15.53	15.23	15.38	16.13	15.28	15.71
Fe2O3 ‡	3.57	4.91	4.24	4.35	5.63	4.99	5.09	4.34	4.72
FeO	9.18	9.03	9.10	9.11	8.08	8.59	8.81	9.26	9.04
MnO	0.17	0.15	0.16	0.04	0.00	0.02	0.02	0.04	0.03
MgO	20.38	20.17	20.28	20.14	20.74	20.44	20.60	20.08	20.34
Total	100.65	99.93	100.29	99.80	99.73	99.76	101.20	99.93	100.57
Al	0.0079	0.0048	0.0063	0.0064	0.0048	0.0056	0.0000	0.0016	0.0008
Ti	12.9518	12.7502	12.8516	12.6802	12.5313	12.6057	12.5174	12.7397	12.6280
Cr	2.4696	2.4565	2.4631	2.6102	2.5586	2.5844	2.6784	2.5635	2.6212
Fe3+ ‡	0.5633	0.7837	0.6728	0.6960	0.9003	0.7982	0.8045	0.6931	0.7491
Fe2+	1.6092	1.6021	1.6057	1.6191	1.4367	1.5279	1.5476	1.6444	1.5957
Mn	0.0302	0.0269	0.0286	0.0072	0.0000	0.0036	0.0036	0.0072	0.0054
Mg	6.3679	6.3758	6.3718	6.3814	6.5684	6.4749	6.4484	6.3508	6.3999
Total	23.9998	24.0000	23.9999	24.0004	24.0001	24.0003	23.9999	24.0002	24.0000
Mg#	79.83	79.92	79.87	79.76	82.05	80.91	80.65	79.43	80.04
Cr#	16.01	16.15	16.08	17.07	16.96	17.01	17.63	16.75	17.19
Y Al	81.03	79.74	80.39	79.32	78.37	78.84	78.23	79.64	78.93
Y Cr	15.45	15.36	15.41	16.33	16.00	16.16	16.74	16.03	16.38
Y Fe3+	3.52	4.90	4.21	4.35	5.63	4.99	5.03	4.33	4.68

Carbonate analyses

Interaction experiments at 2.0GPa

WHR series

WHR-CARMET (1000 °C, 20hrs)

	CC1	CC2	Ave.
FeO*	0.83	1.06	0.95
MnO	0.00	0.00	0.00
MgO	2.47	5.38	3.93
CaO	55.58	53.55	54.57
Total	58.88	59.99	59.44
Fe	0.0217	0.0267	0.0243
Mn	0.0000	0.0000	0.0000
Mg	0.1152	0.2419	0.1797
Ca	1.8631	1.7313	1.7960
C ‡	2.0000	2.0000	2.0000
Total	4.0000	4.0000	4.0000
FeCO ₃	1.09	1.34	1.21
MnCO ₃	0.00	0.00	0.00
MgCO ₃	5.76	12.10	8.98
CaCO ₃	93.16	86.57	89.80

Cryptocrystalline material

Interaction experiments at 2.0GPa

Interaction with SILMET (1000°C, 20 hours)

<u>Beam d.</u>	<u>HR-SILMET(A)</u>			<u>HR-SILMET</u>		
	<u>Melt-1</u> <u>(5µm)</u>	<u>Melt-2</u> <u>(5µm)</u>	<u>Ave.</u>	<u>Melt-1</u> <u>(5µm)</u>	<u>Melt-2</u> <u>(5µm)</u>	<u>Ave.</u>
S102	47.62	46.95	47.29	48.35	46.67	47.51
TiO2	1.89	2.01	1.95	2.04	2.03	2.04
Al2O3	11.27	9.39	10.33	11.63	10.23	10.93
Cr2O3	0.08	0.04	0.06	0.06	0.13	0.10
FeO*	5.17	5.30	5.24	4.68	4.57	4.63
MnO	0.00	0.00	0.00	0.00	0.00	0.00
MgO	12.99	15.36	14.18	12.55	14.41	13.48
CaO	12.36	13.19	12.78	13.46	13.47	13.47
Na2O	1.55	1.20	1.38	1.13	0.88	1.01
K2O	4.55	3.06	3.81	5.33	4.15	4.74
Total	97.48	96.50	96.99	99.23	96.54	97.89
Mg#	81.74	83.78	82.83	82.69	84.89	83.85

APPENDIX C

LEAST-SQUARES MASS BALANCE CALCULATIONS

Least-squares mass balance calculation
to estimate the proportion of the phases stable
at 3.0 GPa and 1125°C in PLZ

Bulk composition used:

PLZ starting material (Table 3.2)

Phases used in the calculation

	<u>Reference</u>		<u>Calculated proportions</u>
Olivine	PLZ31	AppendixB2	40.0
Orthopyroxene	PLZ31	AppendixB2	30.2
Clinopyroxene	PLZ31	AppendixB2	16.1
Garnet	PLZ31	AppendixB2	7.6
Phlogopite	PLZ31	AppendixB2	5.6
FeO			0.4

Bulk PLZ composition

	<u>Observed</u>	<u>Calculated</u>	<u>Square of residual</u>
SiO ₂	47.60	47.60	0.000
TiO ₂	0.30	0.28	0.000
Al ₂ O ₃	4.28	4.28	0.000
FeO*	6.80	6.80	0.000
MgO	35.83	35.83	0.000
CaO	4.37	4.37	0.000
Na ₂ O	0.20	0.17	0.001
K ₂ O	0.62	0.63	0.000
Total	100.00	99.96	
	<u>Sum of the squares of residuals=</u>		0.001

Notes Reference indicates where the composition
of the phase can be found

Least-squares mass balance calculation
to estimate the proportion of the phases stable
at 3.0 GPa and 1225°C in PLZ

Bulk composition used:

PLZ starting material (Table 3.2)

Phases used in the calculation

	<u>Reference</u>		<u>Calculated proportions</u>
Olivine	PLZ30	AppendixB2	41.0
Orthopyroxene	PLZ30	AppendixB2	30.2
Clinopyroxene	PLZ30	AppendixB2	12.5
Garnet	PLZ30	AppendixB2	6.8
Phlogopite	PLZ30	AppendixB2	1.8
Melt	PLZ40	Table 4.4	7.1
FeO			0.6

Bulk PLZ composition

	<u>Observed</u>	<u>Calculated</u>	<u>Square of residual</u>
SiO ₂	47.60	47.60	0.000
TiO ₂	0.30	0.34	0.002
Al ₂ O ₃	4.28	4.28	0.000
FeO*	6.80	6.80	0.000
MgO	35.83	35.83	0.000
CaO	4.37	4.37	0.000
Na ₂ O	0.20	0.26	0.004
K ₂ O	0.62	0.59	0.001
Total	100.00	100.07	
	<u>Sum of the squares of residuals=</u>		0.006

Notes Reference indicates where the composition
of the phase can be found

Least-squares mass balance calculation
to estimate the proportion of the phases stable
at 3.0 GPa and 1000°C in CPL

Bulk composition used:

CPL starting material (Table 3.2)

Phases used in the calculation

	<u>Reference</u>		<u>Calculated proportions</u>
Olivine	CPL11	AppendixB3	37.1
Orthopyroxene	CPL11	AppendixB3	22.6
Clinopyroxene	CPL11	AppendixB3	23.5
Garnet	PLZ31	AppendixB2	7.6
Phlogopite	CPL11	AppendixB3	5.5
Magnesite	CPL11	AppendixB3	3.7

Bulk CPL composition

	<u>Observed</u>	<u>Calculated</u>	<u>Square of residual</u>
SiO ₂	45.87	45.85	0.000
TiO ₂	0.30	0.34	0.002
Al ₂ O ₃	4.12	4.25	0.017
FeO*	6.55	6.32	0.053
MgO	34.51	34.56	0.003
CaO	6.20	6.20	0.000
K ₂ O	0.59	0.55	0.002
CO ₂	1.86	1.85	0.000
Total	100.00	99.92	
		<u>Sum of the squares of residuals=</u>	0.076

Notes Reference indicates where the composition
of the phase can be found

Least-squares mass balance calculation
to estimate the proportion of the phases stable
at 3.0 GPa and 1050°C in CPL

Bulk composition used:

CPL starting material (Table 3.2)

Phases used in the calculation

	<u>Reference</u>		<u>Calculated proportions</u>
Olivine	CPL9	AppendixB3	36.4
Orthopyroxene	CPL9	AppendixB3	27.1
Clinopyroxene	CPL9	AppendixB3	18.8
Garnet	PLZ31	AppendixB2	8.4
Phlogopite	CPL9	AppendixB3	5.4
Dolomite	CPL9	AppendixB3	3.9

Bulk CPL composition

	<u>Observed</u>	<u>Calculated</u>	<u>Square of residual</u>
SiO ₂	45.87	45.84	0.001
TiO ₂	0.30	0.33	0.001
Al ₂ O ₃	4.12	4.24	0.014
FeO*	6.55	6.34	0.044
MgO	34.51	34.56	0.003
CaO	6.20	6.20	0.000
K ₂ O	0.59	0.54	0.002
CO ₂	1.86	1.86	0.000
Total	100.00	99.91	

Sum of the squares of residuals= 0.065

Notes Reference indicates where the composition
of the phase can be found

Least-squares mass balance calculation
to estimate the proportion of the phases stable
at 3.0 GPa and 1100°C in CPL

Bulk composition used:

CPL starting material (Table 3.2)

Phases used in the calculation

	<u>Reference</u>		<u>Calculated proportions</u>
Olivine	CPL16	AppendixB3	38.4
Orthopyroxene	CPL16	AppendixB3	26.3
Clinopyroxene	CPL16	AppendixB3	18.4
Garnet	CPL16	AppendixB3	10.1
Phlogopite	CPL16	AppendixB3	2.5
Melt	Melt-1	Table 5.6	4.3

Bulk CPL composition

	<u>Observed</u>	<u>Calculated</u>	<u>Square of residual</u>
SiO ₂	45.87	45.87	0.000
TiO ₂	0.30	0.34	0.002
Al ₂ O ₃	4.12	4.08	0.002
FeO*	6.55	6.59	0.002
MgO	34.51	34.51	0.000
CaO	6.20	6.20	0.000
K ₂ O	0.59	0.58	0.000
CO ₂	1.86	1.86	0.000
Total	100.00	100.03	
		<u>Sum of the squares of residuals=</u>	0.005

Notes Reference indicates where the composition
of the phase can be found

Least-squares mass balance calculation
to estimate the proportion of the phases stable
at 2.0 GPa and 1000°C in HAR-CARMET before interaction

Bulk composition used:

HAR-CARMET starting material (Table 5.7)

Phases used in the calculation

	<u>Reference</u>		<u>Calculated proportions</u>
Olivine	HAR	AppendixB4	45.6
Orthopyroxene	HAR	AppendixB4	44.4
CARMET	Table 5.7		9.9
FeO			0.1

Bulk PLZ composition

	<u>Observed</u>	<u>Calculated</u>	<u>Square of residual</u>
SiO2	43.84	43.85	0.000
TiO2	0.04	0.03	0.000
Al2O3	1.40	1.34	0.004
FeO*	7.15	7.15	0.000
MgO	39.54	39.54	0.000
CaO	3.13	3.14	0.000
Na2O	0.31	0.30	0.000
K2O	0.40	0.40	0.000
CO2	4.19	4.19	0.000
Total	100.00	99.94	

Sum of the squares of residuals= 0.004

Notes Reference indicates where the composition
of the phase can be found

Least-squares mass balance calculation
to estimate the proportion of the phases stable
at 2.0 GPa and 1000°C in HAR-CARMET after interaction

Bulk composition used:

HAR-CARMET starting material (Table 5.7)

Phases used in the calculation

	<u>Reference</u>	<u>Calculated proportions</u>
Olivine	HAR-CARMET Appendix B4	59.7
Orthopyroxene	HAR-CARMET Appendix B4	19.6
Clinopyroxene	HAR-CARMET Appendix B4	13.6
Phlogopite	Ideal Table 6.4	2.7
CO ₂		4.2
FeO		0.2

Bulk PLZ composition

	<u>Observed</u>	<u>Calculated</u>	<u>Square of residual</u>
SiO ₂	43.84	43.80	0.002
TiO ₂	0.04	0.02	0.000
Al ₂ O ₃	1.40	1.62	0.048
FeO*	7.15	7.15	0.000
MgO	39.54	39.54	0.000
CaO	3.13	3.14	0.000
Na ₂ O	0.31	0.16	0.023
K ₂ O	0.40	0.32	0.006
CO ₂	4.19	4.19	0.000

Total 100.00 99.94

Sum of the squares of residuals= 0.079

Notes Reference indicates where the composition
of the phase can be found

Least-squares mass balance calculation
to estimate the proportion of the phases stable
at 2.0 GPa and 1000°C in WHR-CARMET before interaction

Bulk composition used:

WHR-CARMET starting material (Table 5.7)

Phases used in the calculation

	<u>Reference</u>		<u>Calculated proportions</u>
Olivine	WHR	AppendixB4	65.4
Clinopyroxene	WHR	AppendixB4	21.8
Spinel	WHR	AppendixB4	2.6
CARMET	Table 5.7		9.8
FeO			0.4

Bulk PLZ composition

	<u>Observed</u>	<u>Calculated</u>	<u>Square of residual</u>
SiO ₂	38.41	38.28	0.017
Al ₂ O ₃	2.16	2.28	0.014
Cr ₂ O ₃	0.59	0.47	0.014
FeO*	7.32	7.32	0.000
MgO	38.58	38.60	0.000
CaO	7.85	7.89	0.002
Na ₂ O	0.48	0.49	0.000
K ₂ O	0.40	0.40	0.000
CO ₂	4.19	4.16	0.001
Total	99.98	99.89	

Sum of the squares of residuals= 0.049

Notes Reference indicates where the composition
of the phase can be found

Least-squares mass balance calculation
to estimate the proportion of the phases stable
at 2.0 GPa and 1000°C in WHR-CARMET after interaction

Bulk composition used:

WHR-CARMET starting material (Table 5.7)

Phases used in the calculation

	<u>Reference</u>	<u>Calculated proportions</u>
Olivine	WHR-CARMET Appendix B4	67.8
Clinopyroxene	WHR-CARMET Appendix B4	18.7
Spinel	WHR-CARMET Appendix B4	2.3
Calcite	WHR-CARMET Appendix B4	7.0
Phlogopite	Ideal Table 6.4	2.6
CO ₂		1.1
FeO		0.5

Bulk PLZ composition

	<u>Observed</u>	<u>Calculated</u>	<u>Square of residual</u>
SiO ₂	38.41	38.45	0.002
Al ₂ O ₃	2.16	2.31	0.023
Cr ₂ O ₃	0.59	0.48	0.012
FeO*	7.32	7.32	0.000
MgO	38.58	38.58	0.000
CaO	7.85	7.85	0.000
Na ₂ O	0.48	0.17	0.096
K ₂ O	0.40	0.33	0.005
CO ₂	4.19	4.19	0.000
Total	99.98	99.68	

Sum of the squares of residuals= 0.137

Notes Reference indicates where the composition
of the phase can be found

Least-squares mass balance calculation
to estimate the proportion of the phases stable
at 2.0 GPa and 1000°C in HAR-SILMET before interaction

Bulk composition used:

HAR-SILMET starting material (Table 4.7)

Phases used in the calculation

	<u>Reference</u>		<u>Calculated proportions</u>
Olivine	HAR	AppendixB4	38.1
Orthopyroxene	HAR	AppendixB4	37.2
SILMET	Table 4.7		24.6
FeO			0.1

Bulk PLZ composition

	<u>Observed</u>	<u>Calculated</u>	<u>Square of residual</u>
SiO2	48.12	48.12	0.000
TiO2	0.43	0.42	0.000
Al2O3	4.22	4.16	0.004
FeO*	7.27	7.27	0.000
MgO	34.76	34.76	0.000
CaO	3.06	3.07	0.000
Na2O	0.59	0.58	0.000
K2O	1.56	1.56	0.000
Total	100.01	99.94	
	<u>Sum of the squares of residuals=</u>		0.004

Notes Reference indicates where the composition
of the phase can be found

Least-squares mass balance calculation
to estimate the proportion of the phases stable
at 2.0 GPa and 1000°C in HAR-SILMET after interaction

Bulk composition used:

HAR-SILMET starting material (Table 4.7)

Phases used in the calculation

	<u>Reference</u>	<u>Calculated proportions</u>
Olivine	HAR-SILMET(B)Appendix B4	29.6
Orthopyroxene	HAR-SILMET(B)Appendix B4	36.5
Clinopyroxene	HAR-SILMET(B)Appendix B4	17.7
Phlogopite	HAR-SILMET(B)Appendix B4	10.0
Phlogopite	HAR-SILMET(B)Appendix B4	5.0
FeO		1.2

Bulk PLZ composition

	<u>Observed</u>	<u>Calculated</u>	<u>Square of residual</u>
SiO2	48.12	48.10	0.000
TiO2	0.43	0.44	0.000
Al2O3	4.22	4.36	0.020
FeO*	7.27	7.27	0.000
MgO	34.76	34.76	0.000
CaO	3.06	3.07	0.000
Na2O	0.59	0.21	0.144
K2O	1.56	1.52	0.002
Total	100.01	99.73	

Sum of the squares of residuals= 0.166

Notes Reference indicates where the composition of the phase can be found; CRYPT refers to cryptocrystalline assemblage

REFERENCES

- Abrecht, J. and Hewitt, D.A., 1988. Experimental evidence on the substitution of Ti in biotite. *American Mineralogist*, 73, pp. 1275-1284.
- Anderson, D.L., 1987. The depths of mantle reservoirs. In: Mysen, B.O. (editor), *Magmatic Processes: Physicochemical Principles*. The Geochemical Society, Special Publication 1, pp. 3-12.
- Anderson, D.L. and Bass, J.D., 1984. Mineralogy and composition of the upper mantle. *Geophysical Research Letters*, 11, pp. 637-640.
- Arai, S. and Takahashi, N., 1989. Formation and compositional variation of phlogopites in the Horoman peridotite complex, Hokkaido, northern Japan: implications for origin and fractionation of metasomatic fluids in the upper mantle. *Contributions to Mineralogy and Petrology*, 101, pp. 165-175.
- Arima, M. and Edgar, A.D., 1981. Substitution mechanisms and solubility of titanium in phlogopites from rocks of probable mantle origin. *Contributions to Mineralogy and Petrology*, 77, pp. 288-295.
- Arima, M. and Edgar, A.D., 1983. High pressure experimental studies on a katungite and their bearing on the genesis of some potassium-rich magmas of the west branch of the African Rift. *Journal of Petrology*, 24, pp. 166-187.
- Bailey, D.K., 1972. Uplift, rifting and magmatism in continental plates. *Journal of Earth Sciences (Leeds)*, 8, pp. 225-239.
- Bailey, D.K., 1980. Volcanism, Earth degassing and replenished lithosphere mantle. *Philosophical Transactions of the Royal Society of London*, A297, pp.309-322.
- Bailey, D.K., 1982. Mantle metasomatism - continuing chemical change within the Earth. *Nature*, 296, pp. 525-530.
- Bailey, D.K., 1983. The chemical and thermal evolution of rifts. *Tectonophysics*, 94, pp. 585-597.

- Bailey, D.K., 1985. Fluids, melts, flowage and styles of eruption in alkaline ultramafic magmatism. *Transactions of the Geological Society of South Africa*, 88, pp. 449-457.
- Bailey, D.K., 1987. Mantle metasomatism - perspective and prospect. In: Fitton, J.G and Upton, B.G.J. (editors), *Alkaline Igneous Rocks*. Geological Society of London, Special Publications, 30, pp. 1-13.
- Beeré, W., 1975. A unifying theory of the stability of penetrating liquid phases and sintering pores. *Acta Metallurgica*, 23, pp. 131-138.
- Berman, R.G., 1988. Internally-consistent thermodynamic data for minerals in the system $\text{Na}_2\text{O}-\text{K}_2\text{O}-\text{CaO}-\text{MgO}-\text{FeO}-\text{Fe}_2\text{O}_3-\text{Al}_2\text{O}_3-\text{SiO}_2-\text{TiO}_2-\text{H}_2\text{O}-\text{CO}_2$. *Journal of Petrology*, 29, pp. 445-522.
- Bodinier, J.L., Dupuy, C. and Dostal, J., 1988. Geochemistry and petrogenesis of Eastern Pyrenean peridotites. *Geochimica et Cosmochimica Acta*, 52, pp. 2893-2907.
- Bodinier, J.L., Vasseur, G., Vernieres, J., Dupuy, C. and Fabriès, J., 1990. Mechanisms of mantle metasomatism: geochemical evidence from the Lherz orogenic peridotite. *Journal of Petrology*, 31, pp. 597-628.
- Boettcher, A., 1987. Foreword. In: Menzies, M.A. and Hawkesworth, C.J. (editors), *Mantle Metasomatism*. Academic Press. London, p. xv.
- Boyd, F.R., 1989. Compositional distinction between oceanic and cratonic lithosphere. *Earth and Planetary Science Letters*, 96, pp. 15-26.
- Boyd, F.R., and England, J.L., 1960. Apparatus for phase equilibrium measurements at pressures up to 50kbar and temperatures to 1750°C. *Journal of Geophysical Research*, 65, pp. 741-748.
- Boyd, F.R. and Nixon, P.H., 1975. Origins of the ultramafic nodules from some kimberlites of northern Lesotho and the Monastery mine, South Africa. *Physics and Chemistry of the Earth*, 9, pp. 431-454.
- Brey, G., Brice, W.R., Ellis, D.J., Green, D.H., Harris, K.L. and Ryabchikov, I.D., 1983. Pyroxene-carbonate reactions in the upper mantle. *Earth and Planetary Science Letters*, 62, pp. 63-74.

- Bryan, W.B., Finger, L.W. and Chayes, F., 1969. Estimating proportions in petrographic mixing equations by least-squares approximation. *Science*, 163, pp. 926-927.
- Carroll Webb, S.A. and Wood, B.J., 1986. Spinel-pyroxene-garnet relationships and their dependence on Cr/Al ratio. *Contributions to Mineralogy and Petrology*, 92, pp. 471-480.
- Carswell, D.A., 1975. Primary and secondary phlogopites and clinopyroxenes in garnet lherzolite xenoliths. *Physics and Chemistry of the Earth*, 9, pp. 417-429.
- Cox, K.G., Bell, J.D. and Pankhurst, R.J., 1979. *The interpretation of igneous rocks*. George Allen & Unwin, London, 450p.
- Cox, K.G., Smith, M.R. and Beswetherick, S., 1987. Textural studies of garnet lherzolites: evidence of exsolution origin from high-temperature harzburgites. In: Nixon, P.H. (editor), *Mantle Xenoliths*. John Wiley & Sons, Chichester, pp. 537-550.
- Dawson, J.B., 1982. Contrasting types of mantle metasomatism. *Terra Cognita*, 2, pp. 232-233.
- Dawson, J.B., 1984. Contrasting types of upper-mantle metasomatism? In: Kornprobst, J. (editor), *Kimberlites II: the mantle and crust-mantle relationships*. Elsevier, Amsterdam, pp. 289-294.
- Dawson, J.B. and Smith, J.V., 1977. The MARID (mica-amphibole-rutile-ilmenite-diopside) suite of xenoliths in kimberlite. *Geochimica et Cosmochimica Acta*, 41, pp. 309-323.
- Deines, P., 1989. Stable isotope variations in carbonatites. In: Bell K. (editor), *Carbonatites - Genesis and evolution*. Unwin Hyman, London, pp. 301-359.
- Deines, P. and Gold, D.P., 1973. The isotopic composition of carbonatites and kimberlite carbonates and their bearing on the isotopic composition of deep-seated carbon. *Geochimica et Cosmochimica Acta*, 37, pp. 1295-1319.
- Delaney, J.S., Smith, J.V., Carswell, D.A. and Dawson, J.B., 1980. Chemistry of micas from kimberlites and xenoliths - II. Primary- and secondary-textured micas from peridotite xenoliths. *Geochimica et Cosmochimica Acta*, 44, pp. 857-872.

- Edgar, A.D. and Arima, M., 1984. Experimental studies on K-metasomatism of a model pyrolite mantle and their bearing on the genesis of ultrapotassic magmas. In: *Petrology - Igneous and Metamorphic Rocks. Proceedings of the 27th International Geological Congress, 9*, VNU Science Press, pp. 509- 541.
- Edgar, A.D., Green, D.H. and Hibberson, W.O., 1976. Experimental petrology of a highly potassic magma. *Journal of Petrology*, 17, pp. 339-356.
- Edgar, A.D., Condliffe, E., Barnett, R.L. and Shirran, R.J., 1980. An experimental study of an olivine ugandite magma and mechanisms for the formation of its K-enriched derivatives. *Journal of Petrology*, 21, pp. 475-497.
- Edgar, A.D., Lloyd, F.E., Forsyth, D.M. and Barnett, R.L., 1989. Origin of glass in upper mantle xenoliths from the quaternary volcanics of Gees, West Eifel, Germany. *Contributions to Mineralogy and Petrology*, 103, pp. 277-286.
- Eggler, D.H., 1975. Peridotite-carbonate relations in the system $\text{CaO-MgO-SiO}_2\text{-CO}_2$. *Carnegie Institution of Washington Year Book*, 74, pp. 468-474.
- Eggler, D.H., 1976. Composition of the partial melt of carbonated peridotite in the system $\text{CaO-MgO-SiO}_2\text{-CO}_2$. *Carnegie Institution of Washington Yearbook*, 75, pp. 623-626.
- Eggler, D.H., 1978. The effect of CO_2 upon partial melting of peridotite in the system $\text{Na}_2\text{O-CaO-Al}_2\text{O}_3\text{-MgO-SiO}_2\text{-CO}_2$ to 35kb, with an analysis of melting in a peridotite- $\text{H}_2\text{O-CO}_2$ system. *American Journal of Science*, 278, pp. 305-343.
- Eggler, D.H., 1983. Upper mantle oxidation state: Evidence from olivine-orthopyroxene-ilmenite assemblages. *Geophysical Research Letters*, 10, pp. 365-368.
- Eggler, D.H., 1987. Solubility of major and trace elements in mantle metasomatic fluids: Experimental constraints. In: Menzies, M.A. and Hawkesworth, C.J. (editors), *Mantle Metasomatism*. Academic Press, London, pp. 21-41.
- Eggler, D.H., 1989. Carbonatites, primary melts, and mantle dynamics. In: Bell K. (editor), *Carbonatites - Genesis and evolution*. Unwin Hyman, London, pp. 561-579.

- Eggler, D.H. and Baker, D.R., 1982. Reduced volatiles in the system C-O-H: Implications to mantle melting, fluid formation, and diamond genesis. In: Akimoto, S. and Manghani, M.H. (editors), *Advances in Earth and Planetary Sciences 12, High Pressure Research in Geophysics*. Tokyo: Center for Academic Publications, pp. 237-250.
- Ehrenberg, S.N., 1979. Garnetiferous ultramafic inclusions in minette from the Navajo volcanic field. In: Boyd, F.R. and Meyer, H.O.A. (editors), *The mantle sample: inclusions in kimberlites and other volcanics. Proceedings of the 2nd International Kimberlite Conference, 2*, American Geophysical Union, Washington, D.C., pp. 330-344.
- Ehrenberg, S.N., 1982. Petrogenesis of garnet lherzolite and megacrystalline nodules from The Thumb, Navajo Volcanic Field. *Journal of Petrology*, 23, pp. 507-547.
- Erlank, A.J., 1973. Kimberlite potassic richterite and the distribution of potassium in the upper mantle. *First International Kimberlite Conference, Cape Town, Extended Abstracts of Papers*, pp. 155-158.
- Erlank, A.J., Waters, F.G., Hawkesworth, C.J., Haggerty, S.E., Allsopp, H.L., Rickard, R.S. and Menzies, M.A., 1987. Evidence for mantle metasomatism in peridotite nodules from the Kimberley pipes, South Africa. In: Menzies, M.A. and Hawkesworth, C.J. (editors), *Mantle Metasomatism*. Academic Press, London, pp. 221-311.
- Esperança, S. and Holloway, J.R., 1986. The origin of the high K-latites from Camp Creek, Arizona: constraints from experiments with variable fO_2 and a_{H_2O} . *Contributions to Mineralogy and Petrology*, 95, pp. 207-216.
- Esperança, S. and Holloway, J.R., 1987. On the origin of some mica-lamprophyres: experimental evidence from a mafic minette. *Contributions to Mineralogy and Petrology*, 95, pp. 207-216.
- Falloon, T.J. and Green, D.H., 1987. Anhydrous partial melting of MORB pyrolite and other peridotite compositions at 10kbar: implications for the origin of primitive MORB glasses. *Mineralogy and Petrology*, 37, pp. 181-219.
- Falloon, T.J. and Green, D.H., 1988. Anhydrous partial melting of peridotite from 8 to 35kb and the petrogenesis of MORB. *Journal of Petrology, Special Lithosphere Issue*, pp. 379-414.

- Falloon, T.J. and Green, D.H., 1989. The solidus of carbonated fertile peridotite. *Earth and Planetary Science Letters*, 94, pp. 364-370.
- Falloon, T.J. and Green, D.H., 1990. Solidus of carbonated fertile peridotite under fluid-saturated conditions. *Geology*, 18, pp. 195-199.
- Falloon, T.J., Green, D.H., Hatton, C.J. and Harris, K.L., 1988. Anhydrous partial melting of a fertile and depleted peridotite from 2 to 30kb and application to basalt petrogenesis. *Journal of Petrology*, 29, pp. 1257-1282.
- Foley, S.F., 1989. Experimental constraints on phlogopite chemistry in lamproites: 1. The effect of water activity and oxygen fugacity. *European Journal of Mineralogy*, 1, pp. 411-426.
- Foley, S.F., Taylor, W.R. and Green, D.H., 1986. The effect of fluorine on phase relationships in the system $KAlSiO_4$ - Mg_2SiO_4 - SiO_2 at 28 kbar and the solution mechanism in silicate melts. *Contributions to Mineralogy and Petrology*, 93, pp. 46-55.
- Forbes, W.C. and Flower, M.F.J., 1974. Phase relations of titan-phlogopite, $K_2Mg_4TiAl_2Si_6O_{20}(OH)_4$: a refractory phase in the upper mantle? *Earth and Planetary Science Letters*, 22, pp. 60-66.
- Ford, C.E., 1978. Platinum-iron alloy sample containers for melting experiments on iron-bearing rocks, minerals, and related systems. *Mineralogical Magazine*, 42, pp. 271-275.
- Frey, F.A. and Prinz, M., 1978. Ultramafic inclusions from San Carlos, Arizona: petrologic and geochemical data bearing on their petrogenesis. *Earth and Planetary Science Letters*, 38, pp. 129-176.
- Fuchs, K. and Wedepohl, K.H., 1983. Relation of geophysical and petrological models of upper mantle structure of the Rhenish Massif. In: Fuchs, K., von Gehlen, K., Mälzer, H., Murawski, H., and Semmel, A. (editors), *Plateau Uplift - The Rhenish Shield - A case history*. Springer Verlag, Berlin, pp. 352-363.
- Fujii, T. and Scarfe, C.M., 1984. Composition of liquids coexisting with spinel lherzolite at 10kbar and the genesis of MORBs. *Contributions to Mineralogy and Petrology*, 90, pp.18-28.

- Fujii, T. and Scarfe, C.M., 1985. Compositions of liquids coexisting with spinel lherzolite at 10 kbar and the genesis of MORBs. *Earth and Planetary Science Letters*, 90, pp. 18-28.
- Gasparik, T. and Lindsley, D.H., 1982. Phase equilibria at high pressure of pyroxenes containing monovalent and trivalent ions. In: Prewitt, C.T. (Editor), *Pyroxenes*. Mineralogical Society of America, *Reviews in Mineralogy*, 7, pp. 309-339.
- Gittins, J., 1989. The origin and evolution of carbonatite magmas. In: Bell K. (editor), *Carbonatites - Genesis and evolution*. Unwin Hyman, London, pp. 580-600.
- Goldschmidt, V.M., 1922. On the metasomatic processes in silicate rocks. *Economic Geology*, 17, pp. 105-123.
- Green, D.H., 1973. Experimental melting studies on a model upper mantle composition at high pressure under water-saturated and water-undersaturated conditions. *Earth and Planetary Science Letters*, 19, pp. 37-53.
- Green, D.H., 1976. Experimental testing of "equilibrium" partial melting of peridotite under water-saturated, high-pressure conditions. *Canadian Mineralogist*, 14, pp. 255-268.
- Green, D.H. and Ringwood, A.E., 1970. Mineralogy of peridotitic compositions under upper mantle conditions. *Physics of the Earth and Planetary Interiors*, 3, pp. 359-371.
- Green, D.H. and Wallace, M.E., 1988. Mantle metasomatism by ephemeral carbonatite melts. *Nature*, 336, pp. 459-462.
- Gupta, A.K. and Green, D.H., 1988. The liquidus surface of the system Forsterite-Kalsilite-Quartz at 28kb under dry conditions, in presence of H₂O, and of CO₂. *Mineralogy and Petrology*, 39, pp. 163-174.
- Gurney, J.J., Harte, B. and Cox, K.G., 1975. Mantle xenoliths in the Matsoku kimberlite pipe. *Physics and Chemistry of the Earth*, 9, pp. 507-523.
- Haggerty, S.E., 1989a. Mantle metasomes and the kinship between carbonatites and kimberlites. In: Bell K. (editor), *Carbonatites - Genesis and evolution*. Unwin Hyman, London, pp. 546-560.

- Haggerty, S.E., 1989b. Upper mantle opaque mineral stratigraphy and the genesis of metasomites and alkali-rich melts. In: Kimberlites and Related Rocks, Vol 2: Their mantle/crust setting - Diamonds and diamond exploration. Geological Society of Australia, Publication no. 14. Blackwell Scientific Publications, pp. 687-699.
- Harte, B., 1983. Mantle peridotites and processes - the kimberlite sample. In: Hawkesworth, C.J. and Norry, M.J. (editors), Continental basalts and mantle xenoliths. Shiva Publishing, Nantwich, UK, pp. 46-91.
- Harte, B., 1987. Metasomatic events recorded in mantle xenoliths: an overview. In: Nixon, P.H. (editor), Mantle xenoliths. John Wiley & Sons, Chichester, pp. 625-640.
- Harte, B. and Hawkesworth, C.J., 1989. Mantle domains and mantle xenoliths. In: Kimberlites and Related Rocks, vol. 2, Their mantle/crust setting, diamonds and diamond exploration. Geological Society of Australia, Special Publication 14, Blackwell Scientific Publications, pp. 649-686.
- Harte, B., Cox, K.G. and Gurney, J.J., 1975. Petrography and geological history of upper mantle xenoliths from the Matsoku kimberlite pipe. Physics and Chemistry of the Earth, 9, pp. 477-506.
- Harte, B., Winterburn, P.A. and Gurney, J.J., 1987. Metasomatic and enrichment phenomena in garnet peridotite facies mantle xenoliths from the Matsoku kimberlite pipe, Lesotho. In: Menzies, M.A. and Hawkesworth, C.J. (editors), Mantle Metasomatism. Academic Press, London, pp. 145-220.
- Holland, T.J.B., 1980. The reaction albite \rightarrow jadeite + quartz determined experimentally in the range 600°-1200°C. American Mineralogist, 65, pp. 129-134.
- Holloway, J.R., 1987. igneous fluids. In: Carmichael, I.S.E. and Eugster, H.P. (editors), Thermodynamic modelling of geological materials: minerals, fluids and melts. Mineralogical Society of America, Reviews in Mineralogy, 17, pp. 211-233.
- Hunter, R.H. and McKenzie, D., 1989. The equilibrium geometry of carbonate melts in rocks of mantle composition. Earth and Planetary Science Letters, 92, pp. 347-356.

- Jaques, A.L. and Green, D.H., 1979. Determination of liquid compositions in high-pressure melting of peridotite. *American Mineralogist*, 64, pp. 1312-1321.
- Jaques, A.L. and Green, D.H., 1980. Anhydrous melting of peridotite at 0-15 kb pressure and the genesis of tholeiitic basalts. *Contributions to Mineralogy and Petrology*, 73, pp. 287-310.
- Johannes, W., Bell, P.M., Mao, H.K., Boettcher, A.L., Chipman, D.W., Hays, J.F., Newton, R.C. and Seifert, F., 1971. An inter-laboratory comparison of piston-cylinder pressure calibration using the albite breakdown reaction. *Contributions to Mineralogy and Petrology*, 32, pp. 24-38.
- Jones, A.P., Smith, J.V. and Dawson, J.B., 1982. Mantle metasomatism in 14 veined peridotites from Bulfontein mine, South Africa. *Journal of Geology*, 90, pp. 435-453.
- Kempton, P.D., Harmon, R.S., Stosch, H.-G., Hoefs, J. and Hawkesworth, C.J., 1988. Open-system O-isotope behaviour and trace element enrichment in the sub-Eifel mantle. *Earth and Planetary Science Letters*, 89, pp. 273-287.
- Kramers, J.D., Roddick, J.C.M. and Dawson, J.B., 1983. Trace element and isotope studies on veined, metasomatic and "MARID" xenoliths from Bulfontein, South Africa. *Earth and Planetary Science Letters*, 65, pp. 90-106.
- Kress, V.C. and Carmichael, I.S.E., 1988. Stoichiometry of the iron oxidation reaction in silicate melts. *American Mineralogist*, 73, pp. 1267-1274.
- Kushiro, I., 1969. The system forsterite-diopside-silica with and without water at high pressures. *American Journal of Science*, 267A, pp. 269-294.
- Kushiro, I., 1972. Effect of water on the composition of magmas formed at high pressures. *Journal of Petrology*, 13, pp. 311-334.
- Lindsley, D.H., 1982. Phase equilibria of pyroxenes at pressures > 1 atmosphere. In: Prewitt, C.T. (Editor), *Pyroxenes*. Mineralogical Society of America, *Reviews in Mineralogy*, 7, pp. 289-308.
- Lindsley, D.H. and Dixon, S.A., 1976. Diopside-enstatite equilibria at 850°C to 1400°C, 5 to 35 kb. *American Journal of Science*, 276, pp. 1285-1301.

- Lloyd, F.E., 1981. Upper-mantle metasomatism beneath a continental rift: clinopyroxenes in alkali mafic lavas and nodules from South West Uganda. *Mineralogical Magazine*, 44, pp. 315-323.
- Lloyd, F.E., 1987. Characterization of mantle metasomatic fluids in spinel lherzolites and alkali clinopyroxenites from the west Eifel and south west Uganda. In: Menzies, M.A. and Hawkesworth, C.J. (editors), *Mantle Metasomatism*. Academic Press, London, pp. 91-123.
- Lloyd, F.E. and Bailey, D.K., 1975. Light element metasomatism of the continental mantle: the evidence and the consequences. *Physics and Chemistry of the Earth*, 9, pp 389-416.
- Lloyd, F.E., Arima, M and Edgar, A.D., 1985. Partial melting of a phlogopite-clinopyroxenite nodule from south-west Uganda: an experimental study bearing on the origin of highly potassic continental rift volcanics. *Contributions to Mineralogy and Petrology*, 91, pp. 321-329.
- Lloyd, F.E., Nixon, P.H., Hornung, G. and Condliffe, E., 1987. Regional K-metasomatism in the mantle beneath the west branch of the East African Rift: alkali clinopyroxenite xenoliths in highly potassic magmas. In: Nixon, P.H. (editor), *Mantle Xenoliths*. John Wiley & Sons, Chichester, pp. 641-659.
- Lloyd, F.E., Edgar, A.D., Forsyth, D.M. and Barnett, R.L., 1990a. The paragenesis of upper mantle xenoliths from the Quaternary volcanics south-east of Gees, West Eifel, Germany. *Mineralogical Magazine*, (in press).
- Lloyd, F.E., Huntingdon, A.T., Davies, G.R. and Nixon, P.H., 1990b. Phanerozoic volcanism of south west Uganda: a case for regional K and LILE enrichment of the lithosphere beneath a domed and rifted continental plate. Kampunzu, A.B. and Lubala (editors), *Magmatism in extensional structural settings*. Springer Verlag, Heidelberg, (in press).
- Luth, R.W., Virgo, D., Boyd, F.R. and Wood, B.J., 1990. Ferric iron in mantle-derived garnets. *Contributions to Mineralogy and Petrology*, 104, pp. 56-72.
- Luth, W.C., 1967. Studies in the system $KAlSi_3O_8$ - Mg_2SiO_4 - SiO_2 - H_2O : I. Inferred phase relations and petrologic applications. *Journal of Petrology*, 8, pp. 372-416.

- Mattioli, G.S. and Wood, B.J., 1988. Magnetite activities across the $MgAl_2O_4$ - Fe_3O_4 spinel join, with application to thermobarometric estimates of upper mantle oxygen fugacity. *Contributions to Mineralogy and Petrology*, 98, pp. 148-162.
- Mattioli, G.S., Baker, M.B., Rutter, M.J. and Stolper, E.M., 1989. Upper mantle oxygen fugacity and its relationship to metasomatism. *Journal of Geology*, 97, pp. 521-536.
- McKenzie, D., 1984. The generation and compaction of partially molten rock. *Journal of Petrology*, 25, pp. 713-765.
- McKenzie, D., 1985. The extraction of magma from the crust and mantle. *Earth and Planetary Science Letters*, 74, pp. 81-91.
- McKenzie, D., 1989. Some remarks on the movement of small melt fractions in the mantle. *Earth and Planetary Science Letters*, 95, pp. 53-72.
- McKenzie, D. and Bickle, M.J., 1988. The volume and composition of melt generated by extension of the lithosphere. *Journal of Petrology*, 29, pp. 625-679.
- McNeil, A.M., 1987. Experimental studies of Na metasomatism of a model mantle pyrolite: implications for the natural system. M.Sc. Thesis, University of Western Ontario, London, Canada. 116p.
- McNeil, A.M. and Edgar, A.D., 1987. Sodium-rich metasomatism in the upper mantle: Implications of experiments on the pyrolite- Na_2O -rich fluid system at 950°C, 20 kbar. *Geochimica et Cosmochimica Acta*, 51, pp. 2285-2294.
- Meen, J.K., 1987. Mantle metasomatism and carbonatites; An experimental study of a complex relationship. In: Morris, E.M. and Pasteris, J.D. (editors), *Mantle metasomatism and alkaline magmatism*. Geological Society of America, Special Paper 215, pp. 91-100.
- Meen, J.K., Ayers, J.C. and Fregeau, E.J., 1989. A model of mantle metasomatism by carbonated alkaline melts: trace-element and isotopic compositions of mantle source regions of carbonatite and other continental igneous rocks. In: Bell K. (editor), *Carbonatites - Genesis and evolution*. Unwin Hyman, London, pp. 464-499.

- Mengel, K., and Green, D.H., 1989. Stability of amphibole and phlogopite in metasomatized peridotite under water-saturated and water-undersaturated conditions. In: Kimberlites and Related Rocks, Vol 1: Their composition, occurrence, origin and emplacement. Geological Society of Australia, Publication no. 14. Blackwell Scientific Publications, pp. 571-581.
- Menzies, M.A. and Hawkesworth, C.J. (editors), 1987. Mantle Metasomatism. Academic Press, London, 472p.
- Menzies, M.A. and Murthy, V.R., 1980. Nd and Sr isotope geochemistry of hydrous mantle nodules and their alkali basalts: implications for local heterogeneities in metasomatically veined mantle. Earth and Planetary Science Letters, 46, pp. 323-334.
- Menzies, M.A., Rogers, N.W., Tindle, A. and Hawkesworth, C.J., 1987. Metasomatic and enrichment processes in lithospheric peridotites, an effect of asthenosphere-lithosphere interaction. In: Menzies, M.A. and Hawkesworth, C.J. (editors), Mantle Metasomatism. Academic Press, London, pp. 313-361.
- Mertes, H. and Schmincke, H.-U., 1985. Mafic potassic lavas of the Quaternary West Eifel volcanic field. Contributions to Mineralogy and Petrology, 89, pp. 330-345.
- Modreski, P.J. and Boettcher, A.L., 1972. The stability of phlogopite + enstatite at high pressures: a model for micas in the interior of the earth. American Journal of Science, 272, pp. 852-869.
- Modreski, P.J. and Boettcher, A.L., 1973. Phase relationships of phlogopite in the system K_2O - MgO - CaO - Al_2O_3 - SiO_2 - H_2O to 35 kilobars: a better model for micas in the interior of the earth. American Journal of Science, 273, pp. 385-414.
- Mori, T. and Green, D.H., 1978. Laboratory duplication of phase equilibria observed in natural garnet lherzolites. Journal of Geology, 86, pp. 83-97.
- Morimoto, N. (Chairman), 1988. Nomenclature of pyroxenes. Subcommittee on Pyroxenes, Commission on New Minerals and Mineral Names. American Mineralogist, 73, pp. 1123-1133.
- Morris, E.M. and Pasteris, J.D. (editors), 1987. Mantle metasomatism and alkaline magmatism. Geological Society of America, Special Paper 215, 383p.

- Myers, J. and Eugster, H.P., 1983. The system Fe-Si-O: Oxygen buffer calibrations to 1500K. *Contributions to Mineralogy and Petrology*, 82, pp. 75-90.
- Mysen, B.O., 1977. The solubility of H₂O and CO₂ under predicted magma genesis conditions and some petrological and geophysical implications. *Reviews of Geophysics and Space Physics*, 15, pp. 351-361.
- Mysen, B.O. and Boettcher, A.L., 1975. Melting of a hydrous mantle: I. Phase relations of natural peridotite at high pressures and temperatures with controlled activities of water, carbon dioxide, and hydrogen. *Journal of Petrology*, 16, pp. 520-548.
- Navon, O., Hutcheon, I.D., Rossman, G.R. and Wasserburg, G.J., 1988. Mantle-derived fluids in diamond micro-inclusions. *Nature*, 335, pp. 784-789.
- Nixon, P.H. (editor), 1987. *Mantle xenoliths*. John Wiley & Sons, Chichester, 844p.
- O'Neill, H.St.C. and Wall, V.J., 1987. The olivine-orthopyroxene-spinel oxygen geobarometer, the nickel precipitation curve, and the oxygen fugacity of the earth's upper mantle. *Journal of Petrology*, 28, pp. 1169-1191.
- Olafsson, M. and Eggler, D.H., 1983. Phase relations of amphibole, amphibole-carbonate, and phlogopite-carbonate peridotite: petrologic constraints on the asthenosphere. *Earth and Planetary Science Letters*, 64, pp. 305-315.
- Papike, J.J., 1982. Pyroxene mineralogy of the moon and meteorites. In: Prewitt, C.T. (Editor), *Pyroxenes*. Mineralogical Society of America, *Reviews in Mineralogy*, 7, pp. 495-525.
- Papike, J.J., Cameron, K.L. and Baldwin, K., 1974. Amphiboles and pyroxenes: characterization of Other than Quadrilateral components and estimates of ferric iron from microprobe data. *Geological Society of America, Abstracts with Programs*, 6, pp. 1053-1054.
- Presnall, D.C., Brenner, N.L. and O'Donnell, T.H., 1973. Drift of Pt/Pt10Rh and W3Re/W25Re thermocouple in single-stage piston-cylinder apparatus. *American Mineralogist*, 58, pp. 771-777.

- Raheim, A. and Green, D.H., 1974. Experimental determination of the temperature and pressure dependence of the Fe-Mg partition coefficient for coexisting garnet and clinopyroxene. *Contributions to Mineralogy and Petrology*, 48, pp. 179-203.
- Richardson, S.W., Bell, P. and Gilbert, M.C., 1968. Kyanite-sillimanite equilibrium between 700°C and 1500°C. *American Journal of Science*, 266, pp. 513-541.
- Robert, J.L., 1976. Titanium solubility in synthetic phlogopite solid solutions. *Chemical Geology*, 17, pp. 213-227.
- Roden, M.F. and Murthy, V.R., 1985. Mantle metasomatism. *Annual Review of Earth and Planetary Sciences*, 13, pp. 269-296.
- Roeder, P.L. and Emslie, R.F., 1970. Olivine liquid equilibrium. *Contributions to Mineralogy and Petrology*, 29, pp. 275-289.
- Ryabchikov, I.D. and Boettcher, A.L., 1980. Experimental evidence at high pressure for potassic metasomatism in the mantle of the Earth. *American Mineralogist*, 65, pp. 915-919.
- Ryabchikov, I.D. and Green, D.H., 1978. The role of carbon dioxide in the petrogenesis of highly potassic magmas. In: *Problems of the petrology of the Earth's crust and upper mantle*. Trudy Instituta Geologii Geofiziki, So An SSR 403, Nauka, Novosibirsk, Nauka Publishers, pp. 49-64.
- Ryabchikov, I.D., Green, D.H., Wall, V.J. and Brey, G., 1981. The oxidation state of carbon in the environment of the low velocity zone. *Geokhimiya*, No.2, pp. 221-232.
- Ryabchikov, I.D., Schreyer, W. and Abraham, K., 1982. Compositions of aqueous fluids in equilibrium with pyroxenes and olivines at mantle pressures and temperatures. *Contributions to Mineralogy and Petrology*, 79, pp. 80-84.
- Ryabchikov, I.D., Brey, G., Kogarko, L.N. and Bulatov, V.K., 1989a. Partial melting of carbonated peridotite at 50kbar. *Geokhimiya*, No.1, pp. 3-9 (in Russian, with English Abstract).

- Ryabchikov, I.D., Baker, M. and Wyllie, P.J., 1989b. Phosphate-bearing carbonatite melts equilibrated with mantle lherzolites at 30 kbar. *Geokhimiya*, No.5, pp. 725-729. (In Russian).
- Schmincke, H.-U., Lorenz, V. and Seck, H.A., 1983. Quaternary Eifel volcanic fields. In: Fuchs, K., von Gehlen, K., Mälzer, H., Murawski, H., and Semmel, A. (editors), *Plateau Uplift - The Rhenish Shield - A case history*. Springer Verlag, Berlin, pp. 139-151.
- Schneider, M.E. and Eggler, D.H., 1984. Compositions of fluids in equilibrium with peridotite: implications for alkaline magmatism-metasomatism. In: Kornprobst, J. (editor), *Kimberlites: I, kimberlites and related rocks. Developments in Petrology, 11A*, Elsevier, Amsterdam, pp. 383-394.
- Schneider, M.E. and Eggler, D.H., 1986. Fluids in equilibrium with peridotite minerals: Implications for mantle metasomatism. *Geochimica et Cosmochimica Acta*, 50, pp. 711-724.
- Seck, H.A. and Wedepohl, K.H., 1983. Mantle xenoliths in the Rhenish Massif and the northern Hessian Depression. In: Fuchs, K., von Gehlen, K., Mälzer, H., Murawski, H., and Semmel, A. (editors), *Plateau Uplift - The Rhenish Shield - A case history*. Springer Verlag, Berlin, pp. 343-351.
- Spera, F.J., 1984. Carbon dioxide in petrogenesis III: role of volatiles in the ascent of alkaline magma with special reference to xenolith-bearing mafic lavas. *Contributions to Mineralogy and Petrology*, 88, pp. 217-232.
- Spera, F.J., 1987. Dynamics of translithospheric migration of metasomatic fluid and alkaline magma. In: Menzies, M.A. and Hawkesworth, C.J. (editors), *Mantle Metasomatism*. Academic Press, London, pp. 1-19.
- Stolper, E.M., 1980. A phase diagram for mid-ocean ridge basalts: preliminary results and implications for petrogenesis. *Contributions to Mineralogy and Petrology*, 74, pp. 13-27.
- Stosch, H.-G. and Lugmair, G.W., 1986. Trace element and Sr and Nd isotope geochemistry of peridotite xenoliths from the Eifel (West Germany) and their bearing on the evolution of the subcontinental lithosphere. *Earth and Planetary Science Letters*, 80, pp. 281-298.

- Stosch, H.-G. and Seck, H.A., 1980. Geochemistry and mineralogy of two spinel peridotite suites from Dreiser Weiher, West Germany. *Geochimica et Cosmochimica Acta*, 44, pp. 457-470.
- Stosch, H.-G., Carlson, R.W. and Lugmair, G.W., 1980. Epidiosic mantle differentiation: Nd and Sr isotopic evidence. *Earth and Planetary Science Letters*, 47, pp. 263-271.
- Streckeisen, A.L. (Chairman), 1973. Plutonic rocks: classification and nomenclature recommended by the IUGS subcommission on the systematics of igneous rocks. *Geotimes*, 18 (10), pp. 26-30.
- Takahashi, E. and Kushiro, I., 1983. Melting of a dry peridotite at high pressures and basalt magma genesis. *American Mineralogist*, 68, pp. 859-879.
- Toramaru, A. and Fujii, N., 1986. Connectivity of melt phase in a partially molten peridotite. *Journal of Geophysical Research*, 91, pp. 9239-9252.
- Trønnes, R.G., 1985. The incorporation of Ti in phlogopite in a simplified, synthetic system: a potential geothermobarometer for upper mantle and lower crustal rocks. Ph.D. Thesis, University of Western Ontario, London, Canada. 133p.
- Trønnes, R.G., Edgar, A.D. and Ariam, M., 1985. A high pressure-high temperature study of TiO_2 solubility in Mg-rich phlogopite: implications to phlogopite chemistry. *Geochimica et Cosmochimica Acta*, 49, pp. 2323-2329.
- von Knorring, O. and Du Bois, C.G.B., 1961. Carbonatitic lava from Fort Portal area in western Uganda. *Nature*, 192, pp. 1064-1065.
- Waff, H.S. and Bulau, J.R., 1979. Equilibrium fluid distribution in an ultramafic partial melt under hydrostatic stress conditions. *Journal of Geophysical Research*, 84, pp. 6109-6114.
- Wallace, M.E. and Green, D.H., 1988. An experimental determination of primary carbonatite magma composition. *Nature*, 335, pp. 343-346.
- Wallace, P. and Carmichael, I.S.E., 1989. Minette lavas and associated leucitites from the Western Front of the Mexican Volcanic Belt: petrology, chemistry and origin. *Contributions to Mineralogy and Petrology*, 103, pp. 470-492.

- Waters, F.G., 1987. A suggested origin of MARID xenoliths in kimberlites by high pressure crystallization of an ultrapotassic rock such as lamproite. *Contributions to Mineralogy and Petrology*, 95, pp. 523-533.
- Waters, F.G. and Erlank, A.J., 1988. Assessment of the vertical extent and distribution of mantle metasomatism below Kimberley, South Africa. *Journal of Petrology*, Special Lithosphere Issue, pp. 185-204.
- Waters, F.G., Erlank, A.J. and Daniels, L.R.M., 1989. Contact relationships between MARID rock and metasomatised peridotite in a kimberlite xenolith. *Geochemical Journal*, 23, pp. 11-17.
- Watson, E.B., 1982. Melt infiltration and magma evolution. *Geology*, 10, pp. 236-240.
- Watson, E.B. and Brenan, J.M., 1987. Fluids in the lithosphere, 1. Experimentally-determined wetting characteristics of CO₂-H₂O fluids and their implications for fluid transport, host-rock physical properties, and fluid inclusion formation. *Earth and Planetary Science Letters*, 85, pp. 497-515.
- Wendlandt, R.F. and Eggler, D.H., 1980. The origins of potassic magmas: 2. Stability of phlogopite in natural spinel lherzolite and in the system KAlSiO₄-MgO-SiO₂-H₂O-CO₂ at high pressures and high temperatures. *American Journal of Science*, 280, pp. 421-458.
- Wendlandt, R.F. and Mysen, B.O., 1980. Melting phase relations of natural peridotite + CO₂ as a function of degree of partial melting at 15 and 30 kbar. *American Mineralogist*, 65, pp. 37-44.
- Wilshire, H.G., 1987. A model of mantle metasomatism. In: Morris, E.M. and Pasteris, J.D. (editors), *Mantle metasomatism and alkaline magmatism*. Geological Society of America, Special Paper 215, pp. 47-60.
- Wilshire, H.G. and Shervais, J.W., 1975. Al-augite and Cr-diopside ultramafic xenoliths in basaltic rocks from western United States; Structural and textural relationships. *Physics and Chemistry of the Earth*, 9, pp. 257-272.

- Windom, K.E. and Unger, C.P., 1988. Stability of the assemblage albite plus forsterite at high temperatures and pressures with petrologic implications. *Contributions to Mineralogy and Petrology*, 98, pp. 390-400.
- Witt, G. and Seck, H.A., 1987. Temperature history of sheared mantle xenoliths from the West Eifel, West Germany: evidence for mantle diapirism beneath the Rhenish Massif. *Journal of Petrology*, 28, pp. 475-493.
- Witt, G. and Seck, H.A., 1989. Origin of amphibole in recrystallized and porphyroclastic mantle xenoliths from the Rhenish Massif: implications for the nature of mantle metasomatism. *Earth and Planetary Science Letters*, 91, pp. 327-340.
- Woermann, E. and Rosenhauer, M., 1985. Fluid phases and the redox state of the Earth's mantle: extrapolations based on experimental, phase-theoretical and petrologic data. *Fortschritte der Mineralogie*, 63, pp. 263-349.
- Wood, B.J. and Banno, S., 1973. Garnet-orthopyroxene and orthopyroxene-clinopyroxene relationships in simple and complex systems. *Contributions to Mineralogy and Petrology*, 42, pp. 109-124.
- Wood, B.J. and Virgo, D., 1989. Upper mantle oxidation state: Ferric iron contents of lherzolite spinels by ^{57}Fe Mössbauer spectroscopy and resultant oxygen fugacity. *Geochimica et Cosmochimica Acta*, 53, pp. 1277-1291.
- Wyllie, P.J., 1978. Mantle fluid compositions buffered in peridotite- CO_2 - H_2O by carbonates, amphibole, and phlogopite. *Journal of Geology*, 86, pp. 687-713.
- Wyllie, P.J., 1987. Metasomatism and fluid generation in mantle xenoliths. In: Nixon, P.H. (editor), *Mantle Xenoliths*. John Wiley & Sons, Chichester, pp. 609-621.
- Wyllie, P.J., 1988. Magma genesis, plate tectonics, and chemical differentiation of the earth. *Reviews of Geophysics*, 26, pp. 370-404.
- Wyllie, P.J., 1989a. Origin of carbonatites: evidence from phase equilibrium studies. In: Bell K. (editor), *Carbonatites - Genesis and evolution*. Unwin Hyman, London, pp. 500-545.

- Wyllie, P.J., 1989b. The genesis of kimberlites and some low-SiO₂, high-alkali magmas. In: Kimberlites and Related Rocks, Vol 1: Their composition, occurrence, origin and emplacement. Geological Society of Australia, Publication no. 14. Blackwell Scientific Publications, pp. 603-615.
- Wyllie, P.J. and Huang, W.L., 1975. Influence of mantle CO₂ in the generation of carbonatites and kimberlites. Nature, 257, pp. 297-299.
- Wyllie, P.J. and Huang, W.-L., 1976. Carbonation and melting reactions in the system CaO-MgO-SiO₂-CO₂ at mantle pressures with geophysical and petrological applications. Contributions to Mineralogy and Petrology, 54, pp. 79-107.
- Wyllie, P.J. and Rutter, M., 1986. Experimental data on the solidus for peridotite-CO₂, with applications to alkaline magmatism and mantle metasomatism. EOS, 67, pp. 390.
- Wyllie, P.J., Huang, W.-L., Otto, J. and Byrnes, A.P., 1983. Carbonation of peridotites and decarbonation of siliceous dolomites represented in the system CaO-MgO-SiO₂-CO₂ to 30kbar. Tectonophysics, 100, pp. 359-388.
- Yoder, H.S. and Kushiro, I., 1969. Melting of a hydrous phase: phlogopite. American Journal of Science, 267A, pp. 558-582.